The Dissertation Committee for Yuying Wu Certifies that this is the approved version of the following dissertation:

Mitigation Methods for Piperazine Oxidation in Post-Combustion Carbon Capture

Committee:

Gary T. Rochelle, Supervisor

Dave Allen

Gyeong Hwang

George S. Goff

Mitigation Methods for Piperazine Oxidation in Post-Combustion Carbon Capture

by

Yuying Wu

Dissertation

Presented to the Faculty of the Graduate School of

The University of Texas at Austin

in Partial Fulfillment

of the Requirements

for the Degree of

Doctor of Philosophy

The University of Texas at Austin

August, 2022

Dedication

To my parents

Acknowledgements

First, I want to thank my supervisor Dr. Rochelle. You are always a good teacher, sharing your knowledge and enthusiasm with the students. You are always responsive and patient, happy to discuss about every little bit of data, and provided me guidance when I am lost. Thank you for taking me on the backpacking trips, which I enjoyed so much but would never dare to try by myself. You are the best supervisor I can ever thought of and joining the Rochelle group is the best decision I made.

I would like to thank Fred Closmann, who taught me a lot in how the pilot work is different from bench-scale work. Thank you for keeping the pilot plant running and helping me interpreting the data. Your experience and advice are valuable, and you are like a second supervisor to me.

I also want to thank Maeve Cooney, who proofread all my reports and manuscripts. Thank you for correcting my grammar mistakes and showing me how to write better. Thank you also for organizing the meetings and taking care of all the paperwork.

I wish to express my gratitude to all my committee members: Prof. Dave Allen, Prof. Gyeong Hwang, and Dr. George Goff. Thank you for your valuable time and input into this research.

I want to thank the Rochelle Group Members (Texas Carbon Engineers) for the help in the group. Thank you to Paul Nielsen and Kent Fischer, who guided me as I joined the group, taught me how to use and maintain the instruments, and answered so many questions from me. Thank you to Korede Akinpelumi, who kept the FTIR working in the campaign and generated great data. Thank you to Ching-Ting Liu and Tianyu Gao, besides being excellent lab members, you are also great friends and helped relieved my stress. Thank you to Miguel Abreu and Yee Lee Chen, for taking the night shifts at the SRP

campaign and doing analysis on the samples. Thank you to Chih-I Chen and Athreya Suresh Babu, for the work you have done on the SRP samples. Thank you to Ariel Plantz for reading and reviewing my chapters. And thank you to Daniel Culpepper and Janelle Engel for making the beautiful HTOR and ASAP boxes.

I am grateful to all the engineers and staffs at the National Carbon Capture Center in Alabama. Without you, we will not be able to finish the campaign tests. I also want to thank all the staff working at the SRP. Jamie Church, Jarett Spinhirne, and Juan-Ramon Campos, thank you for all the work you have done supporting our test campaign. Thank you to Matthew Landsman for troubleshooting and maintaining the ICP-OES, which contributed a huge part of the data.

I also want to extend my thanks to all the supporting staff: Adam Kennedy, who modified and made the glassware I used in the experiments; Rife Randy and Denzil Smith, who helped so much on IT-related //problems; Valerie Croft, Susan McCoy, and Nohemi Cazares, who dealt with all the purchase orders and shipping and receiving of samples.

Finally, special thanks to my family. Mom and Dad, thank you for encouraging me to do what I wish to. Despite the long distance between us, I can feel your care and love. I also want to thank my fiancé Ke Zhang, who inspires me and supports me in both research and life. I look forward to our life together.

Abstract

Mitigation Methods for Piperazine Oxidation in Post-Combustion Carbon Capture

Yuying Wu, Ph. D.

The University of Texas at Austin, 2022

Supervisor: Gary T. Rochelle

Piperazine is a promising second-generation solvent for amine scrubbing in post-combustion CO_2 capture. However, the oxidative degradation of PZ can cause environmental problems and economic loss. This work presents the effects of two mitigation methods: carbon treating and N_2 sparging, on the PZ oxidation in long-term operations.

The species and their respective quantities adsorbed by the activated carbon were tested in a bench-scale device. The carbon was then tested in the High Temperature Oxidation Reactor (HTOR), where the solvent oxidizes at a reasonably fast rate. Pilot plant campaigns were also performed at the UT Austin SRP and the National Carbon Capture Center (NCCC) and the effects were verified.

When dissolved Fe is removed by carbon treating or other methods, available soluble Fe in the system dissolves and replaces the dissolved Fe. Therefore, all available Fe and ligands need to be removed for the mitigation to be effective. The sources of soluble Fe include fly ash and the corrosion of stainless steel, and the ligands are degradation products.

All PZ degraded solvents have two absorbance peaks at 320 nm and 538 nm. The 320 nm peak is caused by dissolved metals, especially Fe, complexed by degradation products. The 320 nm peak is related to the amine degradation level and can be used as a simple and efficient method to estimate the amine degradation rate.

The pilot plant data suggest that NO_2 can oxidize PZ significantly, possibly through radical reactions. 0.01 mmol/kg-hr absorption of NO_2 increased the PZ oxidation rate from 1.2 mmol/kg-hr to 2.5 mmol/kg-hr.

Table of Contents

List of Tables

List of Figures

Chapter 1. Introduction

1.1 Post-Combustion Carbon Capture (PCCC)

Global Warming has been recognized as one of the greatest challenges in the 21st century, and anthropogenic CO_2 emissions are the most significant driving force (IPCC, 2014). The most significant point sources of CO_2 are coal and natural gas electricity generation, representing more than 54% of the total carbon dioxide emissions from energy consumption in the US in 2021 (EIA, 2022). While much of fossil fuel power generation will be replaced by renewables, there will still be a need for decarbonized fossil fuel capacity to back-up renewables.

1.2 Amine Scrubbing and Solvent of Interest

Amine scrubbing is the most mature and well-studied technology CCS technology that can be deployed industrially in a relatively short time scale (Rochelle et al, 2011). The lean solvent is cooled down and sent back to the absorber for a new cycle. A typical design is shown as Figure 1-1. At least 90% of CO_2 is absorbed by aqueous lean amine solvent at low temperature and atmospheric pressure. The rich solvent is heated to high temperature to reverse the reaction and release CO_2. After water is condensed, pure CO_2 is compressed to be either sequestered or used for enhanced oil recovery.

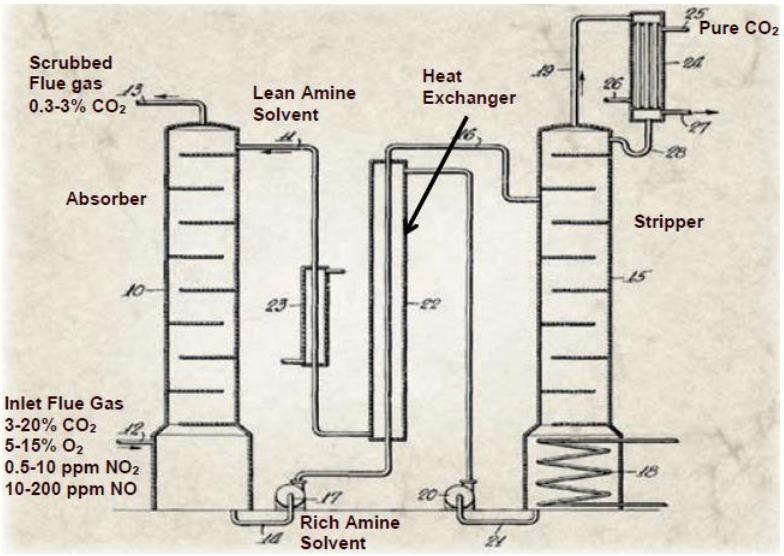

Figure 1-1: Simplified amine scrubbing process (Bottoms 1930) modified for clarity and to include post-combustion flue gas conditions

1.3 Sources of Amine loss

One important challenge at commercial scale is the loss of solvent by thermal and oxidative degradation, reaction with contaminants in flue gas, volatile and aerosol emissions, leaks, and the solvent reclaiming process (Nielsen, 2018). Cost of amine makeup can contribute as much as 10% of the CO_2 capture cost (Rao and Rubin, 2002). The losses from degradation and emissions will also create safety and environmental hazards.

Thermal degradation of amines occurs at high temperatures in the cross exchangers and stripper, where the amine reacts with CO_2 to form amine carbamate polymers (Polderman, 1955). It is the most important source of degradation in acid gas treating.

Thermal degradation is well-studied and is manageable by running the stripper at a lower temperature. For example, the thermal degradation of monoethanolamine (MEA) is manageable up to 120 ℃ (Davis, 2009), and the thermal degradation of piperazine (PZ) is manageable up to 150 ℃ (Freeman, 2011)

Oxidative degradation is observed to be the most significant source of amine loss

in pilot plants with post-combustion flue gas (Strazisar et al., 2003; da Silva et al., 2012; Nielsen, 2018). Oxidation products include heat stable salts (Rooney et al., 1998), amides (Sexton, 2008), ammonia, and aldehydes (Voice, 2014). The oxidation is related to the mass transfer of oxygen, the existence of catalysts and inhibitors, the continuous cycling of solvent between low and high temperatures (Voice, 2014), and application of N_2 sparging (Closmann, 2011; Nielsen, 2018). This work will focus on the oxidative degradation of solvents.

Losses from volatile amine emissions and aerosols is also an important source. The volatile amine loss can be minimized by applying a water wash section at the top of the absorber. The aerosol emission can be mitigated by eliminating the aerosol nuclei in the flue gas (Beaudry, 2017) and increasing the temperature of the absorber top (Akinpelumi et al, 2021).

The impurities in the flue gas can also cause amine losses. NO_2 in the flue gas can react with secondary amines to form nitrosamines, which decompose at high temperature (Fine, 2014). SO_2 in the flue gas can be absorbed as sulfate. Together with the formate, acetate, glycolate, and oxalate from amine degradation, the heat stable salts increase the solvent viscosity. The heat stable salts can also react with amines to form amides, therefore lowering the CO_2 capacity.

1.4 PIPERAZINE

While MEA is well-studied and commonly used as the baseline solvent as it has been widely used in natural gas sweetening commercially, it is not a suitable solvent to use for amine scrubbing in post-combustion capture units. The fast thermal degradation rate of MEA limits the temperature and pressure of the stripper. However, the requirement to compress the captured CO_2 for sequestration means that a high-pressure stripper will have better overall energy (Rochelle et al, 2011). MEA is also prone to oxidize at low

temperatures, making the overall MEA loss rate high even when operated with a low-temperature stripper.

Piperazine (PZ) has been proposed as a 2nd-generation solvent for amine scrubbing in post-combustion CO_2 capture. Its low volatility, high rate of CO_2 absorption, and high capacity (Dugas, 2009; Freeman, 2011) make it an excellent solvent for the amine scrubbing process. PZ has good thermal stability, allowing the stripper to operate at higher temperature and pressure to reduce the overall energy cost. PZ is more resistant to oxidative degradation than MEA as well, therefore making PZ a much better solvent than MEA. This work will focus on the study of 5 m PZ.

Other solvents, including Shell CANSOLV DC-103™ and DC-201™, and MHI KS-1 ™ and KS-21™ have also been tested and reported as promising solvents. However, these solvents are all proprietary, and no detailed studies have been published. Another open-source solvent, CESAR-1, which is a mixture of PZ and Amino-2-methyl-1-propanol (AMP), has also been tested in several pilot plants including Technology Centre Mongstad (TCM) (Benquet et el, 2021) and the pilot plant at Niederaussem (Moser et el., 2021).

1.5 Previous Work Done on PZ

Freeman 2011 systematically studied the thermal degradation of PZ and determined the T_{max} of PZ was 163 ℃ (Freeman, 2011), where trade-off between energy requirements and amine loss is optimized (Davis, 2009).

Fine showed that NO_2 reacts with PZ via a free-radical absorption mechanism to form amine radicals and nitrite, forming n-nitrosopiperazine (MNPZ) at absorber condition (Fine, 2015). 1 mol of nitrite can oxidize 1.5 mol of PZ in a cyclic reactor (Nielsen, 2018)

Sexton, Freeman, Closmann, and Voice proved that the PZ oxidation is much more significant in cyclic operating conditions than at a constant temperature. Closmann

proposed that an amine stable at absorber conditions will oxidize in the hot rich side of the cross exchanger and between the cross exchanger due to the dissolved oxygen. Voice proposed that the oxidation can be caused by oxygen carriers including peroxides and dissolved metals (Sexton, 2008 ; Freeman, 2011; Closmann 2011; Voice, 2013).

Oxidation degradation of the alkanolamine can be reduced in amine scrubbing unit by stripping the rich solvent with a scavenging gas, such as the CO_2 or N_2 prior to any heating of the solvent (Chakravarti & Gupta, 1999). Closmann proposed applying N_2 sparging to remove the dissolved oxygen in the solvent before entering the high temperature section and mitigate amine oxidation. 1 L/min N_2 was confirmed to be effective on 7 m MDEA in bench-scale cycling device (Closmann, 2011). Nielsen tested the effects of N_2 sparging on 5 m PZ in bench-scale cycling device, and the production of NH_3, formate, EDA, and PZ-one all decreased (Nielsen, 2018).

Goff proposed the use of oxidation inhibitors to deplete the dissolved O_2 or free radicals (Inhibitor A (KI), Na_2SO_3, and formaldehyde) in the solvent and decrease the amine oxidation rate (Goff, 2005). Sexton tested the effects of Inh A on PZ solvent at constant temperature. 100 mM Inh A decreased the formate and EDA formation by over 90% with the presence of Fe and Cu. 100 mM Inh A can completely inhibit PZ oxidation with only Fe present (Sexton, 2008). Nielsen tested the mitigation effects in a bench-scale cycling system and discovered the addition of Inh A increases NH_3 from the EDA degradation but did not affect the PZ oxidation (Nielsen, 2018).

1.6 RESEARCH OBJECTIVES

The primary objective of this research is to develop and design feasible methods to mitigate amine oxidation, focusing on carbon treating and N_2 sparging.

This work proposed and studied the use of carbon treating as a long-term method

to mitigate oxidation. The species and the quantities of degradation and corrosion products were studied in bench-scale, and the effects were tested in two different pilot plants. While granular activated carbon has been widely used in industry to remove contaminants and to capture mercury compounds, the use of activated carbon is scarce in amine scrubbing process. A very limited period of carbon testing was performed at Technology Centre Mongstad (TCM) on MEA degradation, but no firm conclusions were drawn (Morken et el., 2019).

Study of N_2 sparging was continued based on the results of Nielsen. While Nielsen focused on treating solvent at early stages, this work presents the results of N_2 sparging on degraded solvent. The combination of carbon treating and N_2 sparging was tested. The effect was tested at pilot plants and the designs were optimized for pilot-scale and commercial scale.

Chapter 2. Methods

2.1 Preparation of PZ Loaded solvent

Loaded PZ solvents were prepared with ultra-pure deionized water, commercially purchased PZ solid (anhydrous, 99% from Sigma Aldrich) and CO_2 from cylinders. The method was described in detail in Hilliard, 2008. The mass of the PZ and the water are measured before added into the glass column as shown in Figure 2-1. The column with the chemicals is connected to a CO_2 inlet line, and then tared before CO_2 is fed slowly through the sparger. The flow rate of the CO_2 is kept small so that no CO_2 leaves the liquid level, which prevents the evaporation of water and keeps the calculated concentration and loading of the solvent accurate. Unloaded PZ has a low solubility in water, and the minimum loading to prevent 5 m PZ from precipitation at room temperature is 0.24 mol CO_2/equivalent N.

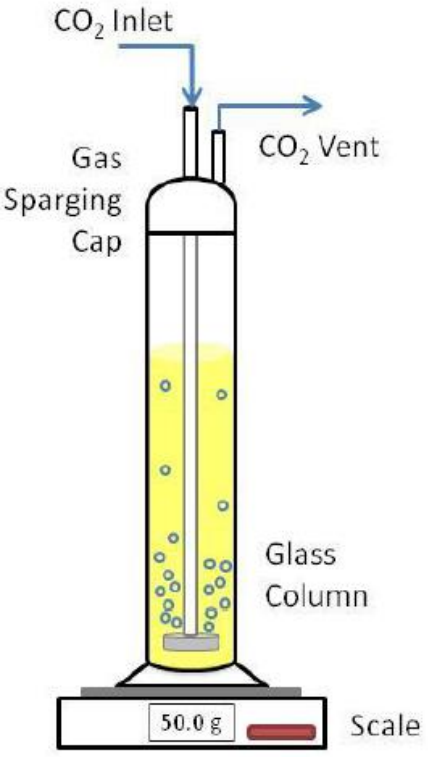

Figure 2-1: Schematic of gravimetric solution preparation (Freeman, 2011)

2.2 ANALYTICAL METHODS

2.2.1 Anion IC

The concentration of heat stable salts including formate, acetate, glycolate, and oxalate generated from PZ degradation was measured with anion ion chromatography. From 2017 to 2020, a Dionex ICS-3000 Ion Chromatography System was used, and the separation of ions was performed on an IonPac AG15 guard column and an IonPac AS15 analytical column. The program was developed by Sexton and Voice (Sexton, 2008; Voice, 2013) and described in detail by Nielsen (Nielsen, 2018). Since 2020, anion IC was performed with a Dionex™ ICS-6000 Capillary HPIC™ system and the same guard column and column were used. The scripts are included in Appendix A. Standards between 0.01 mmol/kg to 0.5 mmol/kg were used to obtain the elution time of the species and a calibration curve for the concentration. Table 2-1 includes the species in most degraded samples and their elution time.

Table 2-1: Species quantified by Anion IC and the elution time

Species	Time (minutes)
glycolate	19.3
acetate	19.9
formate	20.7
propionate	22.2
chloride	24.5
nitrite	26.0
sulfate	29.9
oxalate	30.0
nitrate	32.7

2.2.1.1 Total Heat Stable Salts

The heat stable salts can react with amines to form amides, and the total heat stable salt method breaks the bond between the salts and the amine. The samples are treated with 10 N NaOH 1:1 volumetrically for 24 hours. The treated samples are then diluted 50 times in a 1.5 mL plastic vial. The same scripts are used to analyze for heat stable salts and total heat stable salts.

2.2.2 Cation IC

The concentration of PZ and other cation degradation products was measured with cation chromatography. From 2017 to 2020, a Dionex ICS-2100 Ion Chromatography system was used. The separation of ions was performed on an IonPac CG 17 guard column and an IonPac CS 17 analytical column. The program was developed by Namjoshi and Davis (Davis, 2008; Namjoshi, 2015) and described in detail by Nielsen (Nielsen, 2018). Since 2020, the cation IC was performed with a Dionex™ ICS-6000 Capillary HPIC™ system and the same guard column and column were used. The scripts are included in Appendix A. Standards between 0.01 mmol/kg to 0.5 mmol/kg were used to obtain the elution time of the species and a calibration curve for the concentration. The samples are diluted 10000 times gravimetrically in a 1.5 mL plastic vial, and 25 µL of samples are required for each injection. Table 2-2 includes the species in most degraded samples and their elution time.

Table 2-2: Species quantified by Cation IC and the elution time

Species	Full Name	CAS #	Time (minutes)
NH_4^+			5.0
PZ-one	2-oxopiperazine	5625-67-2	6.8
FPZ	1-formylpiperazine	7752-92-2	7.4
EDA	ethylenediamine	107-15-3	17.9
PZ	piperazine	110-85-0	20.2
HEP	1-(2-hydroxyethyl)piperazine	103-76-4	21.7
MPZ	1-methylpiperazine	109-01-3	22.4
EPZ	1-ethylpiperazine	5308-25-8	23.7
DMPZ	1,4-dimethylpiperazine	106-58-1	25.2
AEP	aminoethylpiperazine	140-31-8	29.3

2.2.3 HPLC

Nitrosamines and aldehydes were analyzed with a Dionex Ultimate 3000 reverse-phase High Performance Liquid Chromatography unit with UV detection with an Acclaim™ Polar Advantage II C18 5 µm 120 Å 4.6 x 150 mm column.

2.2.3.1 Nitrosamines

Mononitrosopiperazine (MNPZ) had the same elution time as formylpiperazine (FPZ), and the two species were not separated by adjusting the HPLC method. In order to quantify the MNPZ accurately in the samples, the samples were treated with 10 N NaOH on a 1:1 base gravimetrically for 24 hrs before analysis. The samples were then diluted 20 times gravimetrically with DDI water in a 1.5 mL plastic vial. The MNPZ peak elutes at

5.5 minutes in a full 15-minute run. These methods were described in detail by Nielsen (Nielsen, 2018).

2.2.3.2 Aldehydes

The aldehydes in the degraded samples were quantified after reaction with 2,4-dinitrophonylhydrazine (DNPH). A stock solution was prepared with 0.4 wt% DNPH in ACN, methanol, and 10 mM ammonium carbonate buffer. The samples were diluted with the stock solution by 20 times gravimetrically. The solution was allowed to react 16 to 24 hrs before analysis to ensure the over 95% of the aldehydes reacted with DNPH. The UV-absorbance at 365 nm was used to quantify the concentration. PZ-DNPH elutes at 2.2 min, PZOH-DNPH elutes at 2.5 min, and unreacted DNPH elutes at 9.1 min in a full 15-minute run. The method is described in detail by Nielsen (Nielsen, 2018).

2.2.4 Alkalinity

The total alkalinity of the amine solvent was quantified with a Metrohm Titrando series automatic titrator operated with PC Control software. The method was described in detail by Freeman (Freeman, 2011). 0.2 g of samples were diluted with 60 mL DDI water in a glass beaker, and titration was performed with 0.1 N aqueous H_2SO_4 at a rate of 0.1 mL every 10 seconds. The end point was determined when the second equivalence point was reached, and the total alkalinity was calculated from the mass of the PZ solvent and the volume of H_2SO_4.

2.2.5 ICP-OES

ICP-OES was used to analyze metals by the specific wavelength of UV light emitted in argon plasma flame at 7000K. A Varian 10-ES Axial ICP-OES (Varian Inc., Palo Alto, CA) is used for this analysis (Nielsen, 2018). The system is controlled through

ICP Expert II® software. 0.32 mL samples were diluted into 8 mL with 2 wt % nitric acid to allow for multiple analyses, and standards between 0.5 ppm and 25 ppm were prepared for each run. For samples with low metal concentrations, a small dilution factor was used to allow a reasonable signal to noise ratio. Since PZ can interfere the absorbance of light in the measurement, the standards were prepared with the same concentration of PZ added to eliminate the interference. For each element, two to three wavelengths that have high intensity and are not interfered by other metals are used, and three measurements were performed at each wavelength. The average results from the measurements of the three wavelength were reported, and the standard deviation is usually within 2% to 3%. The same metal species with different oxidation states are not differentiated, and the results represent the total amount of certain metal species in the samples. The characteristic wavelengths of the commonly analyzed metals are listed in Table 2-3.

Table 2-3: Characteristic wavelengths for ICP-OES metal quantification

Elements	**Measure Wavelengths (nm)**		
Lithium (Li)	670.783	610.365	
Potassium (K)	766.491	769.897	
Iron (Fe)	234.350	238.204	259.940
Chromium (Cr)	205.560	206.158	267.716
Nickel (Ni)	216.555	221.648	231.604
Manganese (Mn)	257.610	259.372	260.568
Copper (Cu)	213.598	224.700	324.754

2.2.6 UV-Vis

The UV-Vis measurements were performed with two instruments: a NanoDrop™ One Microvolume UV-Vis Spectrophotometer, and a Varian Cary 5000 UV-Vis-NIR

Spectrophotometer. The NanoDrop worked well with samples that have high absorbance, while the Varian Cary can only measure in a range between 0 to 2.5 A. 1.5 µL of sample was analyzed with the NanoDrop first to get an estimation of absorbance range. The sample was then diluted to close to 1 A with water for a second measurement with the Varian Cary. 3.5 mL of the diluted sample was injected in a disposable cuvette with a light path of 10 nm. A dilution-corrected absorbance was reported by multiplying the measured absorbance and the dilution factor. The instrument was calibrated with zero transmittance and water blank each time before the analysis.A typical UV-Vis spectrum is shown in Figure 2-2. While a complete spectrum from 0 to 1500 nm was measured, only data from 200 to 800 were representative because the cuvette absorbs all light below 200 nm and water absorbs significantly in the IR region. Compared to the loaded PZ sample, the degraded samples have two significant peaks at 320 nm and 538 nm. Since 538 nm is within visible range, the color of the samples is directly related to this peak. These two peaks were observed in all the samples collected in the HTOR, NCCC, and SRP using 5 m PZ as solvent. Smaller peaks were also oberserved in the region between 350 nm and 500 nm, but these peaks are hard to quantify since they overlap on each other. UV-Vis peaks at 270 nm, 278 nm, 305 nm, and 313 nm were reported in MEA degradation. The peak at 313 nm was caused by the accumulation of N-(2-hydoxyethyl)imidazole, and is strongly correlated with the heat stable salts, which is defined as the total molar concentration of anions as a mass of MEA (Reynolds et al, 2015).

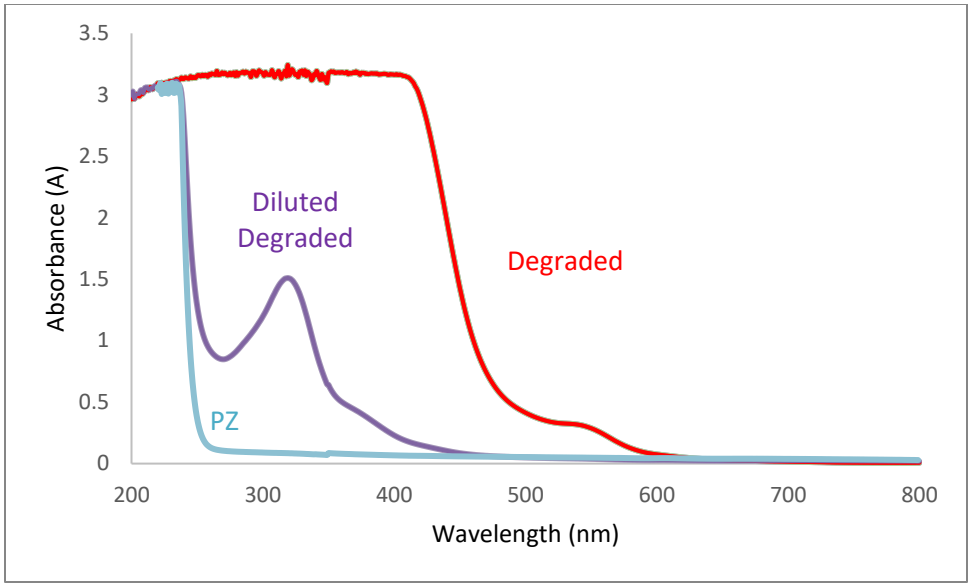

Figure 2-2: Typical UV-Vis spectrum of NCCC solvents

The samples were diluted to different concentrations to test if samples are transparent and follow Beer's law. As shown in Figure 2-3, the absorbance had a linear relationship with the concentration, indicating that the absorbance was measured accurately by assuming no reflective light, and the estimation of samples with high absorbance is accurate after dilution.

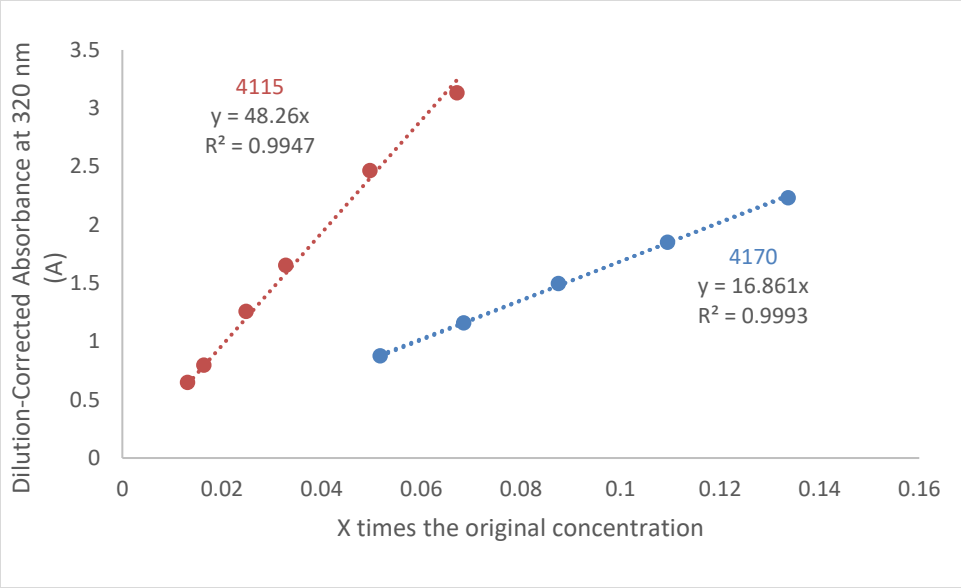

Figure 2-3: Relationship between dilution-Corrected absorbance at 320 nm and dilution factor

Different metal ions were added into degraded samples. While the addition of $NH_4Fe(SO_4)$ did not produce any peak at 320 nm or 538 nm, the addition of $NH_4Fe(SO_4)_2 \cdot 12H_2O$ was found to replicate the peak at 320 nm, shown as the purple curve in Figure 2-4. $NH_4Fe(SO_4)_2 \cdot 12H_2O$ in water alone absorbs at 293 nm instead of 320 nm, indicating that the 320 nm peak was caused by products of Fe^{3+} and the degradation products.

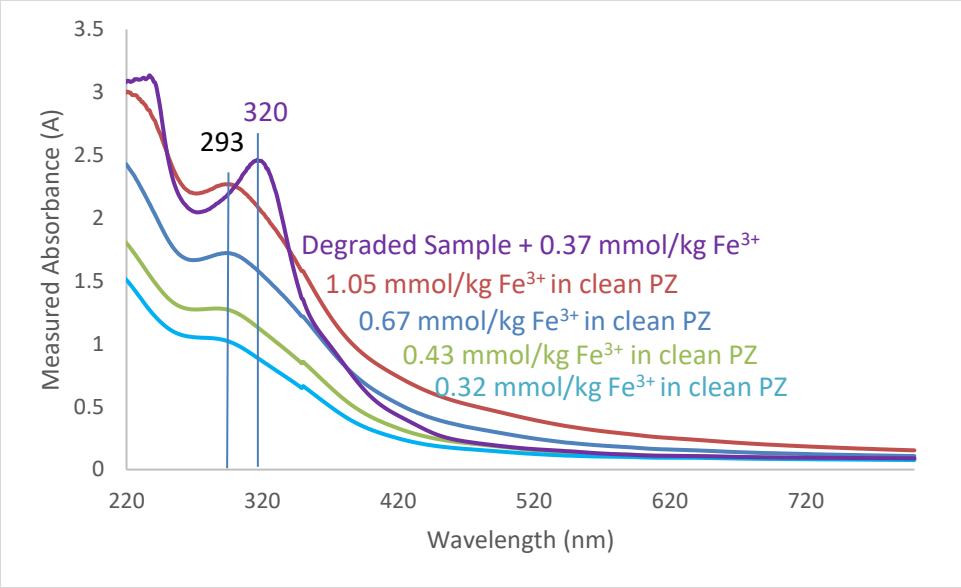

Figure 2-4: Absorbance of Fe^{3+} in clean PZ and degraded sample

There is a linear relationship between the increase in absorbance and the added Fe^{3+} concentration shown in Figure 2-5, indicating that there is an excesse amount of degradation product ready to complex with the Fe^{3+}.

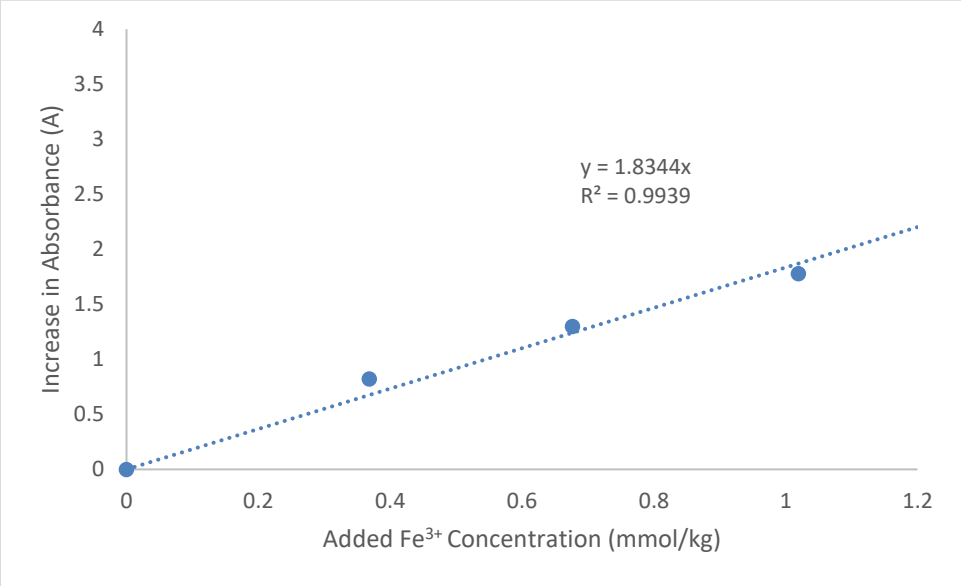

Figure 2-5: Calibration curve of Fe^{3+}complex at 320 nm

While it was found that Fe^{3+} absorbs at 320 nm in degraded samples, Fe^{3+} is not the only species contributing to the 320 nm peak as the Fe^{3+} concentration calculated by UV-Vis was much higher than the Fe concentration given by ICP. More metals were tested in clean and degraded piperazine, which has an absorbance of 1.4 at 320 nm. As shown in Figures 3-6 to 3-8, Ni^{2+}, Cr^{3+}, and Mn^{2+} all absorb close to 320 nm, and can add to the peak intensity at 320 nm. The absorbance due to added Ni^{2+} and Cr^{3+} is much smaller in the degraded sample than in clean PZ, suggesting that they can react with certain degradation products and no longer absorb in that range. It is probable that the 320 nm peak represents some overall metal level in the solvent.

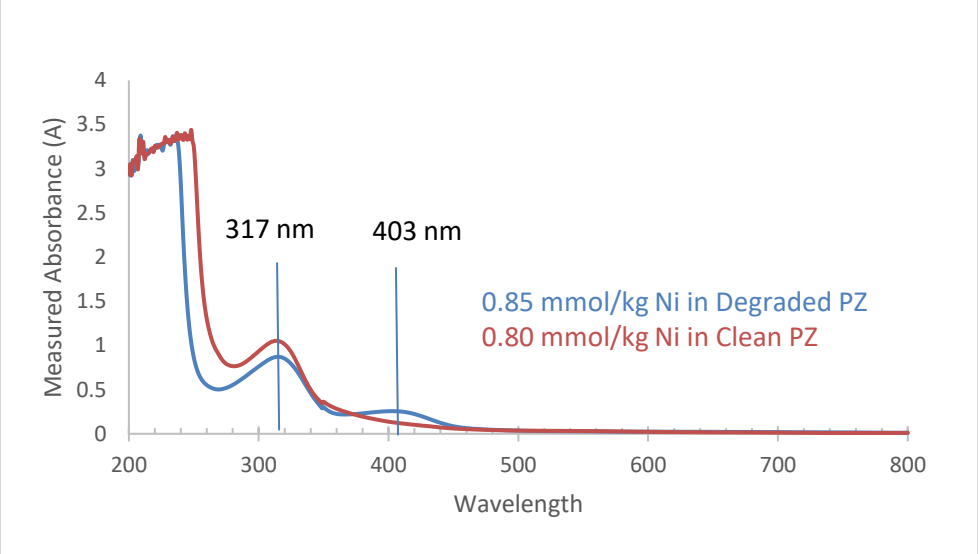

Figure 2-6: Addition of $Ni(NO_3)_2$ in clean PZ and degraded sample

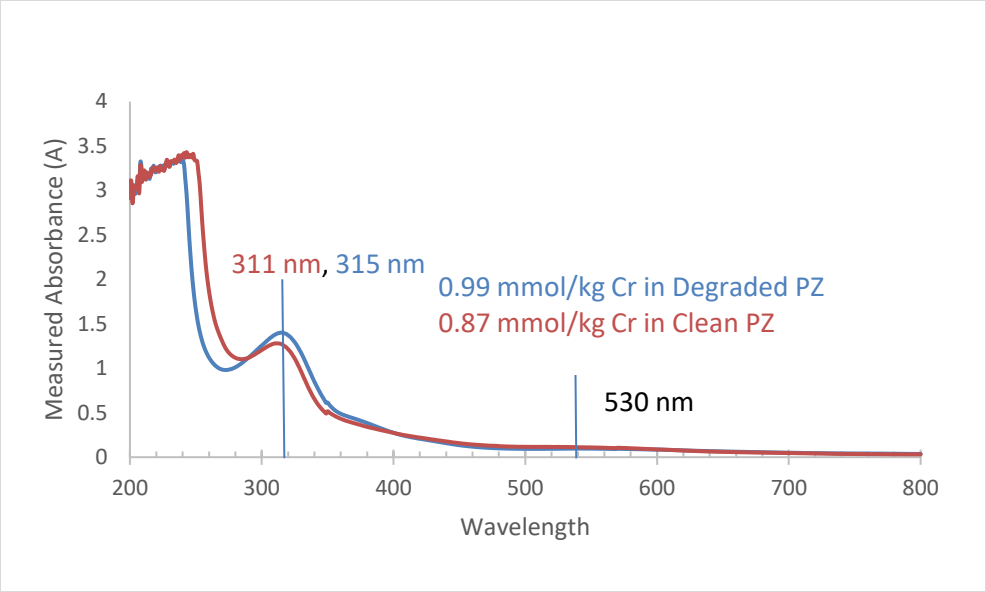

Figure 2-7: Addition of $Cr(NO_3)_3$ in clean PZ and degraded sample

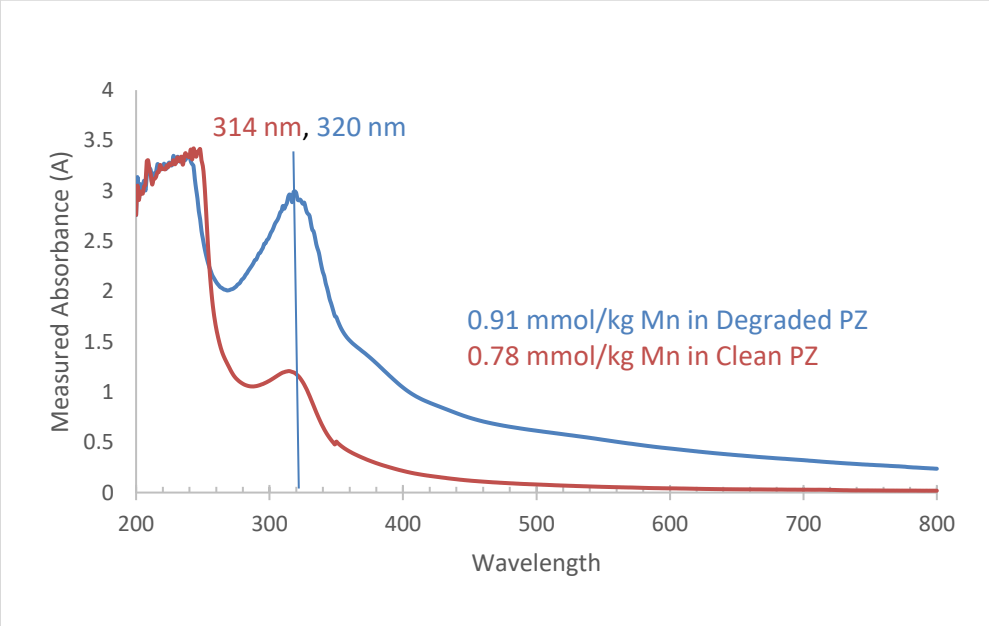

Figure 2-8: Addition of $Mn(NO_3)_2$ in clean PZ and degraded Sample

When the degraded samples were treated with H_2SO_4, the absorbance peak at 320 nm shifted to 304 nm. As shown in Figures 3-9 and 3-10, both $FeNH_4(SO_4)_2$ and $FeCl_3$ in

H_2SO_4 absorb at 304 nm, indicating the 304 nm resulted from Fe^{3+} in H_2SO_4. $Fe(NH_4)_2(SO_4)$ and $FeSO_4$ had no absorbance when added to H_2SO_4.

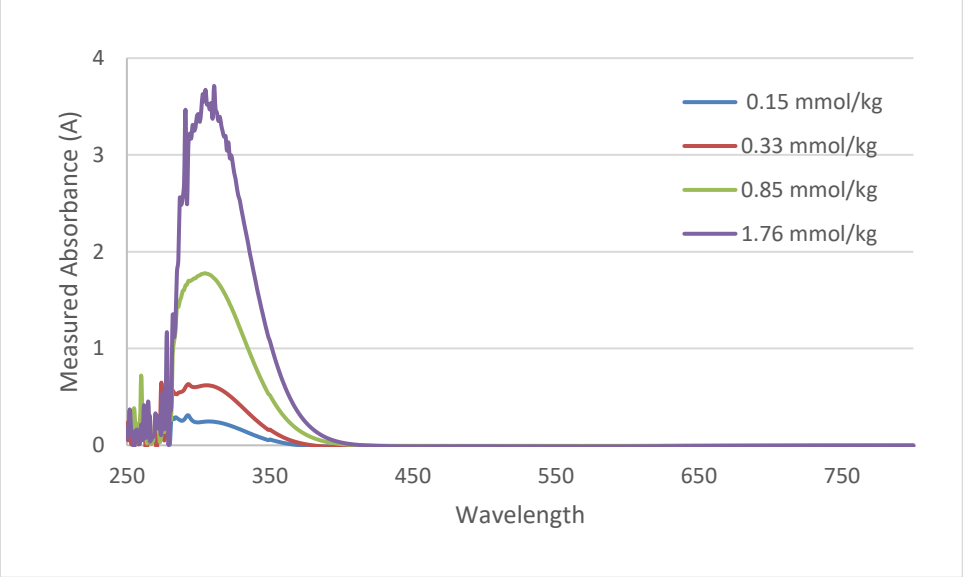

Figure 2-9: UV-Vis standards for $FeNH_4(SO_4)_2$ in H_2SO_4

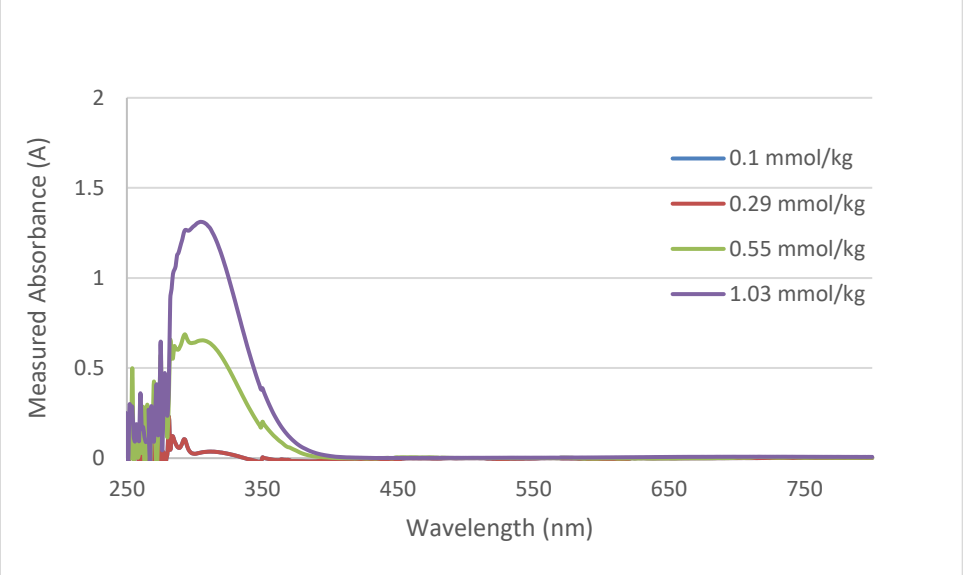

Figure 2-10: UV-Vis standards for $FeCl_3$ in H_2SO_4

Calibration curves were created to obtain the absorptivity of Fe^{3+} in H_2SO_4 with different anion species. As shown in Figure 2-11, while Fe^{3+} in H_2SO_4 share the same absorbance peak, the absorptivity was different depending on the anion form. Therefore, the peak at 304 nm only suggests the existence of Fe^{3+} and cannot be used to quantify the Fe^{3+} due to the dependence of anion species.

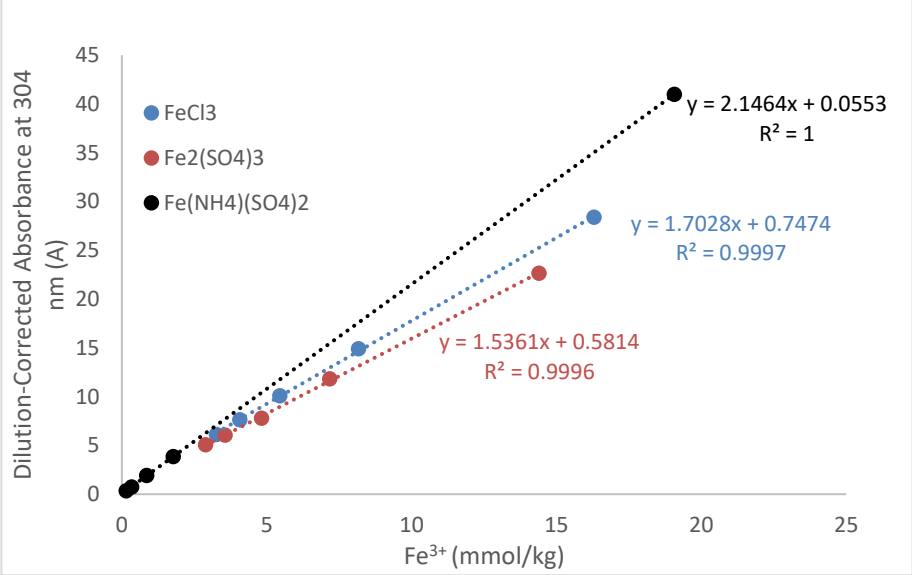

Figure 2-11: UV-Vis standards for Fe^{3+} in H_2SO_4

2.2.7 FTIR

A Temet Gasmet^{TM} DX-4000 portable FTIR analyzer was used to analyze the outlet gas from the HTOR apparatus. A rackmount Gasmet^{TM} CX-4000 FTIR analyzer was used for NCCC and SRP pilot campaigns. 5 SLPM gas was heated and sent into the sample cell at 180 °C , and the light absorption in the wavenumber range of 4200 and 600 cm^{-1} was measured. Measurements were taken every 200 ms, and the average values over 3 minutes were recorded and reported. For each component, two to three analysis ranges are used to quantify the concentration, and the ranges are listed in Table 2-4. The standard deviation is within ±3%. The ranges are selected so that they have high absorption and minimize the

residual. A zero flush was performed automatically every morning at 8:00 am, and a background was taken every one or two weeks of operation.

Table 2-4: FTIR analysis ranges

Compound	Range 1 (cm^{-1})	Range 2 (cm^{-1})	Range 3 (cm^{-1})
H_2O (vol %)	3200-3401		
CO_2 (vol %)	910-1003	3425-3616	2165-2251
NH_3 (ppm)	915-988	2423-2560	
PZ (ppm)	2470-2540	2580-2800	

2.3 EXPERIMENTAL DEVICES

2.3.1 Carbon Adsorption Column (CAC)

A 25-mL burette was used to perform the carbon adsorption experiment. As shown in Figure 2-11, the column was filled with carbon, and the bottom was plugged with glass wool. The solvent flowing out from the column is fed through a peristaltic pump, which transfers the solvent back to the top of the column at a rate of 0.5 mL/s. The mass of the carbon in the column and the total solvent amount are measured to calculate the carbon-to-solvent ratio, and the solvent is collected from the top for further analysis.

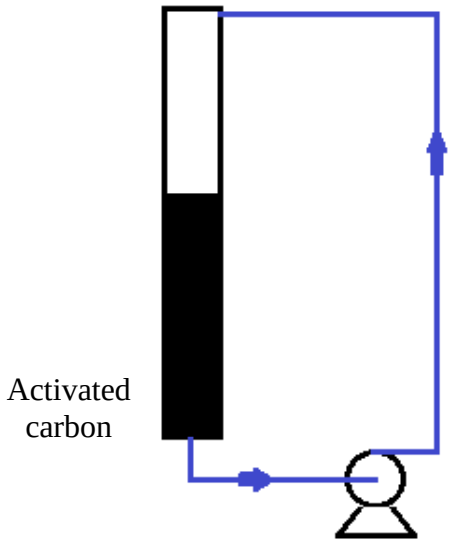

Figure 2-12: Carbon adsorption column setup

2.3.2 High Temperature Oxidation Reactor (HTOR)

The bench-scale experiments were performed in the high temperature oxidation reactor (HTOR), which cycles amine between a low-temperature reactor and a high-temperature oil bath up to 150 ℃ . This apparatus simulates solvent oxidation in the amine scrubbing process, with the reactor simulating the absorber, and the oil bath simulating the stripper. The total inventory is 1.6 L, and the solvent has a flow rate of 0.2 L/min. The inventory at low temperature is 1.0 L, and the inventory at hot rich condition is 0.6 L. The gas rate is 7.5 L/min prepared by mixing compressed air with CO_2. The concentration of the CO_2 is determined to provide thedesired loading of the solvent, which cannot exceed 0.3 to prevent flashing occurring at the high temperature. Nitrogen sparging can be applied to the bubble removal vessel to remove dissolved oxygen as described in detail by Nielsen (Nielsen, 2018). A glass column which is 15 cm in inner diameter and 300 mm tall was added between the peristaltic pump and the bubble removal vessel to serve as carbon bed.

The carbon bed is 15.9 mm in diameter and 1 ft tall and can hold a maximum of 17 g carbon. The HTOR configuration is shown in Figure 2-13.

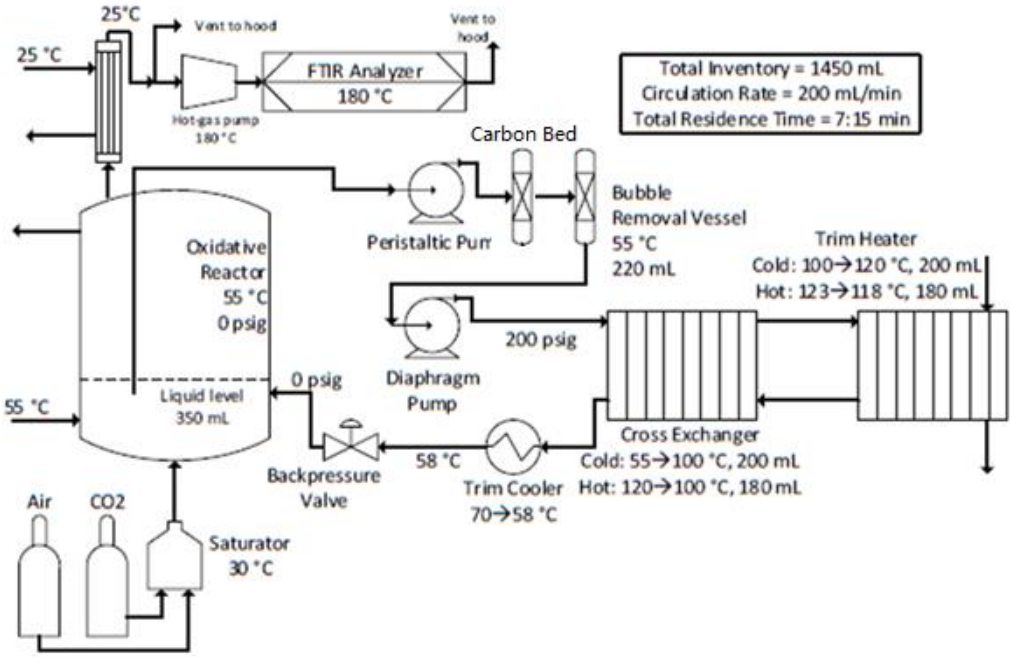

Figure 2-13: HTOR apparatus P&ID

2.4 CHARACTERIZATION OF THE ACTIVATED CARBON

A FEI Quanta 650 FEG Scanning Electron Microscope was used to observe the surface of the carbon after adsorbing the solvent. The carbon samples were ground and stuck to a sample holder, and a focused electron beam was scanned across the surface to create an image as well as the elemental composition of the sample. Since the energy can penetrate several layers beneath the top layer of atoms, the EDX result can only qualitatively represent the surface. The energy was set to 15 kV, and the picture of the samples was taken at the scale of 1 μm.

Besides the solvents, the carbon was also analyzed with SEM and EDX. Three types of samples were analyzed: the unused carbon, the used carbon from the NCCC 2019

Campaign, and used carbon rinsed with H_2SO_4. The images are shown below in Figure 2-14, and the wt % of different elements are shown in Table 2-5. The unused carbon is mostly clean, but there were some impurities in it, primarily oxygen. There are crystals found on the surface of the used carbon and the H_2SO_4 rinsed carbon. They both have a higher concentration in oxygen, and a small Fe concentration was observed. However, the EDX results cannot serve as a quantitative result since it cannot control the depth of the measurement.

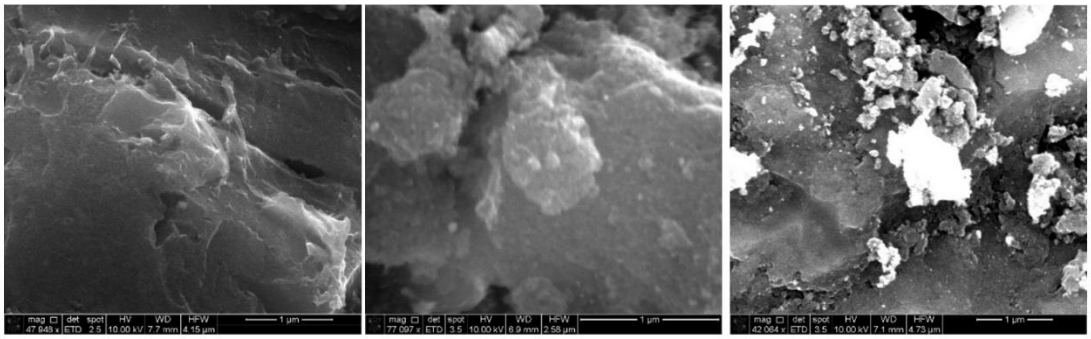

Figure 2-14: SEM images of carbon samples (left: unused carbon; middle: used carbon from NCCC; right: carbon used in NCCC and rinsed with H_2SO_4)

Table 2-5: Elemental composition of carbon surface by EDX

Element	wt %		
	Clean C	**Used C**	**H_2SO_4 Rinsed C**
C	95.58	88.71	88.05
N	0.66	1.65	1.84
O	3.02	7.82	6.91
Al	0.22	0.74	0.55
S	0.55	0.43	0.02
Fe		0.61	0.25

Chapter 3. Bench-Scale Carbon Adsorption Column

This chapter includes the description and results of 27 experiments performed in the carbon adsorption column (CAC) to understand the removal of degradation and corrosion products by activated carbon. The activated carbon used in these experiments is 8*30 mesh, lignite based granular activated carbon, same as the carbon used in the carbon treating in NCCC and SRP campaigns, which will be discussed in Chapter 6.

3.1 Summary of CAC Experiment

The CAC can hold a maximum of 100 mL solvent, which is a relatively small reservoir of solvent compared to the 0.5 mL to 4 mL of samples need to be collected for each analysis. As a result, the final condition, instead of the initial condition, is used when interpreting the results. The solvents used in these experiments included clean PZ and two degraded solvents collected from a campaign performed in the National Carbon Capture Center (NCCC): #3537 and #3706. #3537 experienced 1340 hours of operation, and #3706 experienced 2100 hours of operation.

Table 3-1: Summary of CAC experiments

Experiment Number	Solvent	Initial Solvent Mass (g)	Final Solvent Mass (g)	Clean or Used Carbon	Carbon Mass (g)	Final C/S Ratio
1	#3706	74.7	49.3	N/A	0.0	0
2-1	Clean 5 m PZ	90.0	77.7	Clean	3.4	0.043
2-2	#3706	82.4	77.6	CAC 2-1	3.4	0.044
3	#3537	104.1	76.3	Clean	3.0	0.039
4	#3537	96.7	78.8	Clean	4.3	0.054
5	#3537	86.0	51.7	Clean	1.0	0.020
6	#3537	94.5	76.5	Clean	3.5	0.046
7	#3537	87.8	73.5	Clean	3.7	0.050
8	#3537	87.5	78.4	Clean	2.1	0.026
9	#3537	88.6	82.2	Clean	1.7	0.021
10	#3537	89.2	83.8	Clean	1.3	0.016
11	#3537	86.6	64.5	Clean	4.6	0.071
12	#3706	78.6	45.8	Clean	1.9	0.042
13	#3706	87.0	63.6	Clean	5.2	0.081
14	#3706	86.0	61.3	Clean	2.1	0.035

15	#3706	82.8	80.7	Clean	3.5	0.043
16	#3706	87.0	80.9	Clean	5.2	0.065
17	#3706	83.8	63.1	Clean	4.4	0.117
18	#3706+$Fe_2(SO_4)_3$	81.4	26.1	Clean	3.1	0.119
19	#3706+$Fe_2(SO_4)_3$	81.7	29.2	Clean	3.1	0.106
20-1	#3706	82.7	65.6	Clean	0.3	
20-2	#3706	48.7	29.8	20-1	0.3	
21-1	Water	78.5	N/A	NCCC	3.2	
21-2	0.2 N H_2SO_4	74.6	N/A	NCCC	3.2	
21-3	0.2 N H_2SO_4	77.8	N/A	NCCC	3.2	
21-4	25 mmol/kg EDTA	68.0	N/A	NCCC	3.2	
22	0.2 N H_2SO_4	141.8	N/A	Clean	0.5	
23	5 m PZ + 17.3 mmol/kg AEP	89.8	64.4	Clean	1.6	0.026

3.2 ZERO AND BASELINE CONDITIONS IN CAC

3.2.1 Zero Condition – Solvent Cycling without Carbon

Before interpreting the data, a baseline condition was performed to understand if there was any further reaction going on in the column. In CAC 1, no carbon was used, and the solvent was cycled in the column for 170 hours. ICP, Cation IC, Anion IC, and UV-

Vis were used to analyze for the degradation and corrosion products in the solvents. The results are shown in Figure 3-1, 4-2, and 4-3 and 4-4. Since all the species stayed relatively constant, it is concluded that no further reactions are going on, and no correction of water balance is required while interpreting the data.

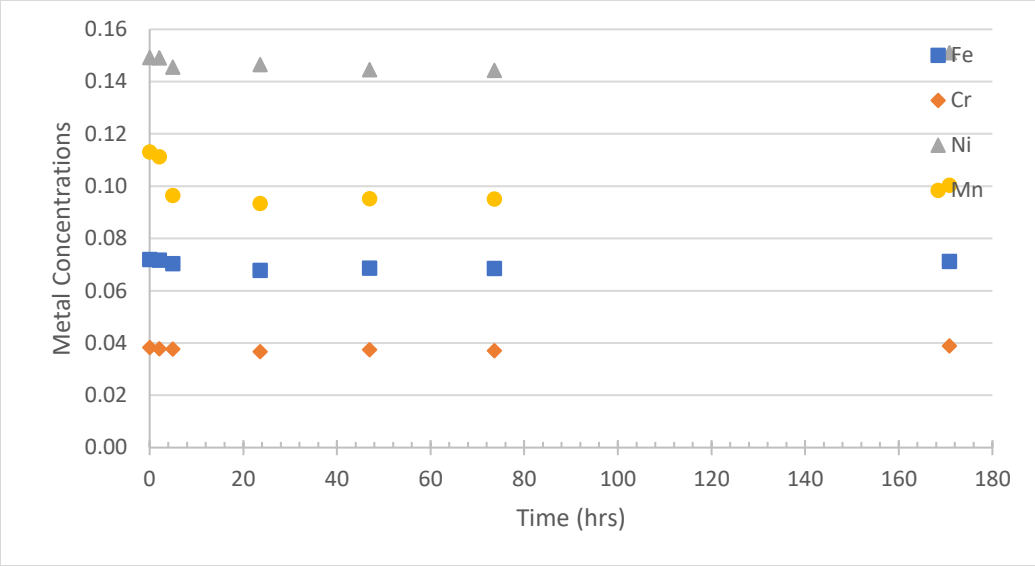

Figure 3-1: Concentrations of metal species in CAC 1 (baseline, no carbon)

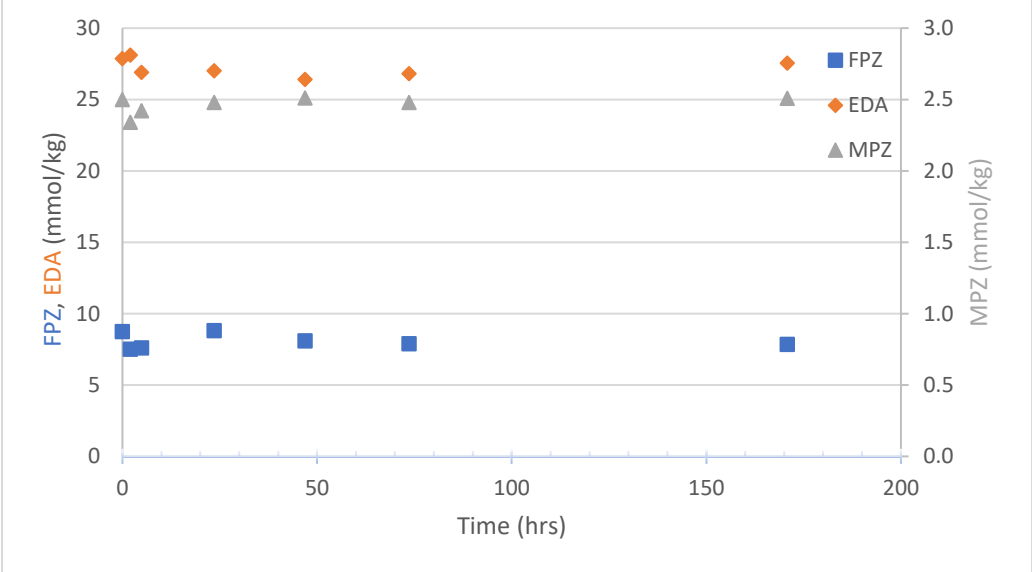

Figure 3-2: Concentrations of cation species in CAC 1 (baseline, no carbon)

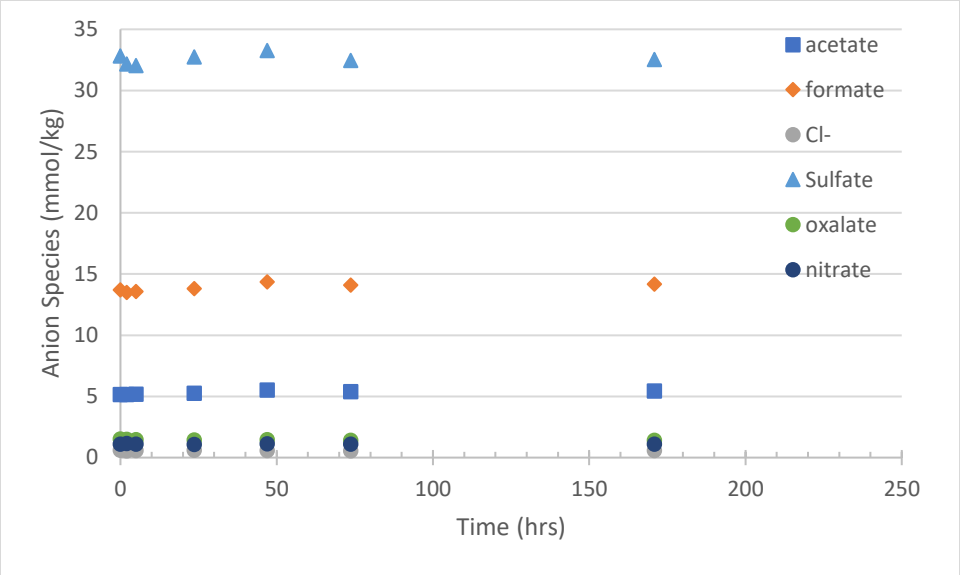

Figure 3-3: Concentrations of anion species in CAC 1 (baseline, no carbon)

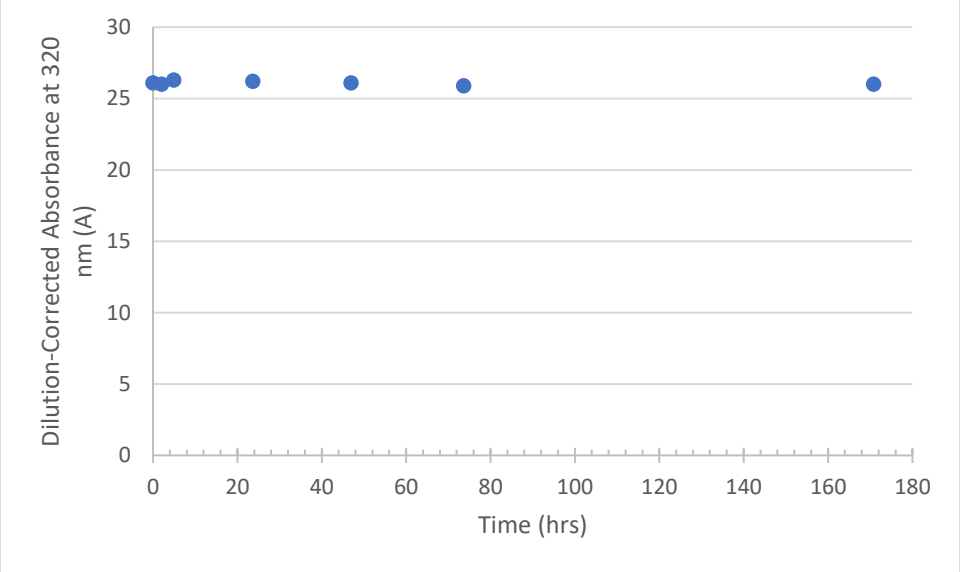

Figure 3-4: Dilution-corrected absorbance at 320 nm in CAC 1 (baseline, no carbon)

3.2.2 Baseline Condition – Compatibility Test with Clean PZ

Since the carbon treating is used to remove the degradation or corrosion products from the solvent, it is important to make sure the carbon does not adsorb piperazine. In CAC 2, 90.0 g clean PZ and and 3.4 g of clean carbon were used at the start. After 70 hours

of operation, the clean PZ was drained from the column, and 82.4 g of #3706 was added to the column, and another 192 hours of operation was performed. The alkalinity of the solvent was measured and plotted in Figure 3-5. During the operation with clean PZ, the alkalinity of the solvent stayed constant, indicating that none of the PZ was removed by the carbon. When the degraded solvent was treated, the alkalinity of the solvent decreased by 7% and reached equilibrium. This shows that the carbon bed removed certain degradation products that contributed to the alkalinity of the solvent. As a result, the carbon bed was proved to be compatible with PZ solvent and effective in removing degradation products from the solvent.

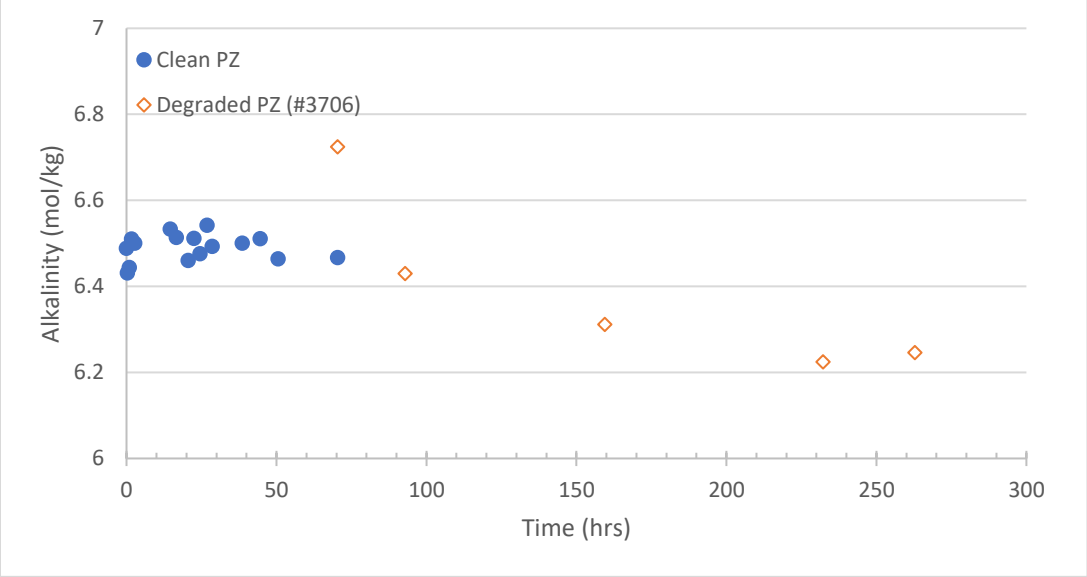

Figure 3-5: Alkalinity in CAC 2 (clean and degraded PZ, clean carbon)

3.3 Tests with Degraded Solvents in CAC

3.3.1 Typical Results from a CAC Experiment

CAC experiments 3 to 17 were performed to test the species that can be removed by the carbon bed. The dilution-corrected absorbance at 320 nm was used as an indication of experiment status. The experiments ended after when the absorbance reached a constant

value, which indicated that the carbon and the solvent had reached equilibrium and cannot remove any degradation products from the solvent further. The time of the first sample with equilibrium concentrations was reported as equilibrium time. Since the samples were collected once every one or two days, the equilibrium time reported may be longer than the actual time required to reach equilibrium.

CAC 3 started with 2.967 g of carbon and 104.0 g of #3537 solvent. Samples were collected frequently at the beginning of the experiment to capture the rate behavior, and much less frequently at the latter half of the experiment to understand the equilibrium. The experiment ended with 76.2792 g of solvent, and the carbon to solvent ratio increased from 0.029 to 0.039. Figure 3-6 shows the dilution-corrected absorbance at 320 nm in CAC 3. The 320 nm absorbance decreased significantly in the first 20 hours, and the rate slowed down afterwards. The equilibrium absorbance was reached after 187 hours at 0.72 A.

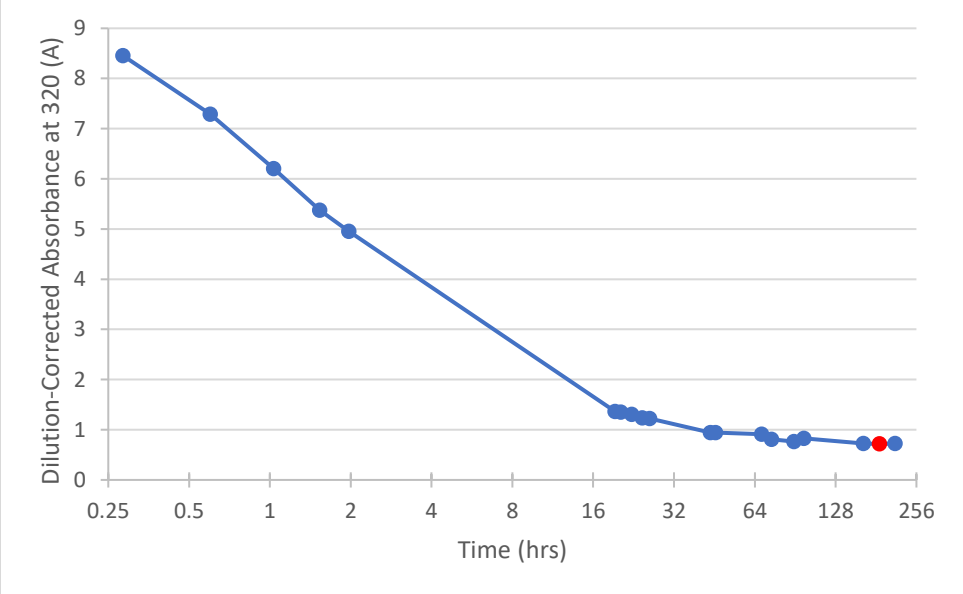

Figure 3-6: UV-Vis results of CAC 3 (end with 76.4 g #3537, 3.0 g clean carbon)

As shown in Figure 3-7, the Ni concentration stayed relatively constant, and is not adsorbed by the carbon bed. The Fe, Cr, and Mn concentration decreased significantly,

indicating that the carbon bed can remove the dissolved Fe, Cr, and Mn. 70% of the Fe was removed, and the Fe reached an equilibrium concentration of 0.011. 64% of the Cr was removed, and the equilibrium Cr concentration reached 0.02 mmol/kg. 77% of the Mn was removed, and the equilibrium Mn concentration reached 0.01 mmol/kg. The concentrations of the metals decreased fast initially, and the removal effects were less significant after 50 hours of operation. Since the removal rate of the metals is much higher than the commonly observed accumulation rate, the equilibrium concentration was more important in long term field operations.

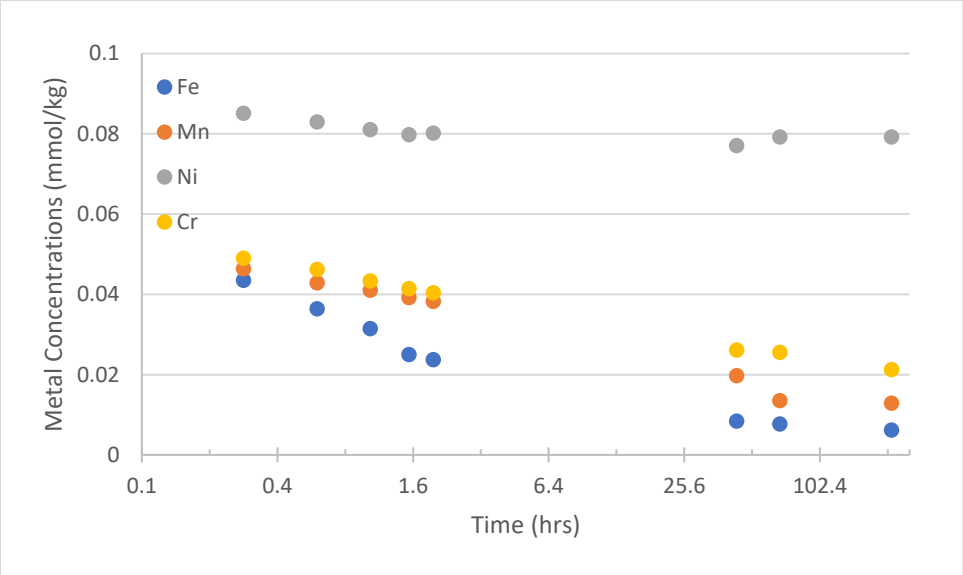

Figure 3-7: Stainless steel metals in CAC 3 (end with 76.4 g #3537, 3.0 g clean carbon)

As shown in Figure 3-8, the free formate, acetate, oxalate, and nitrate decreased in the first 50 hours, and reached an equilibrium after 213 hours of carbon treating. 27% of formate, 18% of sulfate, 26% of oxalate, and 33% of nitrate were removed.

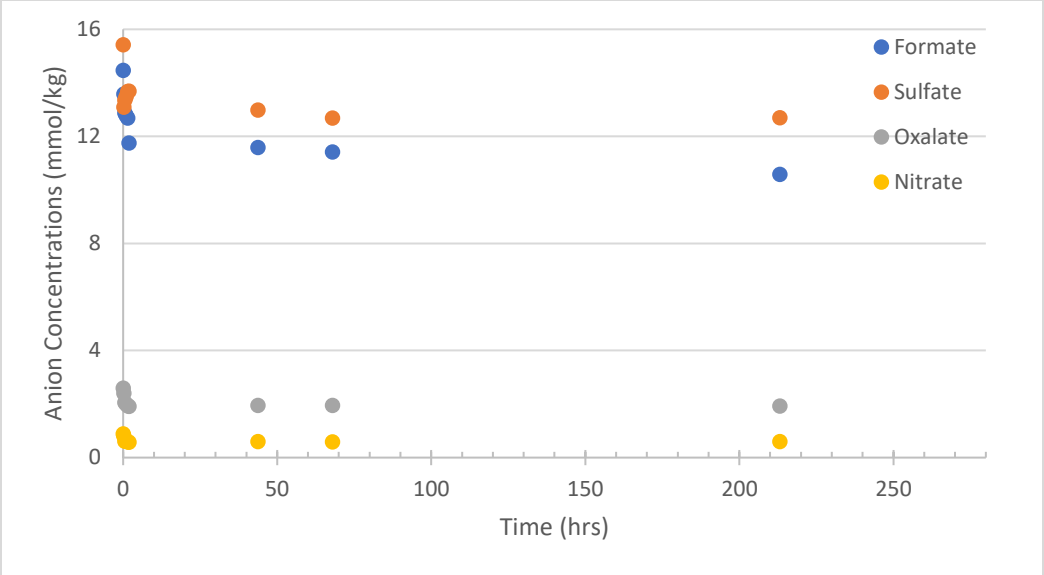

Figure 3-8: Anion results in CAC 3 (rnd with 76.4 g #3537, 3.0 g clean carbon)

The n-formylpiperazine (FPZ), ethylenediamine (EDA) and 1-methylpiperazine (MPZ) concentrations are plotted in Figure 3-9. 33% of FPZ, 24% of EDA, and 43% MPZ were removed by the carbon after 213 hours of treating.

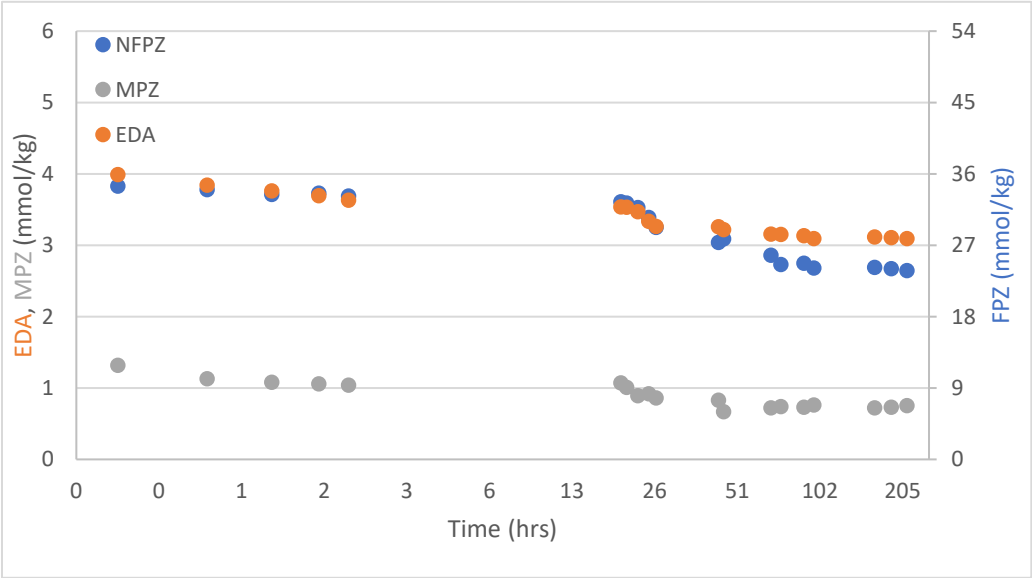

Figure 3-9: Cation results in CAC 3 (end with 76.4 g #3537, 3.0 g clean carbon)

The alkalinity of the samples in CAC 3 were quantified and plotted in Figure 3-10. The alkalinity decreased fast in the first 50 hours and reached a steady state where 5% of the alkalinity was removed. This indicates that the carbon removes certain degradation products that contribute to the alkalinity. Since equilibrium was reached where most of the alkalinity remained, it can be confirmed that PZ is not removed by the carbon.

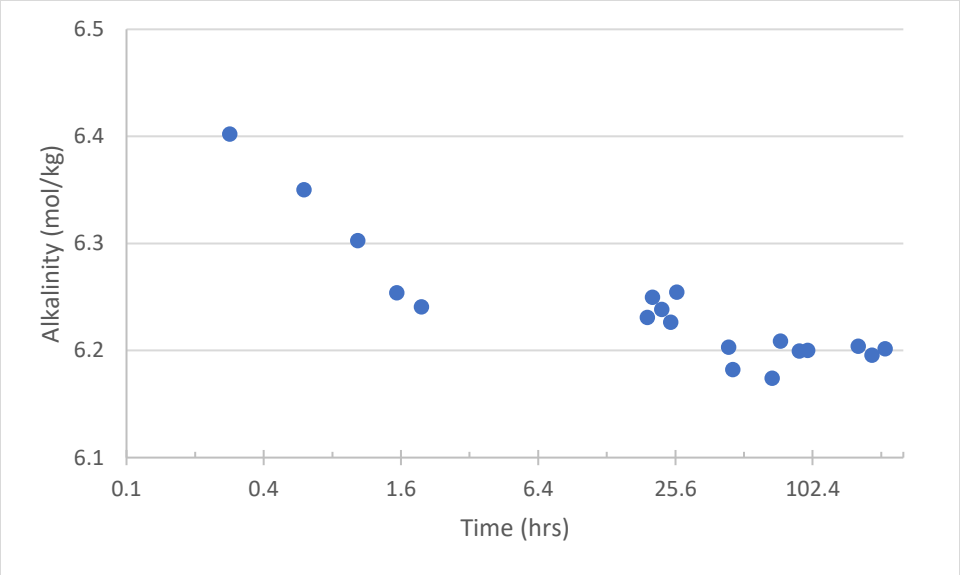

Figure 3-10: Alkalinity results in CAC 3 (end with 76.4 g #3537, 3.0 g clean carbon)

3.3.2 UV-Vis Results with #3537

The UV-Vis results of all the CAC experiments using #3537 as solvents are plotted in Figure 3-11. All the UV-Vis results show the same trend of decreasing fast initially and reaching an equilibrium after 100 to 200 hours of operation. Runs with higher C/S ratio reach equilibrium faster, but the final equilibrium absorbances are similar to each other. More details about the equilibrium are discussed in Section 4.6.

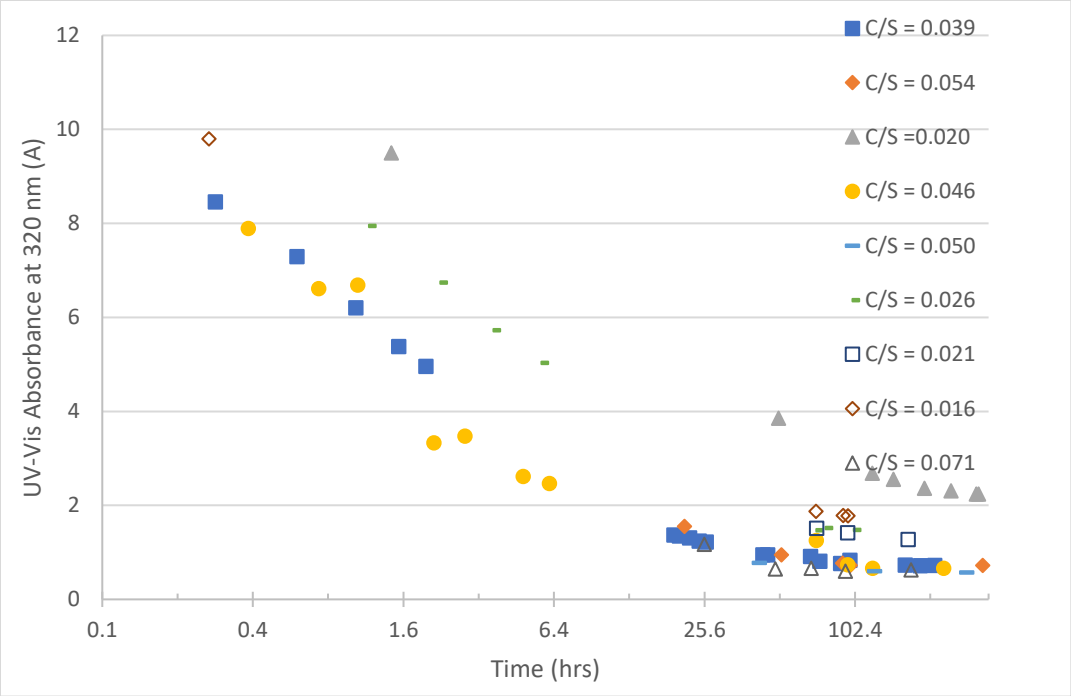

Figure 3-11: UV-Vis results of CAC 3 to 11 (C/S represents the carbon to solvent ratio at the end of the experiments)

3.3.3 Metal Results with #3537

The Ni results of the CAC experiments using #3537 as solvents are plotted in Figure 3-12. The Ni concentrations were constant, so the carbon bed cannot adsorb or remove the Ni in solvent.

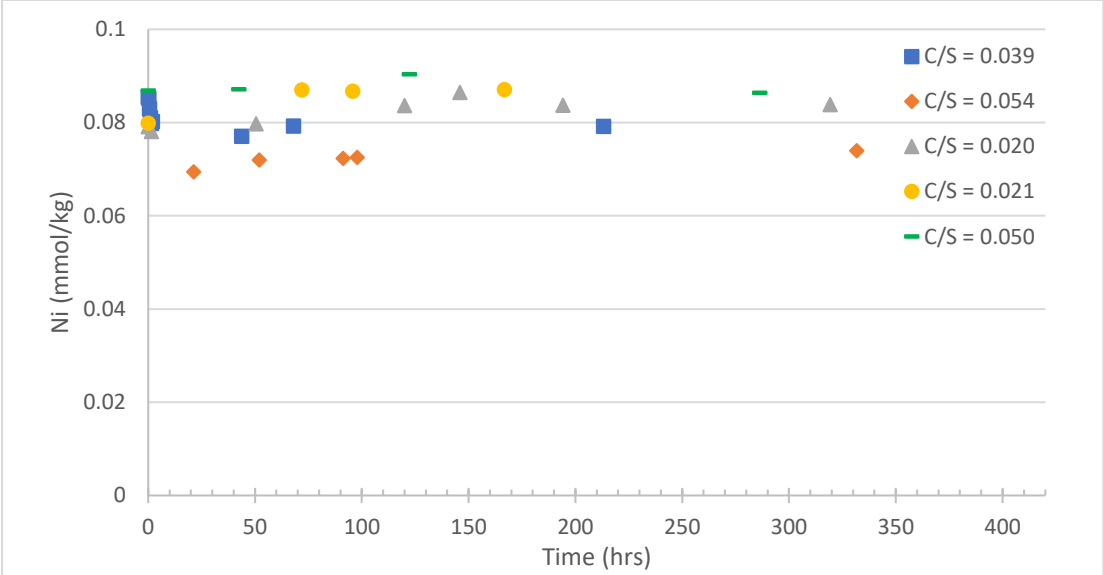

Figure 3-12: Ni results of CAC 3, 4, 5, 7, and 9 (C/S represents the carbon to solvent ratio at the end of the experiments)

The Fe results of all the CAC experiments using #3537 as solvents are plotted in Figure 3-13. The Fe concentration decreased significantly in the first 50 hours and reached steady state after 200 to 330 hours of operation.

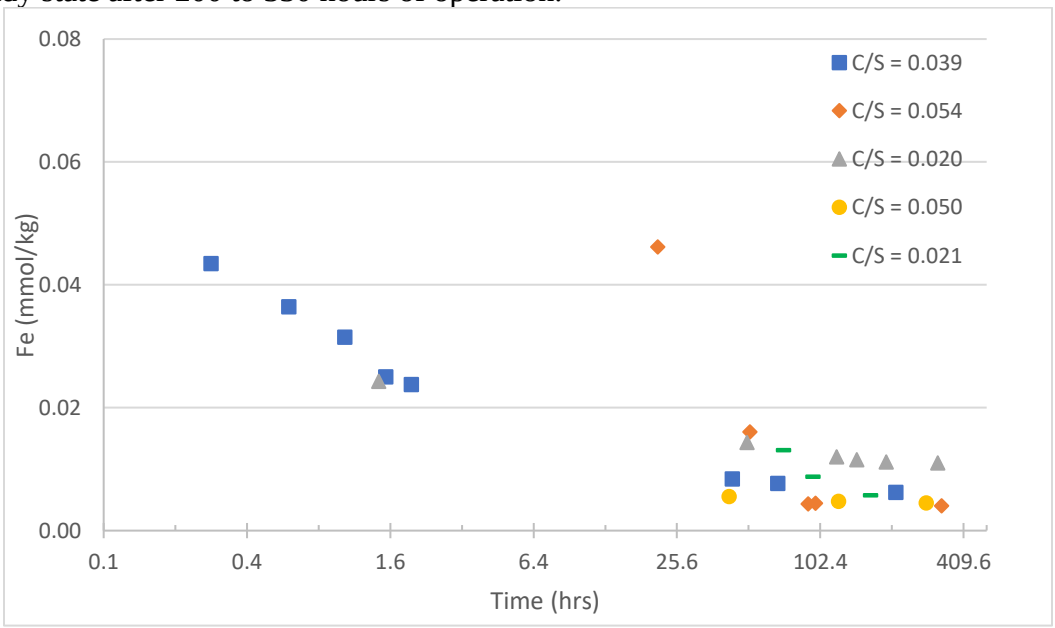

Figure 3-13: Fe results of CAC 3, 4, 5, 7, and 9 (C/S represents the carbon to solvent ratio at the end of the experiments)

Table 3-2 shows the percentage of Fe removed by the carbon treating and the time to reach equilibrium in all the experiment using #3537 as solvent. In all the experiments, Fe concentration decreased by 80% or more after carbon treating, indicating that the carbon is effective in Fe removal, and is a promising method to treat solvents in a commercial plant.

Table 3-2: Fe removal and equilibrium time in CAC experiments treating #3537

Experiment #	End C/S (g/g)	Equilibrium Time (hrs)	Percentage of Fe Removal
3	0.039	213	89%
4	0.054	332	93%
5	0.020	319	81%
7	0.050	286	79%
9	0.021	167	79%

The Cr results of all the CAC experiments using #3537 as solvents are plotted in Figure 3-14. The Cr concentration curve behaved like the Fe concentration. It decreased significantly in the first 50 hours and reached steady state after 200 to 330 hours of operation.

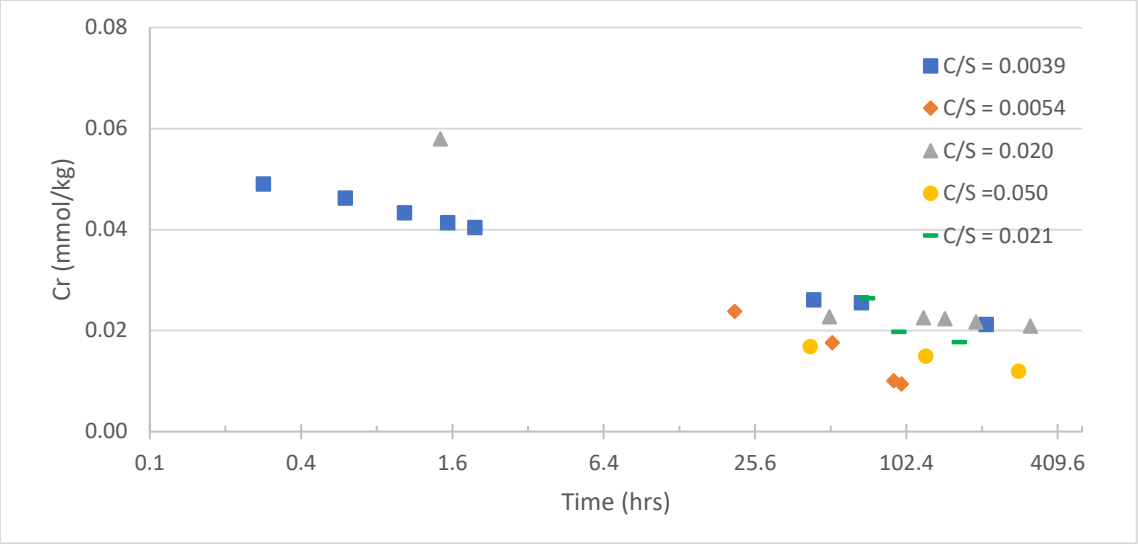

Figure 3-14: Cr results of CAC 3, 4, 5, 7, and 9 (C/S represents the carbon to solvent ratio at the end of the experiments)

Table 3-3 shows the percentage of Cr removed by the carbon treating and the time to reach equilibrium in all the experiment using #3537 as solvent. In all the experiments, Cr concentration decreased by 70% or more after carbon treating. No strong selectivity between Fe and Cr was observed. Since the solvent is considered hazardous if the Cr concentration is above 5 ppm, the ability to remove Cr from the solvent can reduce the cost of waste treatment when solvent is disposed after long terms of operation.

Table 3-3: Cr removal and equilibrium time in CAC experiments treating #3537

Experiment #	End C/S (g/g)	Equilibrium Time (hrs)	Percentage of Cr Removal
3	0.039	213	73%
4	0.054	332	86%
5	0.020	319	70%
7	0.050	286	83%
9	0.021	167	74%

The Mn results of all the CAC experiments using #3537 as solvents are plotted in Figure 3-15. The Mn concentration curve behaved like the Fe and Cr concentration.

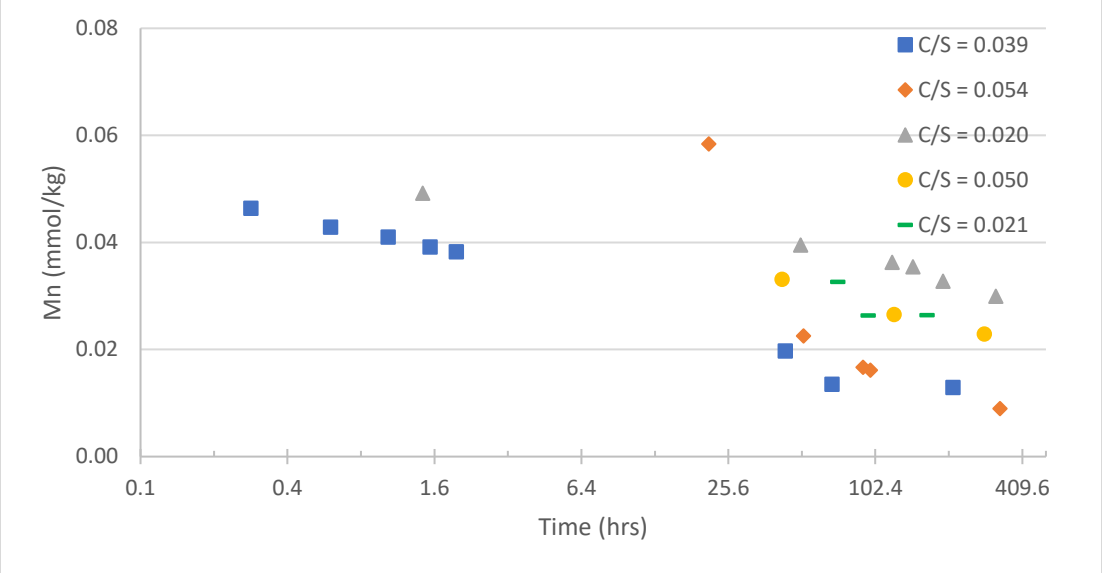

Figure 3-15: Mn results of CAC 3, 4, 5, 7, and 9 (C/S represents the carbon to solvent ratio at the end of the experiments)

Table 3-4 shows the percentage of Mn removed by the carbon treating and the time to reach equilibrium in all the experiment using #3537 as solvent. The carbon bed is proved to be capable of removing Fe, Cr, and Mn from the solvent.

Table 3-4: Mn removal and equilibrium Time in CAC experiments treating #3537

Experiment #	End C/S (g/g)	Equilibrium Time (hrs)	Percentage of Mn Removal
3	0.039	213	77%
4	0.054	332	87%
5	0.020	319	57%
7	0.050	286	68%
9	0.021	167	63%

3.3.4 UV-Vis Results with #3706

The UV-Vis results of all the CAC experiments using #3706 as solvents are plotted in Figure 3-16. All the UV-Vis results are similar to the trend shown in Figure 3-9, which used #3537 as initial solvents.

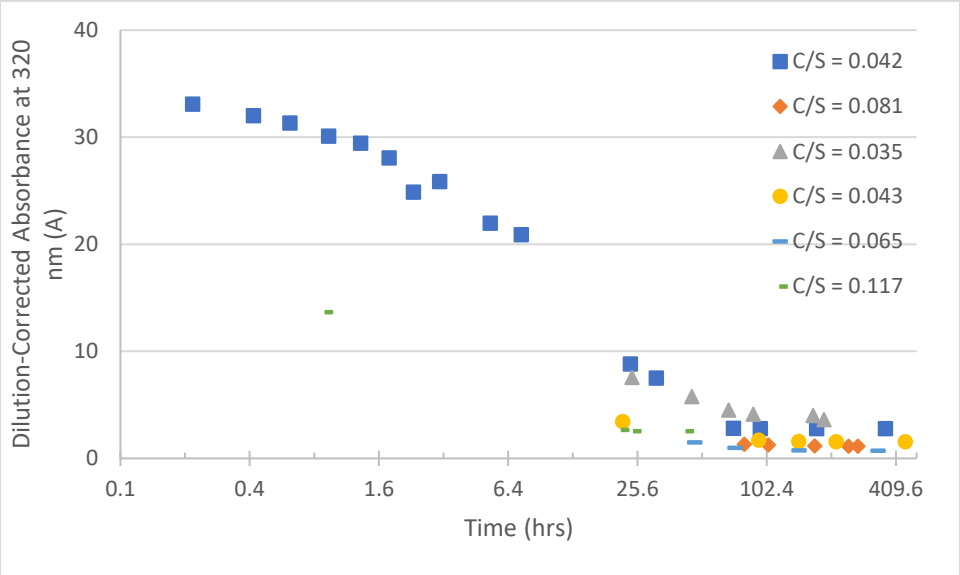

Figure 3-16: Compiled UV-Vis results of CAC 12 to 17 with #3537 (C/S represents the carbon to solvent ratio at the end of the experiments)

3.3.5 Metal Results with #3706

The Ni results of the CAC experiments using #3706 as solvents are plotted in Figure 3-17. As in the results shown in Figure 3-10 treating #3537, The Ni concentrations were constant. ICP was run on only three of the six experiments performed with #3706 since the metal concentration already showed uniform trends in CAC experiments treating #3537.

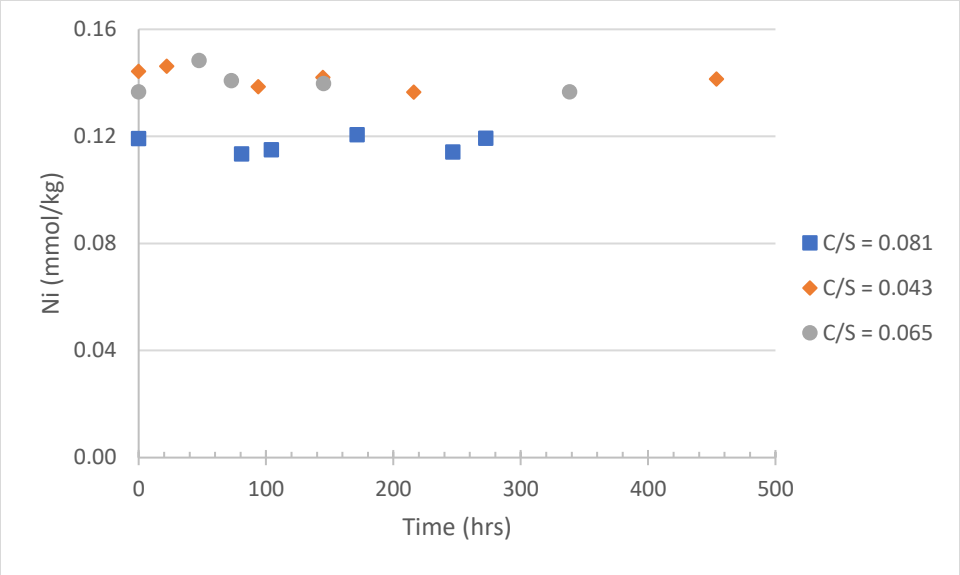

Figure 3-17: Ni results of CAC 13, 15, and 16 (C/S represents the carbon to solvent ratio at the end of the experiments)

The Fe results of the CAC experiments using #3706 as solvents are plotted in Figure 3-18. The Fe concentration decreased initially and reached a steady state just as shown in Figure 3-14. This indicates that the carbon can remove Fe from solvents with different levels of degradation.

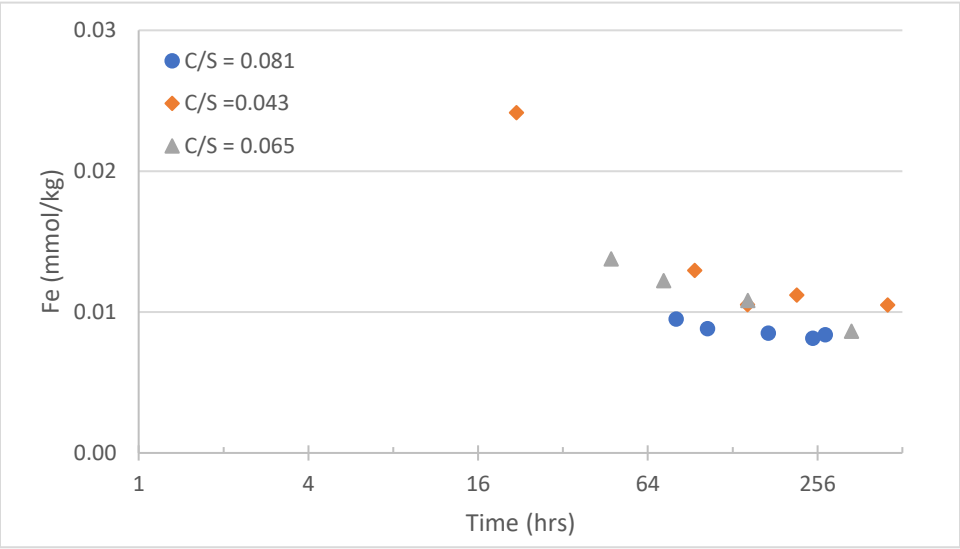

Figure 3-18: Fe results of CAC 13, 15 and 16 (C/S represents the carbon to solvent ratio at the end of the experiments)

Table 3-5 shows the percentage of Fe removed by the carbon treating and the time to reach equilibrium in the experiment using #3706 as solvent. Fe concentration decreased by 80% or more after carbon treating, as in the results shown in Table 3-2.

Table 3-5: Fe removal and equilibrium time in CAC experiments treating #3706

Experiment #	End C/S (g/g)	Equilibrium Time (hrs)	Percentage of Fe Removal
13	0.081	273	90%
15	0.043	454	83%
16	0.065	338	86%

The Cr results of the CAC experiments using #3706 as solvents are plotted in Figure 3-19. The Cr concentration decreased initially and reached a steady state just as shown in Figure 3-15. This indicates that the carbon can remove Cr from solvents with different levels of degradation.

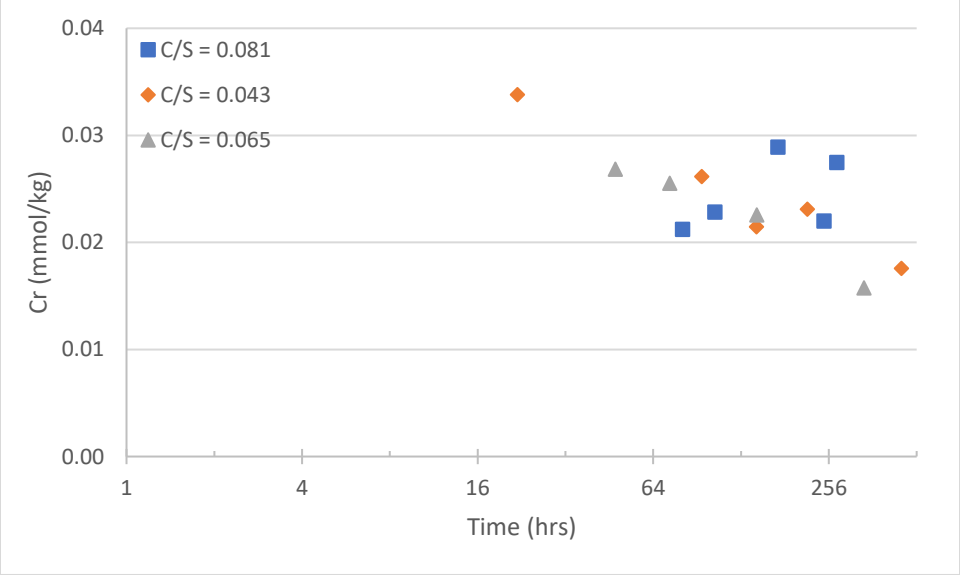

Figure 3-19: Cr results of CAC 13, 15 and 16 (C/S represents the carbon to solvent ratio at the end of the experiments)

Table 3-6 shows the percentage of Cr removed by the carbon treating and the time to reach equilibrium in the experiment using #3706 as solvent. Cr concentration decreased by 80% after carbon treating, as in the results shown in Table 3-3.

Table 3-6: Cr removal and equilibrium time in CAC experiments treating #3706

Experiment #	End C/S (g/g)	Equilibrium Time (hrs)	Percentage of Cr Removal
13	0.081	273	78%
15	0.043	454	81%
16	0.065	338	80%

The Mn results of the CAC experiments using #3706 as solvents are plotted in Figure 3-20. The Mn concentration has a similar behavior as shown in Figure 3-16. This proves the ability of the carbon treating to remove Mn from solvents with different levels of degradation.

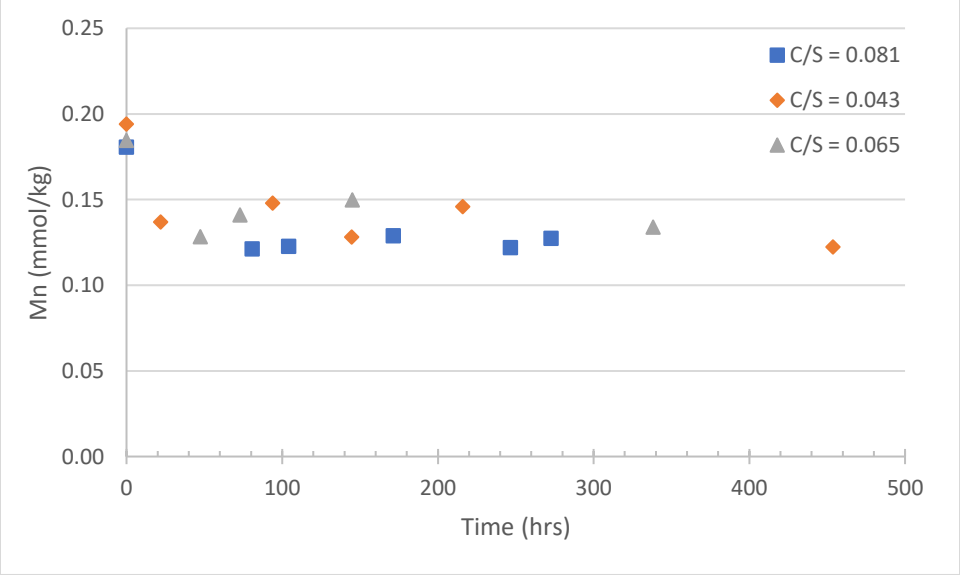

Figure 3-20: Mn results of CAC 13, 15, and 16 (C/S represents the carbon to solvent ratio at the end of the experiments)

Table 3-7 shows the percentage of Mn removed by the carbon treating and the time to reach equilibrium in the experiment using #3706 as solvent. The Mn Concentration only decreased by 27% to 37%, which is much smaller than 57% to 87% in the results shown in Table 3-4 using #3537 as solvent. One explanation is that the selectivity is higher for Fe and Cr compared to Mn, and the Fe and Cr take up the active sites. As a result, fewer Mn is adsorbed when more Fe and Cr are adsorbed.

Table 3-7: Mn removal and equilibrium time in CAC experiments treating #3706

Experiment #	End C/S (g/g)	Equilibrium Time (hrs)	Percentage of Mn Removal
13	0.081	273	29%
15	0.043	454	37%
16	0.065	338	27%

3.3.6 Heat Stable Salts and Degradation Products Results

The formate results of the CAC experiments are plotted in Figure 3-21. The open points are experiments with #3537, and the solid points are experiments with #3706. The formate concentration shows a small decrease in all the experiments, which indicates that the formate was removed by the carbon treating. It is also possible that the removal of FPZ by carbon resulted in more formation of FPZ by formate and piperazine, therefore resulting a decrease in the formate concentration.

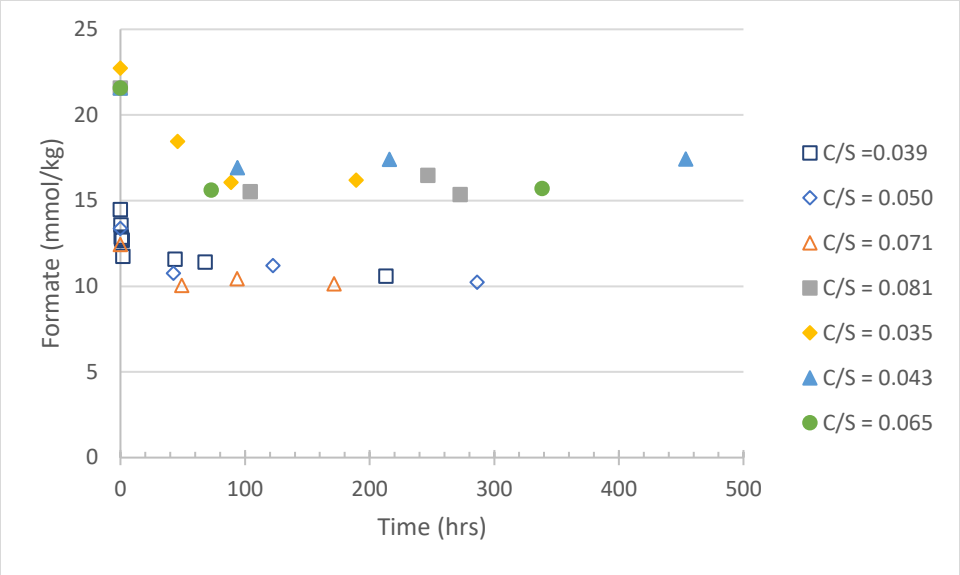

Figure 3-21: Formate results of CAC 3, 7, 11, 13, 14, 15, and 16 (C/S represents the carbon to solvent ratio at the end of the experiments)

Table 3-8 shows the percentage of formate removed by the carbon treating and the time to reach equilibrium. The formate concentration decreased by 18% to 29%, which is much smaller than the amount of metals removed by carbon treating. While carbon treating is capable of removing formate from the solvent, it cannot achieve a low equilibrium concentration.

Table 3-8: Formate removal and equilibrium time in CAC experiments

Experiment #	Initial Solvent	End C/S (g/g)	Equilibrium Time (hrs)	Percentage of Formate Removal
3	#3537	0.039	213	27%
7	#3537	0.050	286	23%
11	#3537	0.071	167	18%
13	#3706	0.081	273	29%
14	#3706	0.035	189	29%
15	#3706	0.043	454	19%
16	#3706	0.065	338	27%

The sulfate results of the CAC experiments are plotted in Figure 3-22. The open points are experiments with #3537, and the solid points are experiments with #3706. The sulfate results are similar to the formate concentration shown in Figure 3-18.

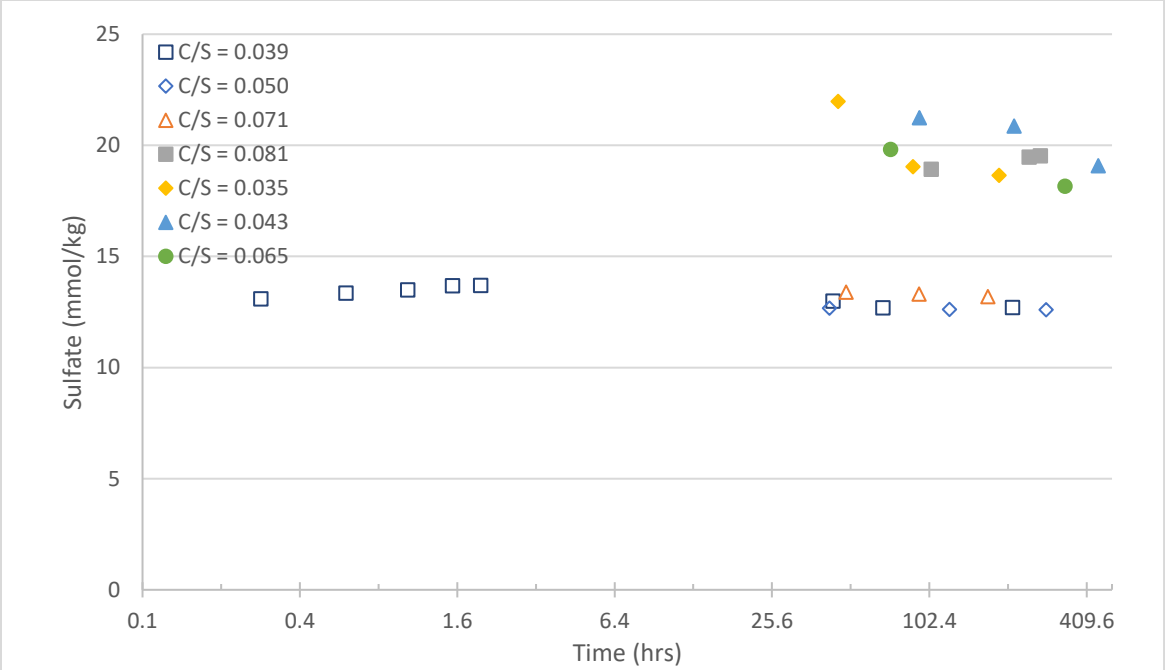

Figure 3-22: Sulfate results of CAC 3, 7, 11, 13, 14, 15, and 16 (C/S represents the carbon to solvent ratio at the end of the experiments)

Table 3-9 shows the percentage of sulfate removed by the carbon treating and the time to reach equilibrium. The sulfate concentration decreased by 16% to 23%. The ability of carbon bed to remove sulfate is small and may be less useful in commercial plant operations.

Table 3-9: Sulfate removal and equilibrium time in CAC experiments

Experiment #	Initial Solvent	End C/S (g/g)	Equilibrium Time (hrs)	Percentage of Sulfate Removal
3	#3537	0.039	213	18%
7	#3537	0.050	286	16%
11	#3537	0.071	167	16%
13	#3706	0.081	273	16%
14	#3706	0.035	189	21%
15	#3706	0.043	454	23%
16	#3706	0.065	338	27%

The nitrate results of the CAC experiments are plotted in Figure 3-23. The open points are experiments with #3537, and the solid points are experiments with #3706. The nitrate results are similar to the formate and sulfate results shown in Figure 3-18 and 4-19.

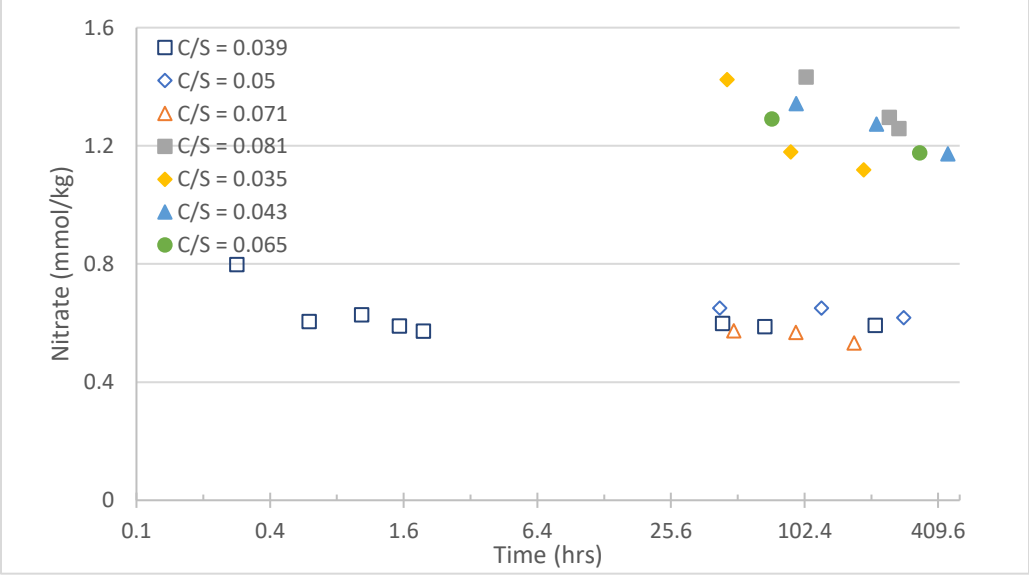

Figure 3-23: Nitrate results of CAC 3, 7, 11, 13, 14, 15, and 16 (C/S represents the carbon to solvent ratio at the end of the experiments)

Table 3-10 shows the percentage of nitrate removed by the carbon treating and the time to reach equilibrium. The nitrate concentration decreased by 18% to 39%.

Table 3-10: Nitrate removal and equilibrium time in CAC experiments

Experiment #	Initial Solvent	End C/S (g/g)	Equilibrium Time (hrs)	Percentage of Nitrate Removal
3	#3537	0.039	213	33%
7	#3537	0.050	286	18%
11	#3537	0.071	167	24%
13	#3706	0.081	273	35%
14	#3706	0.035	189	39%
15	#3706	0.043	454	36%
16	#3706	0.065	338	36%

The oxalate results of the CAC experiments are plotted in Figure 3-24. The open points are experiments with #3537, and the solid points are experiments with #3706. All the heat stable salts presented similar behavior.

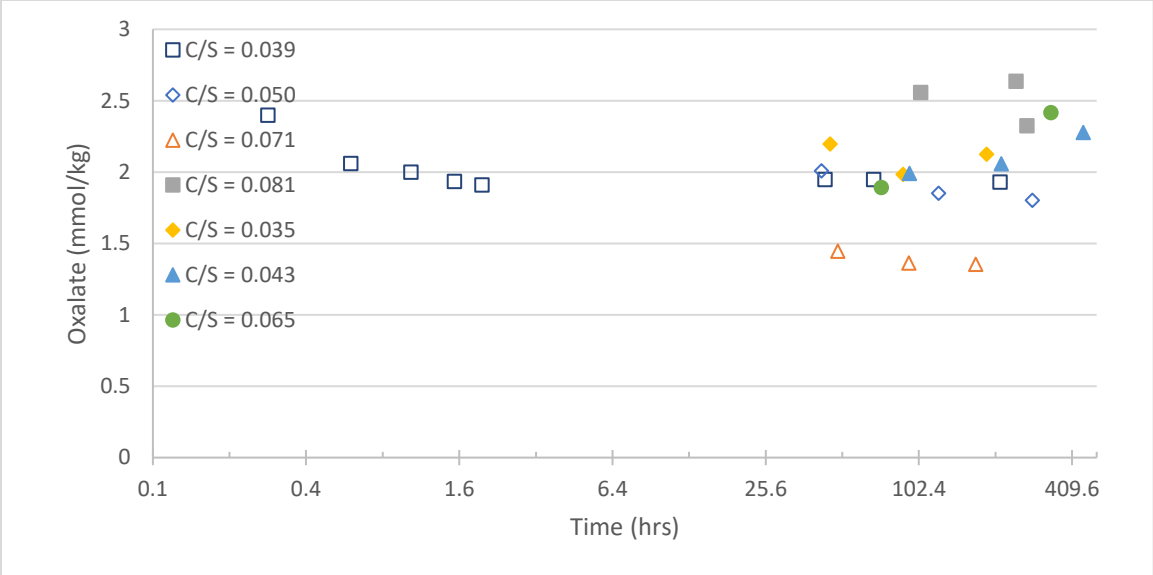

Figure 3-24: Oxalate results of CAC 3, 7, 11, 13, 14, 15, and 16 (C/S represents the carbon to solvent ratio at the end of the experiments)

Table 3-11 shows the percentage of oxalate removed by the carbon treating and the time to reach equilibrium. The sulfate concentration decreased by 23% to 42%.

Table 3-11: Oxalate removal and equilibrium time in CAC experiments

Experiment #	Initial Solvent	End C/S (g/g)	Equilibrium Time (hrs)	Percentage of oxalate Removal
3	#3537	0.039	213	26%
7	#3537	0.050	286	23%
11	#3537	0.071	167	35%
13	#3706	0.081	273	42%
14	#3706	0.035	189	42%
15	#3706	0.043	454	37%
16	#3706	0.065	338	36%

The FPZ concentration of the CAC experiments are plotted in Figure 3-25. The open points are experiments with #3537, and the solid points are experiments with #3706. The FPZ concentration showed a small decrease in the experiment

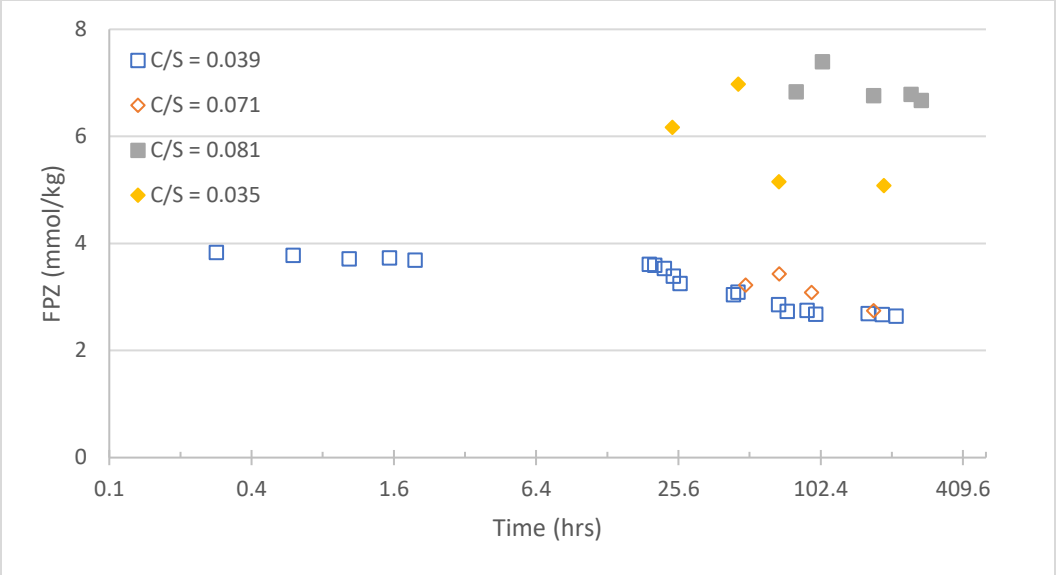

Figure 3-25: FPZ results of CAC 3, 11, 13, and 14 (C/S represents the carbon to solvent ratio at the end of the experiments)

Table 3-12 shows the percentage of FPZ removed by the carbon treating and the time to reach equilibrium. FPZ concentration decreased by 20% to 36%.

Table 3-12: FPZ removal and equilibrium time in CAC experiments

Experiment #	Initial Solvent	End C/S (g/g)	Equilibrium Time (hrs)	Percentage of FPZ Removal
3	#3537	0.039	213	33%
11	#3537	0.071	167	26%
13	#3706	0.081	273	20%
14	#3706	0.035	189	36%

The EDA concentration of the CAC experiments are plotted in Figure 3-26. The

open points are experiments with #3537, and the solid points are experiments with #3706. The EDA concentration showed a small decrease in the experiment.

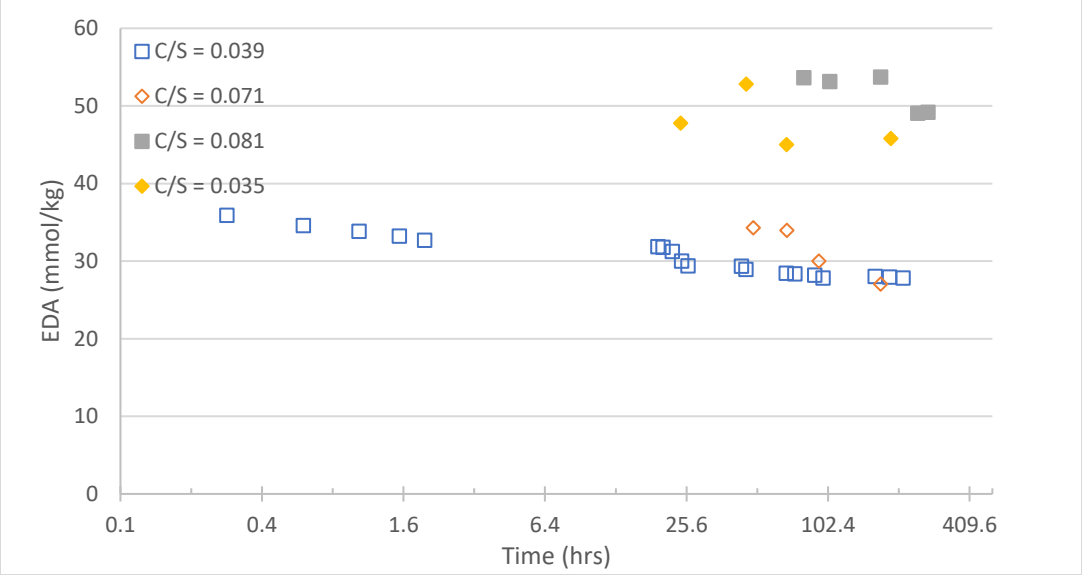

Figure 3-26: EDA results of CAC 3, 11, 13, and 14 (C/S represents the carbon to solvent ratio at the end of the experiments)

Table 3-13 shows the percentage of EDA removed by the carbon treating and the time to reach equilibrium. EDA concentration decreased by 11% to 24%.

Table 3-13: EDA removal and equilibrium time in CAC experiments

Experiment #	Initial Solvent	End C/S (g/g)	Equilibrium Time (hrs)	Percentage of EDA Removal
3	#3537	0.039	213	24%
11	#3537	0.071	167	22%
13	#3706	0.081	273	11%
14	#3706	0.035	189	20%

The MPZ concentration of the CAC experiments are plotted in Figure 3-27. The open points are experiments with #3537, and the solid points are experiments with #3706.

The MPZ concentration decreased in the experiment.

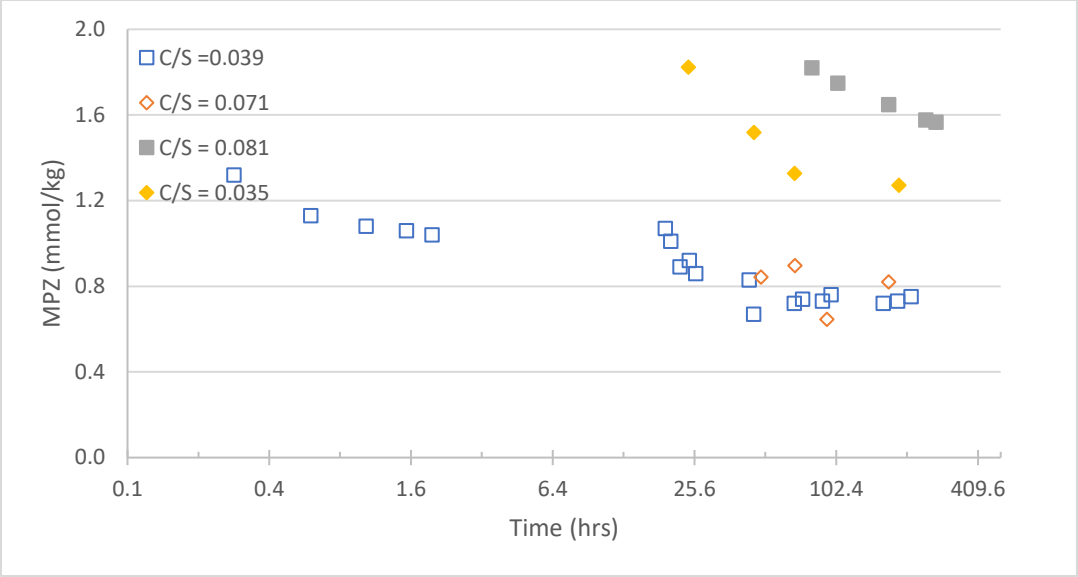

Figure 3-27: MPZ results of CAC 3, 11, 13, and 14 (C/S represents the carbon to solvent ratio at the end of the experiments)

Table 3-14 shows the percentage of MPZ removed by the carbon treating and the time to reach equilibrium. MPZ concentration decreased by 34% to 43%.

Table 3-14: MPZ removal and equilibrium time in CAC experiments

Experiment #	Initial Solvent	End C/S (g/g)	Equilibrium Time (hrs)	Percentage of MPZ Removal
3	#3537	0.039	213	43%
11	#3537	0.071	167	34%
13	#3706	0.081	273	38%
14	#3706	0.035	189	36%

While AEP was not present in #3537 and #3706, it is a thermal degradation product of PZ. A solvent was prepared by adding 17.3 mmol/kg of AEP into 5 m clean PZ. 1.6722 g of clean carbon was used to treat 89.7980 g of solvent, and the final C/S is 0.026. As

shown in Figure 3-28, 46% of AEP was removed when equilibrium was reached at 94.5 hrs.

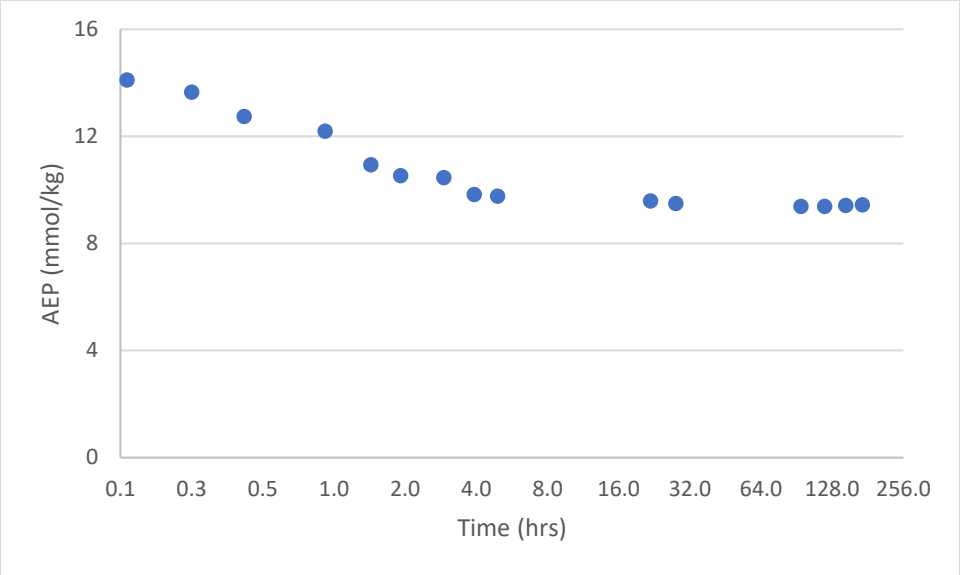

Figure 3-28: Removal of AEP from clean 5 m PZ by carbon

3.3.7 Alkalinity Results with #3537 and #3706

The alkalinity of the samples in CAC 3, 7, 11, 13, and 14 are shown in Figure 3-25 plotted as the alkalinity of the solvent divided by the initial alkalinity. The open points are experiments with #3537, and the solid points are experiments with #3706. Compared to the results with clean PZ plotted in Figure 3-29, the alkalinity of the solvent all decreased, indicating that the carbon bed removes degradation products that has alkalinity, and reducing the alkalinity of the solvent by up to 6%.

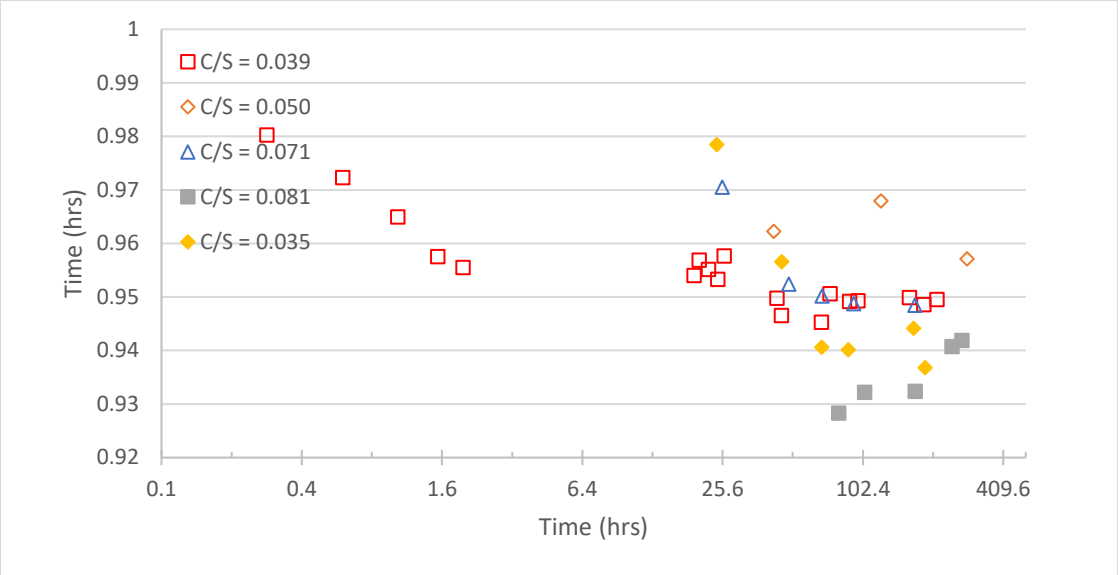

Figure 3-29: Alkalinity/initial alkalinity results of CAC 3, 7, 11, 13, and 14 (C/S represents the carbon to solvent ratio at the end of the experiments)

3.4 Tests with External Source of Fe

In all the previous experiments, the carbon bed removed complexed Fe^{3+}. Two experiments were performed to add Fe^{3+} into the solvent to see if the external source of Fe will behave the same as the already complexed Fe in the solvent. In CAC 18, 3.1 g of clean carbon and 81.4 g of #3706 was used. $Fe_2(SO_4)_3$ was added in excess of the solubility limit to the solvent, and the precipitation was kept in the column. The solvent and the carbon reached equilibrium after 505 hours of operation. The UV-Vis absorbance and the Fe concentration of the solvent are quantified and plotted in Figure 3-30. The solubility limit of Fe in solvent #3706 is 9.88 mmol/kg, and the dilution-corrected absorbance increased to 56.25. Both Fe concentration and absorbance at 320 nm decreased over time, and both reached a level lower than the initial Fe concentration in solvent #3706, indicating that the carbon can remove both the external Fe^{3+} and the Fe originally in the solvent.

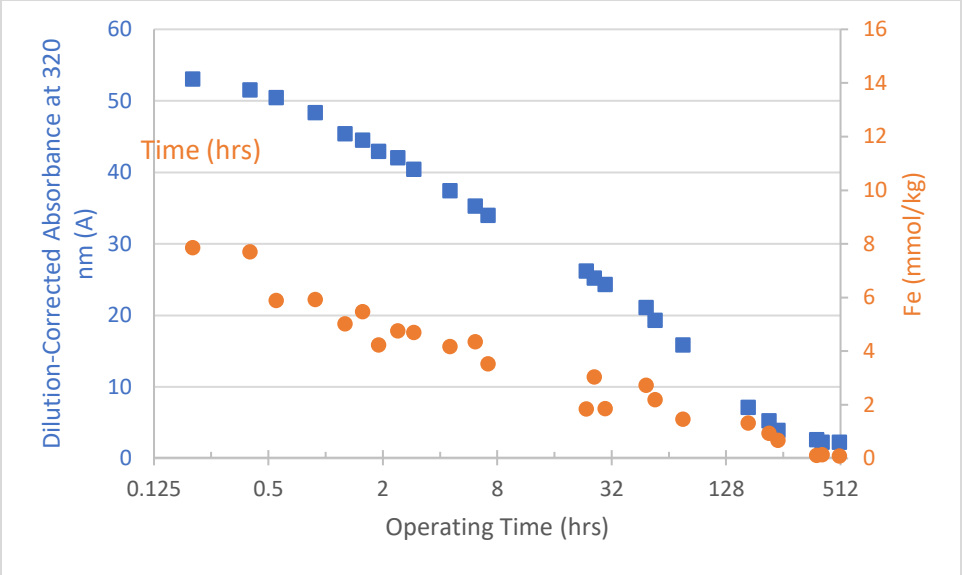

Figure 3-30: UV-Vis absorbance and Fe concentration profile of CAC 18 (clean carbon, #3706 with excess $Fe_2(SO_4)_3$ addition)

In CAC 19, 3.1 g of clean carbon and 81.7 g of NCCC solvent #3706 were used. 0.07 mmol/kg of $Fe_2(SO_4)_3$ was added to the solvent, which doubled the Fe concentration in the solvent. The solvent and the carbon reached equilibrium after 266 hours of operation. The UV-Vis absorbance and the Fe concentration of the solvent are quantified and plotted in Figure 3-31, and they behaved similarly to the CAC 30.

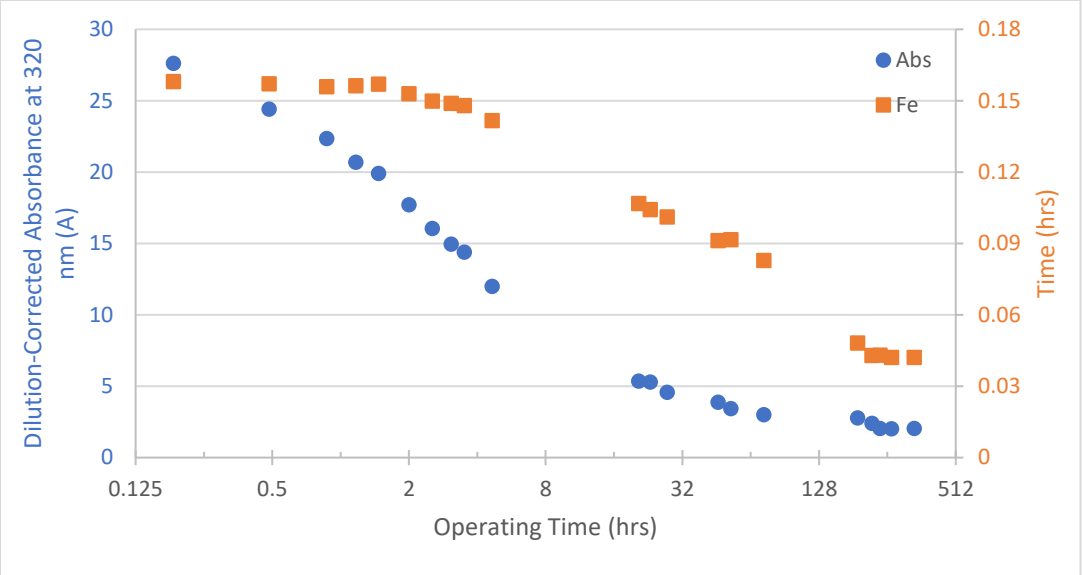

Figure 3-31: UV-Vis absorbance and Fe concentration profile of CAC 19 (clean carbon, 3706 with 0.07 mmol/kg $Fe_2(SO_4)_3$ addition)

3.5 REMOVAL OF LIGANDS

In the previous carbon adsorption experiments, it was found that the carbon bed can remove the complexed Fe^{3+} and result in a decrease in absorbance at 320 nm. However, it was unclear if the carbon bed removes only the Fe^{3+} complexed part or all the ligands. To better understand what is being removed, Fe^{3+} was added to the end solvent from CAC end sample. Figure 3-31 and Figure 3-32 showed the UV-Vis absorbance when different amounts of Fe^{3+} were added to #3706 and #3706 treated by the carbon. In Figure 3-32, the peak at 320 nm increased when Fe^{3+} was added, which matched the conclusion that there were excessive amounts of ligands not complexed with Fe^{3+} in the solvent, and the complexed Fe^{3+} has an absorbance of 320 nm. In Figure 3-33, the peak at 293 nm increased when Fe^{3+} was added, and 293 nm is the absorbance wavelength of ionic Fe^{3+} in clean PZ. This indicates that the ligands were all removed by the carbon, resulting in the Fe^{3+} not getting complexed and a measured absorbance at 293 nm instead of 320 nm. The solubility limit of Fe^{3+} in the solvent decreased from 12.8 mmol/kg to 4.2 mmol/kg. Therefore, carbon

treating is useful in preventing Fe from further dissolving into the degraded solvent if no further ligand is produced in the solvent.

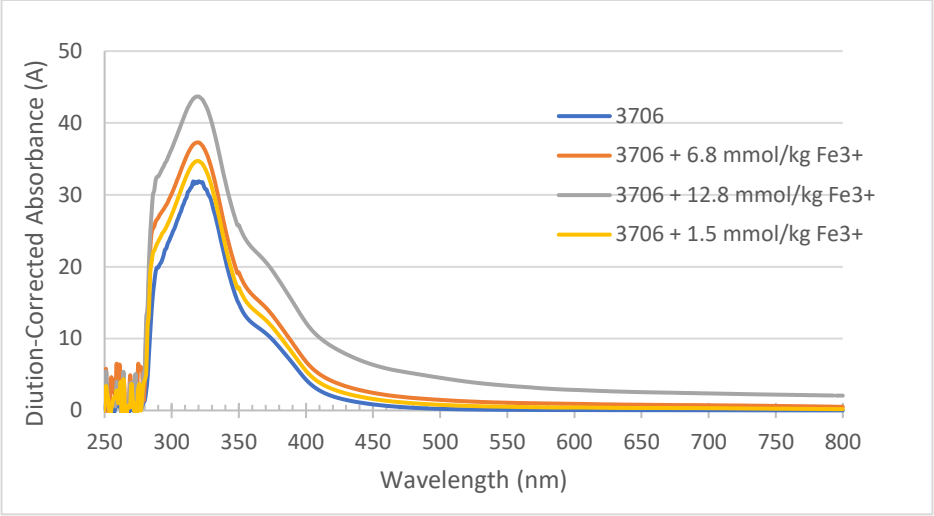

Figure 3-32: UV-Vis absorbance profile of NCCC #3706 with different Fe^{3+} addition

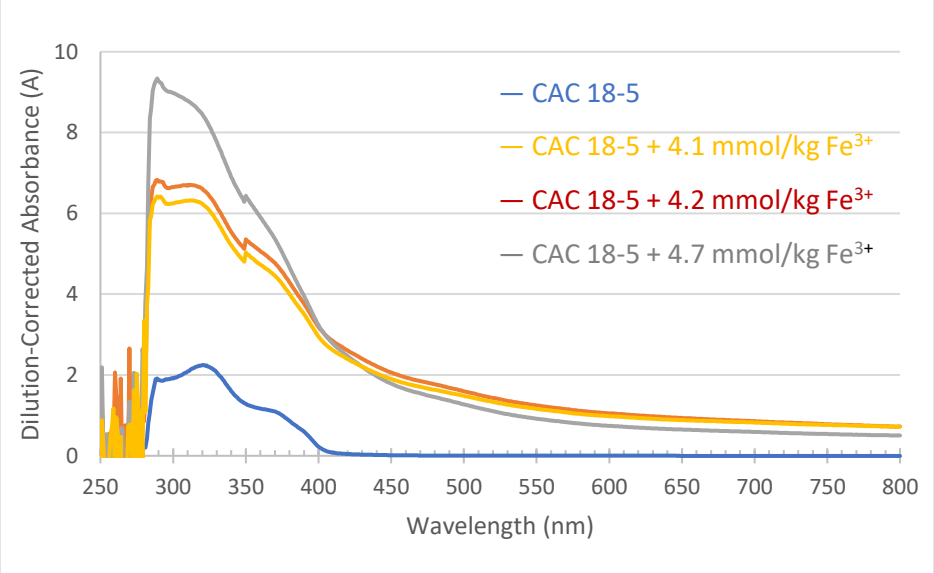

Figure 3-33: UV-Vis absorbance profile of CAC 18 end solvent with different Fe^{3+} addition

3.6 Equilibrium Results with CAC

At the point of equilibrium, the loading of the carbon is calculated, and Figure 3-33 shows the relationship between the loading of carbon and the equilibrium absorbance. The loading of carbon represents the amount of absorbance per unit of carbon, here calculated as:

$$Loading\ of\ carbon = \Delta Absorbance * \frac{g\ of\ solvent}{g\ of\ carbon} \qquad (3-1)$$

While different experiments started with different levels of degradation and different carbon to solvent ratio, the equilibrium absorbance at 320 nm is linearly related to the equilibrium loading of the carbon. The absorbance with added Fe^{3+} was no different from the absorbance of the solvent without adding the Fe. This relationship can be used to estimate the lifetime of the carbon in pilot or commercial plants, which is discussed in more details in Chapter 7.

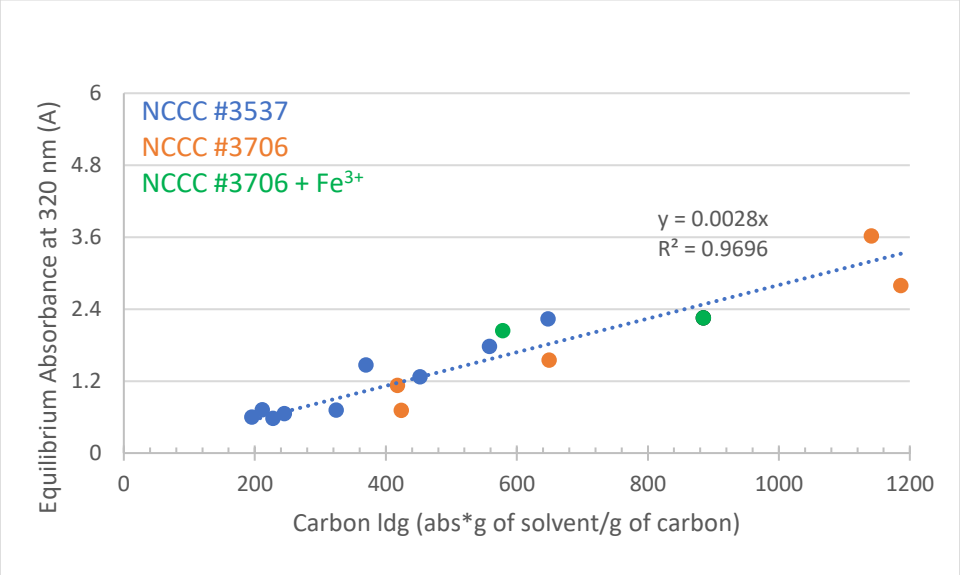

Figure 3-34: Linear relationship between equilibrium absorbance and carbon loading

From the linear relationship, it is suggested that a carbon in equilibrium with a less degraded solvent should be capable of removing degradation products again if allowed to treat a more degraded solvent, and this hypothesis was tested in CAC 20. 0.28 g of clean carbon and 82.7 g of #3706 were charged to the column, and the carbon reached equilibrium with the solvent after 170 hours. After equilibrium, the solvent was drained, and another batch of 41.7 g of #3706 was added to the column. The dilution-corrected absorbance is plotted in Figure 3-35. The carbon which had previously reached equilibrium started adsorbing again, and the rate of adsorbance was lower due to the decreased amounts of active sites. The solvent reached equilibrium after 335 hours, and the equilibrium absorbance was higher than the equilibrium absorbance reached at 170 hours, which is due to a higher carbon loading.

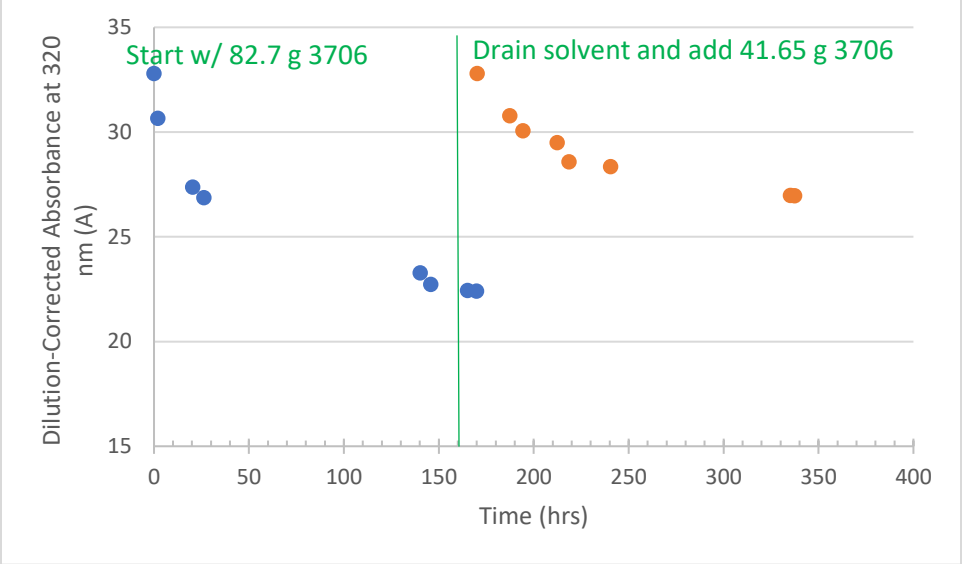

Figure 3-35: UV-Vis absorbance profile of CAC 20 (NCCC clean carbon, #3706)

The relationship between the equilibrium concentration in the liquid and the concentration adsorbed on the carbon for all species is plotted in Figure 3-36. The metal concentrations in the initial solvent were low, which caused larger scatter due to the errors

in the measurements. The species all followed a linear relationship similar to the absorbance data. No selectivity was observed between the anion and cation species.

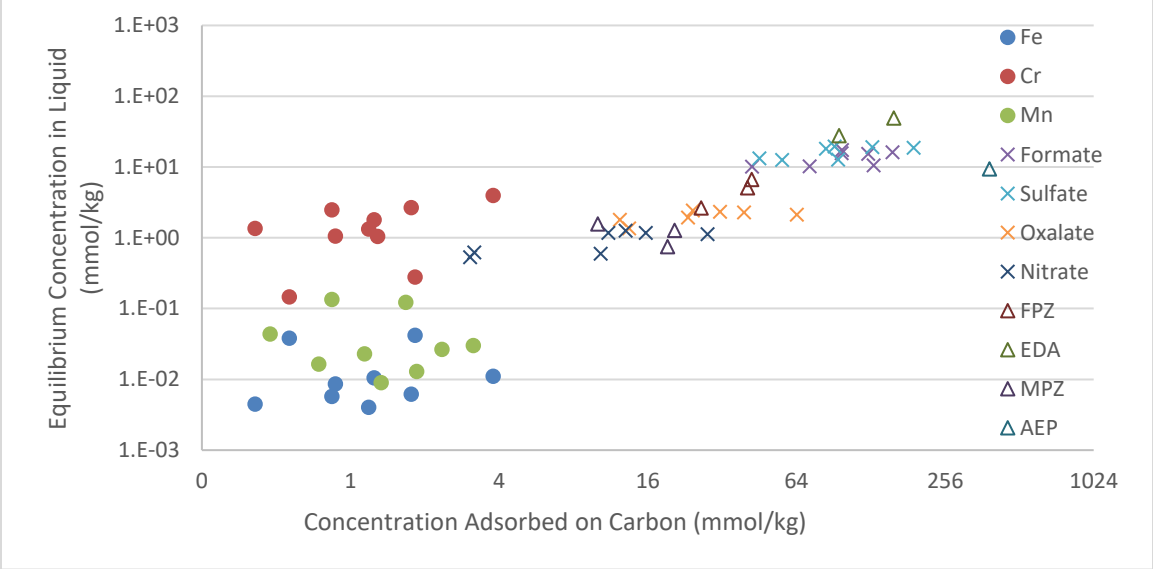

Figure 3-36: Equilibrium results of all the species adsorbed by carbon

3.7 Fe Removal from the Used Carbon with Acids

0.2 N H_2SO_4 was tested to remove the Fe off the used carbon to quantify the adsorption of Fe. 5 batches of 15 mL H_2SO_4 was used to rinse 3 g of NCCC used carbon, and the absorbance of the H_2SO_4. As shown in Figure 3-37, all the H_2SO_4 after rinse shows a UV-Vis peak at 304 nm, while the peak removed by the carbon bed absorbs at 320 nm in the solvent. Peak 304 nm and 320 nm can be complexed metals in different forms in different environments.

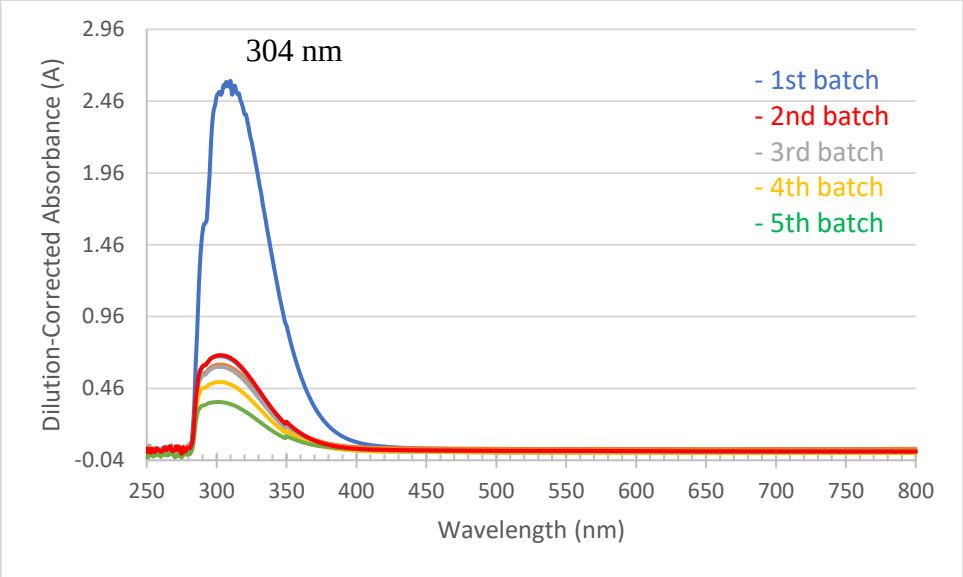

Figure 3-37: UV-Vis absorbance of 0.2 N H_2SO_4 after rinsing used NCCC carbon (0.2 N sulfuric acid used as baseline)

ICP was performed to identify and quantify the metals in the rinsed solvent. 5 g of sulfuric acid was added to different amounts of used NCCC carbon in a 15 mL centrifugal tube and let sit for 48 hours. A clean carbon sample was also prepared as a baseline. The metal ion concentrations are shown in Figure 3-38. Negligible Li, K, Ni, and Cr concentrations were observed in the solvent, and only Fe and Mn were found in the sulfuric acid. The Mn concentration was two orders of magnitude smaller than the Fe concentration. The Fe concentration did not increase after the mass ratio of carbon to H_2SO_4 reached 0.09, indicating that the Fe may have reached saturation in the sulfuric acid, and not all the metals were removed.

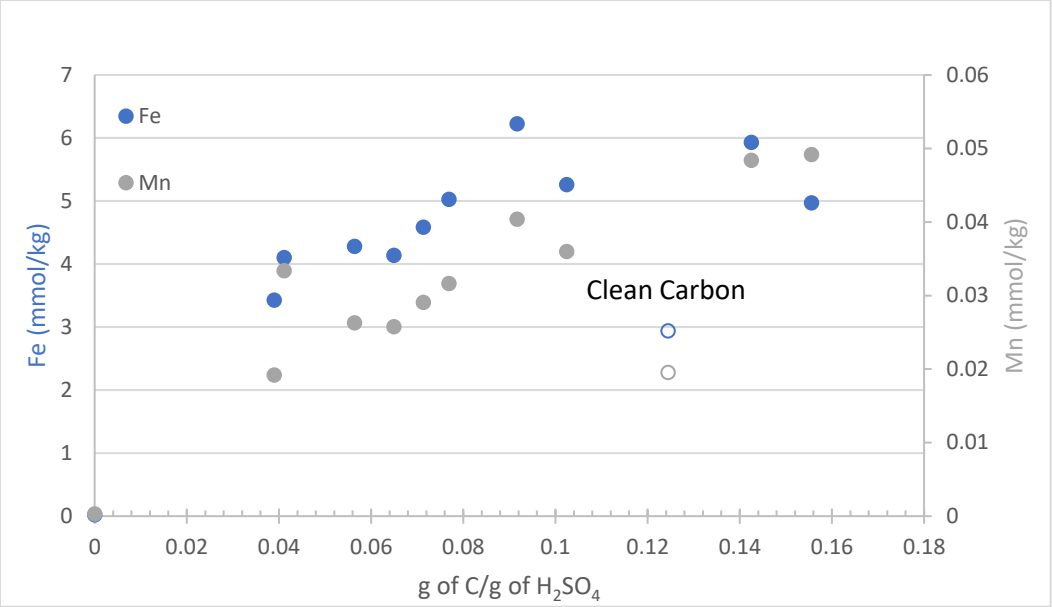

Figure 3-38: Metal concentrations of 0.2 N H_2SO_4 solution after rinsing used NCCC Carbon

To better quantify the amount of Fe removed by the carbon, three CAC experiments were performed. In CAC 21, 3.2301 g of used C was added to the column. The removal effect of water, 0.2 N H_2SO_4, and 25 mmol/kg EDTA was tested. The same carbon was used, and each batch of solvent was drained completely before adding the new batch. The time and solvent addition were shown in Table 3-15.

Table 3-15: Solvent addition in CAC 21

Time (hrs)	Batch Added
0	78.5160 g of H_2O
3	74.6176 g of 0.2 N H_2SO_4
99	77.7892 g of 0.2 N H_2SO_4
287	67.9605 g 25 mmol/kg EDTA in H_2O

The Fe concentration in the solvent is shown in Figure 3-39. There was no Fe removed by the water. Only a short period of time was required for Fe to reach saturation

in the H_2SO_4, and one batch was insufficient to remove all the Fe from the carbon. The concentration of Fe in the EDTA was much lower than in H_2SO_4, indicating that EDTA was not as efficient as H_2SO_4.

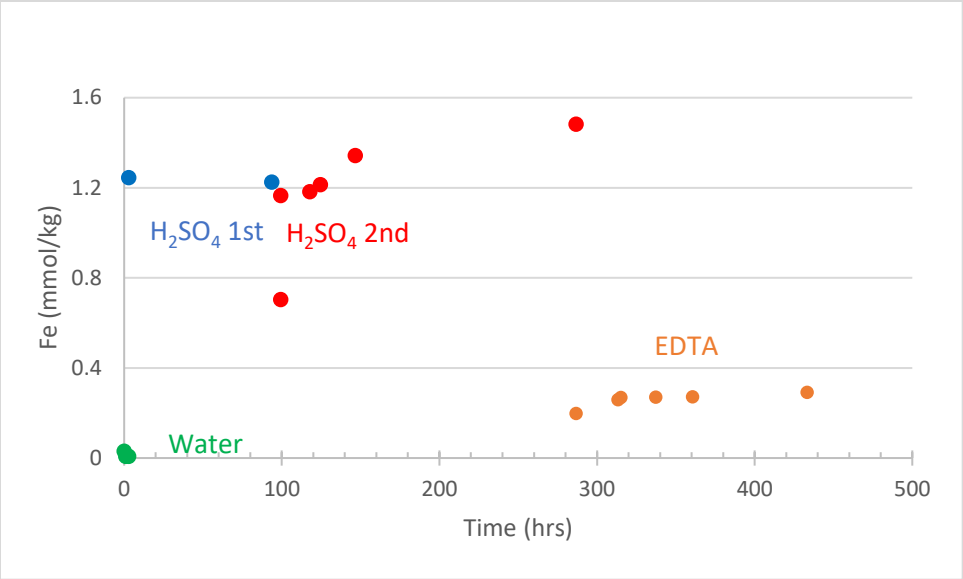

Figure 3-39: Fe removal test from used carbon (water, 0.2 N H_2SO_4, and 25 mmol/kg EDTA)

In CAC 22, excess 0.2 N H_2SO_4 was added to 0.4375 g of NCCC used carbon to quantify the Fe removed more accurately. 11 batches of H_2SO_4 were added, and each batch was drained completely before the new batch was added. The time and amount of H_2SO_4 added is shown in Table 3-16.

Table 3-16: Solvent addition in CAC 22

Time (hours)	Mass of 0.2 N H_2SO_4 (g)
22.47	83.1046
22.72	58.7132
22.97	61.5182
23.23	61.6279
23.48	63.5220
23.90	60.7665
24.15	57.9786

The Fe concentration in the H_2SO_4 is shown in Figure 3-40. The Fe concentration became negligible after 141.8178 g of 0.2 N H_2SO_4 was used to rinse the carbon, and all the Fe was removed from the carbon. From the Fe concentration and the mass of 0.2 N H_2SO_4, it was calculated that there was 36.3 mmol Fe/kg carbon on clean carbon.

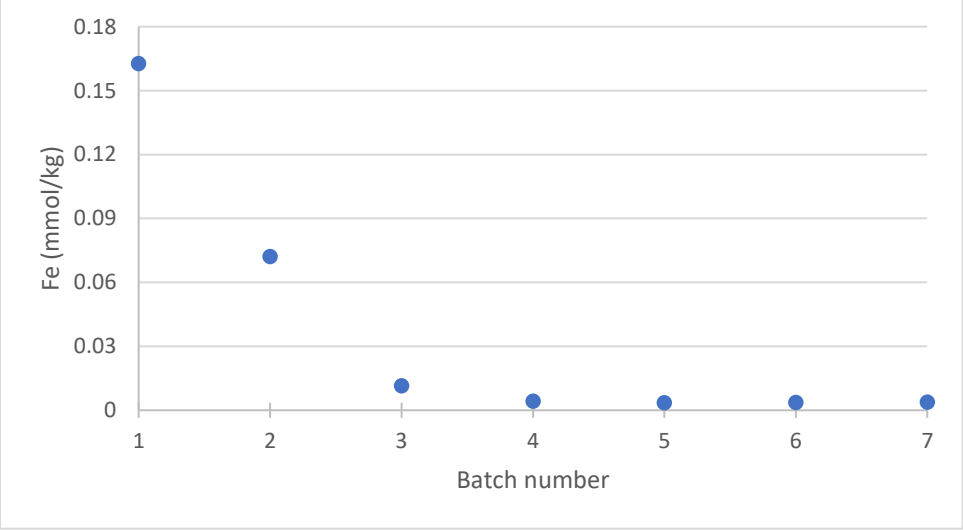

Figure 3-40: Fe in CAC 22 (0.2 N H_2SO_4, NCCC clean carbon)

3.8 CONCLUSIONS

1. The solvent in the Carbon Adsorption Column has a constant concentration of EDA, PZ, MPZ, AEP, formate, sulfate, nitrate, oxalate, Fe, Cr, Ni, and Mn after 170 hours of operation without carbon. No correction of water balance is needed to interpret the CAC data.
2. The carbon bed does not adsorb PZ, which makes treating PZ with carbon possible.
3. The carbon does not adsorb Ni, but can adsorb Fe, Cr, and Mn. More than 70% of Fe, and Cr are removed when equilibrium is reached. The selectivity for Fe and Cr is higher than Mn, so less Mn is removed as more Fe and Cr is removed. The carbon is a viable and economic method to remove Fe and Cr from the solvent.
4. Carbon treating removes heat stable salts, including formate, sulfate, nitrate, and oxalate from the solvent. However, the removal effect is small compared to the removal effects on metals.
5. Carbon treating removes degradation products, including FPZ, EDA, and MPZ from the solvent.
6. Carbon treating reduces the alkalinity of the solvent by up to 6%, indicating that the carbon adsorbs degradation products with alkalinity.
7. When external Fe^{3+} is added to the solvent, the peak at 320 nm increases. Carbon treating can remove the external Fe^{3+} and absorbance no different from the Fe originally in the solvent.
8. The carbon removes all the degradation products that can complex with Fe^{3+}, even if they are not complexed.
9. The equilibrium loading of the carbon is linearly related to the absorbance of the solvent, and this relationship is not related to the initial Fe concentration or degradation level.

10. After the carbon has reached equilibrium, it can still treat solvents with high absorbance. The rate of treatment becomes slower and the second equilibrium absorbance is higher due to the decrease in active sorption sites.
11. H_2SO_4 rinsed off species absorbing at 303 nm from the used carbon, which is the same species absorbing at 320 nm in the sample. By performing ICP on the H_2SO_4, the amount of Fe adsorbed by the carbon can be quantified.
12. The used activated carbon contains 36.3 mmol Fe/kg carbon quantified by the H_2SO_4 rinsing method.

Chapter 4. Bench-Scale Oxidation in Cyclic Apparatus

4.1 Overview of Results from Previous HTOR Experiments

A number of important experiments have been performed in the HTOR apparatus studying the oxidation of PZ at cyclic conditions. These experiments suggest that initially PZ oxidizes to intermediates such as PZOH, PZ-one, and EDA, which then decompose to NH_3, formate, and other degradation products. The loss rate of clean PZ solvent in the HTOR is between 0.7 to 1.6 mmol/kg-hr, and the overall activation energy is 34 ± 7 kJ/mol. The overall NH_3 production rate increases linearly as the solvent becomes more degraded, resulting in a quadratic curve in cumulative NH_3 generation. Fe is solubility limited instead of availability limited, and the solubility increases as the solvent becomes more degraded. Varying temperature between 40 and 55 °C in the absorber has no effect on the PZ oxidation rate. Applying N_2 sparging before cycling the solvent to high temperature can reduce NH_3 production from PZ by 0.4 mmol/kg-hr in the HTOR (Nielsen, 2018).

4.2 Summary of HTOR Experiments

The results of seven HTOR experiments are included in this work. These experiments studied the effects of two mitigation methods and three degradation products or impurities in the system on the oxidation of 5 m PZ. The low temperature is kept at 55 °C , and the high temperature is kept at 150 °C for all HTOR experiments. Table 4-1 shows the experiments that have been performed.

Table 4-1: Summary of HTOR Experiments

Experiment Number	Operating Time (hrs)	Initial Solvent and Treatment
HTOR 22	660	Degraded PP2 Solvent N_2 Sparging
HTOR 23	630	Clean PZ + EDA N_2 Sparging
HTOR 25	890	Clean PZ + Formaldehyde N_2 Sparging
HTOR 27	770	Degraded NCCC Solvent Carbon Bed
HTOR 28	570	Degraded NCCC Solvent Carbon Bed + N_2 Sparging
HTOR 29	660	Degraded NCCC Solvent Carbon Bed + N_2 Sparging

4.3 Effects of Nitrogen Sparging on Degraded 5 m PZ solvent

4.3.1 HTOR 22: Moderately Degraded PZ Cycled from 55 °C to 150 °C

HTOR 22 started with moderately degraded PZ from the PP2 campaign, which contained 20.5 mmol/kg EDA, 16.8 mmol/kg PZ-one, 46.2 mmol/kg total formate, 5.22 mmol/kg total oxalate, 0.42 mmol/kg Fe, 1.61 mmol/kg Cr, 1.54 mmol/kg Ni, and 0.13 mmol/kg Mn. The solvent was cycled from 55 °C to 150 °C with nitrogen sparging at a flow rate of 0.5 L/min. Foaming was observed during the experiments, and 1 mL of antifoam, containing 40 to 44 wt % polypropylene glycol, 4 to 5 wt % octylphenoxy

polyethoxy ethanol, and 2.7 to 2.9 wt % treated amorphous silica, was added to the solvent at 178 hrs, 375 hrs and 515 hrs. The process changes during the experiment are shown in Table 4-2.

Table 4-2: Process changes during HTOR 22

Time (hrs)	Process Change
0	$\alpha = 0.3$, N_2 sparging on
103	N_2 sparging off
154	N_2 sparging on
252	$\alpha = 0.25$
590	$\alpha = 0.35$, N_2 sparging off
658	End of Experiments

In the first 250 hrs, the solvent experienced flashing in the high temperature part due to the high loading of the solvent. Since only liquid can pass the backpressure regulator, gas accumulates in the high temperature part, resulting a decreasing amount of flow entering the high temperature part. As a result, the flow stops completely, and the NH_3 data is no longer representative as it only represents the NH_3 produced in the low temperature part. The NH_3 data from 250 hrs to the end of the experiment is plotted in Figure 4-1. The average ammonia emission rate with lean loading was lower at 0.33 mmol/kg-hr after equilibrium and before antifoam was added. After adding the antifoam, the average rate was 0.60 mmol/kg-hr. Two significant increases in the ammonia rate were observed after the antifoam additions at 375 hrs and 515 hrs. The NH_3 rate stayed constant after the N_2 sparging was turned off at 590 hrs, which may indicate that the anitifoam cancelled out the effects of N_2 sparging. Since the antifoam eliminated the foaming in the sparging column,

the mass transfer of O_2 reduces from liquid phase to gas phase. Similar effects were also observed in the SRP campaign described in detail in Chapter 6.

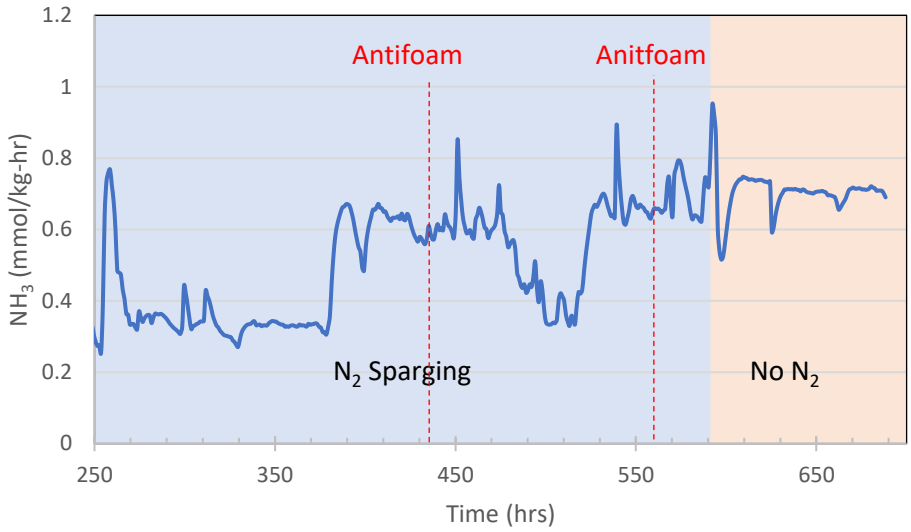

Figure 4-1: HTOR 22 NH_3 rate (55 ℃ to 150 ℃ , PP2 degraded solvent, N_2 sparging, α = 0.25)

The UV-Vis absorbance was measured, and there was only one significant peak at 320 nm, as plotted in Figure 4-2. No peak was observed at 538 nm. In the two regions with N_2 sparging, the absorbance increases at 0.1 A/hr, which is smaller than the 0.5 A/hr in the region without N_2 sparging. This indicates that N_2 sparging can reduce the accumulation of the UV-absorbing compound, and the loading does not influence its production.

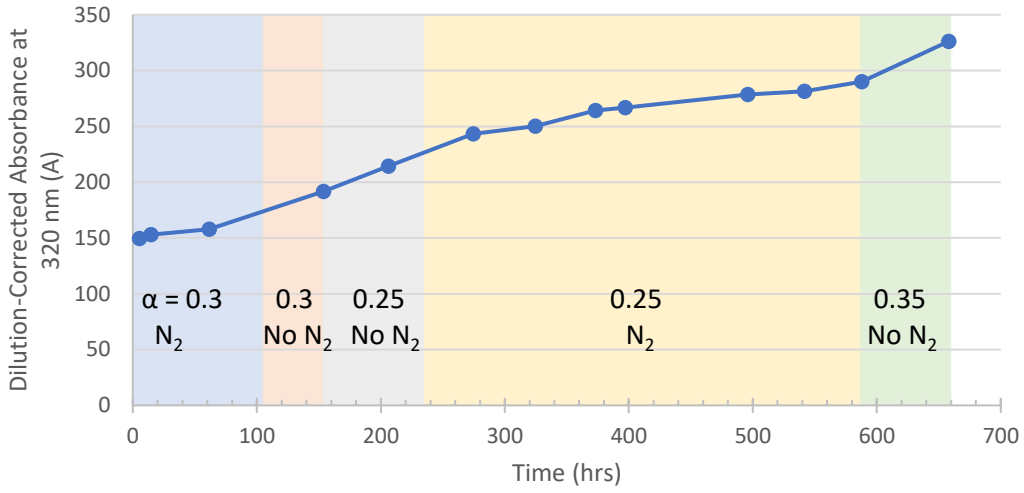

Figure 4-2: Dilution-corrected absorbance at 320 nm in HTOR 22 (55 ℃ to 150 ℃ , PP2 degraded solvent, N_2 Sparging, α = 0.25)

The concentration of the dissolved metals is shown in Figure 4-3. Mn slightly increased from 0.13 mmol/kg to 0.15 mmol/kg. Ni, Fe and Cr showed a similar trend. The metals precipitated out first and showed a steady increase after the system reached equilibrium at lean loading and before adding the antifoam. Ni accumulated to 0.0025 mmol/kg and Fe accumulated to 0.0024 mmol/kg. The two additions of antifoam lowered the concentration of the metals at first, and then metal concentration increased again. The effect of the antifoam decreased over time.

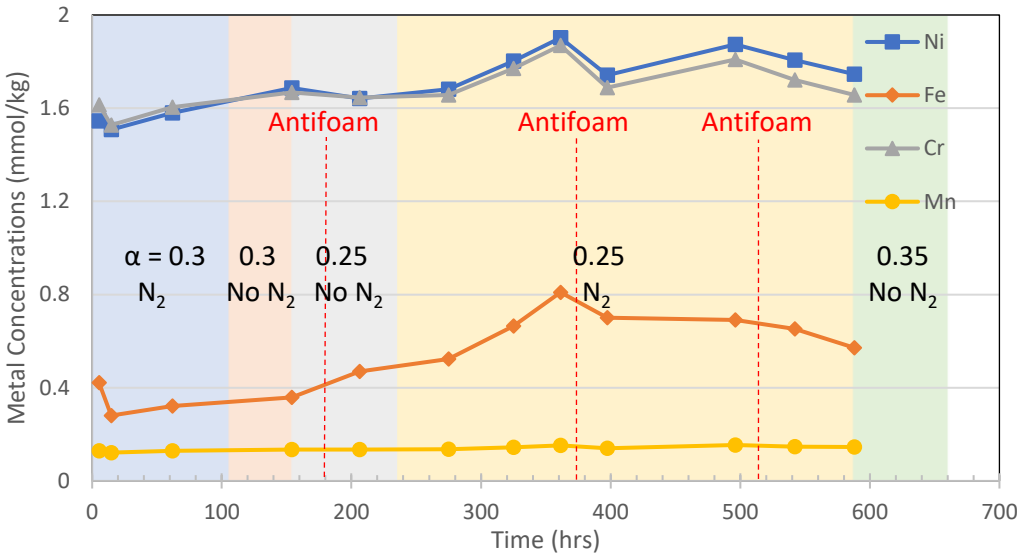

Figure 4-3: Dissolved stainless-steel metals in HTOR 22 (55 ℃ to 150 ℃ , PP2 degraded solvent, N_2 sparging, $\alpha = 0.25$)

The degradation products are plotted in Figure 4-4. EDA decreased at an average rate of 0.020 mmol/kg-hr when the nitrogen sparging was on, and it increased at an average rate of 0.047 mmol/kg-hr when the nitrogen sparging was turned off. Turning off the nitrogen sparging increased the production of 0.067 mmol/kg-hr of EDA, which should mainly come from the oxidation of PZ. Other degradation products did not show an obvious change in production rate when nitrogen sparging was turned off. When antifoam was added to the solvent at 375 hr and 515 hr, the degradation products all decreased. Since the addition of antifoam also caused the increase in ammonia production and decrease in metal concentration, it is possible that adding antifoam could speed up the oxidation or reduce the solubility of the degradation products and metals in the solvent.

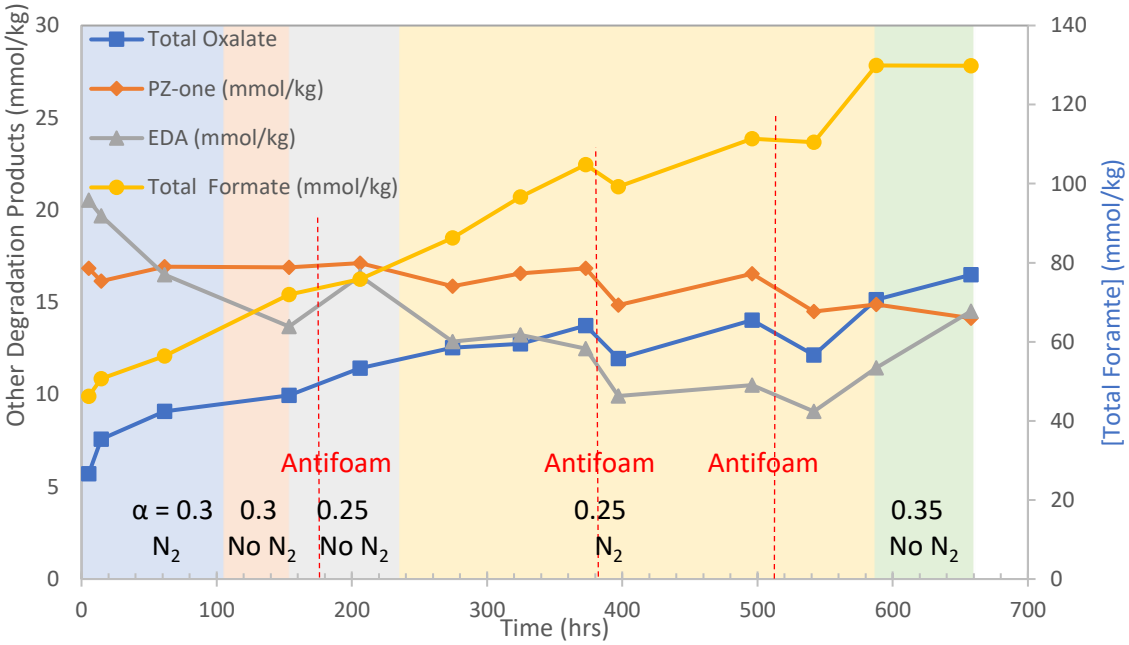

Figure 4-4: Degradation products in HTOR 22 (55 ℃ to 150 ℃ , PP2 degraded solvent, N_2 sparging, α = 0.25)

The PZ over time is shown in Figure 4-5. The average degradation rate of PZ was 0.812 mmol/kg-hr given an initial concentration of 4.17 mol/kg. In the first 200 hrs, the PZ steadily increased. Although it is possible that the FPZ in NCCC run decomposed into PZ and formate in the HTOR experiment, the initial FPZ was 7.23 mmol/kg, and cannot explain the 0.4 mol/kg increase in PZ. One possible reason could be some other PZ-derivatives broke down and formed PZ again at the start. It was also possible that there were errors occurring while measuring concentration. In all future experiments, tracers were added to eliminate the possible human and systematic errors.

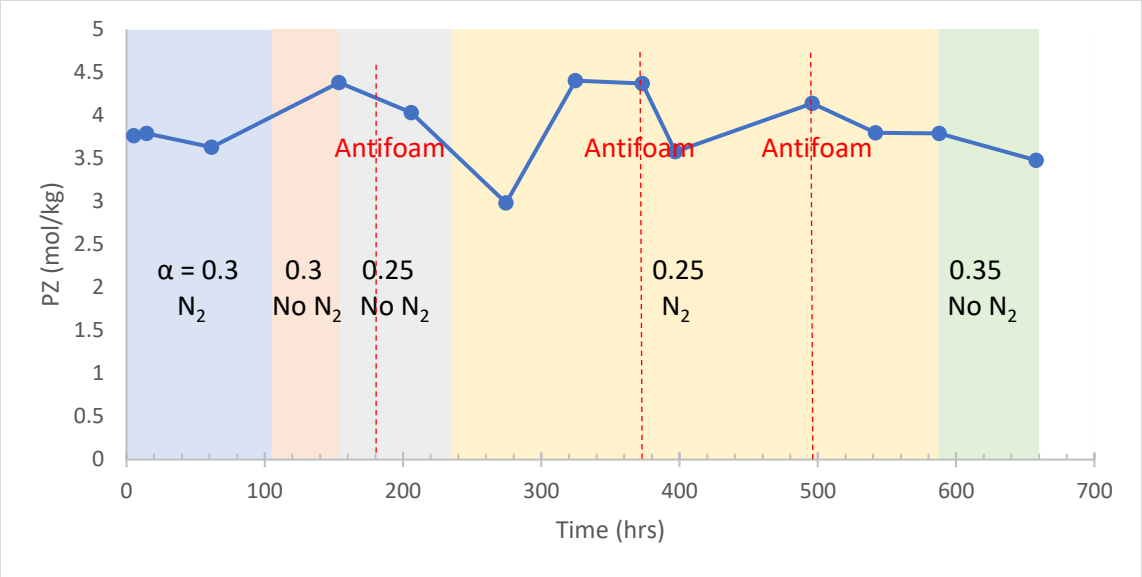

Figure 4-5: PZ in HTOR 22 (55 ℃ to 150 ℃ , PP2 degraded solvent, N_2 sparging, α = 0.25)

4.4 Effects of Degradation Products and Impurities on PZ Oxidation

4.4.1 HTOR 23: Clean 5 m PZ with EDA Cycled from 55 ℃ to 150 ℃

2.22 kg of clean 5 m PZ was prepared by dissolving PZ into water with the sparging of CO_2. Since EDA is one of the major degradation products of PZ oxidation, it is desired to test the effects of EDA on the PZ oxidation process. 18 g of EDA was added to the solution, and 0.206 g of LiOH and 0.396 g of KH_2PO_4 was added to the solvent as tracers. In this experiment, Li tracer worked well in correcting water balance problems, therefore Li was added as a tracer in all HTOR experiments afterwards. The solvent was cycled from 55 ℃ to 150 ℃ for 630 hrs with nitrogen sparging at a flow rate of 0.5 L/min. The inlet CO_2 flow rate was 37.5 mL/min to yield a lean loading of 0.25. The process changes in the experiment are shown in Table 4-3.

Table 4-3: Process changes during HTOR 23

Time (hrs)	Process Change
23	Add 3.2 mL 200 mM FeSO4
412	Add 1 mL antifoam
602	Reduce inlet [O_2] by 66%
629	End of experiment

The accumulation rate of important species at different conditions are summarized in Table 4-4. More detailed results are shown afterwards.

Table 4-4: Summary of degradation and corrosion products, and PZ oxidation rate in HTOR 23

Species	[O_2] = 20%	[O_2] = 6.7%
Gas-phase NH_3 rate (mmol/kg-hr)	Increased from 0.25 to 0.65	0.36
320 nm absorbance (A/hr)	0.23 ± 0.01	0.08
PZ (mmol/kg-hr)	-0.49 ± 0.04	N/A
Fe (μmol/kg-hr)	0.10 ± 0.09	-0.1
EDA (mmol/kg-hr)	-0.15 ± 0.01	-0.04

The ammonia production rate measured by FTIR is shown in Figure 4-6. There is an increase in NH_3 production at 23 hr when Fe^{2+} was added to the solvent. After the iron was in equilibrium with the solvent, the ammonia production rate dropped. At 411 hr, foaming was occurring in the HTOR, and 1 mL of antifoam was added. There was a step

increase of 0.1 mmol/kg-hr in the ammonia production. Compared to the effect of antifoam added in HTOR 22, the increase is smaller, which could be because the solvent is less degraded in HTOR 23 than in HTOR 22. Overall, the ammonia production rate followed the trend seen in previous experiments of increasing steadily as the solvent became more degraded. At the end of the experiment, the O_2 of the inlet gas was decreased to test the role of Fe in the oxidation. Since reducing O_2 decreased the ammonia production, it could be possible that the reduced O_2 caused less Fe^{2+} to be oxidized to Fe^{3+} at the absorber condition, which causes less PZ to be oxidized by Fe^{3+} at the stripper condition.

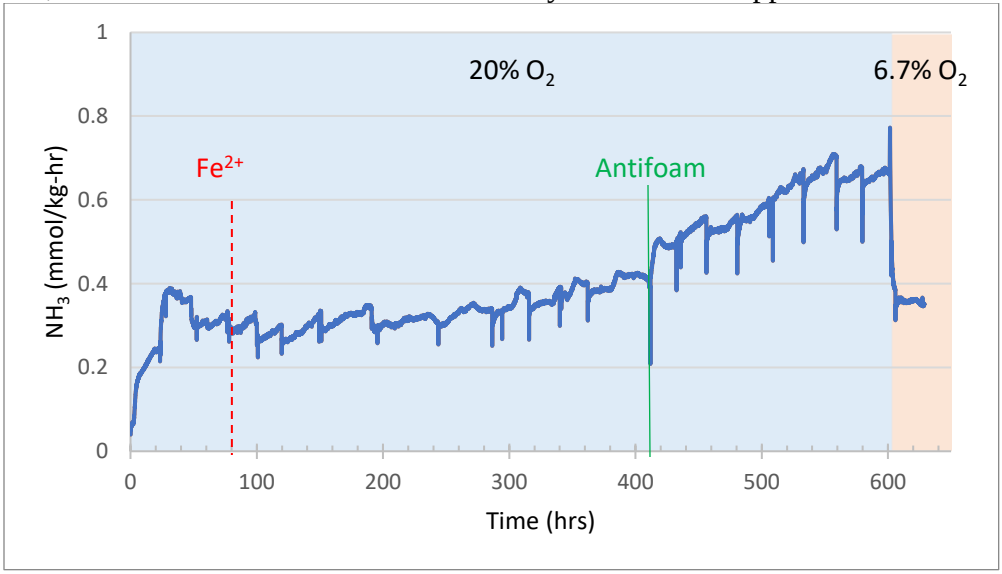

Figure 4-6: NH_3 production rate (clean PZ + EDA, 55 ℃ to 150 ℃ , N_2 sparging)

The cumulative NH_3 production rate of HTOR 23 is shown in Figure 4-7 as clean PZ + EDA w/ Sparging. By comparing with the clean PZ with N_2 sparging, it was found that the cumulative NH_3 production was higher with EDA present, and the difference between the curves increases as the solvent became more degraded. At 629 hr, there was 168.45 mmol/kg more NH_3 being produced when EDA was added to the initial solvent.

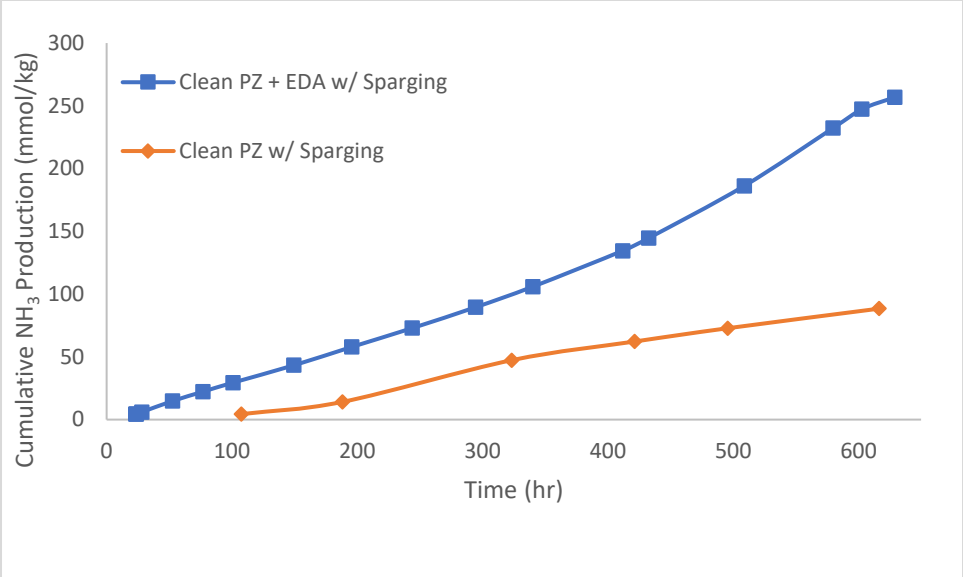

Figure 4-7: Comparison of cumulative NH_3 production with and without EDA

The UV-Vis absorbance was measured, and there was only one significant peak at 320 nm, as plotted in Figure 4-8. From 0 to 600 hrs, the absorbance increases at 0.23 ± 0.01 A/hr. When the oxygen concentration was reduced from 20% to 6.7%, the accumulation rate of absorbance decreased to 0.08 A/hr, which suggests the formation of the UV absorbing compound is first order to the oxygen. However, since only one samples was collected after changing the O_2 concentration, this relationship is not strongly supported.

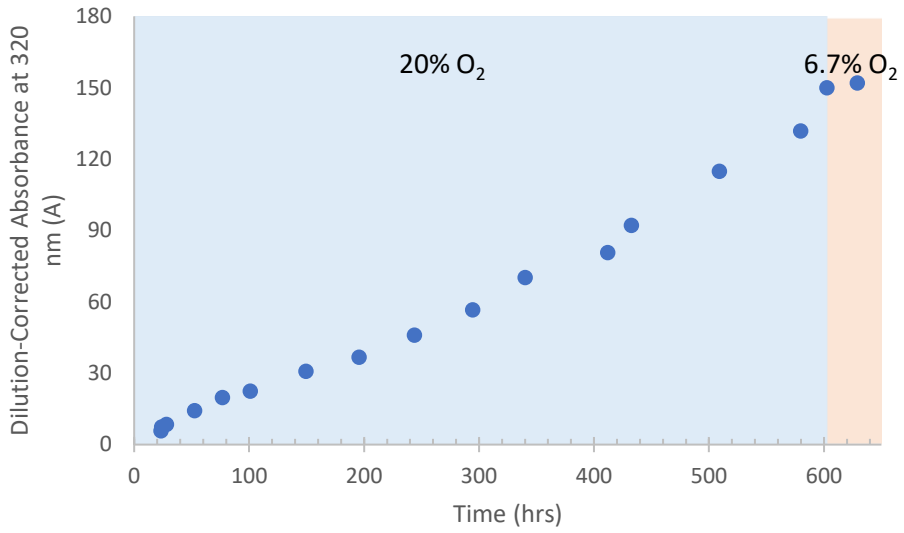

Figure 4-8: UV-Vis absorbance in HTOR 23 (clean PZ + EDA, 55 °C to 150 °C , N_2 sparging)

The concentrations of the tracers were quantified with ICP-OES and plotted in Figure 4-9. Two tracers were showing same trend, suggesting that the using Li and K are reliable. All the degradation products and PZ concentrations shown afterwards were corrected with the Li .

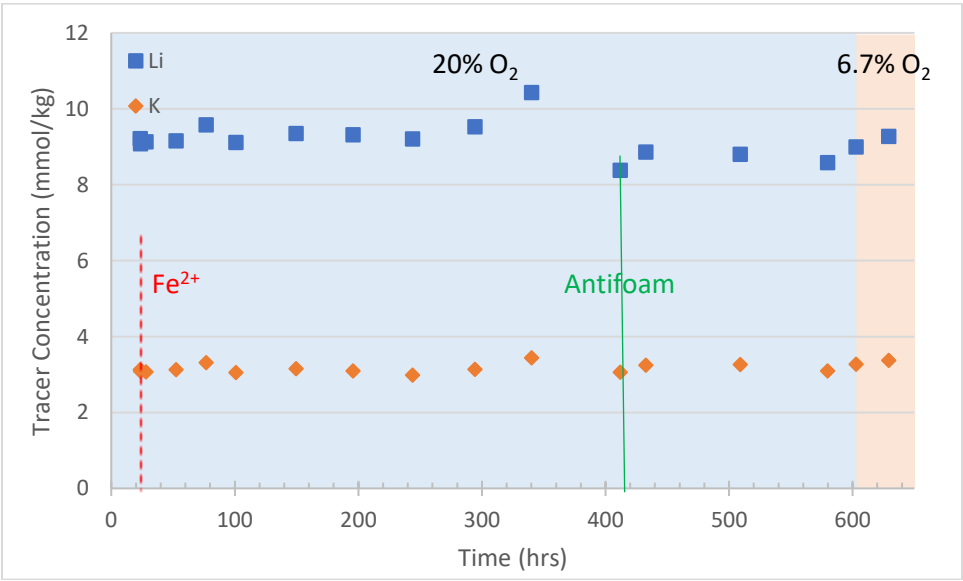

Figure 4-9: Tracer concentrations in HTOR 23 (clean PZ + EDA, 55 °C to 150 °C , N_2 sparging)

The EDA decreased at an average rate of 0.15 ± 0.01 mmol/ kg-hr until 620 hrs. Assuming all the N in the EDA degraded into NH_3, EDA degradation would have made 175 mmol/kg NH_3. This amount of NH_3 matches the difference of NH_3 production with and without EDA added as shown in Figure 6. It can be concluded that adding EDA to PZ solvent does not affect the amount of NH_3 produced by PZ, but it might affect the production of other degradation products. When the oxygen concentration was reduced to 6.7%, the rate of the EDA decomposition slowed down to 0.04 mmol/kg-hr.

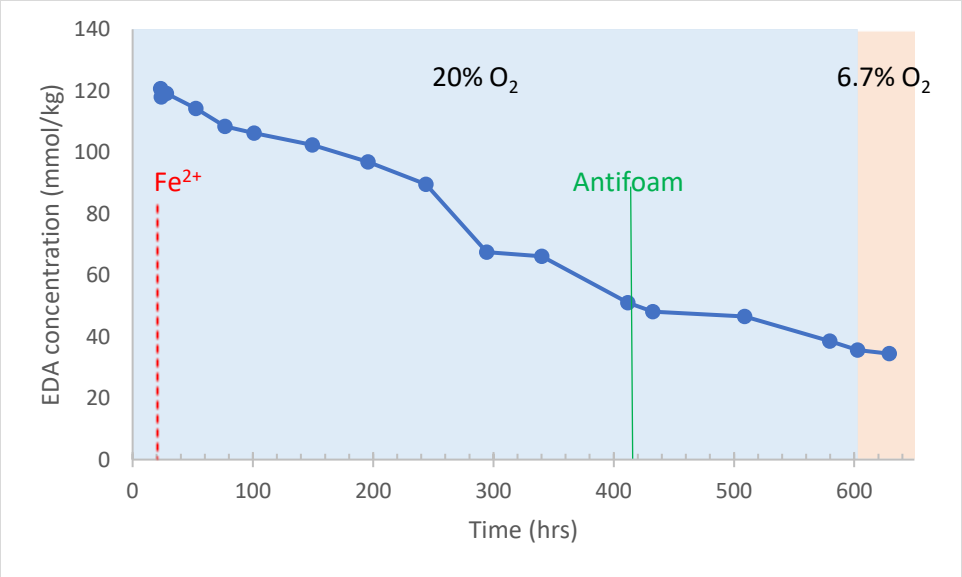

Figure 4-10: EDA concentration normalized w/ Li in HTOR 23 (clean PZ + EDA, 55 ℃ to 150 ℃ , N_2 sparging)

As shown in 5-11, the PZ concentration decreases at 0.49 ± 0.04 mmol/kg-hr, similar to the base condition of clean PZ oxidizing between 55 ℃ to 150 ℃ (Nielsen, 2018). This indicates that EDA does not influence PZ oxidation. The oxidation of EDA does not compete with PZ oxidation either.

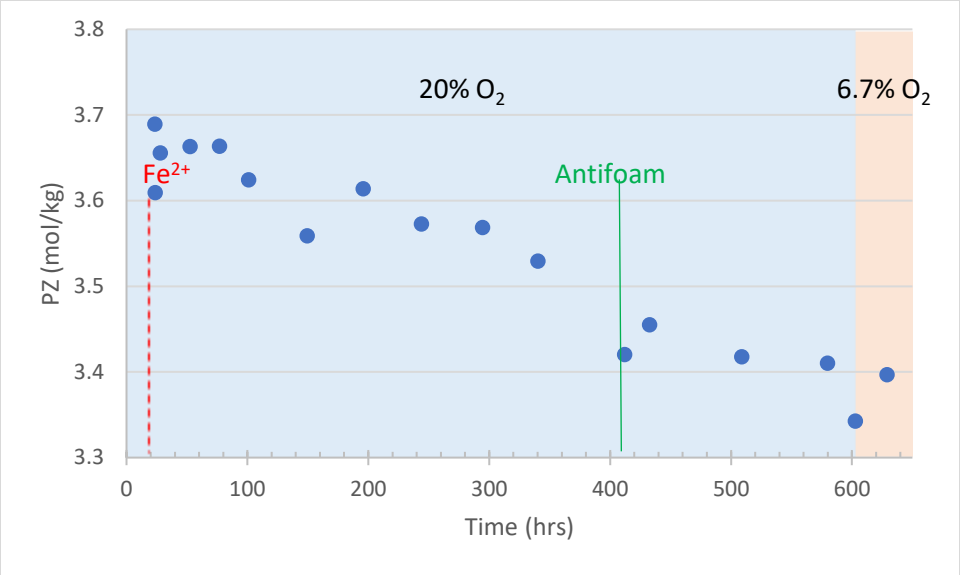

Figure 4-11: PZ normalized w/ Li in HTOR 23 (clean PZ + EDA, 55 ℃ to 150 ℃ , N_2 sparging)

Figure 4-12 shows the Fe concentration. Since Fe is limited by solubility instead of availability, the Fe was not normalized by Li. At 23.4 hr, $FeSO_4$ solution was added into the solvent, resulting a sharp increase in the Fe. After the system was balanced, Fe precipitated out from the solution and reached a level close to the Fe before addition. There is a steady increase of Fe as the solvent become degraded, which is a sign of increase in Fe solubility. The addition of antifoam and reduction O_2 concentration both caused a decrease in the Fe .

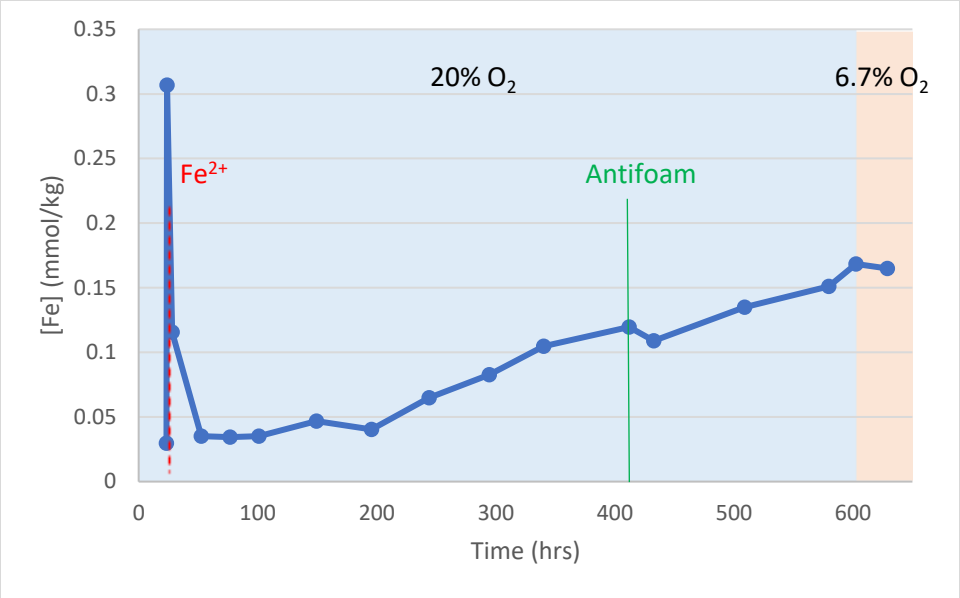

Figure 4-12: Dissolved Fe in HTOR 23 (clean PZ + EDA, 55 ℃ to 150 ℃ , N_2 sparging)

The concentrations of Ni, Cr, and Mn are normalized with Li tracer and plotted in Figure 4-13. The metal concentrations decreased after antifoam was added, and continued increasing when O_2 concentration was reduced. Adding antifoam may change the physical properties of the solvent and affect all the metal concentrations, while reducing O_2 affected the reaction and only caused reduction in Fe. Overall, there is an increase of metal concentrations in the solvent, and the proportions are consistent with the ratios of Cr, Ni and Mn in the stainless-steel, indicating that the metals probably resulted from corrosion of stainless steel. The rate of increase in Cr, Ni and Mn is limited by the corrosion rate instead of the solubility in the solvent.

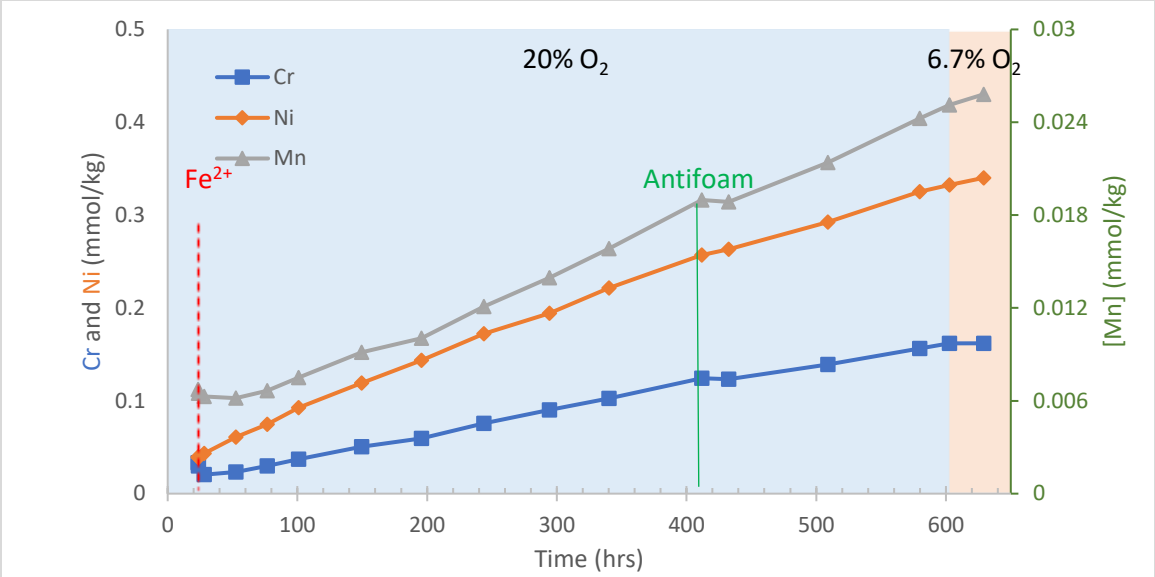

Figure 4-13: Cr, Ni and Mn concentration in HTOR 23 (clean PZ + EDA, 55 ℃ to 150 ℃ , N_2 sparging)

4.4.2 HTOR 25: Clean 5 m PZ with Formaldehyde Cycled from 55 ℃ to 150 ℃ with Nitrogen Sparging

The effects of aldehydes on the PZ oxidation is studied by adding formaldehyde to clean PZ solvent. 2.08 kg of clean 5 m PZ was prepared by dissolving PZ into water with the sparging of CO_2. 1.4495 g of LiOH and 1.0022 g of KH_2PO_4 were added to the solvent as tracers. At the start of the experiment, 3.2619 g of 37 wt % formaldehyde was added, and three more additions were performed during the experiment. Each addition of formaldehyde was equal to around 20 mmol/kg formaldehyde. The solvent was cycled from 55 ℃ to 150 ℃ with nitrogen sparging at a flow rate of 0.5 L/min. The inlet CO_2 flow rate was 37.5 mL/min to yield a lean loading of 0.25. The change of conditions in the experiment is shown in Table 4-5.

Table 4-5: Process changes during HTOR 25

Time (hrs)	Process Change
0	3.2619 g of 37 wt % formaldehyde
23	3.2 mL of 200 mM $FeSO_4$
148	3.1476 g of 37 wt % formaldehyde
335	3.1878 g of 37 wt % formaldehyde
384	N_2 Sparger off
387	N_2 Sparger on
551	3.0068 g of 37 wt % formaldehyde
761	Circulation stopped due to flash
790	Restart circulation
892	End of experiment

The NH_3 production rate is shown and compared with clean PZ in Figure 4-14. When formaldehyde was added to the solvent, the NH_3 production first dropped to 0, and then increased greatly. Formaldehyde can react with NH_3 to form hexamethylenetetramine (Ogata, 1963), causing the drop of NH_3 immediately after addition. It may also react with O_2 and water in the presence of Fe, as shown in Scheme 4-1, which reacted with the precursors of NH_3 and caused increase in NH_3 2 hrs after addition. The effects ceased as formaldehyde evaporates into the gas phase.

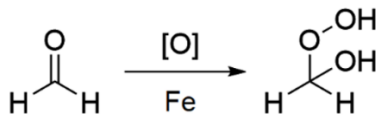

Scheme 4-1: Reaction of formaldehyde with O_2 (Fe as catalyst)

Although the solvent started with 20 mmol/kg formaldehyde, there was no significant increase in the NH_3 production rate compared to the clean PZ since negligible amount of Fe presented in solvent and the reaction was not initiated. After the solvent gets more degraded, the increase of NH_3 production rate due to addition of formaldehyde increased, indicating that the reaction of formaldehyde was related to the degradation extent of the solvent. As the solvents become more degraded, more Fe was present, therefore more peroxides were created, resulting a more significant effect. The first addition generated 5 mmol/kg more NH_3 compared to the baseline experiment with clean PZ. The second addition generated an additional 27.5 mmol/kg more NH_3, and the third addition generated 41.5 mmol/kg more NH_3. At 760 hrs, the system stopped circulation, causing the NH_3 production rate to become 0. Since the NH_3 cannot be released through the reactor, there was a sharp increase of NH_3 when the system started circulation again as degradation continued to occur at high temperature and NH_3 accumulated in solvent.

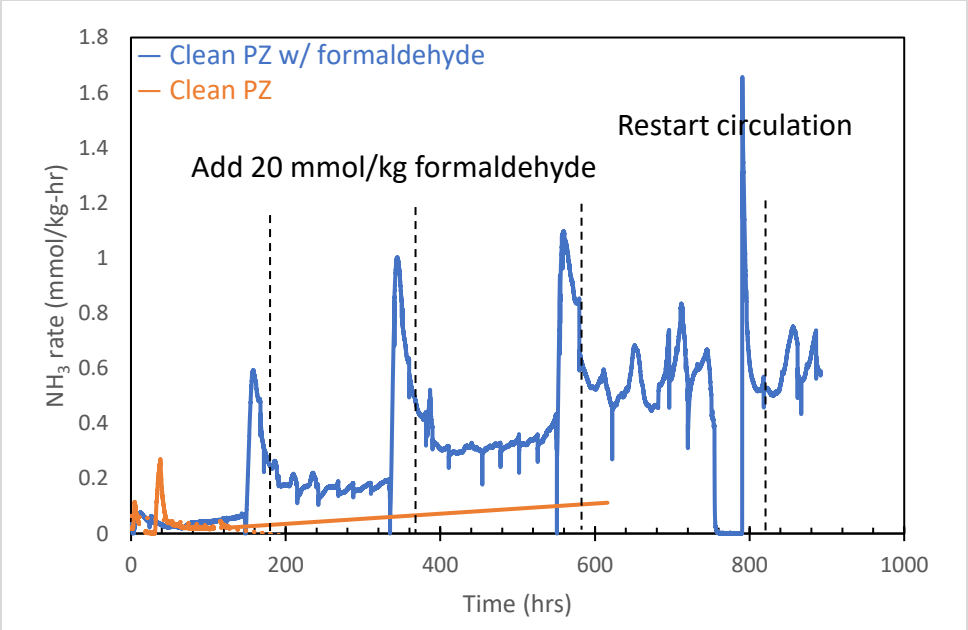

Figure 4-14: NH_3 production rate in HTOR 25 (clean 5 m PZ with formaldehyde, cycled from 55 ℃ to 150 ℃ with N_2 sparging)

The absorbance at 320 nm was measured and plotted in Figure 4-15. When formaldehyde was added to the system at 150 hrs, the accumulation rate increased from 0.04 ± 0.01 A/hr to 0.27 ± 0.01 A/hr. No significant difference was observed when the following two formaldehyde additions were performed. This suggests that the UV-absorbing compound was not a product of formaldehyde and PZ reaction directly, but the formaldehyde initiated the oxidation by creating peroxides.

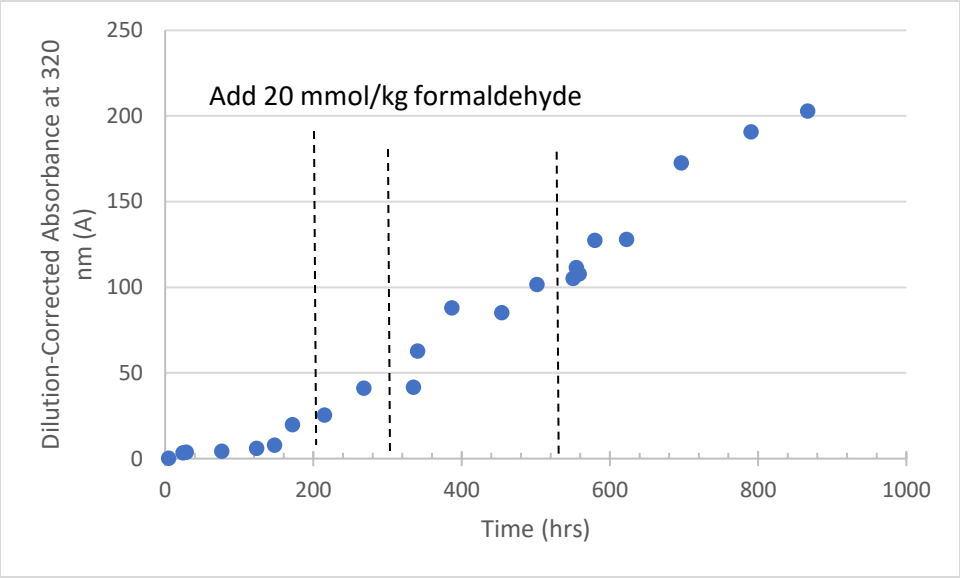

Figure 4-15: Dilution-corrected absorbance at 320 nm in HTOR 25 (clean 5 m PZ with formaldehyde, cycled from 55 °C to 150 °C with N_2 sparging)

Figure 4-16 shows the Fe in comparison with the NH_3 rate. The Fe increased with the addition of the $FeSO_4$ but went back to the initial value quickly due to solubility limit. When formaldehyde was added, a step increase in the Fe was observed, and the highest concentration was achieved when the NH_3 rate reached local maxima. This shows the Fe solubility is related to the solvent oxidation rate instead of the solvent oxidation level. After the formaldehyde was depleted, Fe decreased to a level higher than the concentration before addition. Overall, the Fe accumulated at 0.14 ± 0.03 μmol/kg-hr.

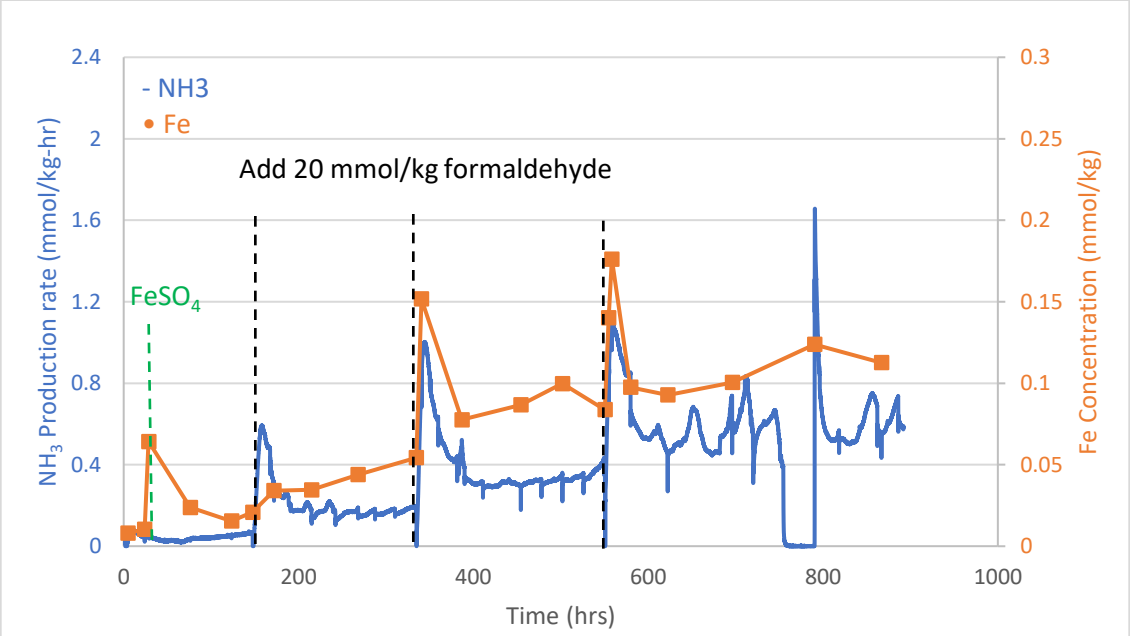

Figure 4-16: Relationship between dissolved Fe and NH_3 production in HTOR 25 (clean 5 m PZ with formaldehyde, cycled from 55 °C to 150 °C with N_2 sparging)

The normalized formate, total formate, and FPZ are plotted in Figure 4-17. The 20 mmol/kg formadehyde addition resulted in an increase of 9.1 mmol/kg total formate and 8.2 mmol/kg FPZ after the addition at 335 hrs, and resulted in an increase of 8.3 mmol/kg total formate and 17.5 mmol/kg FPZ after the addition at 551 hrs. The FPZ and total formate decreased to the original level. This suggests that some formaldehyde reacts with PZ to form FPZ, which degrades into species other than formate. The overall accumulation rate of total formate was 0.065 mmol/kg-hr, and was not affected by the formaldehyde addition. As the solvent became more degraded, the accumulation rate of total formate increased, and the trend followed a quadratic relationship with time. The FPZ accounted for about 60% of the total formate.

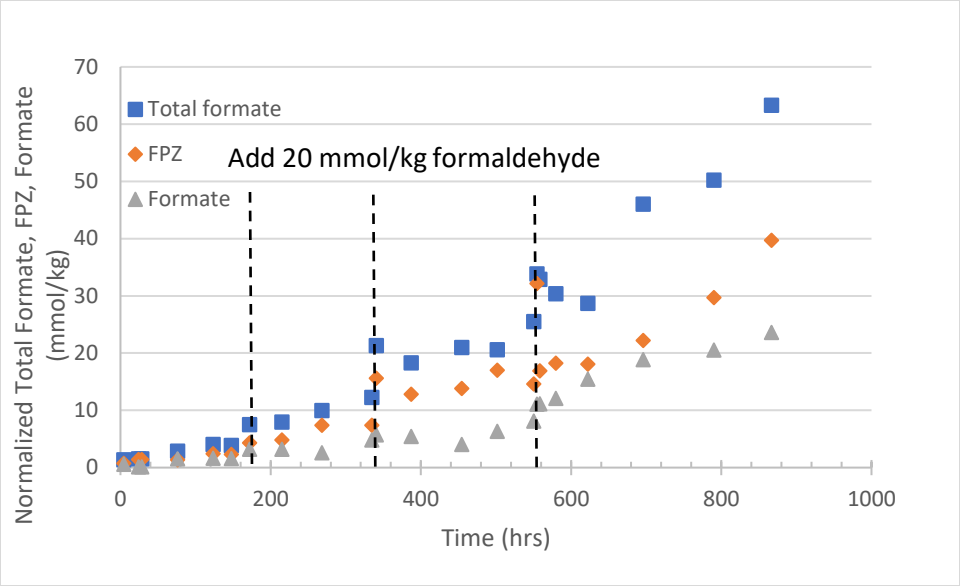

Figure 4-17: Formate, total formate, and FPZ normalized by Li in HTOR 25 (clean 5 m PZ with formaldehyde, cycled from 55 °C to 150 °C with N_2 sparging)

As shown in Figure 4-18, the EDA was not affected by the addition of formaldehyde. After formaldehyde addition, both the EDA concentration and rate of production remained constant at 0.12 ± 0.01 mmol/kg-hr. When EDA reached 48 mmol/kg, the accumulation stopped, and EDA started to degrade.

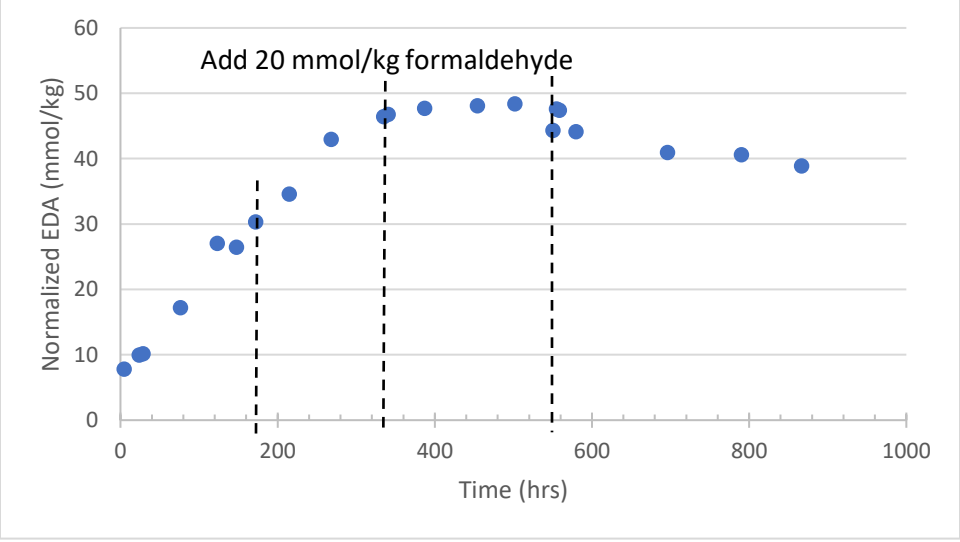

Figure 4-18: EDA normalized by Li in HTOR 25 (clean 5 m PZ with formaldehyde, cycled from 55 °C to 150 °C with N_2 sparging)

The normalized MPZ accumulated at 0.033 ± 0.002 mmol/kg-hr, as shown in Figure 4-19. Similar to EDA, the MPZ concentration and production rate was not affected by the formaldehyde addition. The MPZ was more stable than EDA, and no decomposition had been observed.

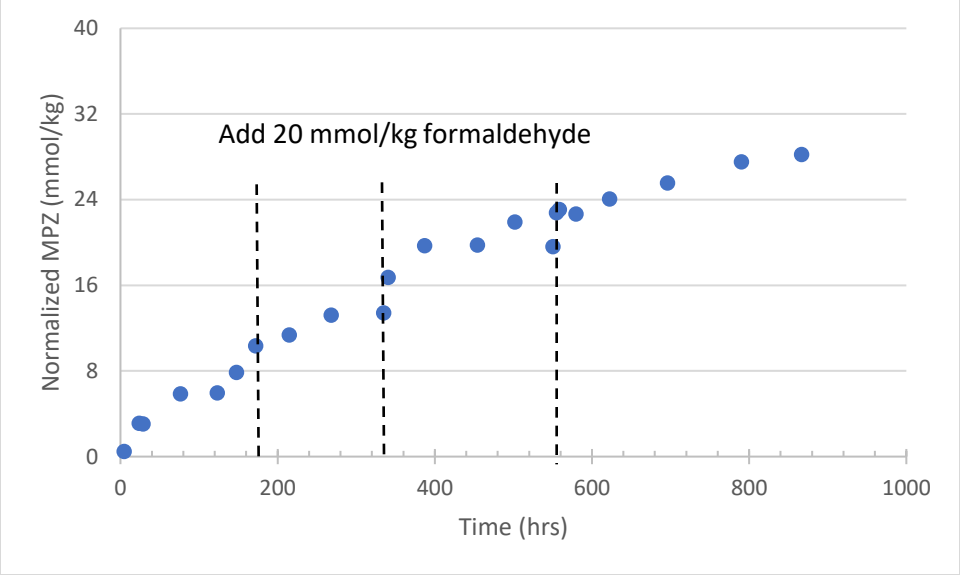

Figure 4-19: MPZ normalized by Li in HTOR 25 (clean 5 m PZ with formaldehyde, cycled from 55 ℃ to 150 ℃ with N_2 sparging)

PZ-one normalized by Li is plotted in Figure 4-20. PZ-one did not vary immediately when the formaldehyde was added. However, it experienced a step two days after addtion, indicating that PZ-one is not a product after several reaction steps. Scheme 4-2 shows possible mechanism to create PZ-one. PZ-one started decreasing after formaldehyde was added at 551 hrs, which indicates that the PZ-one degrading at a faster rate than producing, possibly because the solvent got more degraded, and more catalysts existed to oxidize PZ-one.

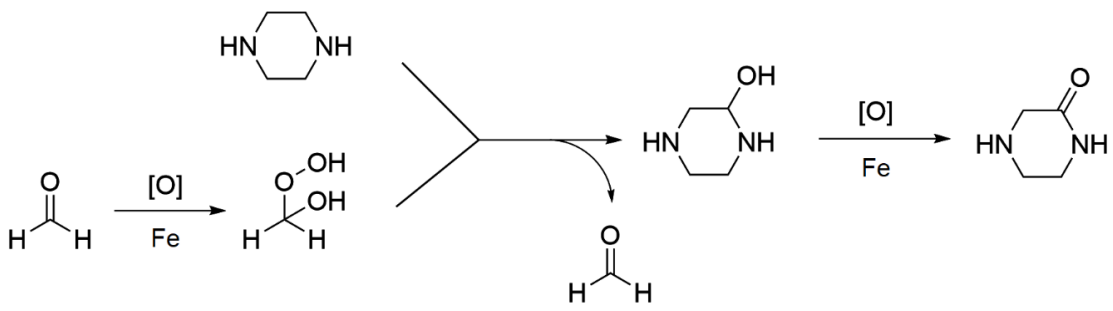

Scheme 4-2: Reaction of formaldehyde with PZ

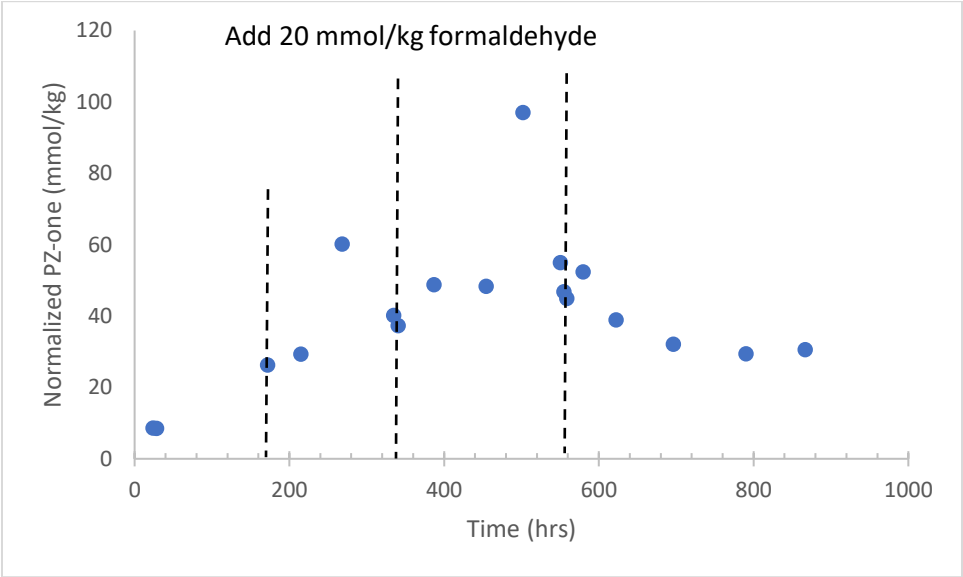

Figure 4-20: PZ-one normalized by Li in HTOR 25 (clean 5 m PZ with formaldehyde, cycled from 55 °C to 150 °C with N_2 sparging)

Shown in Figure 4-21, the PZ loss was estimated at 1.2 ± 0.01 mmol/kg-hr. Although the effects of formaldehyde are not obvious in the graph, the rate was much higher than the 0.5 mmol/kg-hr on 5 m clean PZ with N_2 sparging in the HTOR (Nielsen, 2018). This shows that the addition of formaldehyde can accelerate the PZ oxidation. Besides reactions stated in Scheme 5.1, formaldehyde can also react with PZ through nucleophilic addition, as shown in Scheme 4-3, which requires further work to confirm.

While formaldehyde can polymerize with various molecules, it is unlikely to be the case since formaldehyde monomers are favored under alkaline conditions (Walker, 1964).

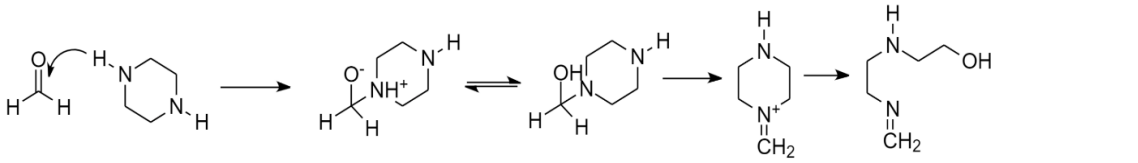

2-((2-(methyleneamino)ethyl)amino)ethan-1-ol

Scheme 4-3: Nucleophilic addition of formaldehyde with PZ

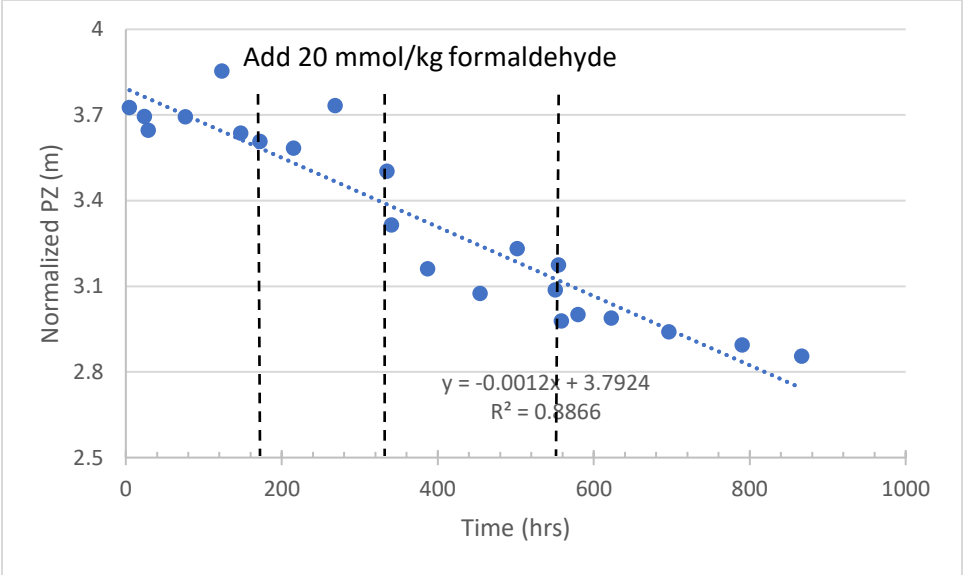

Figure 4-21: PZ normalized by Li in HTOR 25 (clean 5 m PZ with formaldehyde, cycled from 55 ℃ to 150 ℃ with N_2 sparging)

The Cr, Ni, and Mn, normalized by Li, are shown in Figure 4-22. Cr increased at 0.28 ± 0.01 μmol/kg-hr, Ni increased at 0.37 ± 0.01 μmol/kg-hr, and Mn increased at 0.04 ± 0.002 μmol/kg-hr. No changes in concentration or accumulation rate were observed with the addition of formaldehyde, since Cr, Ni, and Mn accumulated in solvent because of corrosion, and the addition of formaldehyde had no effects on the corrosion behavior.

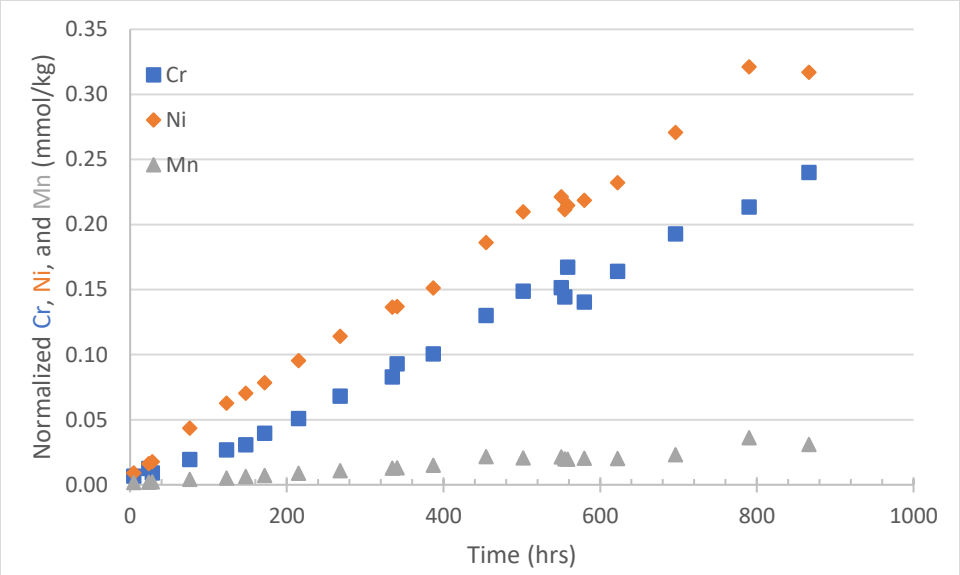

Figure 4-22: Normalized stainless steel metal concentrations (clean 5 m PZ with formaldehyde, cycled from 55 ℃ to 150 ℃ with N_2 sparging)

4.5 Effects of Carbon Treating on PZ Solvent Experiencing Oxidation

4.5.1 HTOR 27: Moderately Degraded PZ from 55 ℃ to 150 ℃ with Carbon Treating

HTOR 27 started with a 1:1 blend of clean 5 m PZ and the end solvent of HTOR 22. The HTOR 22 started with the end solvent from the PP2 campaign, which lasted for 1600 hrs, and the HTOR 22 experiment lasted for 700 hrs, making the end solvent very degraded. The initial solvent contained 0.08 mmol/kg Fe, 47.02 mmol/kg total formate. A 7.5 L/min synthetic flue gas was used by mixing air with CO_2 to maintain a loading of 0.25, which is close to the lean loading in real plant operations. LiOH was used as tracer to correct for the water balance. The solvent was cycled between 55 ℃ and 150 ℃ , and a carbon bed containing 15.5 g of carbon was tested. The time of each process changes is recorded in Table 4-6. Table 4-7 shows a summary of the rates of species measured in the HTOR 27.

Table 4-6: Process changes during HTOR 27

Time (hrs)	Process Change
19.2	Turn on carbon bed
23.6	Bypass carbon bed
67.0	Turn on carbon bed
363.1	Pump down (No Circulation)
404.5	Pump fixed
409.9	Bypass carbon bed
676.2	Turn on carbon bed
766.7	End of experiment

Table 4-7: Accumulation rate of degradation and corrosion products, and PZ oxidation rate

Species	Carbon on 67 – 409 hrs	Carbon off, 409 – 676 hrs	Carbon on, 676 – 767 hrs
Gas-phase NH_3 rate ($mmol/kg\text{-}hr^2$)	Constant at 0.4 mmol/kg-hr	0.002 ± 0.000	Constant at 0.7 mmol/kg
PZ loss (mmol/kg-hr)	-1.4 ± 0.1	-1.8 ± 0.1	-1.4 ± 0.0
320 nm absorbance (A/hr)	Constant at 60 A	0.20 ± 0.01	Constant at 110 A
Total formate (mmol/kg-hr)	0.04 ± 0.00	0.15 ± 0.01	0.12 ± 0.02
Total acetate (mmol/kg-hr)	0.009 ± 0.002	0.039 ± 0.004	0.019 ± 0.008
Total oxalate (mmol/kg-hr)	0.005 ± 0.001	0.022 ± 0.008	0.014 ± 0.004

The NH_3 production rate is shown in Figure 4-23. When the carbon bed was turned on between 67 and 410 hrs, the NH_3 production rate was relatively constant at 0.4 mmol/kg-hr. When the carbon bed was turned off, there was a linear increase in the NH_3 production rate. When the carbon bed was turned on the second time, the NH_3 rate stopped increasing and remained constant at 0.7 mmol/kg. This graph suggests that the carbon bed can inhibit the increase in the NH_3 rate by removing catalytic complexes. It is also possible that the carbon removes precursor of NH_3, therefore reduce the NH_3 production.

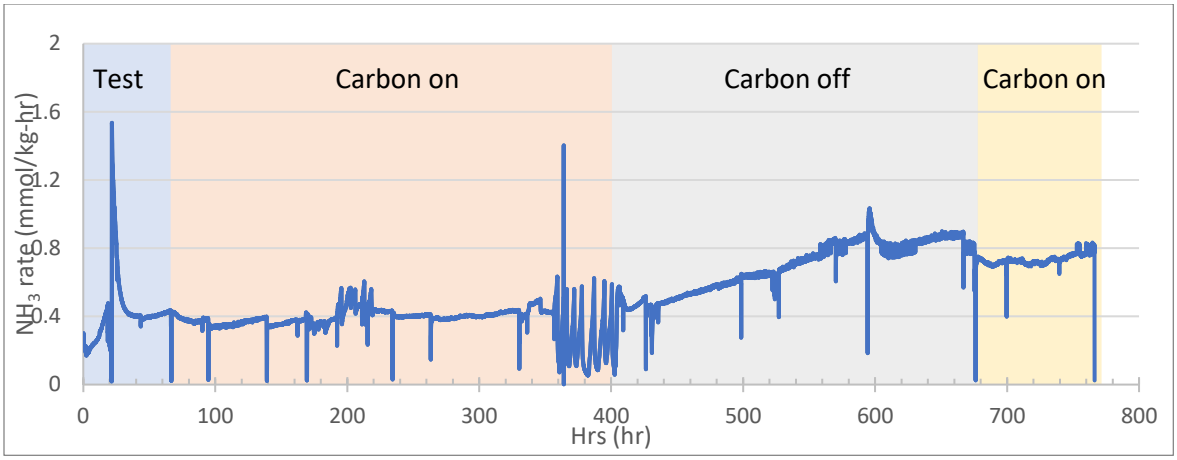

Figure 4-23: NH_3 production rate in HTOR 27 (55 ℃ to 150 ℃ , moderately degraded PZ, carbon bed)

The PZ calculated from IC and alkalinity is shown in Figure 4-24. The PZ concentrations from the two methods matched each other and showed a significant decrease over the duration of the experiment. A leak was found in the HTOR system after the experiment, which explains most of the PZ loss. Li tracer was added at the start, and the concentration can be corrected to show the PZ if there were no leak. However, since the PZ is very low towards the end of the experiment, it might not be representative of 5 m PZ.

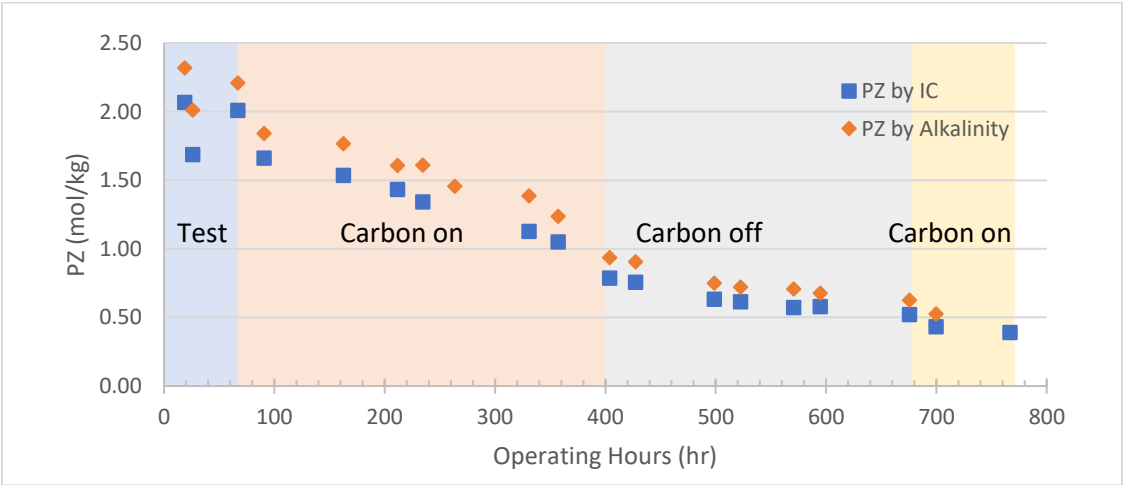

Figure 4-24: Raw PZ concentration and alkalinity in HTOR 27 (55 ℃ to 150 ℃ , moderately degraded PZ, carbon bed)

The normalized PZ concentration is shown in Figure 4-25, and the rate for different periods of time was estimated. When the carbon bed was on, the PZ oxidation rate was 1.4 ± 0.1 mmol/kg-hr, and when the carbon bed was turned off, the PZ oxidation rate was 1.8 ± 0.1 mmol/kg-hr. When the carbon bed turned on the second time, the PZ oxidation rate decreased to 1.4 ± 0.0 mmol/kg-hr again. This shows that the carbon bed reduces the PZ oxidation rate by 0.4 mmol/kg-hr. However, the PZ oxidation rate was much higher than the NH_3 production rate, suggesting that PZ can degrade in pathways that produce fewer than 1 mol of NH_3 per mol of PZ.

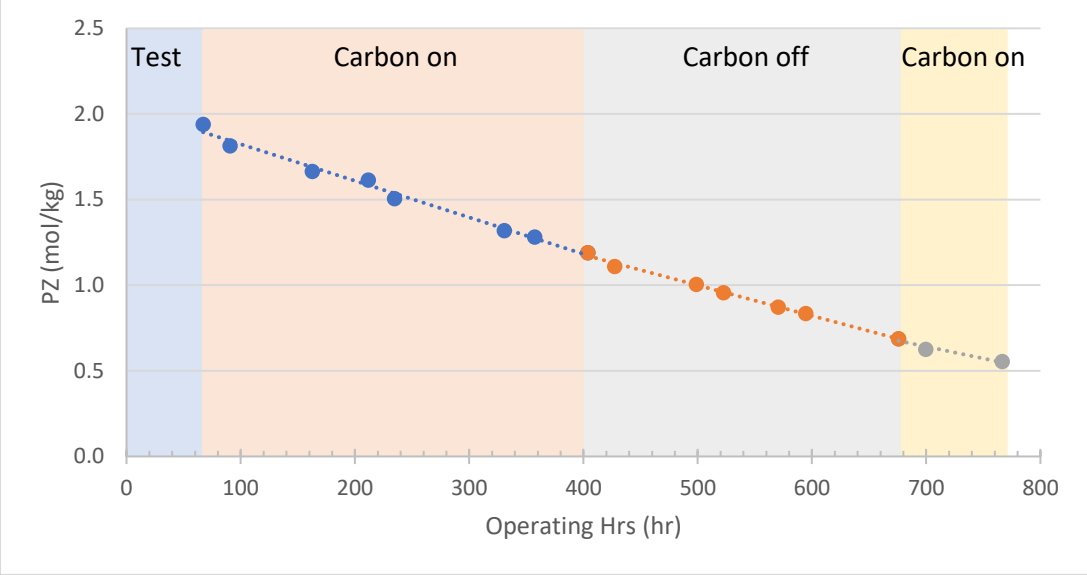

Figure 4-25: Normalized PZ concentration in HTOR 27 (55 ℃ to 150 ℃ , moderately degraded PZ, carbon bed)

Since Fe is affected by oxidation, instead of being simply a result of corrosion, the raw Fe represents the data better than normalized Fe. Figure 4-26 shows that the Fe increased at a higher rate during the period when the carbon bed was off, but it is not clear if this was a result of a higher oxidation rate or a lower Fe level. The reason for the decrease at 400 hrs remained unclear.

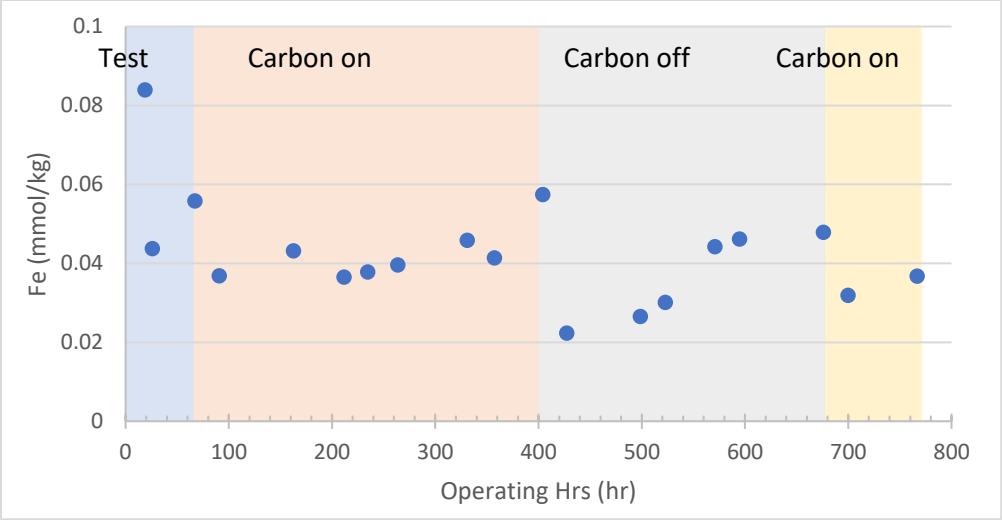

Figure 4-26: Fe in HTOR 27 (55 ℃ to 150 ℃ , moderately degraded PZ, carbon bed)

The normalized stainless-steel metal concentrations are shown in Figure 4-27. Cr, and Mn both exhibited a decrease; Ni stayed relatively constant; and Fe seemed to vary randomly. The decrease in Mn matched the results from the carbon adsoprtion column, although the decrease in Cr did not. The Cr still decreased even when the carbon bed was turned off, and more investigation is required to understand the decrease after turning off the carbon bed.

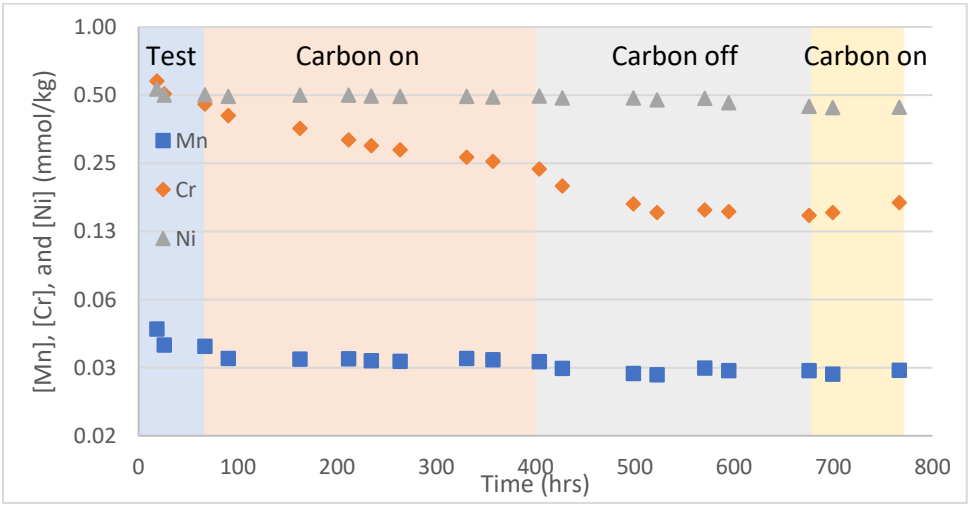

Figure 4-27: Normalized Mn, Cr, and Ni in HTOR 27 (55 ℃ to 150 ℃ , moderately

degraded PZ, carbon bed)

The color of the solvent was quantified using UV-Vis measurement. The dilution-corrected absorbance at 320 nm is shown in Figure 4-28. When the carbon bed was on, the absorbance stayed constant. When the carbon bed was turned off, the absorbance increased at a rate of 0.20 ± 0.01 A/hr. This indicates that the absorbance is resulted from the accumulation of degradation products, and the carbon bed can remove the newly produced products and reach a state where the rate of production is equal to the rate of removal. This also suggests that carbon bed may keep the solvent at a lower absorbance level, which is a lower degradation extent, if the starting solvent clean and the oxidation rate is lean.

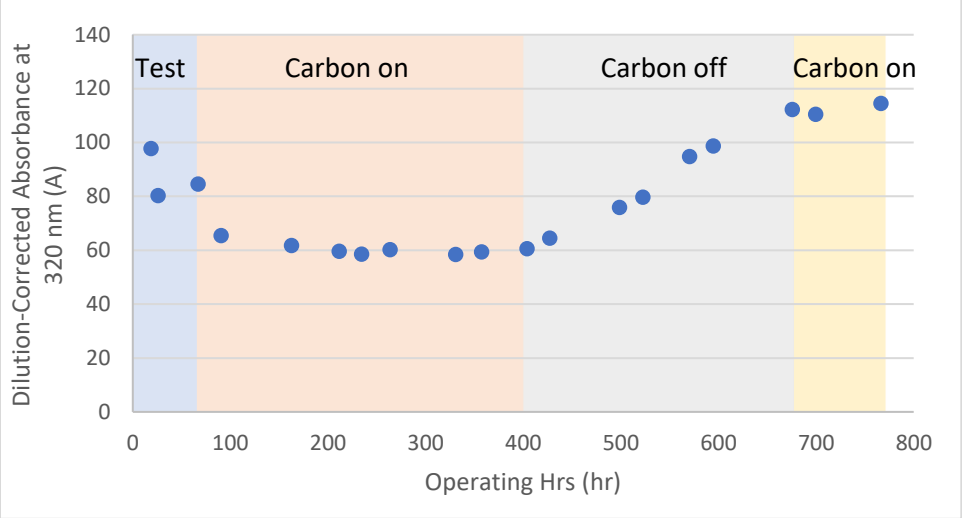

Figure 4-28: Normalized dilution-corrected absorbance in HTOR 27 (55 ℃ to 150 ℃ , moderately degraded PZ, carbon bed, no N_2 sparging)

The normalized EDA is plotted in Figure 4-29. In the first 330 hrs, the EDA accumulated at 0.075 ± 0.005 mmol/kg-hr, and no difference was observed before or after the carbon was turned on, indicating that carbon bed did not remove EDA or any degradation products that react with EDA. After 330 hrs, the EDA started decreasing at 0.047 mmol/kg-hr. This matched the observation that EDA always accumulates at early stages of degradation and starts to decompose when the concentration reached 25 to 40

mmol/kg.

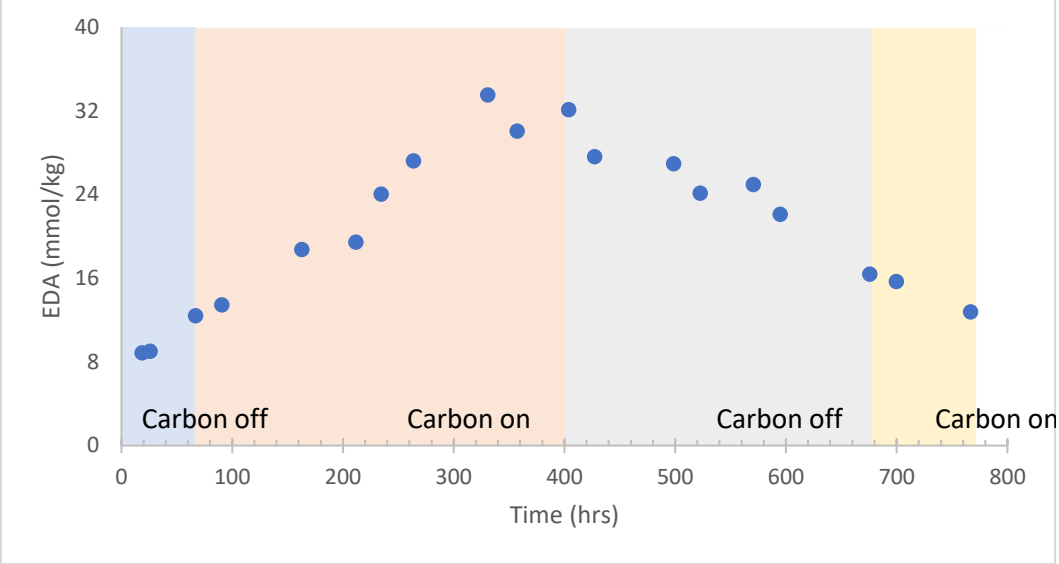

Figure 4-29: EDA normalized by Li in HTOR 27 (55 ℃ to 150 ℃ , moderately degraded PZ, carbon bed)

The normalized MPZ is shown in Figure 4-30. The production rate of MPZ stayed constant at 0.018 ± 0.001 mmol/kg-hr, not affected by the carbon treating.

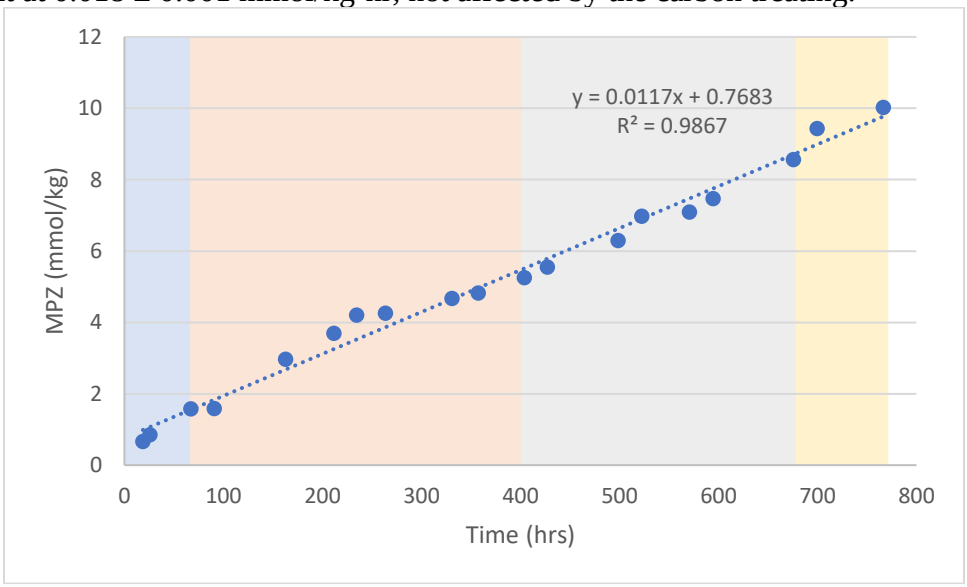

Figure 4-30: MPZ normalized by Li in HTOR 27 (55 ℃ to 150 ℃ , moderately degraded PZ, carbon bed)

The normalized total formate, total acetate, and total oxalate concentrations are shown in Figure 4-31. The total acetate and oxalate stayed low, while the total formate increased to 110 mmol/kg. All the total anions showed a faster increase when the carbon bed was turned off, and a time lag is observed, indicating that the total heat stable salts require multiple steps to form. When the carbon bed is turned on again at 675 hrs, the accumulation of all these three species slowed down. The rate of total formate, total acetate, and total oxalate in each period is summarized in Table 4-7. As discussed in Chapter 4, although carbon treating can remove the anion species in the solvent, the removal rate is usually small, suggesting that the production rates of these anions were smaller when the carbon bed was turned on, and the carbon bed may have removed complexes could be the precursors of the anions or catalysts to reactions that produced these anions.

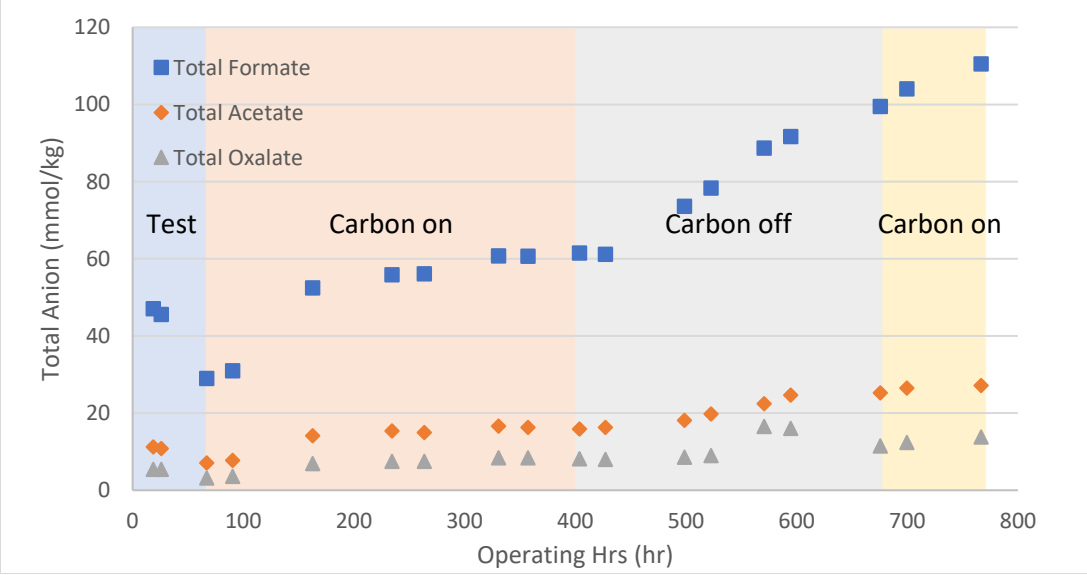

Figure 4-31: Normalized total anions in HTOR 27 (55 ℃ to 150 ℃ , moderately degraded PZ, carbon bed, no N_2 sparging)

The normalized PZ-ol is shown in Figure 4-32. The concentration stays low, but the trend is different in the two periods when carbon bed was off. In previous experiments, PZ-ol always increased at first, and then decreased after the solvent was degraded, mainly

because it was an intermediate in the series of oxidation reactions. In this experiment, the first increase in the PZ-ol may have occurred because the carbon bed removed the catalyst that can oxidize the PZ-ol degradation. When the carbon bed was turned off, the catalyst started accumulating, and accelerated the PZ-ol oxidation. Even though the carbon bed was turned on again at 700 hrs, it did not remove enough catalysts.

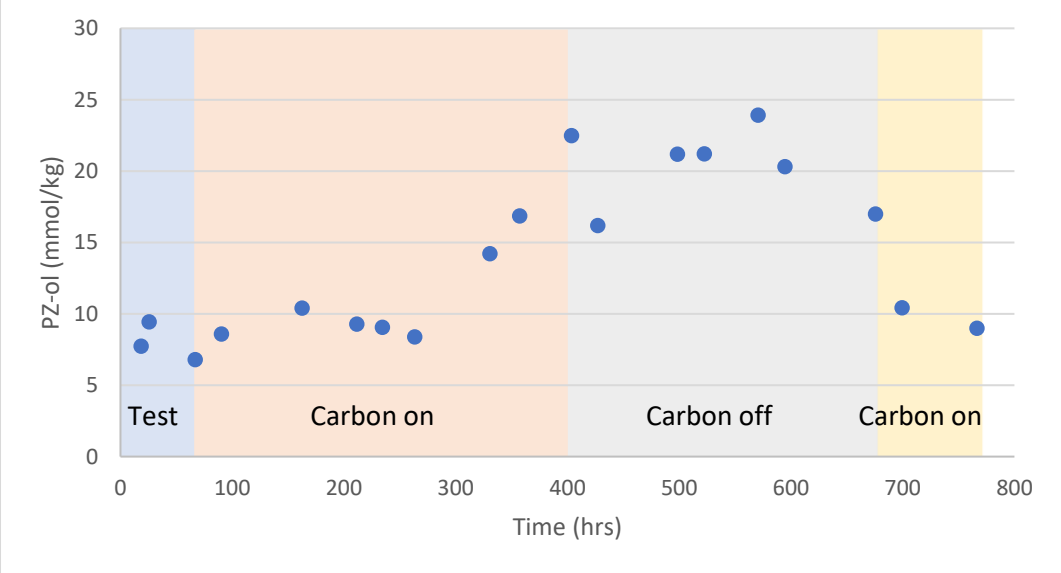

Figure 4-32: Normalized PZ-ol in HTOR 27 (55 ℃ to 150 ℃ , moderately degraded PZ, carbon bed, no N_2 sparging)

No PZ-one peak was observed in the HTOR 27 samples, so the PZ-one is smaller than the detection limit of 8 mmol/kg.

Excess 0.2 N H_2SO_4 was added to 0.8344 g of HTOR 27 used carbon to quantify the Fe removed more accurately. 8 batches of H_2SO_4 were added, and each batch was drained completely before the new batch was added. The time and amount of H_2SO_4 added is shown in Table 4-8.

Table 4-8: 0.2 N H_2SO_4 treatment to HTOR 27 used carbon

Time (hrs)	Mass of 0.2 N H_2SO_4 (g)
0.17	64.9148
0.34	68.9375
0.67	67.2767
1	66.1061
1.33	67.4479
1.67	64.7705
2	46.9824
2.5	24.6478

The dissolved Fe in the H_2SO_4 is shown in Figure 4-33. It became negligible after 267.2351 g of 0.2 N H_2SO_4 was used to rinse the carbon, and almost all the Fe was removed from the carbon. From the Fe concentration and the mass of 0.2 N H_2SO_4, the calculated Fe is 94.07 mmol/kg of carbon on the HTOR 27 used carbon. Since there is 36.3 mmol Fe/kg of carbon on the clean carbon, a total of 0.89 mmol Fe was adsorbed by the carbon in HTOR 27, which corresponds to 0.56 mmol Fe/kg solvent. The difference of Fe concentration before and after carbon treating is much smaller than 0.56 mmol/kg, suggesting that there is a stock of soluble Fe in the system that can dissolve into solvent immediately when the dissolved Fe is removed by the carbon bed.

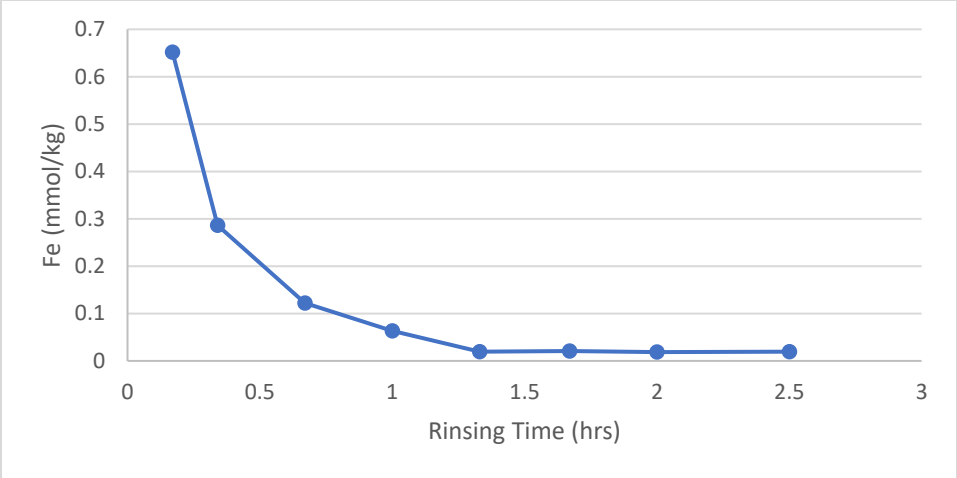

Figure 4-33: Fe in H_2SO_4 after rinsing carbon used in HTOR 27 (55 ℃ to 150 ℃ , moderately degraded PZ, carbon bed, no N_2 sparging)

4.5.2 HTOR 28: Moderately Degraded PZ from 55 ℃ to 150 ℃ with Carbon Treating and Nitrogen Sparging

In HTOR 28, the effect of carbon treating on oxidation was tested. Nitrogen sparging was applied in the middle of the experiment, testing the combined mitigation effect of carbon treating and nitrogen sparging. The experiment started with the NCCC 2019 end solvent, which is a moderately degraded solvent containing 30 mmol/kg total formate, 0.13 mmol/kg Fe, 9.6 mmol/kg EDA and 13.9 mmol/kg PZ-one. The solvent contained 1.6 mmol/kg Li^+, which was used as a tracer in the experiment to account for the water balance. A 7.5 L/min synthetic flue gas was created by mixing air with 0.5% CO_2 to maintain a loading of 0.25, which is close to the lean loading in real plant operations. The solvent was cycled between 55 ℃ and 150 ℃ at 0.2 L/min. The system experienced a severe water balance issue in the first 140 hrs, so the data were only reported after 140 hrs. The process changes in HTOR 28 are recorded in Table 4-9. Foaming was observed at the baseline condition and disappeared within 24 hrs after carbon treating was applied. Table 4-10 shows a summary of the rates of species measured in the HTOR 28.

Table 4-9: Process changes during HTOR 28

Time (hrs)	Process Change
140	Baseline (No carbon nor N_2)
214	Carbon treating
384	N_2 sparging
482	Carbon used up
578	End of experiment

Table 4-10: Summary of degradation and corrosion products, and PZ oxidation rate in HTOR 28

Species	Baseline	Carbon Bed	Carbon Bed + N_2 Sparging	Depleted carbon + N_2 Sparging
Gas-phase NH_3 rate (μmol/kg-hr^2)	2.42 ± 0.01	0.27 ± 0.01	-0.23 ± 0.01	1.40 ± 0.00
PZ (mmol/kg-hr)	-4.0 ± 1.3	-2.8 ± 0.6	-1.4 ± 0.5	-2.0 ± 0.2
320 nm absorbance (A/hr)	1.00 ± 0.10	0.17 ± 0.09	Constant at 200 A	0.69 ± 0.11
Total formate (mmol/kg-hr)	0.14 ± 0.3	0.08 ± 0.01	0.05 ± 0.02	0.06 ± 0.4
Total acetate mmol/kg-hr	0.01 ± 0.04	0.05 ± 0.01	0.10 ± 0.08	0.03 ± 0.03
Fe (μmol/kg-hr)	2.9 ± 0.2	Constant at 0.57 mmol/kg	-0.5 ± 0.3	2.4 ± 0.8
PZ-one (mmol/kg-hr)	0.52 ± 0.12	Constant (160 mmol/kg)	-0.29 ± 0.10	Constant (115 mmol/kg)

The NH_3 production rate, as shown in Figure 4-34, represented the oxidation rate of the PZ solvent. At the baseline condition, the NH_3 rate started low at 0.25 mmol/kg-hr and increased linearly at a rate of 02.42 ± 0.01 μmol/kg-hr^2. The trend of increase stopped when carbon treating was applied, but there was no step change in the NH_3 rate. Between 320 hrs to 357 hrs, the cooler was not working properly, which maintained the solvent after the cross exchanger at 75 ℃ instead of the desired 62 ℃ and caused a higher temperature in the reactor. The NH_3 rate decreased immediately after the cooler was reset, indicating that the oxidation occurs even at the relatively low temperature of 75 ℃ . After the nitrogen sparging was applied, there was a step decrease in the NH_3 rate, and the NH_3 rate started decreasing. In previous HTOR experiments with no carbon bed, the NH_3 rate decreased when nitrogen sparging was applied, but the NH_3 rate still increased as the experiment continued. At 483 hrs, the NH_3 rate started increasing at 1.4 μmol/kg-hr^2even though no operating changes were applied to the system, with the explanation believed to be depleted carbon. From 483 hrs to the end of the experiment, the results represented the mitigation effects of nitrogen sparging only. The slope of the NH_3 rate was 50% smaller with N_2 sparging compared to the baseline condition. The cumulative NH_3 produced throughout the experiment was 183.5 mmol/kg, which corresponded to an oxidation rate of 0.34 mmol PZ/kg-hr. To conclude, the nitrogen sparging reduces the NH_3 production rate and the rate of increase. Carbon treating does not reduce NH_3 production rate but reduces the rate of increase. Combining nitrogen sparging and carbon treating is more effective than applying nitrogen sparging or carbon treating separately.

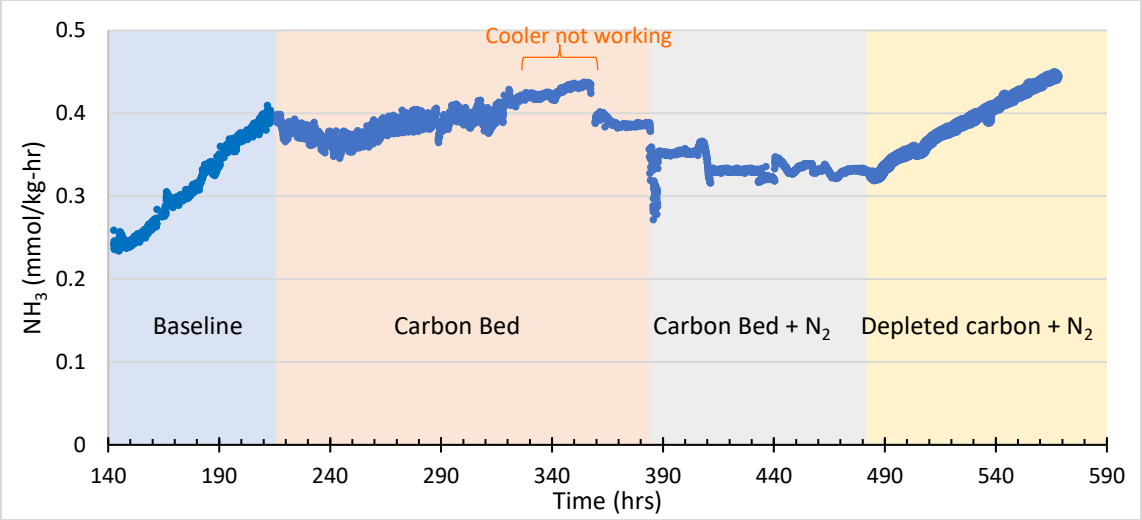

Figure 4-34: NH_3 production rate in HTOR 28 (0.5% CO_2, 55 ℃ to 150 ℃ , NCCC 2019 end solvent, carbon bed, and N_2 sparging)

The PZ concentration normalized by Li is plotted in Figure 4-35. The overall loss rate is 2.1 ± 0.2 mmol/kg-hr. This is 5 times the NH_3 production rate, and since little PZ was observed in the gas outlet, only 1 mol of NH_3 was produced when 5 mols of PZ was oxidized. The oxidation rate of PZ in each time period is included in Table 4-10, but since the concentration of PZ is large, the loss rate is not accurate enough in regions with only 4 or 5 data points.

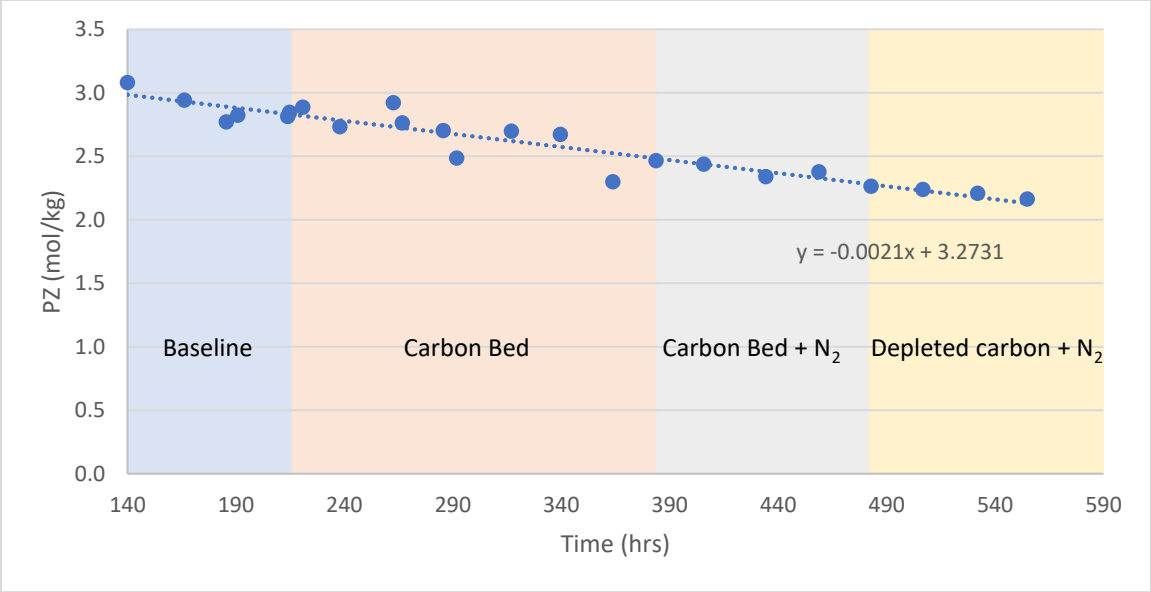

Figure 4-35: Normalized PZ in HTOR 28 (0.5% CO_2, 55 ℃ to 150 ℃ , NCCC 2019 end solvent, carbon bed, and N_2 sparging)

The dilution-corrected absorbance at 320 nm is shown in Figure 4-36. A very similar trend is shown in the 320 nm absorbance and the NH_3 rate as in Figure 4-34. At the baseline condition, the absorbance increased at 1.00 ± 0.10 A/hr. When the carbon bed was turned on, the accumulation rate decreased to 0.17 ± 0.09 A/hr. After the nitrogen sparging was turned on, the absorbance remained constant at 200 A, indicating that nitrogen sparging reduces the production rate of the complexing products. When the carbon bed was depleted, the absorbance increased again at a rate of 0.69 ± 0.11 A/hr.

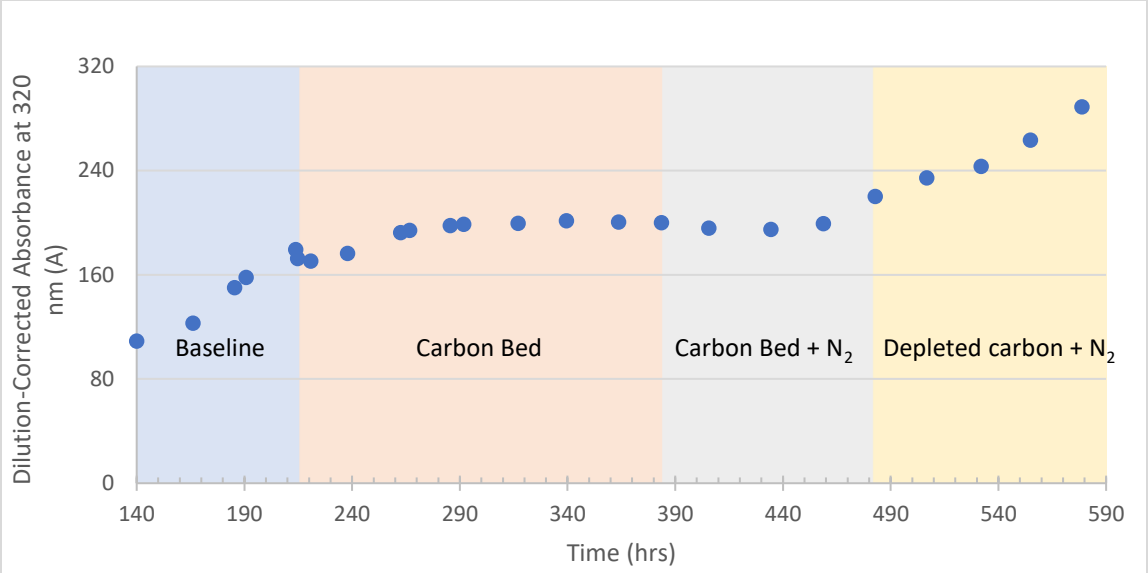

Figure 4-36: Dilution-corrected absorbance in HTOR 28 (0.5% CO_2, 55 °C to 150 °C , NCCC 2019 end solvent, carbon bed, and N_2 sparging)

The Fe concentration is shown in Figure 4-37. Compared to the initial Fe of 0.13 mmol/kg, the Fe throughout the experiment was considerably higher, indicating that the solubility limit in the HTOR is higher than the solubility limit in the NCCC. The Fe increased at the baseline condition at a rate of 2.9 ± 0.2 µmol/kg-hr. When the carbon bed was turned on, the Fe stayed relatively constant, and the Fe decreased at a rate of 0.5 ± 0.3 µmol/kg-hr when the N_2 sparging was turned on. When the carbon was depleted, the Fe started increasing again at 2.4 ± 0.8 µmol/kg-hr. From these sets of data, carbon treating reduces Fe at 2.9 µmol/kg-hr, and N_2 sparging reduces Fe at 0.5 µmol/kg-hr.

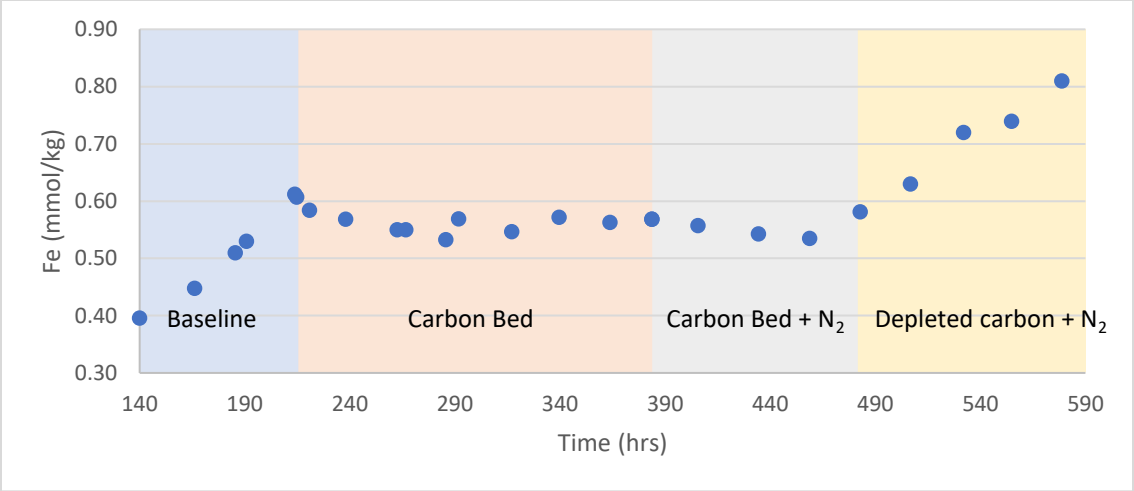

Figure 4-37: Fe in HTOR 28 (0.5% CO_2, 55 °C to 150 °C , NCCC 2019 end solvent, carbon bed, and N_2 sparging)

A strong correlation between NH_3, Fe, and the dilution-corrected absorbance was observed, and the three curves are plotted in Figure 4-38. The strong correlation shows that applying the carbon bed or the nitrogen sparging are both useful in mitigating oxidation and combining these two mitigation methods worked better than using either one of the methods alone.

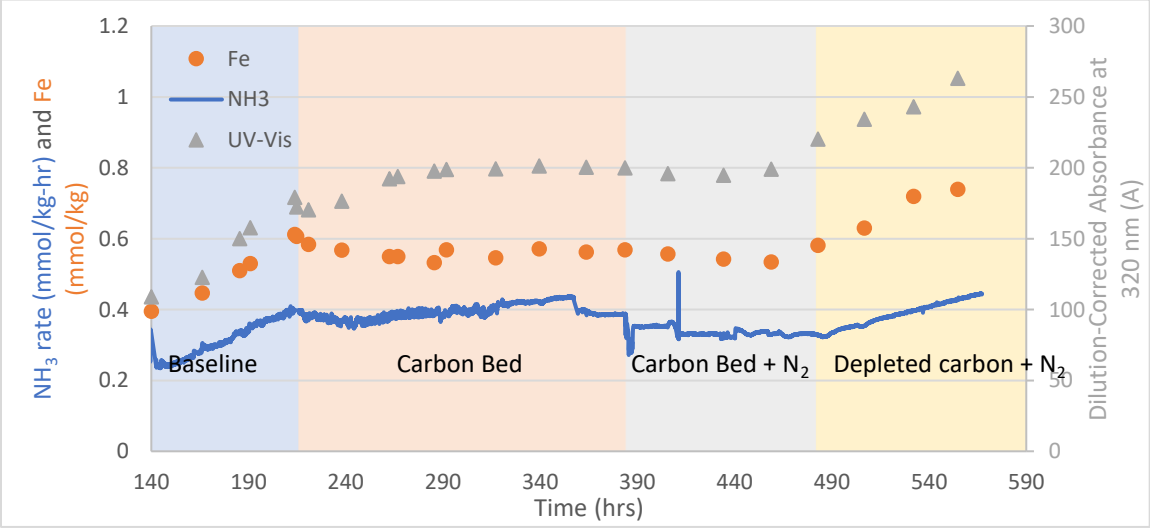

Figure 4-38: Correlation between NH_3, Fe, and dilution-corrected absorbance at 320 nm in HTOR 28 (0.5% CO_2, 55 °C to 150 °C , NCCC 2019 end solvent, carbon bed, and N_2 sparging)

The EDA concentration is plotted in Figure 4-39, EDA continues to decrease, and no significant difference in decomposition rate is observed, so the degradation of EDA is independent of the application of carbon bed or N_2 sparging.

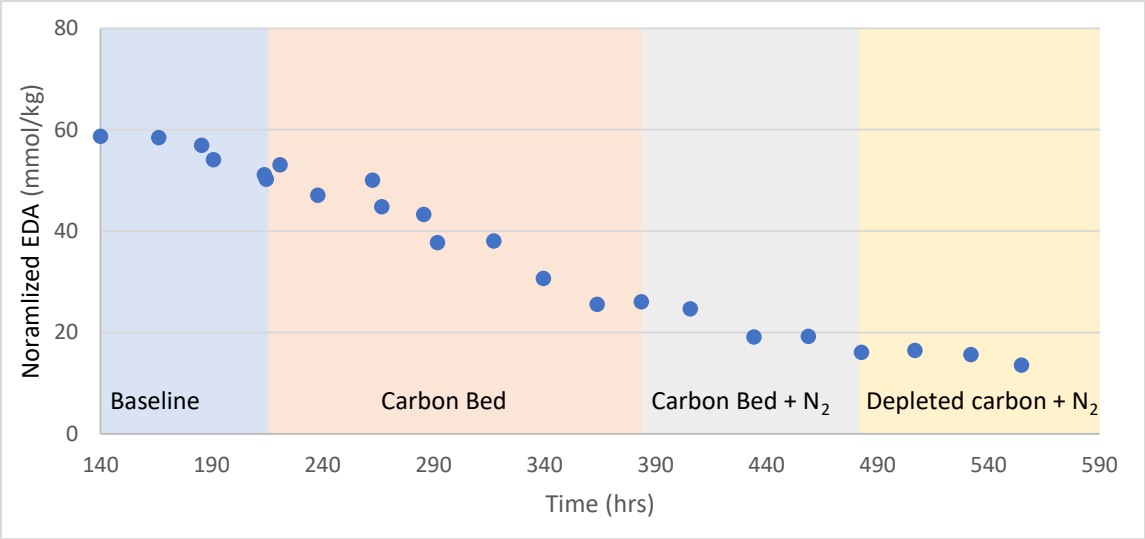

Figure 4-39: EDA normalized by Li in HTOR 28 (0.5% CO_2, 55 ℃ to 150 ℃ , NCCC 2019 end solvent, carbon bed, and N_2 sparging)

The PZ-one concentration is plotted in Figure 4-40. At the baseline condition, the PZ-one increased linearly at 0.52 ± 0.12 mmol/kg-hr, and the PZ-one stopped increasing and leveled out at 160 mmol/kg with the carbon bed. After N_2 sparging was applied, the PZ-one started to decrease at 0.29 ± 0.10 mmol/kg-hr until the effects of the carbon bed diminished.

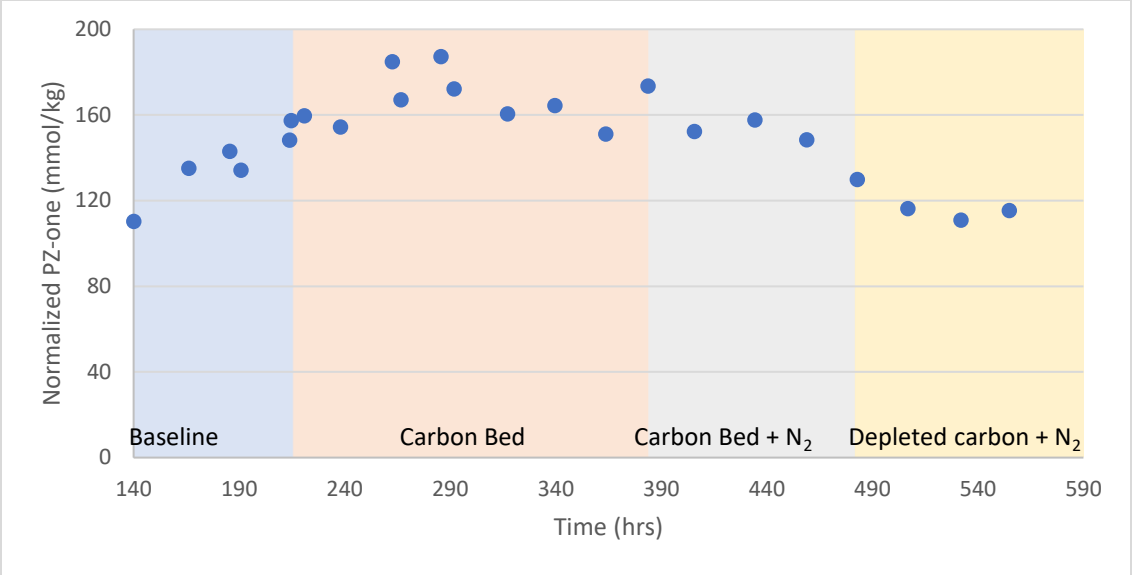

Figure 4-40: PZ-one concentration normalized by Li in HTOR 28 (0.5% CO_2, 55 ℃ to 150 ℃ , NCCC 2019 end solvent, carbon bed, and N_2 sparging)

The concentrations of total anions are plotted in Figure 4-41. A lag is observed while applying the carbon bed, which was consistent with the total heat stable salts results in HTOR 27 plotted in Figure 4-31. The rate of accumulation in different periods is included in Table 4-10. The formate increases fastest at the baseline condition and increases at the smallest rate when applied both carbon treating and N_2 sparging. However, the behavior of the total acetate is opposite, where the smallest rate happened at the baseline condition, and the fastest rate with both mitigation method. This suggests that when carbon treating and N_2 sparging were applied, the production of acetate is favored compared to formate.

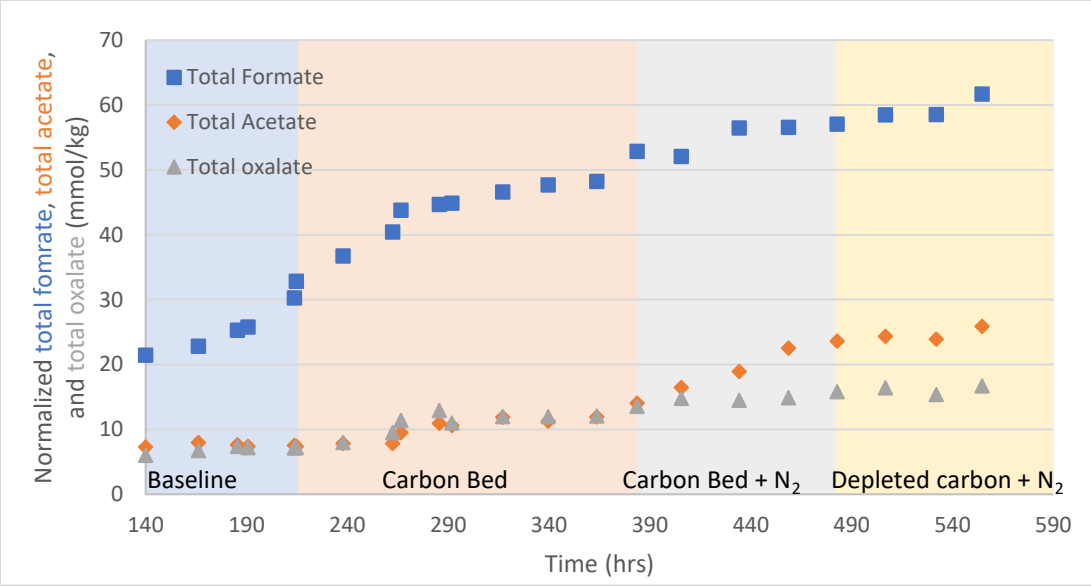

Figure 4-41: Total formate, total acetate, and total oxalate normalized by Li in HTOR 28 (0.5% CO_2, 55 ℃ to 150 ℃ , NCCC 2019 end solvent, carbon bed, and N_2 sparging)

The normalized stainless steel metal ion concentrations are shown in Figure 4-42. All the metal ion concentrations increased when there was no carbon bed applied, which was due to corrosion of stainless steel. The increase of Ni was not a function of carbon treating or nitrogen sparging. The Mn decreased when there was a working carbon bed, which matched the previous observance that the carbon bed can remove dissolved Mn at a low rate. The Cr decreased when the carbon bed was turned on but reached a steady state when the Cr reached 0.32 mmol/kg.

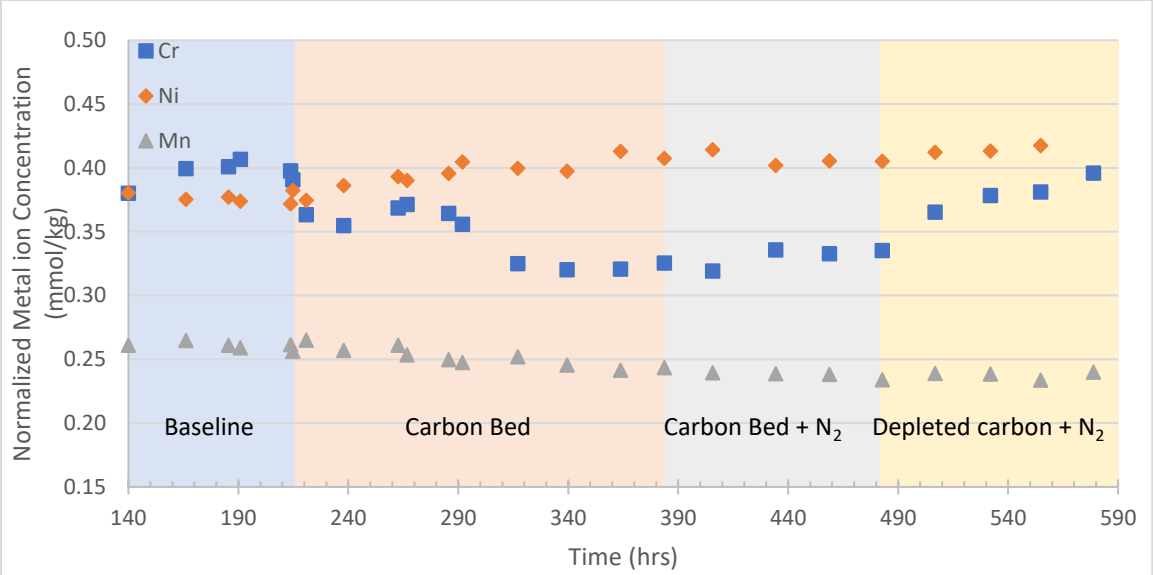

Figure 4-42: Normalized metal ion concentrations in HTOR 28 (0.5 % CO_2, 55 ℃ to 150 ℃ , NCCC 2019 end solvent, carbon bed, and N_2 sparging)

Excess 0.2 N H_2SO_4 was added to 1.2483 g of HTOR 28 end carbon to quantify the Fe removed more accurately. 8 batches of H_2SO_4 were added, and each batch was drained completely before the new batch was added. The time and amount of H_2SO_4 added is shown in Table 4-11. The Fe concentration became negligible after 255.97 g of 0.2 N H_2SO_4 was used to rinse the carbon, and almost all the Fe was removed from the carbon. From the Fe concentration and the mass of 0.2 N H_2SO_4, it is calculated that there were 67.37 mmol Fe/kg of carbon on the SRP used carbon. Since there 36.3 mmol Fe/kg of carbon on the clean carbon, a total of 0.48 mmol Fe was adsorbed by the carbon in the HTOR 28, which corresponds to 0.30 mmol Fe/kg solvent with an inventory of 1.6 L. Similar to results from HTOR 27, this concentration is much larger than the difference of Fe before and after carbon treating, confirming the dissolve of Fe colloids.

Table 4-11: 0.2 N H_2SO_4 treatment to HTOR 28 used carbon

Time (hrs)	Mass of 0.2 N H_2SO_4 (g)	[Fe] in H_2SO_4 (mmol/kg)
0.17	64.40	0.71
0.34	63.49	0.31
0.67	64.58	0.10
1	63.49	0.07
1.33	67.49	0.03
1.67	65.39	0.02
2	69.46	0.03
2.5	69.49	0.03

4.5.3 HTOR 29: Moderately Degraded PZ from 55 ℃ to 150 ℃ with Carbon Treating and Nitrogen Sparging

HTOR 29 was designed to be a parallel experiment of HTOR 28. The experiment started with the NCCC 2019 end solvent, which was the same initial solvent as in HTOR 28. 15.5 g of carbon was applied at the beginning of the experiment and was bypassed at 142 hrs. The system run a baseline condition from 142 to 414 hrs, and then nitrogen sparging was applied till the end of the experiment. A 7.5 L/min synthetic flue gas was created by mixing air with 0.5% CO_2 to maintain a loading of 0.25, which is close to the lean loading in real plant operations. The solvent was cycled between 55 ℃ and 150 ℃ at 0.2 L/min. The process changes in HTOR 29 are recorded in Table 4-12. Table 4-13 shows a summary of the rates of species measured in the HTOR 29.

Table 4-12: Process changes during HTOR 29

Time (hrs)	Process Change
0	Carbon treating
142	Bypassed carbon
414	N_2 sparging
600	N_2 sparging at double liquid depth
664	End of experiment

Table 4-13: Summary of degradation and corrosion products, and PZ oxidation rate in HTOR 29

Species	Carbon Bed	Baseline	N_2 Sparging
Gas-phase NH_3 rate ($\mu mol/kg\text{-}hr^2$)	0.30 ± 0.01	1.51 ± 0.01	0.81 ± 0.02
PZ (mmol/kg-hr)	-1.4 ± 0.2	-2.6 ± 0.4	-1.5 ± 0.5
320 nm absorbance (A/hr)	0.18 ± 0.01	0.52 ± 0.03	0.23 ± 0.02
Total formate (mmol/kg-hr)	0.07 ± 0.02	0.12 ± 0.01	0.05 ± 0.04
FPZ (mmol/kg-hr)	0.06 ± 0.01	0.11 ± 0.01	0.05 ± 0.02
Total oxalate mmol/kg-hr	0.008 ± 0.005	0.045 ± 0.004	0.026 ± 0.004
Fe (μmol/kg-hr)	-1.4 ± 0.2	2.7 ± 0.2	2.3 ± 0.4
PZ-one (mmol/kg-hr)	-0.08 ± 0.05	0.16 ± 0.04	Constant (150 mmol/kg)

The gas phase NH_3 is shown in Figure 4-43. In the first 30 hrs, the NH_3 production dropped from 0.4 mmol/kg-hr to 0.06 mmol/kg-hr, which is due to the stripping of NH_3 dissolved in the stock solvent. With carbon treating, the NH_3 rate increased linearly at 0.30 ± 0.01 $\mu mol/kg\text{-}hr^2$, which is equal to the rate observed in the carbon treated region in

HTOR 28. After the carbon bed is bypassed, NH_3 rate increased at a higher rate at 1.51 ± 0.01 μmol/kg-hr^2, smaller than the 2.42 ± 0.01 μmol/kg-hr^2 observed in the baseline region in HTOR 28. This indicates that the effect of carbon lasted, possibly due to the removal of catalytical degradation products or NH_3 precursors. When the N_2 sparging was turned on, the NH_3 rate decreased by 0.12 mmol/kg-hr, and the acceleration rate was halved to 0.81 ± 0.2 μmol/kg-hr^2. The cumulative NH_3 production was 200.5 mmol/kg in HTOR 29, which corresponds to a PZ oxidation rate of 0.3 mmol/kg-hr.

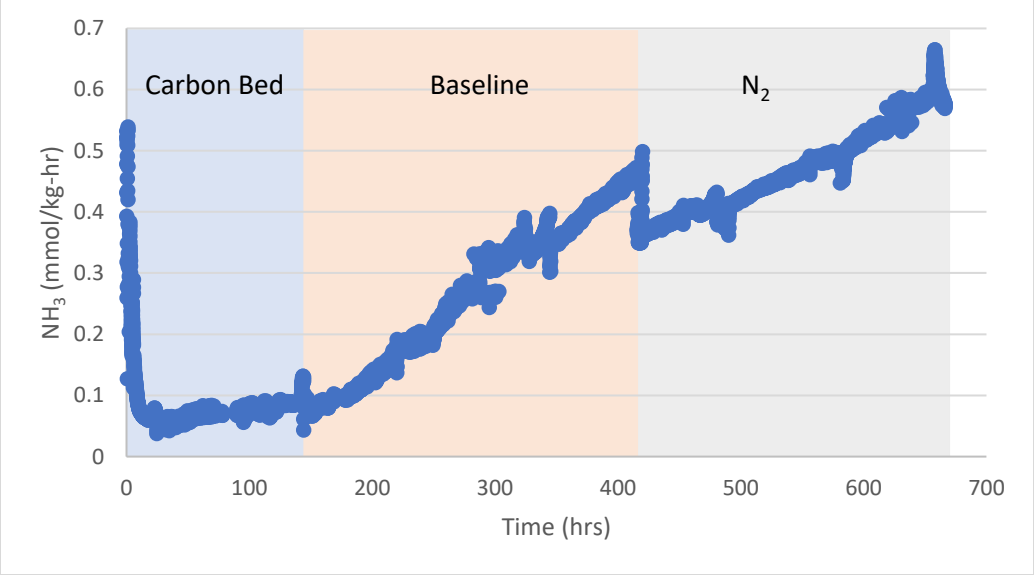

Figure 4-43: NH_3 rate in HTOR 29 (0.5 % CO_2, 55 ℃ to 150 ℃ , NCCC 2019 end solvent, carbon bed, and N_2 sparging)

The PZ concentration normalized by Li is plotted in Figure 4-44. The overall loss rate is 2.0 ± 0.1 mmol/kg-hr. The PZ oxidation rate was 1.4 ± 0.2 mmol/kg-hr in carbon treating, 2.6 ± 0.4 mmol/kg-hr in baseline, and 1.5 ± 0.5 mmol/kg-hr with N_2 sparging. The rate in the baseline was smaller than in HTOR 28, indicating that the effects of carbon treating in the first 140 hrs lasted after the carbon was bypassed due to the removal of possible catalytic products. Therefore, it is better to apply carbon treating in the early stage of oxidation.

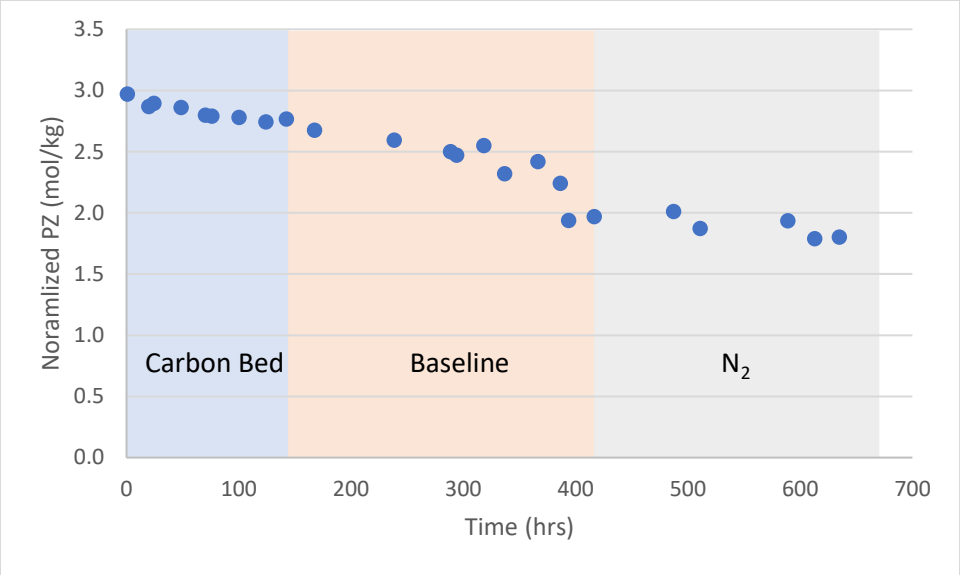

Figure 4-44: PZ normalized by Li in HTOR 29 (0.5 % CO_2, 55 ℃ to 150 ℃ , NCCC 2019 end solvent, carbon bed, and N_2 sparging)

The dilution-corrected absorbance at 320 nm is plotted in Figure 4-45. While being carbon treated, the absorbance increased at 0.18 ± 0.01 A/hr, which was the same rate in the carbon treated region in HTOR 28. When the carbon bed was bypassed, the absorbance increased at 0.52 ± 0.03 A/hr. Compared to the 1 A/hr at the baseline condition in HTOR 28, we see that although the carbon bed was bypassed, the removal slows down the accumulation of UV-absorbing components, thus applying carbon treating in the early stages of oxidation can have a better effect. When N_2 sparging was applied, absorbance increased steadily at 0.23 ± 0.02 A/hr. Combining the results from HTOR 28, N_2 sparging reduces the accumulation rate by 0.3 A/hr, and this rate is not related to the initial rate of accumulation before N_2 sparging. No change is observed when larger liquid depth was used for N_2 sparging.

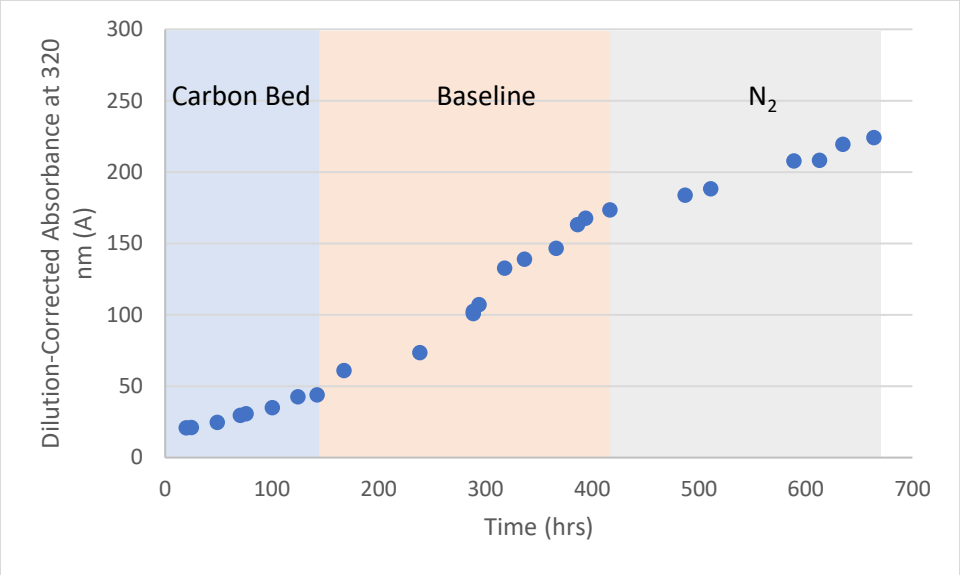

Figure 4-45: Dilution-corrected absorbance at 320 nm in HTOR 29 (0.5 % CO_2, 55 °C to 150 °C , NCCC 2019 end solvent, carbon bed, and N_2 sparging)

The raw Fe concentration is plotted in Figure 4-46. At the start of the experiment, when the carbon bed was applied, Fe decreases at -1.4 ± 0.3 µmol/kg-hr initially after reaching 0.05 mmol/kg. After that, the small concentration of dissolved Fe resulted in a small removal rate, so no further decrease was observed in the Fe. When the carbon bed was bypassed, the Fe accumulation rate increased significantly to 2.7 ± 0.2 µmol/kg-hr, which is the same rate observed in the baseline region in HTOR 28. This suggests that the accumulation of Fe is not dependent on if the solvent has been treated or not. Even after treatment, the Fe continues to increase at the same rate once the carbon bed is bypassed. Therefore, to maintain low Fe in operation, the carbon bed needs to be kept on consistently. When the N_2 sparging was initiated, the Fe increased at 2.3 ± 0.4 µmol/kg-hr, which is the same rate observed between 480 and 580 hrs in HTOR 28. This confirms that N_2 sparging can reduce the Fe accumulation rate, and the depleted carbon has no effects on Fe. When a larger liquid depth was used, the Fe accumulation rate seems to decrease furthermore, but due to the short period of time, this conclusion needs further validation.

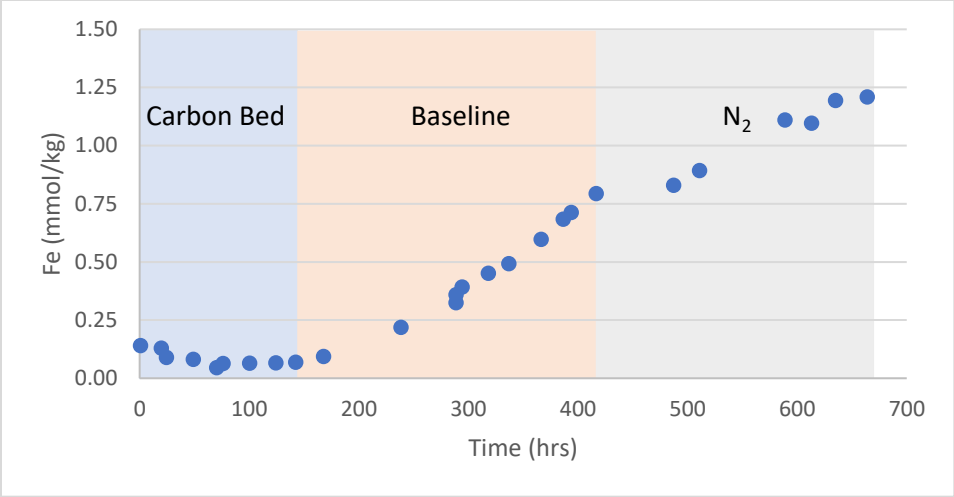

Figure 4-46: Fe in HTOR 29 (0.5 % CO_2, 55 ℃ to 150 ℃ , NCCC 2019 end solvent, carbon bed, and N_2 sparging)

The normalized stainless steel metal ion concentrations are shown in Figure 4-47. Similar to HTOR 28 results, all the metal ion concentrations increased when there was no carbon bed applied, which was due to corrosion of stainless steel. The Cr decreased when the carbon bed was turned on and reached 0.11 mmol/kg. Both the removal rate and accumulation rate were the same as in the HTOR 28.

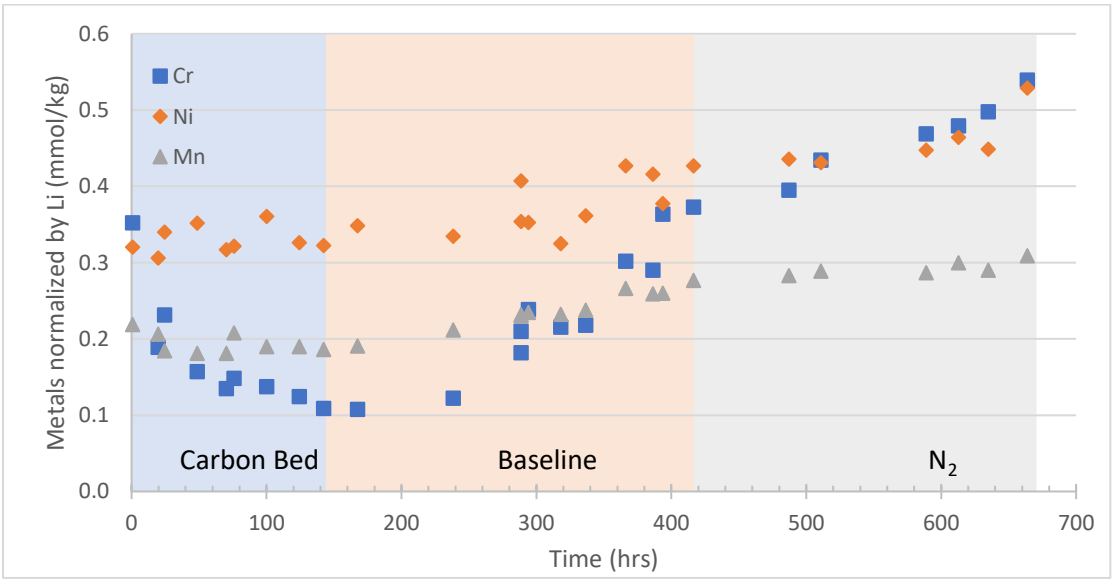

Figure 4-47: Normalized metal ion concentrations in HTOR 29 (0.5 % CO_2, 55 ℃ to 150 ℃ , NCCC 2019 end solvent, carbon bed, and N_2 sparging)

The PZ-one concentration is normalized by Li and plotted in Figure 4-48. At the baseline condition, the PZ-one decreased at 0.08 ± 0.05 mmol/kg-hr with carbon treating and increased linearly at 0.16 ± 0.04 mmol/kg-hr in the baseline. PZ-one stopped increasing and leveled out at 150 mmol/kg with N_2 sparging. This result also matched the results in HTOR, and the accumulation rate in HTOR 29 at baseline condition is smaller than that in HTOR 28, suggesting the benefits of applying carbon treating early.

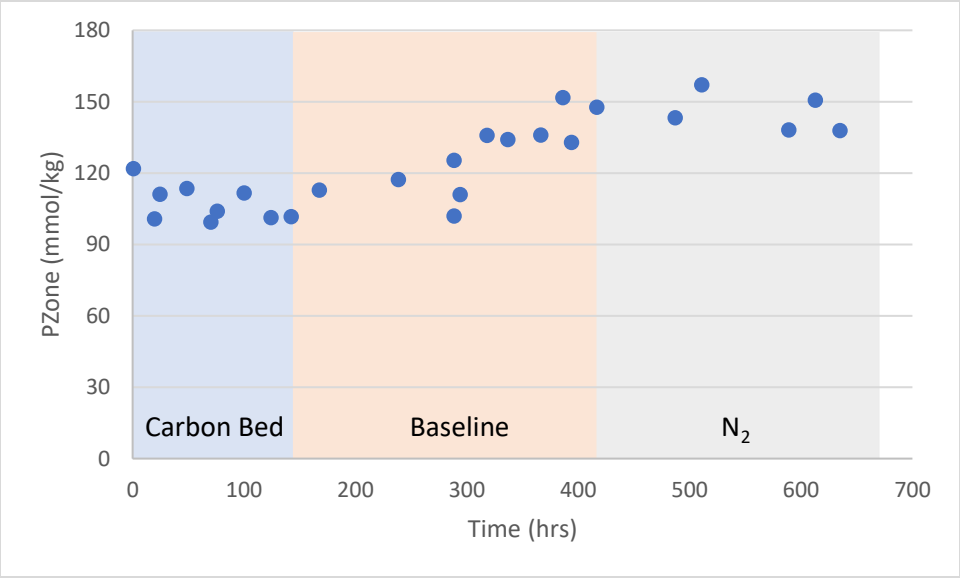

Figure 4-48: Normalized PZ-one concentrations in HTOR 29 (0.5 % CO_2, 55 ℃ to 150 ℃ , NCCC 2019 end solvent, carbon bed, and N_2 sparging)

The EDA normalized by Li is plotted in Figure 4-49, the EDA accumulated steadily until it reached 50 mmol/kg. The concentration decreased after that, and no significant difference in decomposition rate is observed, which is the same result observed in HTOR 28.

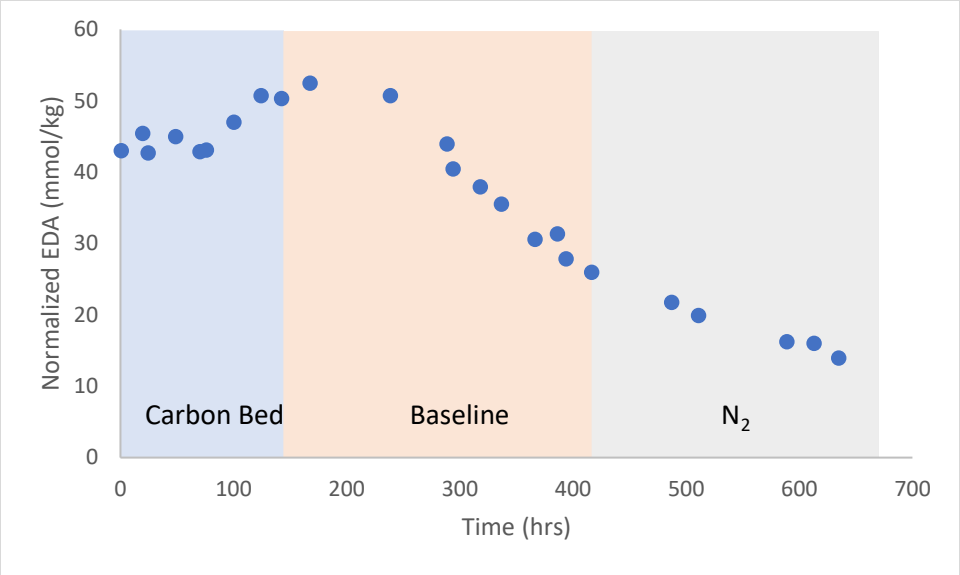

Figure 4-49: Normalized EDA concentrations in HTOR 29 (0.5 % CO_2, 55 ℃ to 150 ℃ , NCCC 2019 end solvent, carbon bed, and N_2 sparging)

The normalized total formate, FPZ, and formate concentrations are plotted in Figure 4-50. Most of the formate existed as FPZ. The formate increased at a small rate and was independent of the operating conditions. The accumulation rate of total formate and FPZ were included in Table 4-13. The highest rate was observed in the baseline region. Compared to HTOR 28, the formate accumulation rate in baseline is smaller, suggesting that carbon treating removed precursors of formate, therefore the effects on formate existed even when the carbon was bypassed. As a result, applying carbon treating in the early stage of oxidation may be more effective.

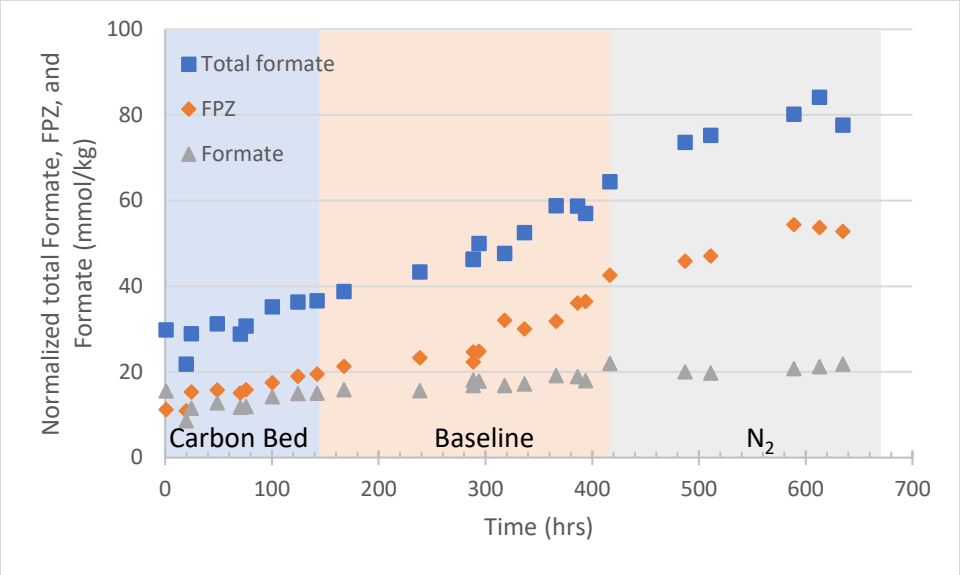

Figure 4-50: Total formate, FPZ, and formate normalized by Li in HTOR 29 (0.5 % CO_2, 55 °C to 150 °C , NCCC 2019 end solvent, carbon bed, and N_2 sparging)

The normalized total acetate, propionate, and oxalate were plotted in Figure 4-51. The total acetate increased at 0.032 ± 0.001 mmol/kg-hr and did not vary due to the operating conditions. The propionate accumulated slowly at 0.002 ± 0.000 mmol/kg-hr. The total oxalate increased at 0.008 ± 0.005 mmol/kg-hr with carbon treating, 0.045 ± 0.004 mmol/kg-hr in baseline, and 0.026 ± 0.004 mmol/kg-hr with N_2 sparging.

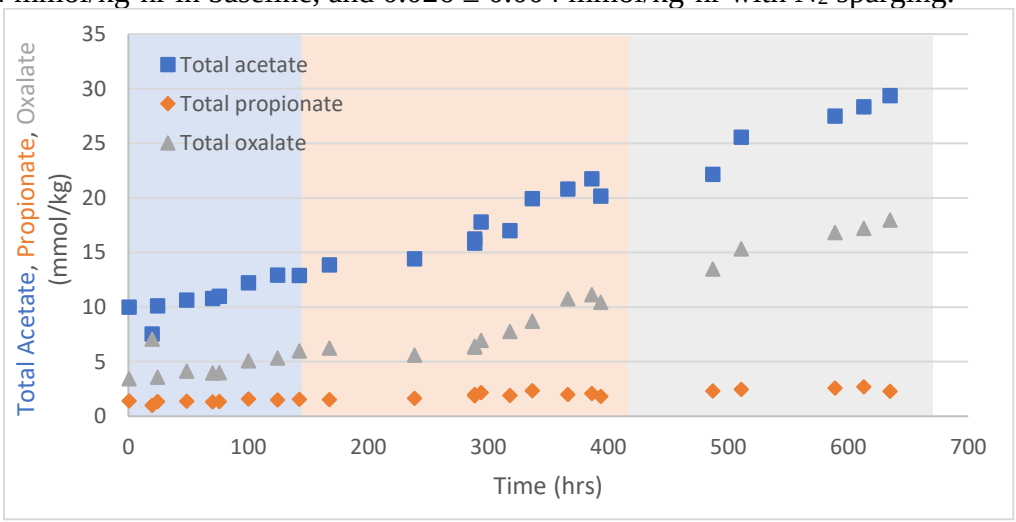

Figure 4-51: Total anions normalized by Li in HTOR 29 (0.5 % CO_2, 55 °C to 150 °C , NCCC 2019 end solvent, carbon bed, and N_2 sparging)

Excess 0.2 N H_2SO_4 was added to 2.955 g of HTOR 29 end carbon to quantify the Fe removed more accurately. 8 batches of H_2SO_4 were added, and each batch was drained completely before the new batch was added. The time and amount of H_2SO_4 added is shown in Table 4-14. The Fe concentration became negligible after 333.88 g of 0.2 N H_2SO_4 was used to rinse the carbon, and almost all the Fe was removed from the carbon. From the Fe concentration and the mass of 0.2 N H_2SO_4, it is calculated that there was 48.4 mmol Fe/kg of carbon on the HTOR end carbon. Since there was 36.3 mmol Fe/kg of carbon on the clean carbon, a total of 0.19 mmol Fe was adsorbed by the carbon in HTOR 29, which corresponds to 0.12 mmol Fe/kg solvent with a total inventory of 1.6 L. Similar to results from HTOR 27 and HTOR 28, this concentration is much larger than the difference of Fe before and after carbon treating, confirming the dissolve of Fe colloids.

Table 4-14: 0.2 N H_2SO_4 treatment to HTOR 29 end carbon

Time (hrs)	Mass of 0.2 N H_2SO_4 (g)	[Fe] in H_2SO_4 (mmol/kg)
0.17	66.03	1.03
0.34	69.24	0.39
0.67	67.66	0.29
1	68.41	0.20
1.33	62.55	0.16
1.67	66.71	0.04
2	69.62	0.02
2.5	66.87	0.02

4.6 COMPARISONS BETWEEN HTOR EXPERIMENTS

The regressed PZ loss rates in HTOR 23, 25, 27, 28, and 29 are compiled in Figure 4-52. Due to the absence of tracers, the PZ in HTOR 22 was largely affected by the water balance, and no meaningful loss rate can be estimated from the data. Therefore, the results from HTOR 22 were not included. The dashed lines are two baseline experiments run previously in HTOR with clean PZ. The PZ loss rate in HTOR 23 was the same as in the HTOR 15, showing that EDA had no catalytic effects on PZ oxidation. In HTOR 25, the PZ loss rate was much higher rate than HTOR 15, indicating that the formaldehyde can react with PZ and accelerate PZ oxidation. The PZ loss rate in HTOR 27 was significantly higher than in other experiments because a leak occurred during the experiment, causing additional solvent loss. The loss rate in HTOR 28 and 29 are higher than the other experiments because they started with a more degraded solvent.

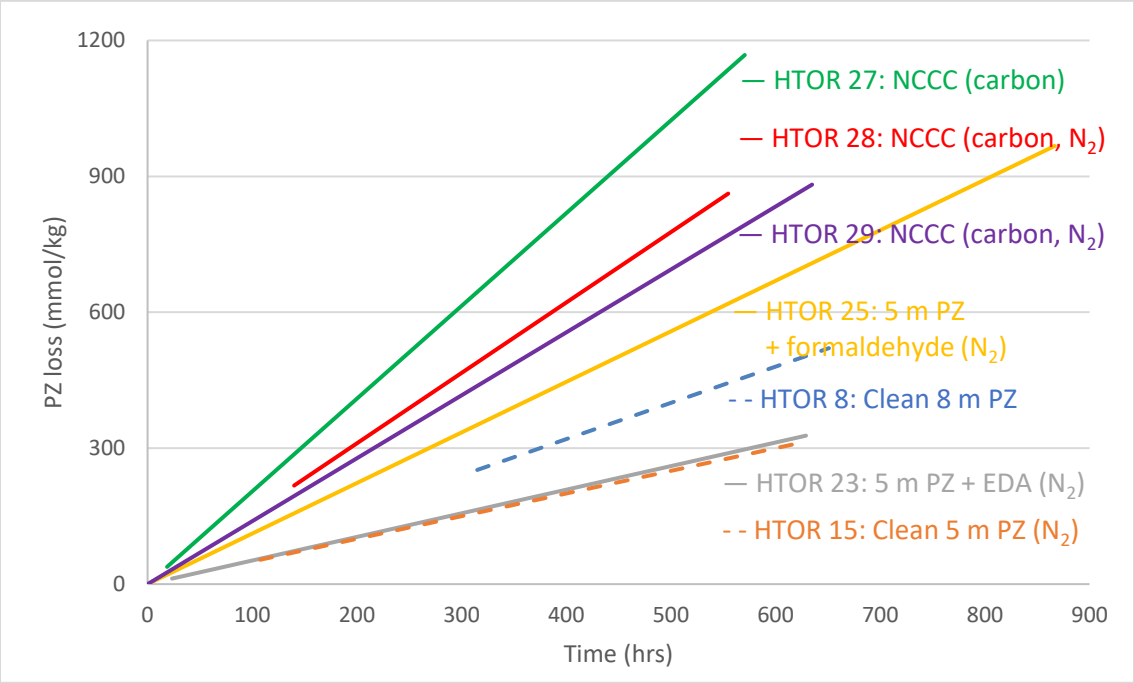

Figure 4-52: PZ loss rate comparison in HTOR experiments

The N balance of the PZ oxidation in all the HTOR experiments are shown in Table 4-15, which includes the newly produced degradation products, the amount of volatile amine loss, and the total loss of PZ. The units for all the species are in mmol/kg. The % N are much higher in HTOR 22, 23, and 25 than in HTOR 27, 28, and 29, and can be caused by two reasons. The carbon bed removed the degradation products generated by oxidation, and therefore the accumulation of degradation products in liquid samples were underestimated. It was also possible that when the solvent become more degraded, unknown degradation products were produced.

Table 4-15: N balance of the HTOR experiments

	HTOR 22	**HTOR 23**	**HTOR 25**	**HTOR 27**	**HTOR 28**	**HTOR 29**
NH_3	313.8	256.8	301.6	407.7	183.4	198.6
Volatile PZ	33.4	77.8	68.2	22.3	27.1	25.2
PZ-one	-2.7		30.5		20.1	16.0
PZ-ol	-1.4			1.2		
EDA	-6.0	-86.2	38.9	3.9	-45.0	-22.0
MPZ	3.8	10.1	28.2	14.2		8.3
FPZ	41.3	14.1	39.7	-1.5	4.5	41.7
PZ loss	286.4	172.5	831.6	1700.0	767.4	846.5
% N	78.7	83.6	42.8	14.4	12.8	19.9

The correlations between the cumulative production and PZ loss rate in the HTOR 23, 25, 27, 28, and 29 are shown in Figure 4-53. While previous experiments suggested

that 1 mol of PZ oxidized into 1 mol of NH_3 (Voice, 2013), different results were observed in these HTOR experiments. HTOR 23 was close to the 1:1 ratio if taking the volatile PZ loss off the total PZ loss. In HTOR 25, the formaldehyde addition caused a smaller NH_3 production per mol of PZ, and this ratio increased after the last formaldehyde addition, indicating that the PZ reaction with formaldehyde produced fewer NH_3 and different final products. The results from HTOR 27, 28, and 29 were close to each other, and the 0.23 mol NH_3 was produced per mol of PZ loss. The results in HTOR 27 should underestimate the ratio because of the PZ leakage. The lower NH_3 production can be caused by the carbon treating, where the precursors of NH_3 got adsorbed and removed from the solvent. It is also possible that the solvent from the NCCC followed different pathways and produced less NH_3.

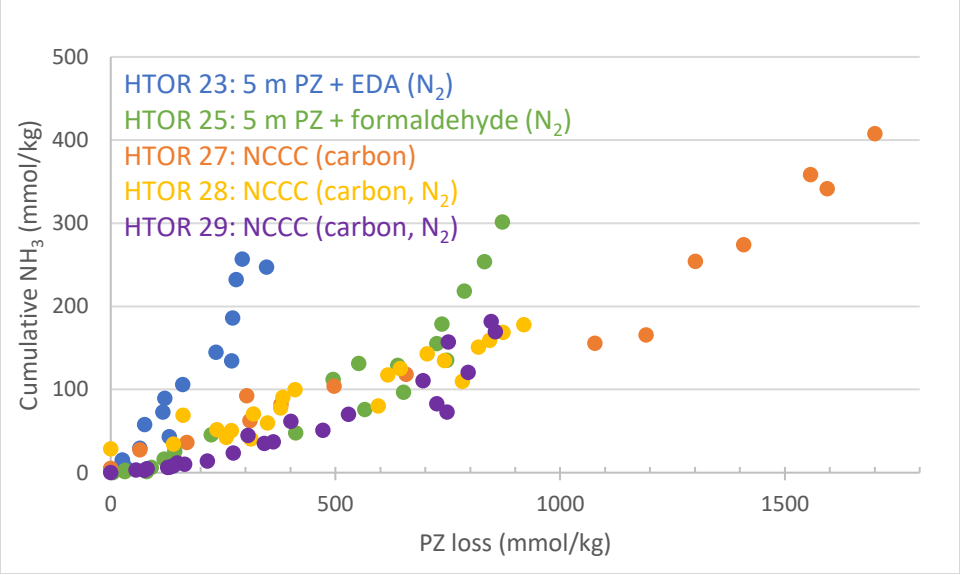

Figure 4-53: Relationship between PZ loss and NH_3 production in HTOR experiments

Despite the previous observation that 7 mols of NH_3 were produced every 1 mol of formate (Nielsen, 2018), the NH_3 to formate production ratio was different in the newly performed HTOR experiments. A more consistent relationship was observed on the ratio

between total formate production and PZ loss. The results in HTOR 27 underestimate the ratio because of the PZ leakage. In all the other experiments, 0.05 ± 0.02 mols of total formate were produced per mole of PZ loss.

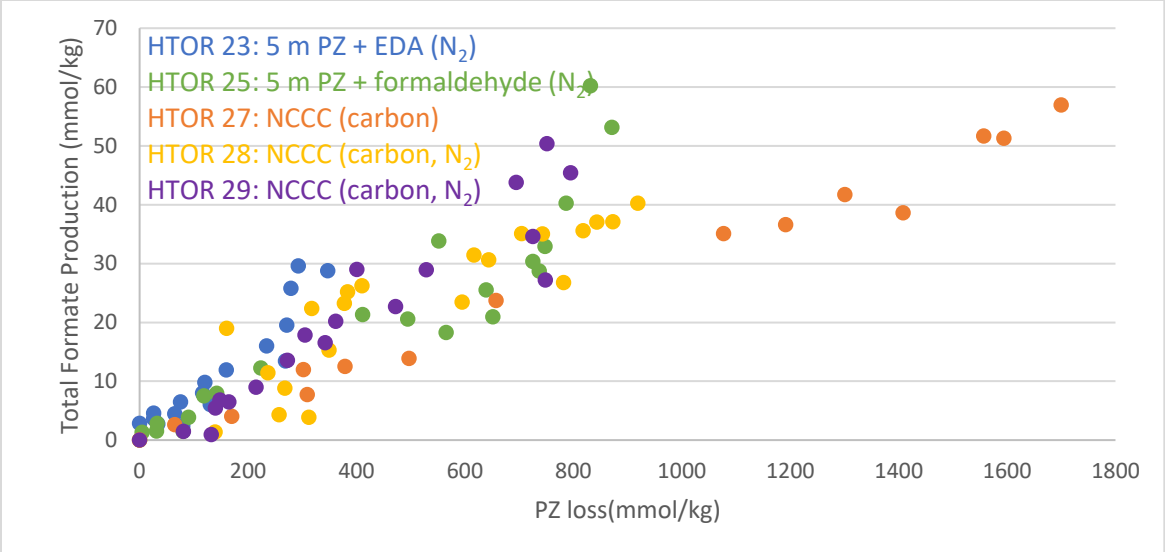

Figure 4-54: Relationship between PZ loss and formate production in HTOR experiments

4.7 CONCLUSIONS

1. All the HTOR samples have strong UV-Vis absorbance at 320 nm. The peak increases as the solvent becomes more degraded, indicating that the absorbance is due to accumulation of degradation or corrosion products.
2. The PZ loss in the HTOR varied between 0.5 mmol/kg-hr and 1.5 mmol/kg-hr. The oxidation rate is higher on degraded solvent.
3. The previous observation of 1 mol of NH_3 production per mol of PZ oxidation only holds true in less degraded solvent. When the solvent is more degraded, different oxidation pathways exist and 1 mol of PZ only produces 0.23 mol of NH_3.

4. For every mol of PZ oxidized, 0.05 mols of total formate were produced. Although a linear relationship was observed between NH_3 production and total formate production, the slopes are not consistent in different HTOR experiments.
5. Increasing the temperature of the trim cooler from 62 to 75 ℃ increased the NH_3 production rate. Therefore, in commercial units, the locations above 75 ℃ are of interest when studying PZ oxidation.
6. Adding EDA into PZ solvent does not affect the oxidation rate of PZ. More NH_3 is observed in the experiment due to EDA degradation, but the NH_3 from PZ holds constant. Therefore, EDA does not affect the degradation of PZ.
7. Adding antifoam diminishes the effect of N_2 sparging. It is possible that the foaming produced extra surface area that strengthens the effects of N_2 sparging.
8. Reducing O_2 in inlet gas by 66% reduced NH_3 production rate by 50% and decreases iron concentration. Other metals were not affected by changing O_2 concentration.
9. Formaldehyde increases NH_3 production rate, and a larger increase is observed in more degraded samples. Dissolved Fe increased along with the increase in NH_3 production rate. Formaldehyde can accelerate PZ oxidation. Possible mechanisms include the nucleophilic addition with PZ, formation of peroxides, and the reaction of peroxides with PZ and degradation solvents in the solvent.
10. Carbon treating is effective in removing degradation and corrosion products and mitigating oxidation in the HTOR. When carbon treating is applied, the second derivative of NH_3 rate decreases, the UV-Vis absorbance at 320 nm decreases, and the accumulation rate of Fe and total formate decreases. Carbon treating can remove Cr and Mn from the solvent and stop the solvent from foaming. 15.5 g of carbon on 1.6 L of NCCC degraded solvent reduces PZ oxidation rate by 0.4 mmol/kg-hr.

11. The Fe removed by the carbon bed is larger than the result calculated from the solvent inventory and concentration difference of Fe in solvent. This is because the Fe colloids or other “soluble” Fe can dissolve into the solvent when the Fe in solvent is adsorbed by the carbon.
12. Combining carbon treating and nitrogen sparging is more effective in oxidation mitigation than applying the methods separately. Observations included decrease in NH_3 production rate, UV-Vis absorbance at 320 nm, accumulation rate of Fe and total formate.
13. The effects of carbon treating lasts when the carbon is bypassed, which is possibly due to the removal of catalytic degradation products. Therefore, it is better to apply carbon treating in the early stage of oxidation
14. EDA always accumulates at the beginning of degradation. After EDA reaches 40 to 50 mmol/kg in the HTOR, the rate of EDA degradation is faster than the rate of EDA production. Such behavior is not affected by the operational changes.

Chapter 5. Pilot-Scale Oxidation

5.1 Overview of Pilot Plant Campaigns

This chapter includes the data from four pilot plant campaigns: two at the National Carbon Capture Center (NCCC) in Wilsonville, Alabama, and two at the Separations Research Program (SRP) at the University of Texas at Austin. The oxidative degradation was studied and compared with previous pilot plant results using PZ, including results from Pilot Plant 2 (PP2), SRP from 2009 to 2015 in Austin, TX, and CSIRO Tarong in Queensland, Australia.

PP2 used a slipstream of real flue gas from a coal-fired boiler, which had been treated with selective catalytic reduction and flue gas desulfurization to reduce SO_x and NO_x. 8 m PZ was used, and the campaign used a simple stripper operating from 120 ℃ to 150 ℃ (Nielsen, 2018).

SRP treated a synthetic flue gas equivalent to 0.1–0.2 MW, typically consisting of air and 12 kPa CO_2 at 350 to 500 ACFM. 5 to 8 m PZ was used, and both simple stripper and advanced stripper configurations were tested. The stripper temperature was controlled at 150 ℃ (Nielsen, 2018). The SRP campaign from 2009 to 2015 started with clean 8 m PZ and added 1 wt% Inh A (potassium iodide) into the solvent (Nielsen, 2017). The SRP campaign in 2018 and 2022 started with clean 5 m PZ prepared at NCCC.

CSIRO Tarong was designed to capture up to 90% of the CO_2 in a 0.1 MW slipstream of coal flue gas from the Tarong Power Station. In late 2012 through early 2013, a campaign was conducted to test the effectiveness of 8 m PZ. Initially, 856 hours of parametric testing were performed to optimize energy performance. After these tests, the plant was operated at steady-state conditions for 425 hours at a stripper operating temperature of 125 ℃ , followed by 421 hours at 155 ℃ to determine the effects of stripper

temperature on energy performance and degradation (Cousins et al., 2015).

Chapter 5.2 is adapted from journal article "Wu Y, Rochelle GT. Effects of Carbon Treating on Piperazine Oxidation in Pilot Plant Testing of PZAS^{TM}. *International Journal of Greenhouse Gas Control*. **2021**; 112:103502"

5.2 CAMPAIGNS AT NCCC

5 m PZ was tested at NCCC with the PZAS^{TM} configuration shown in Figure 5-1 with conditions representing long-term operations in two campaigns. The first campaign lasted from February to August 2018, starting with fresh 5 m PZ solvent, and the second campaign lasted from February to June 2019, using the end solvent from the first campaign. The system was drained and flushed with water between the two campaigns, and the solvent was collected and stored.

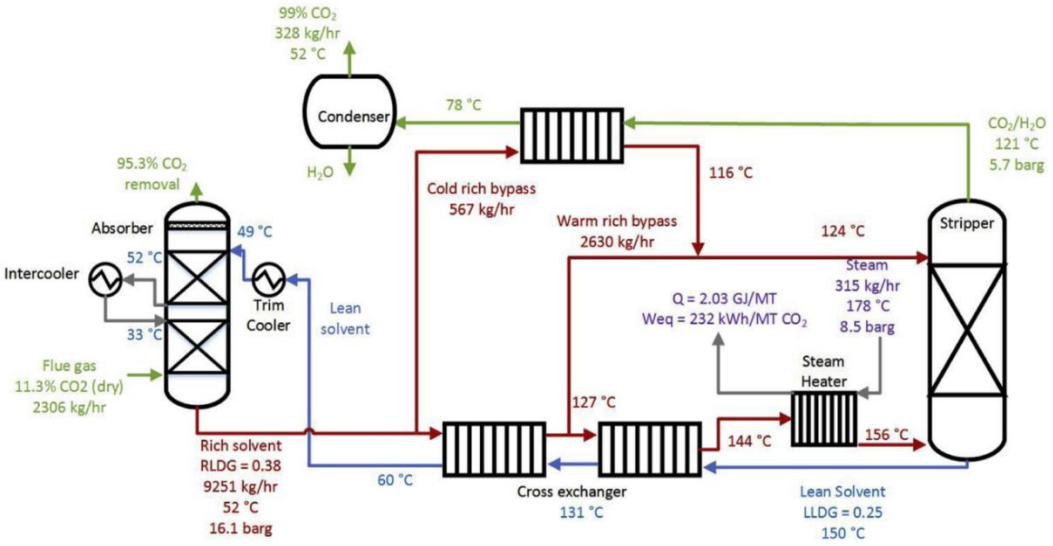

Figure 5-1: Configuration of PZAS^{TM} in the NCCC campaign (Rochelle et al., 2019)

5.2.1 NCCC 2018 Campaign

The NCCC 2018 Campaign tested the performance of 5 m PZ solvent on coal-fired flue gas for 2100 hrs. The system treated 0.6 MWe of coal-fired flue gas that was pre-

treated with a baghouse. Table 5-1 shows the timeline of the NCCC 2018 operations. LiOH and KH_2PO_4 were added at 250 hr as tracers to account for water balance in the system. At 900 hrs, a makeup of 5 m PZ was added. According to the tracer concentration changes, the addition was equal to 25% of the total solvent mass in the system. Initially, the system started with a high ox condition, which operated with 80% stripper sump level. At 1100 hrs, three mitigation methods were applied, including reducing the stripper sump level to 15%, applying 1 scfm N_2 sparging at the absorber sump, and adding thiosulfate in the prescrubber to remove NO_2 in the flue gas. The reduction of stripper sump level reduces the residence time ratio of the solvent at high temperature compared to the total residence time. The dominant oxidation mechanism in the high temperature part is the reaction with the oxidation carriers, and the overall rate of oxidation is mitigated with a smaller part of solvent at high temperature. The operating condition after the mitigation is referred to as PZAS™ low ox condition.

Table 5-1: Process changes in NCCC 2018 Campaign

Time (hrs)	Process Change
0	PZAS™ high ox
600	Simple stripper
880	PZAS™ high ox Low stripper sump level
1100	N_2 sparging, NO_2 pre-treatment
2150	End of campaign

The 24-hr average FTIR results from the campaign are plotted in Figure 5-2. The NH_3 in the inlet gas was 1 to 2 ppm, so the NH_3 produced in the scrubbing process was

between 3 to 6 ppm. The cumulative NH_3 production was 104 mmol/kg in the 2150 hours of operation, which gives an average rate of 0.047 mmol/kg-hr. When the mitigation methods were applied, the NH_3 production decreased from 5.5 ppm to 4.8 ppm, indicating that the methods reduced the PZ oxidation rate by 13%. Compared to the effects of N_2 sparging on bench-scale (Nielsen, 2018), the mitigation effect is small. One possible reason is that the liquid depth of the N_2 sparging was small, resulting in insufficient dissolved oxygen removal to show a significant mitigation.

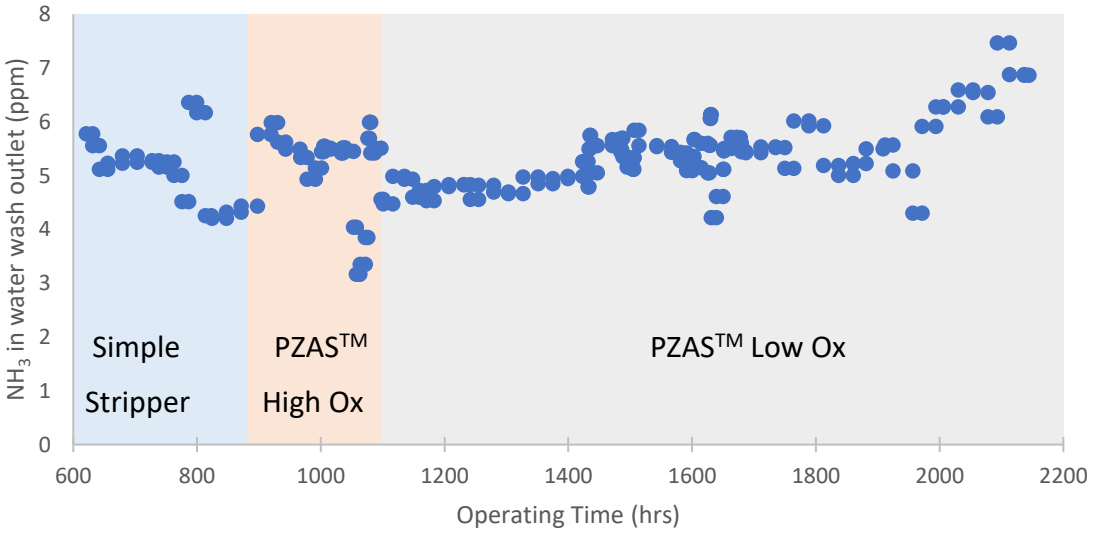

Figure 5-2: NCCC 2018 campaign NH_3 concentration in absorber outlet

All the NCCC 2018 samples had two universal absorbance peaks at 320 nm and 538 nm. The peak at 538 nm was small and fluctuated around 0.05 A. The dilution-corrected absorbance at 320 nm is plotted in Figure 5-3. The peak at 320 nm increased at 0.011 ± 0.0003 A/hr, indicating the peak was a result of degradation or corrosion products

accumulation. The switch from PZAS™ high ox condition to PZAS™ low ox condition did not affect the accumulation rate.

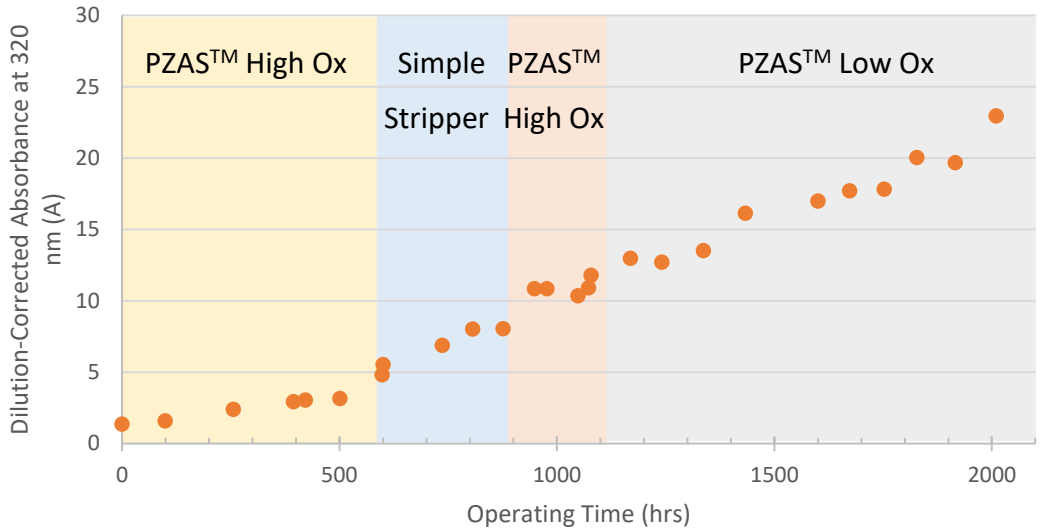

Figure 5-3: Dilution-corrected absorbance at 320 nm in NCCC 2018 campaign

The concentrations of Li and K tracers are plotted in Figure 5-4. The changes in concentration of tracers match each other, indicating that the correction for water balance with either metal is accurate. Since Li gives a stronger and more accurate signal in the ICP-OES analysis, the concentrations of the degradation products are normalized with Li for a consistent comparison with the starting point. The addition of 5 m PZ at 900 hours caused the concentration of tracer to decrease sharply.

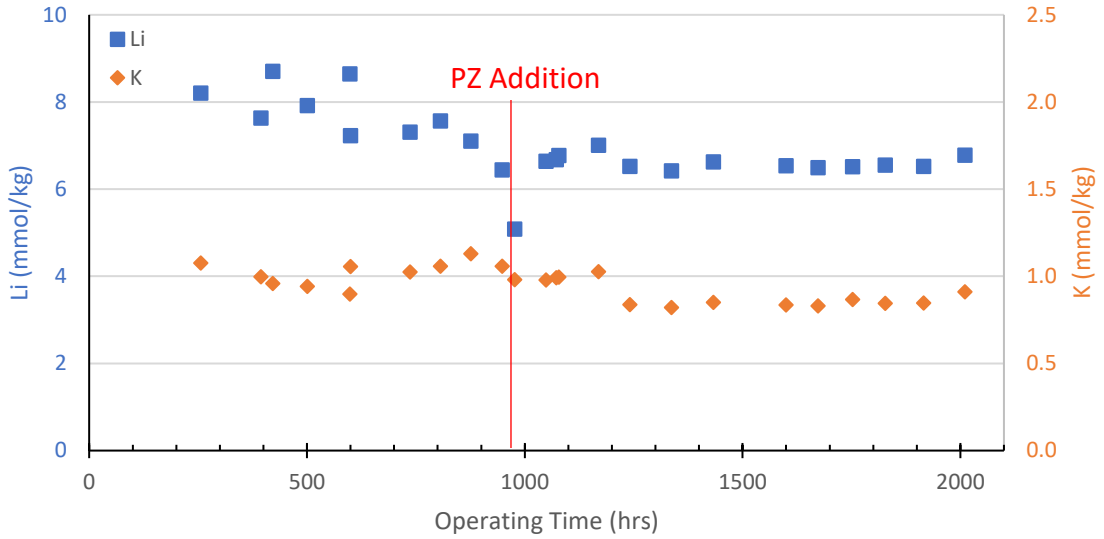

Figure 5-4: Li and K tracers in NCCC 2018 campaign

The PZ concentration was normalized by Li, and the additions of 5 m PZ were accounted for so that Figure 5-5 represents the PZ concentration with constant inventory and no solvent addition. The PZ loss rate was 0.54 ± 0.12 mmol/kg-hr in the first 1100 hrs, and was 0.05 ± 0.13 mmol/kg-hr between 1100 hrs and 2100 hrs. The large standard deviation was the result of a small PZ loss rate relative to the starting concentration of PZ. At the beginning of the campaign, the PZ emission was in the range of 10 to 20 ppm, so a large majority of the PZ loss was because of evaporation and aerosol emission instead of the oxidation of PZ. The transfer of PZ solvent between the PZAS^{TM} and simple stripper can also cause PZ loss which is not quantified.

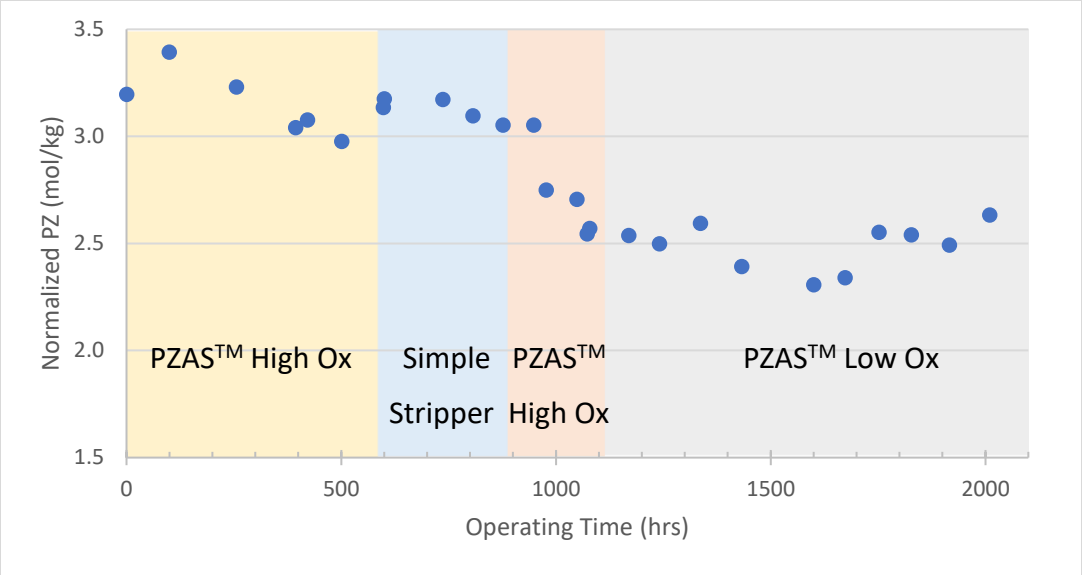

Figure 5-5: PZ Normalized by Li concentration in NCCC 2018 campaign

As shown in Figure 5-6, the total formate accumulated in a quadratic relationship in the first 1100 hrs. No significant changes were observed during the switch to the simple stripper condition, indicating that the PZAS™ design does not affect the total formate production. The average accumulation rate before mitigation is 0.0036 ± 0.0003 mmol/kg-hr. When the mitigation methods were applied, the total formate concentration decreased, which suggests that the production rate of formate decreased while the decomposition rate of formate remained constant. An increase in total formate was observed at 1750 hrs, but no change in process conditions was related to this increase. The average total formate accumulation rate was 0.0018 ± 0.0005 mmol/kg-hr, indicating the mitigation methods can reduce the production rate of formate. The formate and FPZ showed similar behavior as the total formate.

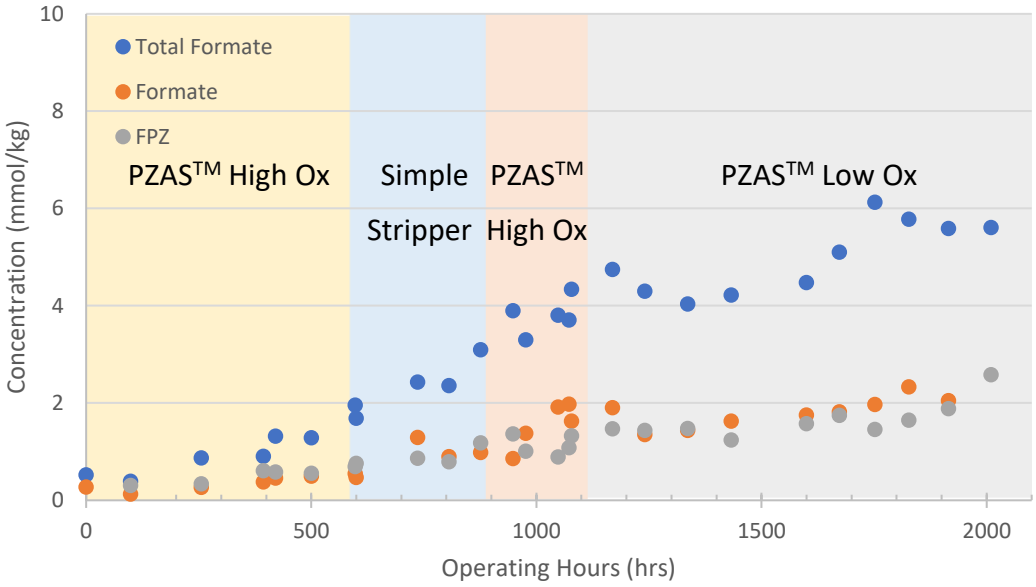

Figure 5-6: Total formate, formate, and FPZ normalized by Li in NCCC 2018 campaign

Since dissolved Fe is solubility limited instead of availability limited, the Fe concentration is not normalized. As shown in Figure 5-7, Fe increased slowly initially at the PZAS™ high condition and reached 0.04 mmol/kg. When switched to simple stripper, a step increase was observed, possibly due to the existence of Fe in the configuration. However, the Fe precipitated out quickly afterwards and stabilized at 0.03 mmol/kg. When the mitigation methods were applied, the Fe decreased initially to 0.02 mmol/kg and stayed constant for 500 hours. As the solvent became more degraded and the oxidation rate increased, the Fe accumulated in the solvent as a result of an increase in the solubility limit.

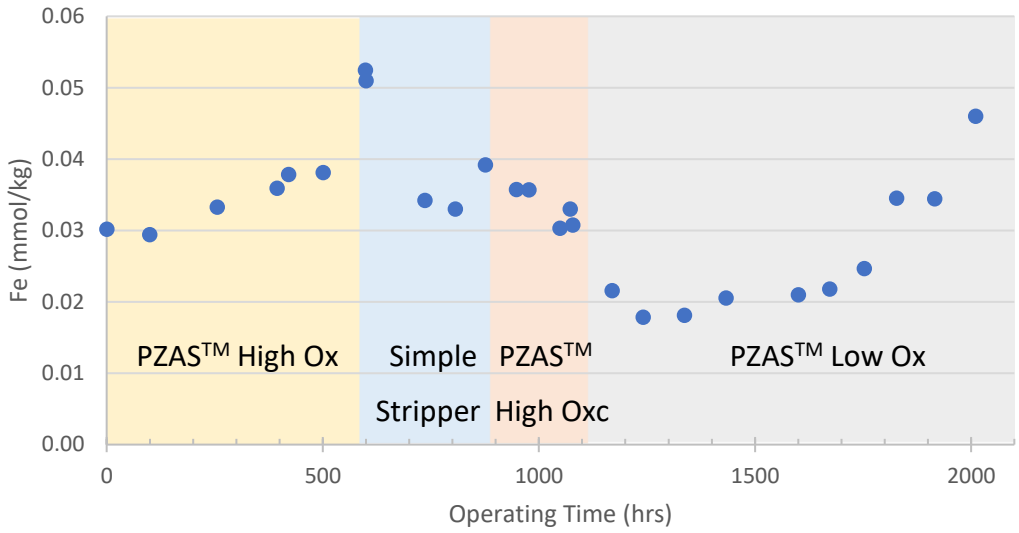

Figure 5-7: Fe in NCCC 2018 campaign

Previous work has suggested that the dissolved Fe is directly related to the extent of solvent degradation (Nielsen, 2018). A comparison of Fe concentration, NH_3 emissions from the water wash, and total formate concentration is shown in Figure 5-8. Compared to total formate, which is directly correlated to the extent of solvent oxidation extent, Fe is more closely related to the NH_3 rate, which represents the oxidation rate. One explanation could be that Fe exists mainly as Fe^{2+} in the absorber inlet and is oxidized into Fe^{3+} before entering the stripper. In the stripper, Fe^{3+} oxidizes the solvent and converts to Fe^{2+}, so at a lower oxidation rate less Fe^{3+} is converted to Fe^{2+}. The excessive Fe^{3+} precipitates out and causes a lower Fe concentration in the absorber inlet.

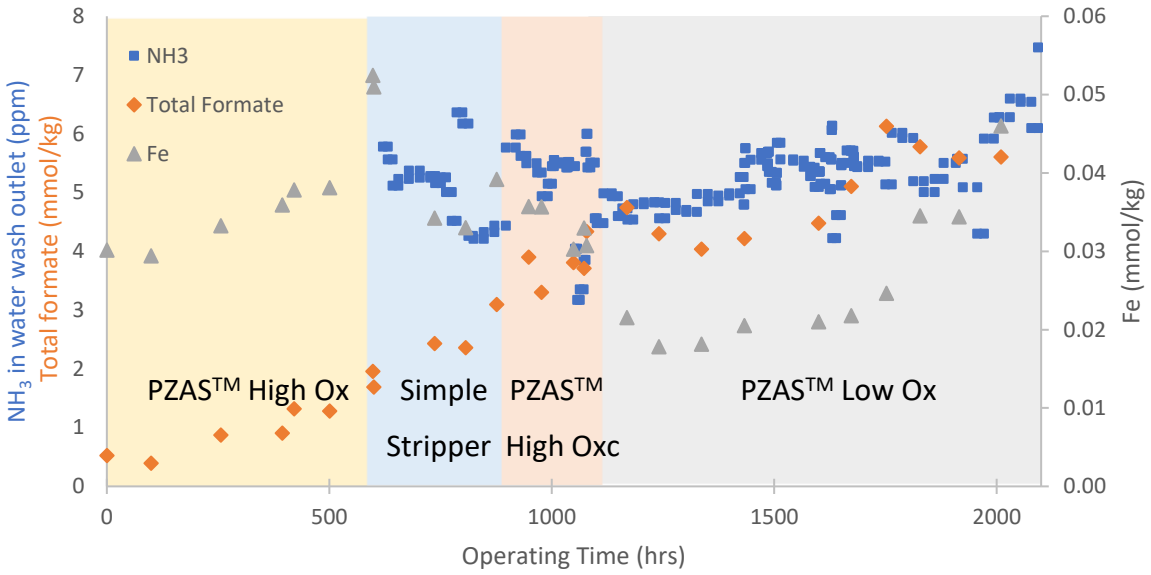

Figure 5-8. Comparison of Fe, normalized total formate, and NH_3 rate in the NCCC 2018 campaign

The normalized EDA is plotted in Figure 5-9. The EDA accumulated steadily at 0.0087 ± 0.0006 mmol/kg-hr. No significant changes were observed during switching of operating conditions, indicating that the production of EDA is not affected by the stripper configuration, the stripper sump level, the dissolved O_2 concentration, or NO_2 in inlet gas.

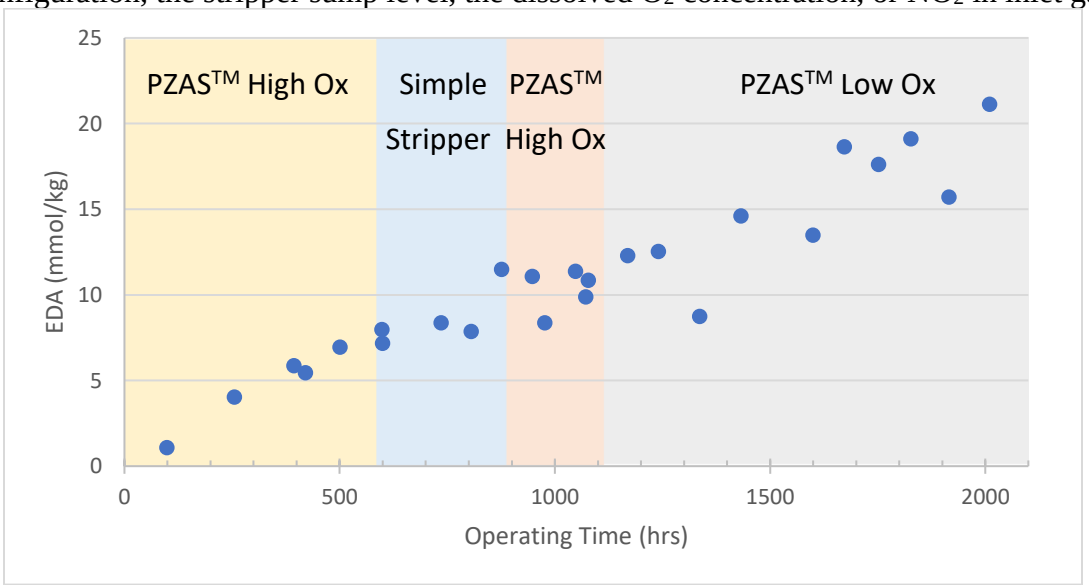

Figure 5-9: EDA normalized by Li in NCCC 2018 campaign

The normalized Ni, Mn, and Cr are plotted in Figure 5-10. In the first 900 hr, all three metals increased linearly, which can be due to corrosion of the stainless steel. The increasing trend stopped when the stripper was switched from simple stripper to PZAS^{TM}. The accumulation rates of Ni and Cr were smaller after the mitigation methods were applied at 1100 hr, which indicated that the corrosion rate became smaller with the mitigation method. Besides corrosion, the carryover of solution from the limestone desulfurization absorber can also be a source of Mn. Therefore, the rate of Mn did not decrease along with Ni and Cr.

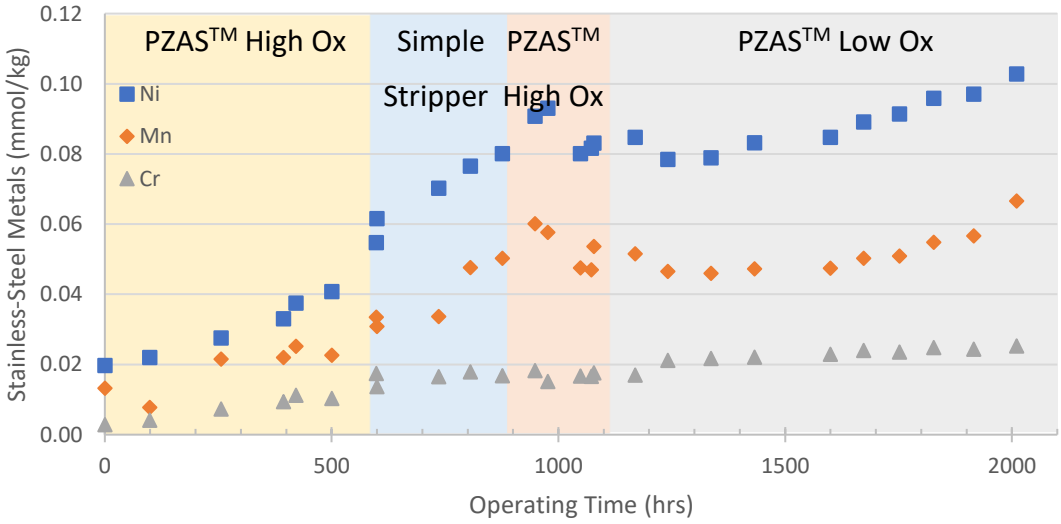

Figure 5-10: Ni, Mn, and Cr normalized by Li in NCCC 2018 campaign

The normalized total sulfate, total acetate, total nitrate, and total oxalate are shown in Figure 5-11. Total sulfate accumulated due to the SO_3 existing in the flue gas and injected during the aerosol testing. Total nitrate accumulated because of NO_2 in flue gas. It increased at 0.0006 ± 0.0001 mmol/kg-hr in the first 1100 hrs, and at 0.0004 ± 0.0001 mmol/kg-hr after the mitigation methods. This shows that, although adding thiosulfate into prescrubber can reduce the amount of NO_2 in flue gas, it did not remove the NO_2 completely. Total acetate accumulated at 0.0010 ± 0.0001 mmol/kg-hr and total oxalate

accumulated at 0.00013 ± 0.00002 mmol/kg-hr throughout the campaign, and no significant changes were caused by operation changes.

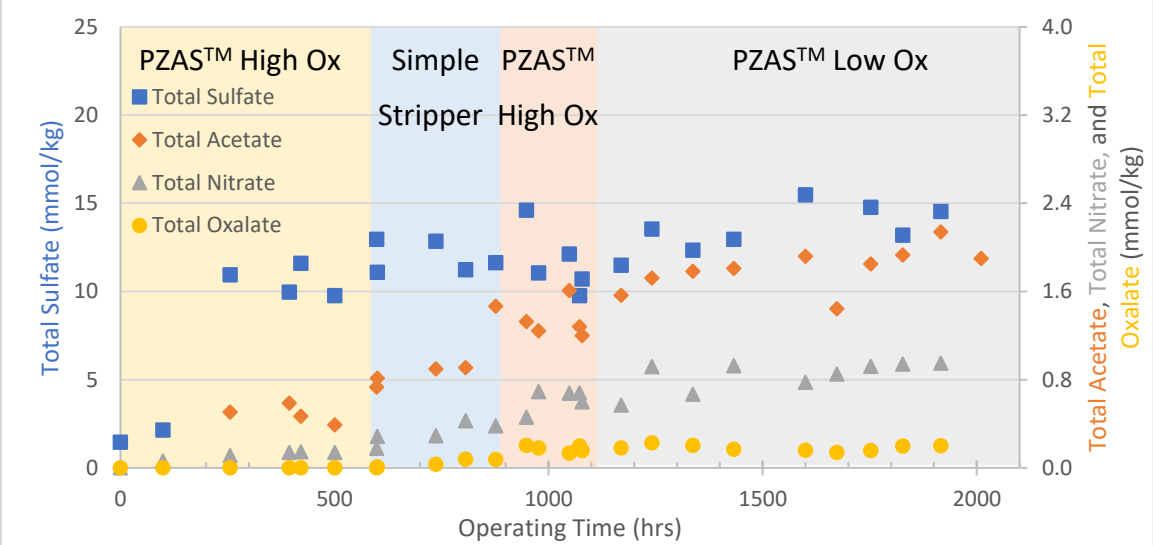

Figure 5-11: Total sulfate, total acetate, total nitrate, and total oxalate normalized by Li in NCCC 2018 campaign

No MPZ was observed in samples before 1100 hrs. After 1100 hrs, the MPZ started accumulating at 0.0051 ± 0.0005 mmol/kg-hr, as shown in Figure 5-12. It is possible that the MPZ was only produced at the low ox condition, but it is also possible that in the first 1100 hrs, the precursor of MPZ was produced, and it started to be oxidized to MPZ when the precursor reached a certain concentration.

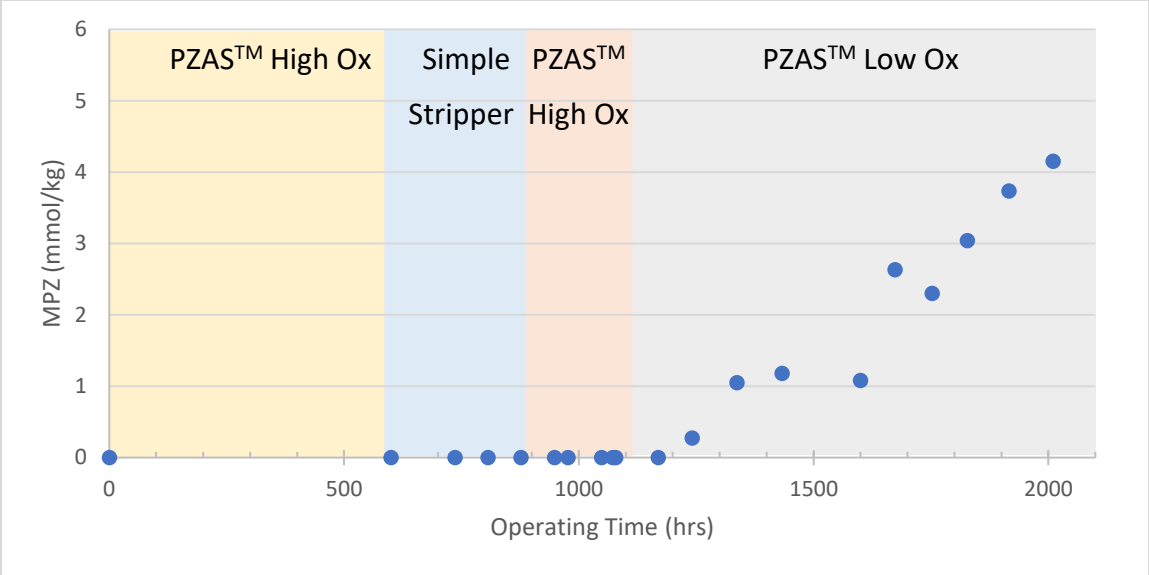

Figure 5-12: MPZ normalized by Li in NCCC 2018 campaign

The normalized total nitrate is plotted in Figure 5-13. The nitrate concentration increased at 0.0006 ± 0.0001 mmol/kg-hr in the first 1100 hrs. The accumulation rate decreased to 0.0004 ± 0.0002 mmol/kg-hr after the NO_2 pretreatment at 1100 hrs. This suggests that NO_2 pretreatment removed a small portion of the NO_2 in the flue gas.

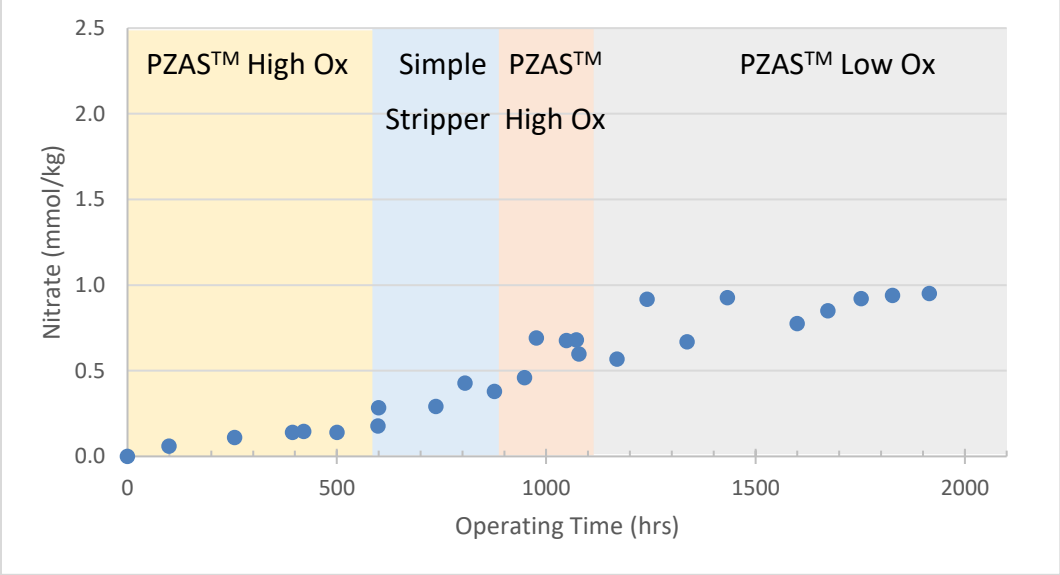

Figure 5-13: Total Nitrate normalized by Li in NCCC 2018 campaign

An average of 0.4 mmol/kg MNPZ was observed in the solvent, which is a result of the low NO_2 in the flue gas and high temperature in the stripper. During the coal campaign, PZ oxidized at 0.047 mmol/kg-hr, corresponding to an oxidation rate of 0.1 kg PZ/tonne CO_2 captured (Rochelle et al., 2019) based on the assumption that 1 mol of PZ degrades into 1 mol of NH_3 (Nielsen, 2018). PZ is oxidizing very slowly in the NCCC 2018 campaign, and one reason could be the use of the AFS**.** In the AFS, only a portion of the solvent, the hot rich bypass, is heated up to about 125 ℃ **.** The solvent was also allowed to flash when heated, so there was little oxygen in solvent to oxidize the solvent in the pipe.

5.2.2 NCCC 2019 Campaign

From February to June 2019, another 2000-hr campaign was performed on the end solvent in NCCC 2018 Campaign. The flue gas was produced from a coal-fired boiler, and it was mixed with air to create a stream containing 4% CO_2 and 15% O_2, equivalent to a 0.64 MW NGCC plant.

N_2 sparging at 1 scfm was applied at the bottom of the absorber. The system was then operated at optimum conditions, and the oxidation behavior was studied in a long-term test. In the latter portion of the campaign, carbon treating was used to remove catalytic metals and oxidation products to mitigate oxidation. A total of 868 lb of 8*30 mesh, lignite-based granular activated carbon was used to treat a 5 gpm slipstream from the absorber outlet, which was then sent back to the absorber. The carbon bed operated between 40 to 50 ℃ , and can hold 200 gallons of solvent, which gives a residence time of 40 min. The system was able to maintain 90% CO_2 removal at the same operating conditions and flow rates before the bed was turned on, indicating that the carbon bed has no or negligible impact on the effectiveness of the solvent. Important degradation and corrosion product results including total formate and dissolved Fe were compared with previous campaigns using

PZ. The major changes in the processes are shown in Table 5-2. The LiOH and KH_2PO_4 added into the solvent in the NCCC 2018 campaign were also used as tracers to correct for water balance.

Table 5-2: Operating conditions in the 2019 NCCC campaign

Time (hrs)	Process Change
2100	150 ℃ stripper temperature
2400	160 ℃ stripper temperature
2460	140 ℃ stripper temperature
2850	150 ℃ stripper temperature
3570	Carbon bed
4100	End of campaign

The NH_3 concentration in the water wash gas outlet was monitored continuously, shown as the blue curve in Figure 5-14. Before 3100 hours, the FTIR reported a high NH_3 residual, suggesting that there was contamination that caused inaccuracy in peak assignment, and the data was not reported. The FTIR was then purged with N_2 to remove any potential contaminants, and the residue was small, indicating an accurate result. Between 3100 and 3500 hours, the NH_3 concentration increased steadily to 6 ppm as the solvent became more degraded. The average NH_3 rate was 0.106 mmol/kg-hr, corresponding to an oxidation rate of 0.3 kg PZ/tonne CO_2 captured. This rate is higher than in the NCCC 2018 campaign, which may be a result of the higher oxygen content in the NGCC flue gas. When the carbon bed was turned on, the NH_3 concentration began to decrease, and reached 3.5 ppm after 400 hours, which was equivalent to 0.056 mmol/kg-hr. Given the ±3% accuracy in the FTIR analysis, this showed that oxidation was mitigated by using the carbon bed, which could remove oxidation catalysts for PZ or its degradation products. If the campaign had continued with the carbon bed on, more catalytic compounds

may have been removed, and the NH_3 rate may have continued to decrease. The NH_3 production rate fluctuated diurnally between 3600 and 4000 hours, which was likely due to the change in NH_3 solubility in water with the temperature difference between day and night. The fluctuation became more significant as the ambient temperature swing coincidentally became greater when the carbon bed testing started.

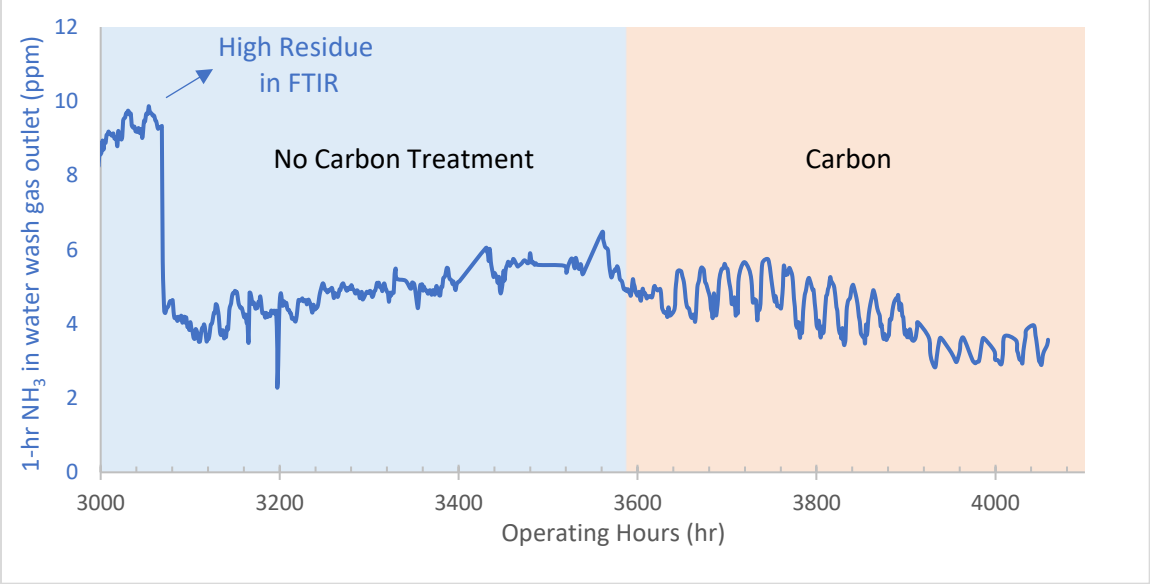

Figure 5-14: NH_3 production rate in water wash outlet in NCCC 2019 Campaign

Previously, NO_2 was found to oxidize PZ (Fine, 2015), and bench-scale results showed that 1 mol of NO_2 oxidizes 1.5 mol PZ by assuming $NaNO_2$ addition has the same effect as NO_2 injection (Nielsen, 2018). Knowing this, the NO_2 concentration in the inlet flue gas was closely monitored as shown in Figure 5-15. While adding sulfite and thiosulfate in the prescrubber proved useful in removing NO_2 (Fine, 2015), the apparent NO_2 remained high at 2 ppm from 3000 to 3450 hours while thiosulfate was added to the prescrubber at 3300 hrs. However, when the NO_2 analyzer was calibrated at 3450 hrs, the NO_2 decreased to <0.2 ppm. It is therefore believed that the high NO_2 results were due to inaccurate analyzer results, and the actual NO_2 was always low during the campaign. This

reasoning is supported by the low NH_3 concentration.

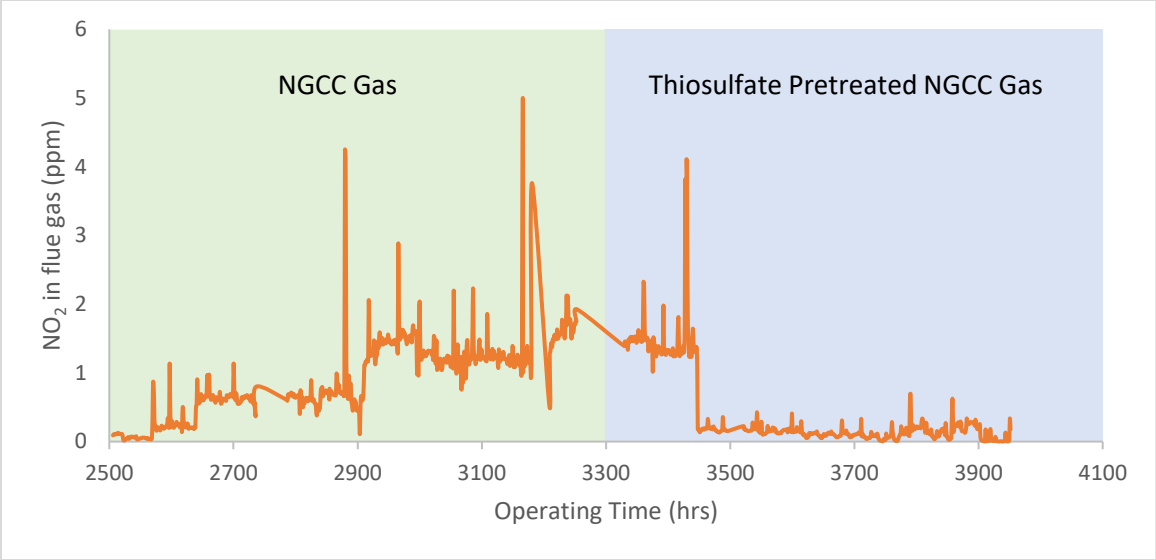

Figure 5-15: NO_2 in flue gas in NCCC 2019 Campaign

The Li and K are plotted in Figure 5-16. The Li and K concentrations dropped significantly compared to the previous campaign, which can be due to precipitation during storage. At 2130, 2400, and 2880 hrs, 5 m fresh PZ was added, and both tracers showed an immediate drop in concentration. Before 3300 hrs, the two tracers behaved similarly, indicating that the inventory is well-represented by the tracers. However, starting at 3500 hrs, K increased much more significantly than Li, and the ratio of the tracer concentrations deviated from the initial ratio of LiOH and KH_2PO_4 added into the solvent, indicating that the carbon bed could have introduced external sources of K. As a result, the tracers were not representative after 3500 hrs.

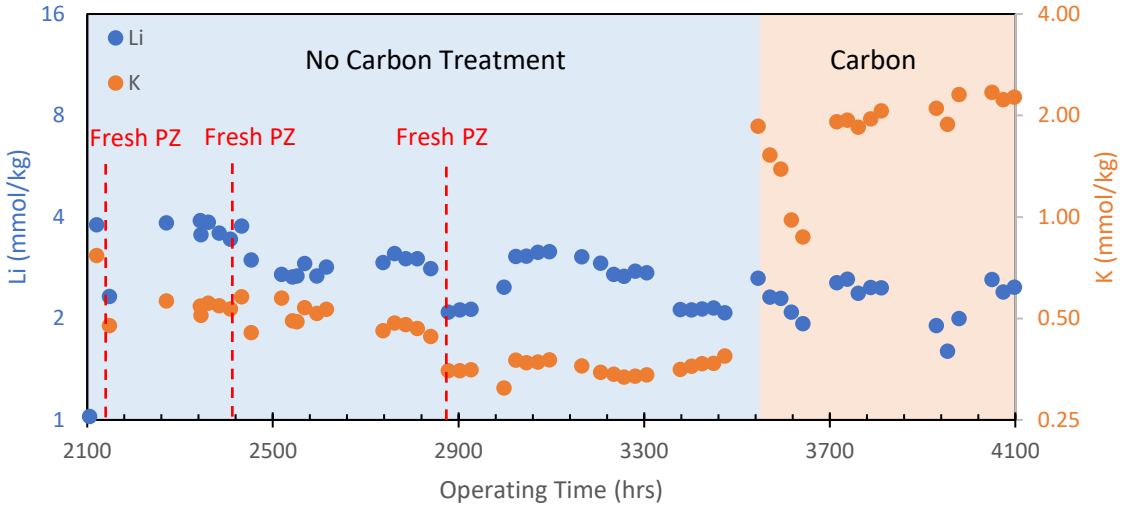

Figure 5-16: Tracer concentrations in NCCC 2019 campaign

Without the tracer data, the inventory in the rich storage tank, the absorber sump, and the stripper sump were estimated to keep track of the total inventory of solvent. As shown in Figure 5-17, the total inventory stayed relatively constant after the carbon bed was turned on at 3570 hrs. While the inventory of packing, heat exchangers, and piping were not included in the estimation, it was assumed that the inventory in these areas of the capture system stayed constant. As a result, the water balance was corrected based on the inventory instead of the tracer concentrations for any data after the application of carbon treating.

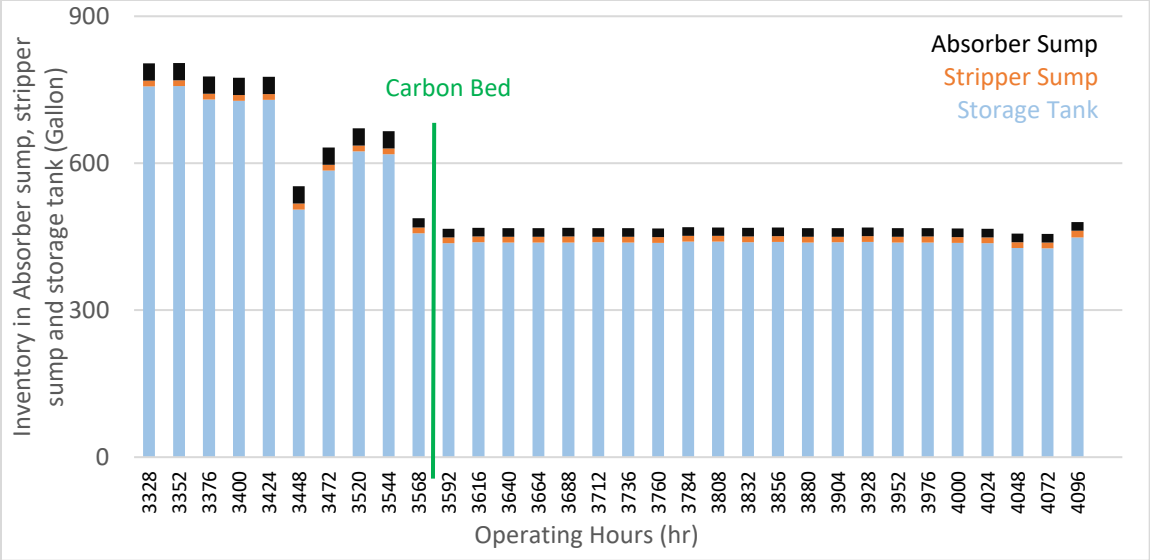

Figure 5-17: Estimated inventory in absorber sump, stripper sump, and storage tank

The carbon bed was turned on at 3600 hr of operation, and color changes were observed in samples collected afterwards. Shown in Figure 5-18, the solvent color becomes lighter over time, and after 9 days of operation, it is very close to the color of the starting solvent, indicating that some degradation products or corrosion products may have been removed by carbon bed. This color effect was also observed after solvent reclaiming was applied on the MEA solvent in Technology Centre Mongstad (Flø et al., 2017), suggesting that the similar products are removed in the carbon bed and reclaiming process.

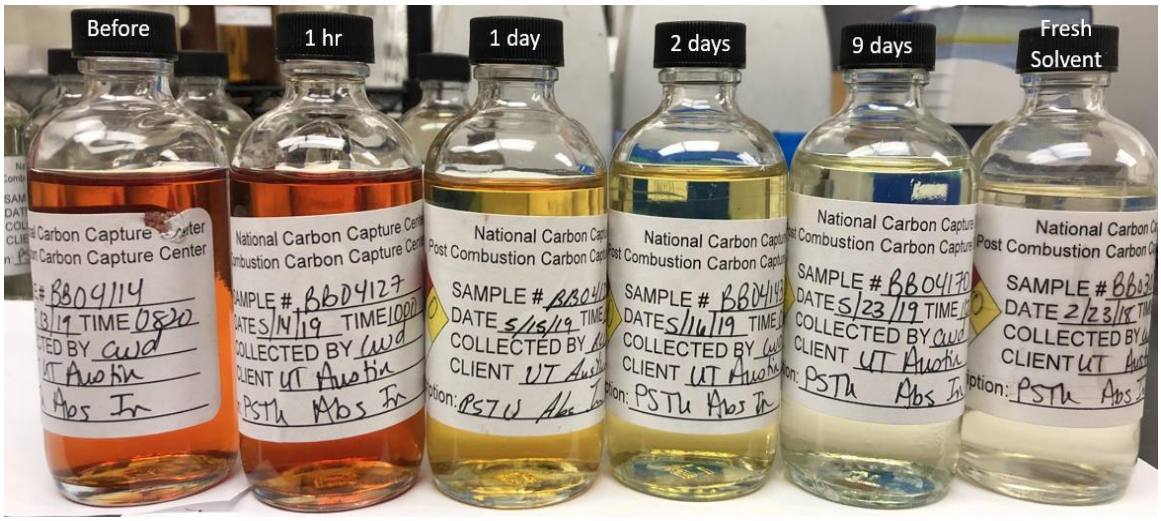

Figure 5-18: Color changes in NCCC 2019 samples after turning on carbon bed

Figure 5-19 shows the concentration of products closely related to oxidation. The dilution-corrected absorbance of NCCC samples at 320 nm is shown in orange. The 320 nm absorbance increased linearly at a rate of 0.020 ± 0.001 A/hr before carbon treating was applied. The peak height reached a maximum of 58.3 A, dropped significantly after the use of the carbon bed, and reached a final absorbance of 17.4 A. This indicates that the peak was caused by degradation products that were removed effectively with the carbon bed. The peak at 538 nm accumulated to 1.1 A, and the carbon treating removed the light absorbing component and the peak deceased to 0.1 after 200 hours of operation.

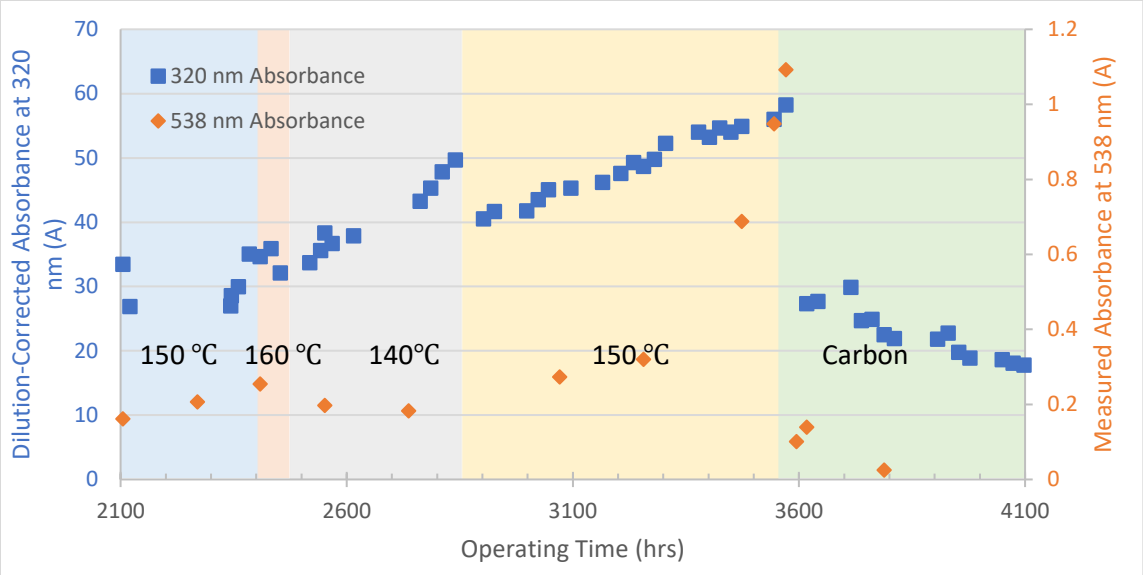

Figure 5-19: Dilution-corrected absorbance at 320 nm and absorbance at 538 nm in NCCC 2019 Campaign

Total formate is plotted in Figure 5-20. There is a delay in formate concentration when the operating conditions varied, and the delay is because of the time required for the equilibrium to be reached. When the stripper temperature was high at 150 ℃ and 160 ℃ , the total formate concentration stayed low. However, when the temperature was reduced to 140 ℃ , the total formate concentration increased at an accelerated rate. This suggests that formate can degrade into other products, and the low temperature resulted in a low formate degradation rate, causing the accumulation of total formate. After the stripper temperature was raised back to 150 ℃ , the degradation rate of formate increased, causing the concentration of formate to decrease until steady state was reached. When the carbon bed was brought online, there was a step increase followed by some fluctuations in the total formate concentration. This increase may be due to an external source of formate and was unlikely due to oxidation of PZ. The total formate increased at a rate of 0.038 ± 0.005 mmol/kg-hr when the stripper temperature was 150 ℃ .

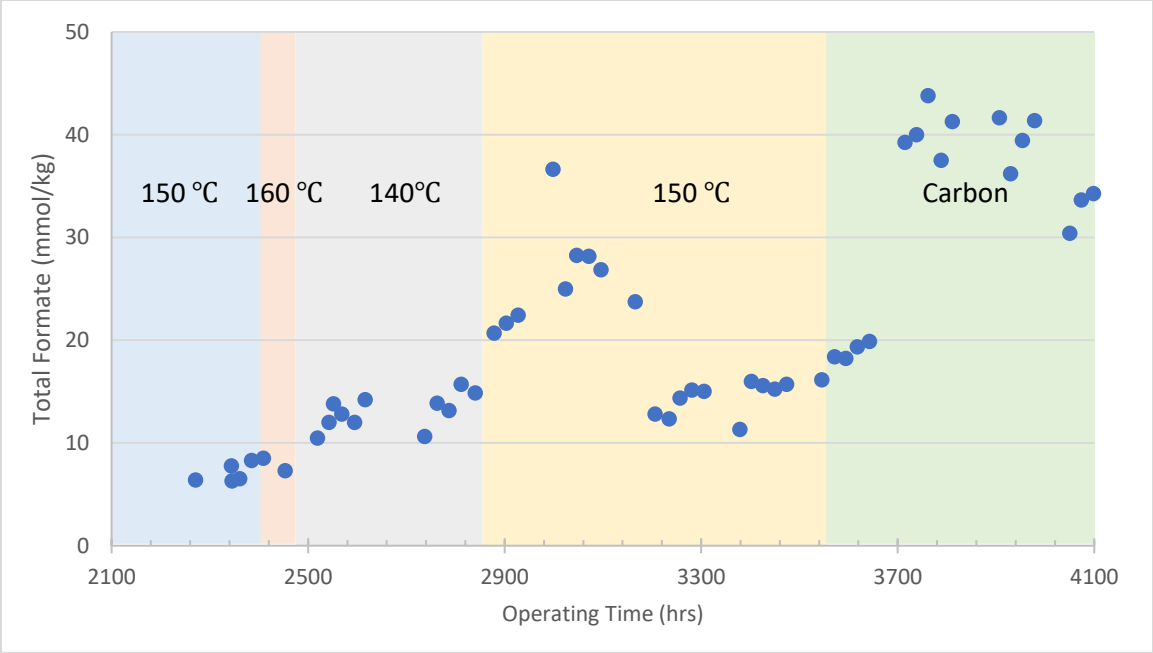

Figure 5-20: Normalized total formate in NCCC 2019 Campaign

As shown in Figure 5-21, the dissolved Fe fluctuated between 2100 and 2900 hrs due to changes in oxidation caused by stripper temperature. As the stripper temperature increased to 160 ℃ , more corrosion occurred, causing an increase in the metals. However, this resembled a step change of Fe addition, and the agents that increased Fe solubility in the solvent did not increase (Nielsen, 2018). As a result, the dissolved Fe precipitated when equilibrium was reached. The accuracy of the ICP-OES is ±2%, which may also explain the fluctuation. Between 2900 and 3500 hrs, the system operated at a stripper temperature of 150 ℃ , and the Fe increased slowly but steadily, similar to the NH_3 concentration. After the carbon treating was applied, Fe increased and then decreased to the level before carbon treating, so the carbon did not reduce the dissolved Fe concentration in solvent.

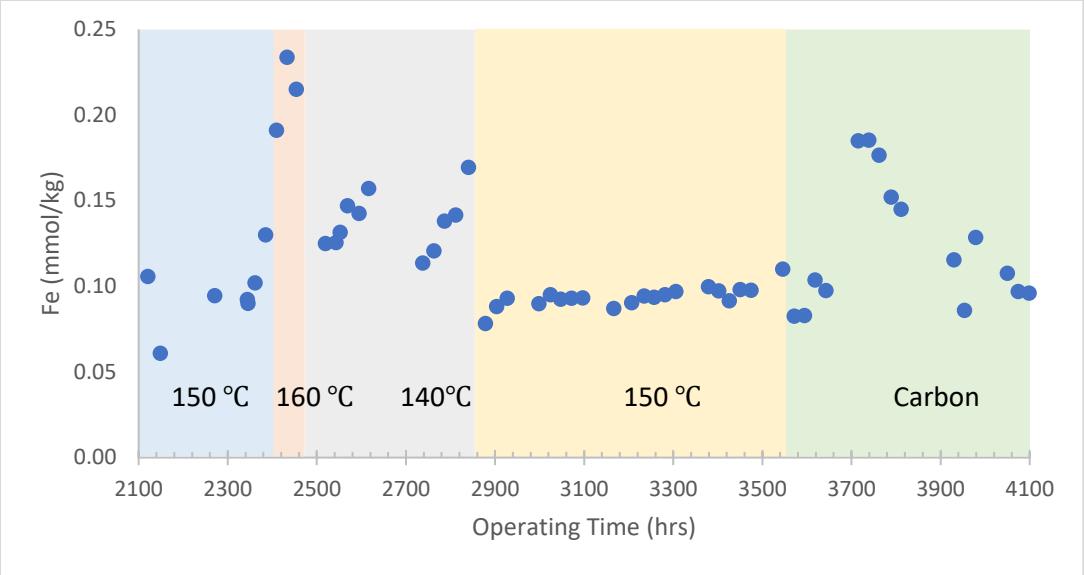

Figure 5-21: Fe in NCCC 2019 campaign

Before the carbon bed was turned on, Cr, Ni, and Mn showed similar behavior, as shown in Figure 5-22, indicating that the concentration changes were mainly due to corrosion. From 2400 hrs to 2460 hrs, the stripper temperature was increased to 160 ℃ , which resulted in a sharp increase of these metals. After the carbon bed was turned on, the Mn and Ni still increased, but the Cr decreased steadily, which is a result of Cr being removed by the carbon bed.

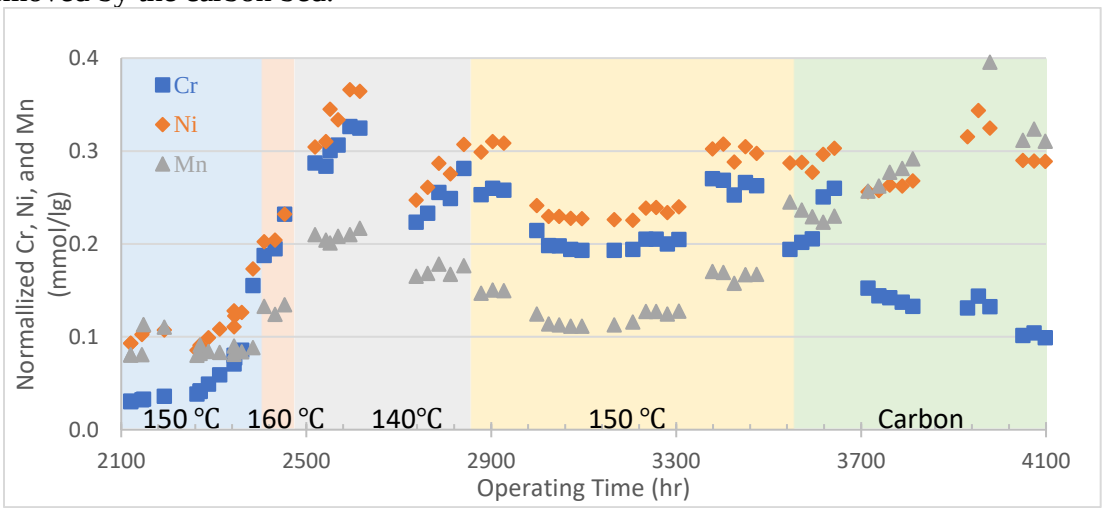

Figure 5-22: Normalized Cr, Ni, and Mn in NCCC 2019 campaign

As plotted in Figure 5-23, the EDA concentration decreased initially between 2100 and 2450 hrs. When the stripper temperature was lowered to 140 ℃ , the EDA increased significantly, indicating that the degradation of EDA was more sensitive to the stripper than the production of EDA, and the low temperature caused a significantly lower EDA degradation rate. When the temperature increased to 150 ℃ again, the EDA dropped since the degradation rate of EDA increased. The EDA concentration decreased steadily at 0.017 ± 0.005 mmol/kg-hr since the temperature effect disappeared at 3400 hrs. The rate was not affected by the carbon treating, suggesting that the carbon does not remove any EDA and its precursors, and does not affect the production and consumption of EDA.

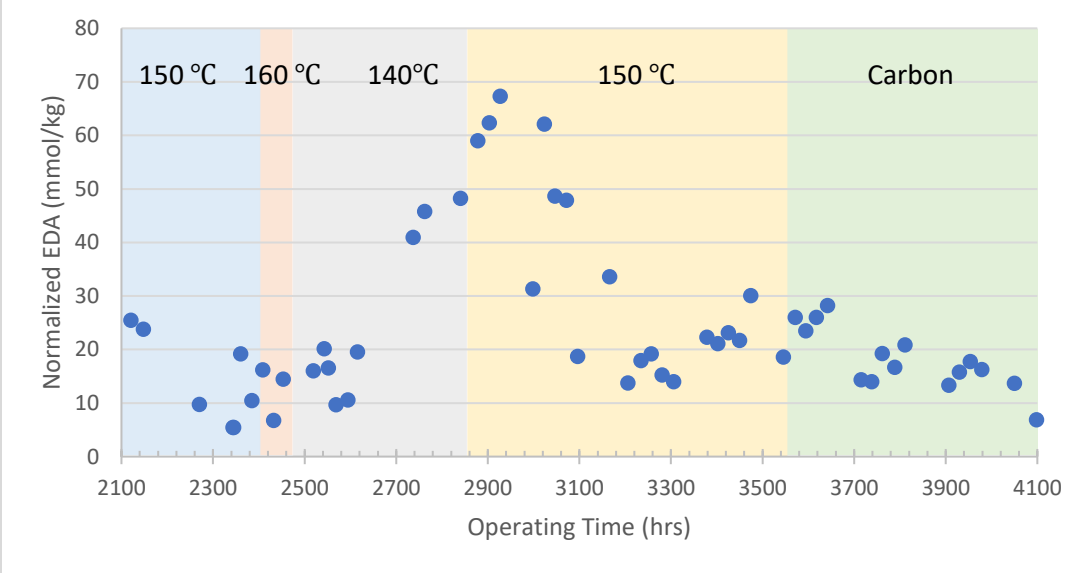

Figure 5-23: Normalized EDA in NCCC 2019 campaign

Figure 5-24 shows PZ-one concentration. PZ-one is an early degradation product of PZ and usually accumulates when the solvent is clean and decomposes when the solvent becomes more degraded (Nielsen, 2018). The PZ-one accumulates faster at a lower stripper temperature, and this may be because the reaction to form PZ-one is faster than the reaction to consume PZ-one at lower temperature. The PZ-one accumulated at 0.038 ± 0.008 mmol/kg-hr at 140 ℃ stripper temperature, and then decomposed when the stripper

temperature increased. After the carbon bed was turned on, PZ-one increased at a faster rate, indicating that the catalysts to oxidize PZ-one has been removed by carbon bed. However, a longer period is required to verify this hypothesis.

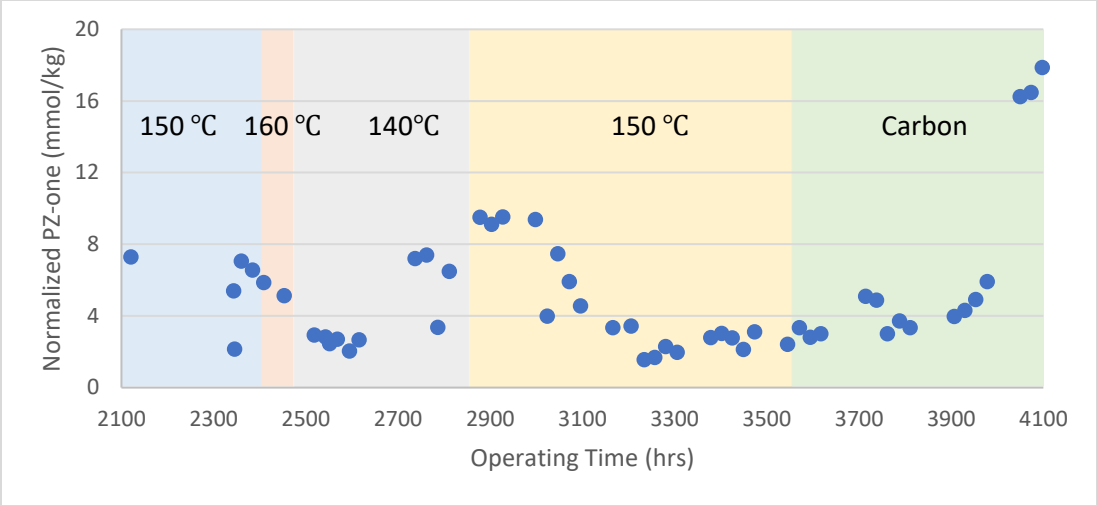

Figure 5-24: Normalized PZ-one in NCCC 2019 campaign

The normalized total nitrate is plotted in Figure 5-25. Over the 2000 hrs of operation, the nitrate accumulated at 0.0006 ± 0.0001 mmol/kg-hr, similar to the rate of accumulation in the first 1100 hrs as shown in Figure 5-13. This indicate the NO_2 absorption rate in the NCCC 2019 campaign was similar to that in NCCC 2018 without NO_2 pretreatment.

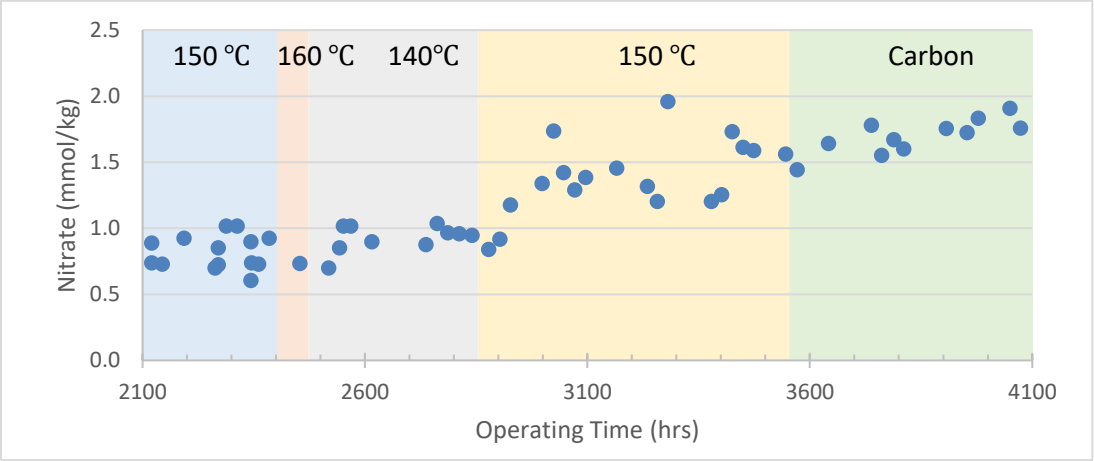

Figure 5-25: Normalized total nitrate in NCCC 2019 campaign

The PZ was normalized by Li, the solvent inventory, and the additions of PZ were corrected. Figure 5-26 represents the PZ concentrations if fresh solvent makeup had not been added to the solvent. A correction factor was calculated by dividing the PZ concentration before solvent makeup and the PZ concentration after solvent makeup, and all the PZ concentrations after solvent makeup were corrected with this factor to estimate the PZ without solvent makeup. The PZ loss was 3.25 ± 0.85 mmol/kg-hr at 150 ℃ from 2100 to 2400 hrs, and 0.63 ± 0.15 mmol/kg-hr at 140 ℃ from 2460 to 2850 hrs. The 160 ℃ condition was too short to get any reliable estimation of PZ loss rate. When the stripper temperature was switched to 150 ℃ from 2850 to 3570 hrs, the PZ loss was 0.50 ± 0.10 mmol/kg-hr. The loss rate decreased to 0.18 ± 0.07 mmol/kg-hr when the carbon treating was applied. Initially, the PZ loss was very high, which is possibly due to leaks of PZ and unstable operating conditions. The loss rate in the 140 ℃ was higher than the second 150 ℃ region, but this does not necessarily mean that PZ oxidizes faster at 140 ℃ . Since the solvent experienced a 60-hr high temperature operation, there can be accumulation of catalytic degradation products that accelerated the oxidation even when the temperature is low. There can also be some delayed effects, causing the high oxidation rate at 160 ℃ to be represented in regions of 140 ℃ , and the low oxidation rate of 140 ℃ to be represented in regions of 150 ℃ . The overall PZ loss rate was 0.26 ± 0.03 mmol/kg-hr in the NCCC 2019 Campaign. There can be two reasons for the much higher rate compared to the 0.106 mmol/kg-hr estimated from the NH_3 data. Since the amount of fresh solvent added each time was not recorded and was estimated using the tracer concentration, the replenishment can be overestimated due to the uneven mixing of the tracers if the sample was taken immediately after fresh solvent had been added. There can also be PZ loss in the gas from the absorber and stripper outlets. The PZ loss rate includes degradation, emissions, leaks, and loss in storage, while the NH_3 data only account for PZ loss due to oxidation.

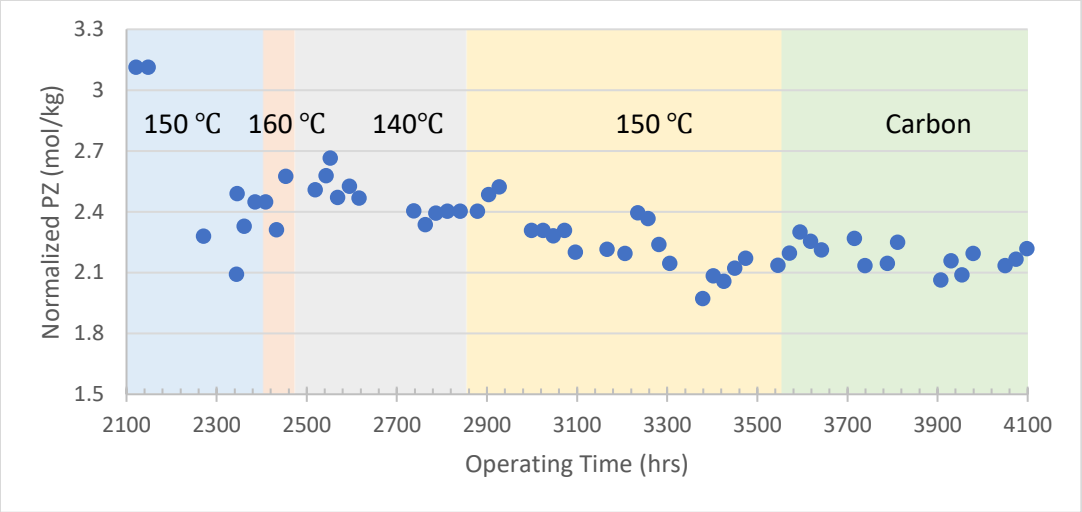

Figure 5-26: Normalized PZ concentration before carbon bed was turned on

LC-MS was performed on samples before and after carbon treatment to identify what was removed by the carbon. While the separation of species was not successful, the molecular weights of all identified species are shown in Figure 5-27 and Figure 5-28. Compounds with high molecular weight were present in samples before treatment, but not after. These compounds may represent the polymerization of PZ and can be removed by carbon treatment.

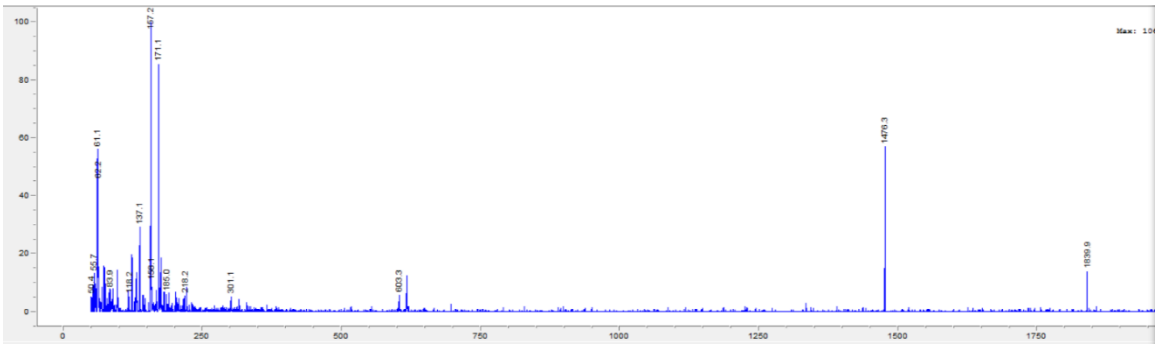

Figure 5-27: LC-MS of NCCC 2019 solvent before carbon treatment

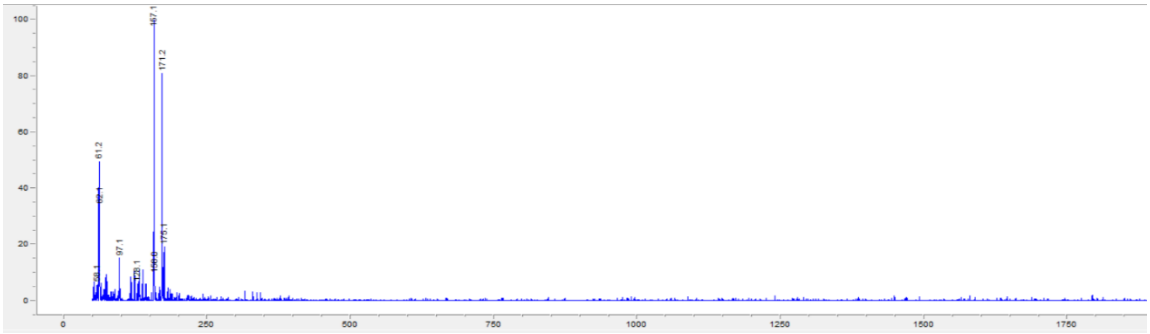

Figure 5-28: LC-MS of NCCC 2019 solvent after carbon treatment

Excess 0.2 N H_2SO_4 was added to 0.5340 g of the NCCC used carbon to quantify the amount of Fe removed by the carbon. 7 batches of H_2SO_4 were added, and each batch was drained completely before the new batch was added. The time and amount of H_2SO_4 added is shown in Table 5-3.

Table 5-3: Solvent addition in CAC 22

Time (hrs)	Mass of 0.2 N H_2SO_4 (g)
0.23	45.6027
0.43	46.4259
0.60	59.5482
0.78	68.6823
0.95	68.1460
1.10	69.0898
1.35	67.3072
1.53	67.8629
1.72	83.8618
1.90	83.0964
2.15	86.7890

The Fe concentration in the H_2SO_4 is shown in Figure 5-29. It became negligible

after 279.4051 g of 0.2 N H_2SO_4 was used to rinse the carbon, and almost all the Fe was removed in this experiment. From the Fe concentration and the mass of 0.2 N H_2SO_4, it is calculated that there was 104.5 mmol Fe/kg of carbon on the NCCC used carbon. The calculation is shown below:

$$Fe\ removed\ by\ Carbon = \frac{\Sigma\left(\left[Fe_{H_2SO_4}\right] \times H_2SO_4\ mass\right)}{carbon\ mass} \qquad (5-1)$$

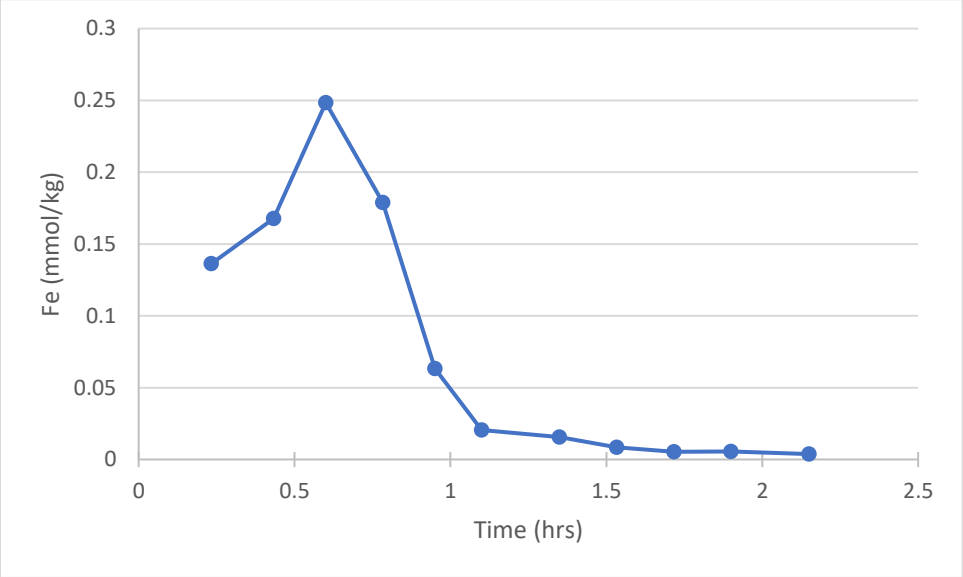

Figure 5-29: Fe in CAC 22 (0.2 N H_2SO_4, NCCC Used Carbon)

The difference between the clean carbon and used carbon was calculated, and the carbon bed removed 6.6 mmol/kg solvent in the NCCC campaign based on the assumptions of 28 canisters, 31 lbs of carbon each canister, and 12000 lbs of solvent inventory. The number may not be accurate since the carbon bed at NCCC was operated with a liquid level of 12 inches, and only a portion of the carbon is used. The activated carbon was not well mixed, and the carbon for analysis was collected at the top of the carbon cartridge. From the Fe concentration data shown in Figure 5-20, the Fe in solvent did not decrease, indicating that whenever the carbon removes the dissolved Fe, more Fe previously in

”solid” form will dissolve into the solvent. Therefore, the whole inventory of available “soluble” Fe must be removed to result in a decrease in Fe concentration.

5.3 CAMPAIGNS IN SRP

SRP treated a synthetic flue gas equivalent to 0.1–0.2 MW, typically consisting of air and CO_2 at 350 to 600 ACFM. 5 m PZ was used, and the stripper temperature was controlled at 150 ℃ (Nielsen, 2018). The process flow diagram of the SRP plant is shown in Figure 5-30, and a picture of the SRP is shown in Figure 5-31.

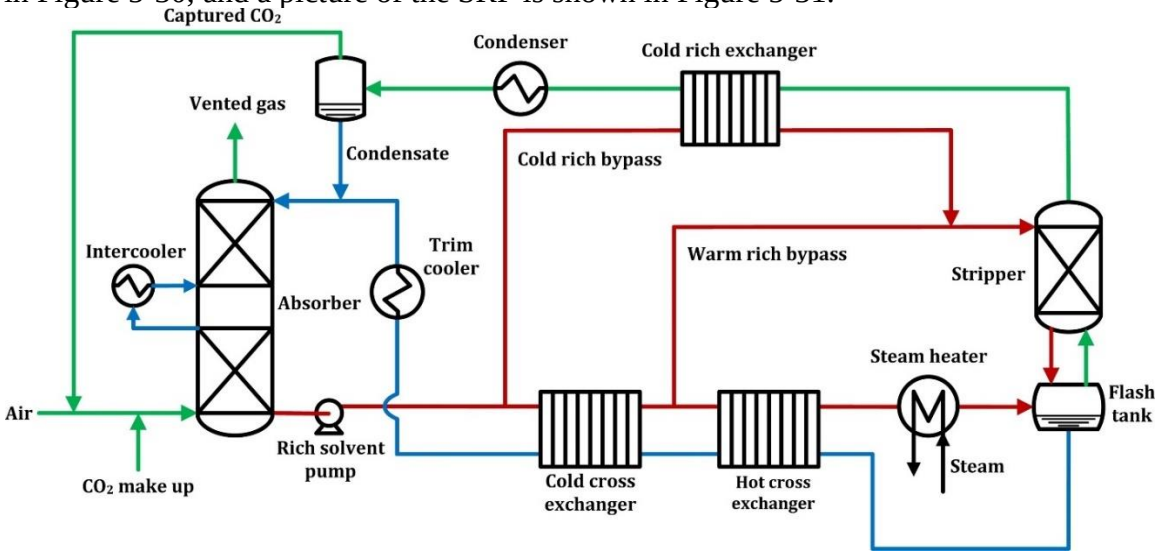

Figure 5-30: Advanced flash stripper configuration with cold and warm rich bypass and cold rich exchanger (Zhang et al., 2017)

Figure 5-31: SRP pilot absorber/stripper and advanced flash stripper skid (bottom left) (Chen et al., 2017)

5.3.1 SRP 2018 Campaign

The SRP 2018 campaign operated from September 18, 2018, to October 4, 2018, using fresh 5 m piperazine (PZ). The changes in operating conditions of the SRP 2018

campaign are shown in Table 5-4.

Table 5-4: Important process changes in the SRP 2018 campaign

Operating Time (hrs)	Important Process Changes
0	19% CO_2 in flue gas
165	3.5% CO_2 in flue gas
264	End of campaign

While 500 g Li_2SO_4 was added at 165 hrs as tracer, the concentrations of tracer fluctuated due to mixing as shown in Figure 5-32. It was believed that the Li was not well mixed until the last two samples collected in the campaign. Therefore, the Li was not used for correction while reporting component concentrations.

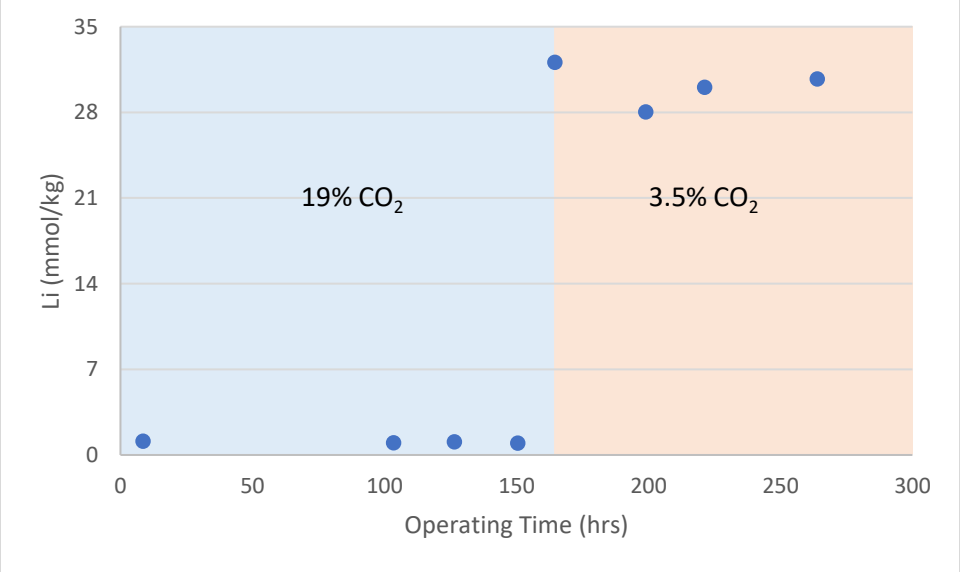

Figure 5-32: Li tracer in samples from SRP 2018 campaigns

The EDA increased steadily at 0.057 ± 0.007 mmol/kg-hr as shown in Figure 5-33. No difference was observed when the CO_2 concentration in the flue gas decreased from 19% to 3.5%.

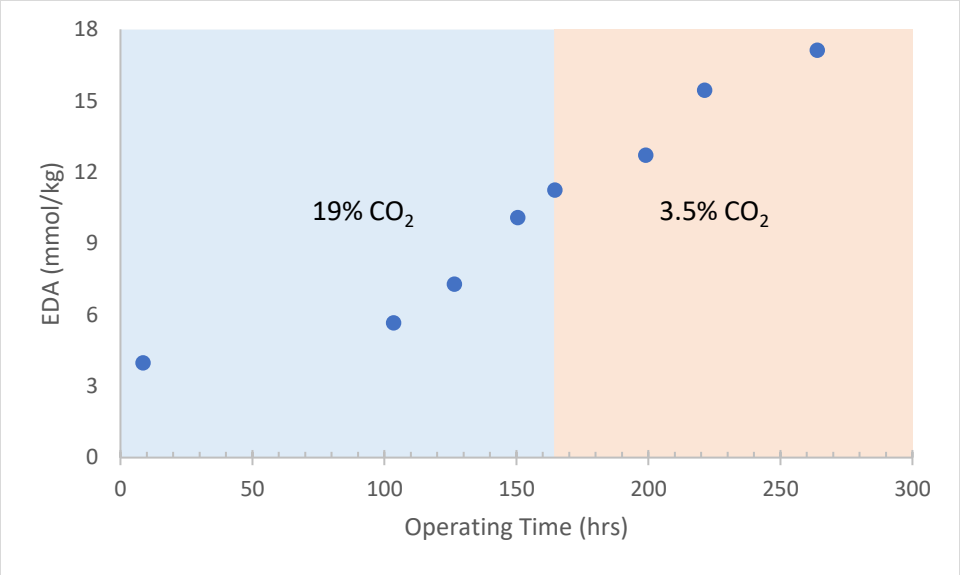

Figure 5-33: EDA in samples from SRP 2018 campaigns

The concentrations of stainless-steel metals are shown in Figure 5-34. The samples start with a high level of Fe, which precipitated out as the campaign progressed. Since the solvent was prepared in February 2018 and was stored in stainless-steel tanks for more than 6 months, it is possible that the Fe come from the corrosion of the containers and decreased because the solubility limit of Fe was low in the scrubbing system. Ni, Cr, and Mn had a similar trend of going down, which may suggest the solvent being diluted in the campaign.

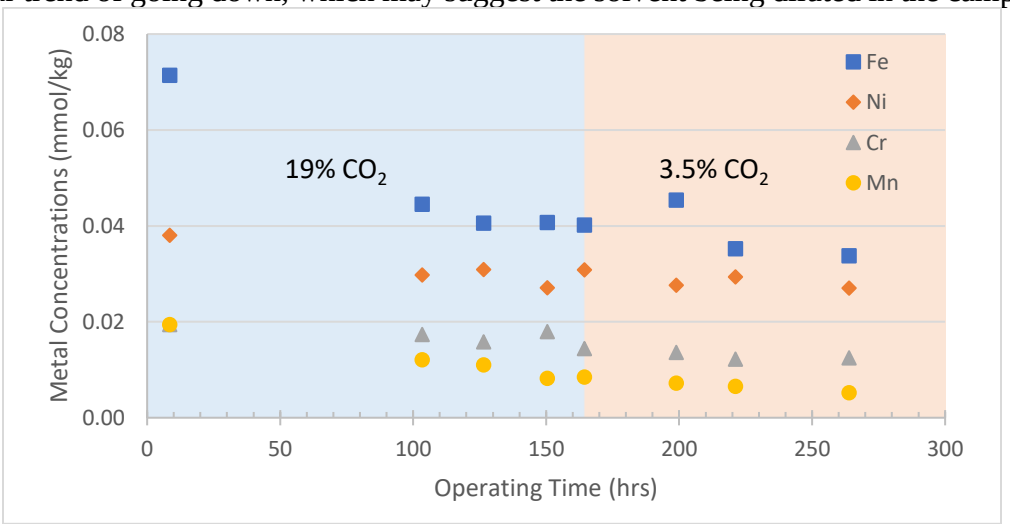

Figure 5-34: Stainless steel metals in SRP 2018 campaign

The concentrations of heat stable salts are listed in Table 5-5. Overall, very little heat stable salt was generated in the 264 hrs of operation. The sulfate source is the Li_2SO_4 added into the solvent instead of any reactions in the system.

Table 5-5: Heat stable salts concentration in SRP 2018 campaign

	Formate	Sulfate	Acetate	Oxalate
Free (mmol/kg)	2.06	6.32	1.00	0.17
Total (mmol/kg)	3.85	8.04	1.21	0.34

The PZ loss rate was 1.46 ± 1.01 mmol/kg-hr with 19% CO_2, and 2.54 ± 1.56 mmol/kg-hr with 3.5% CO_2 in flue gas as shown in Figure 5-35. Since only a few samples were collected, the standard deviation is very large, and the rate is not representative of the true PZ loss.

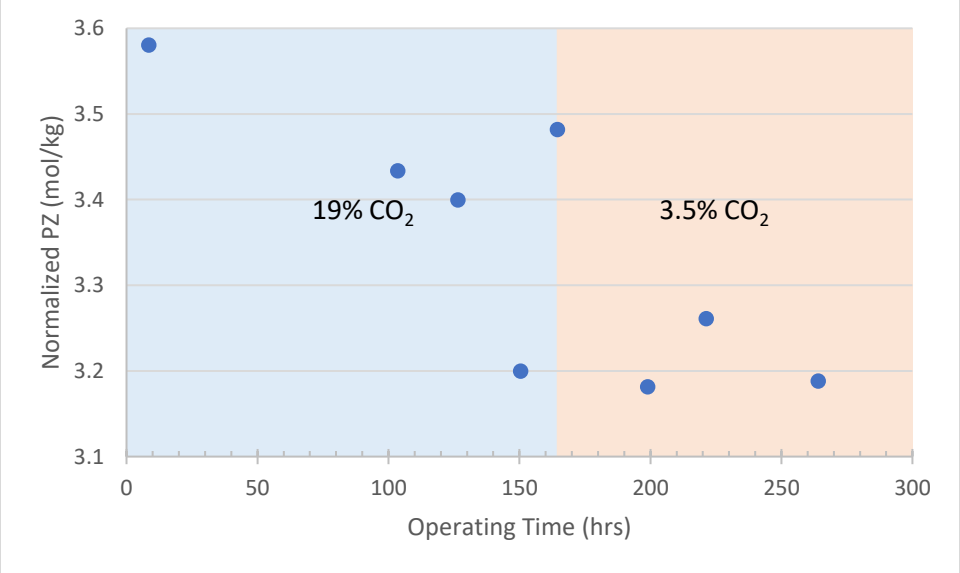

Figure 5-35: Unnormalized PZ concentration during the SRP campaign

5.3.2 SRP 2022 Campaign

The SRP 2022 campaign started with the end solvent of SRP 2018 campaign. The

initial solvent contained 7.55 mmol/kg EDA, 2.03 mmol/kg total formate, 0.012 mmol/kg Fe, and 5.12 mmol/kg Li. The concentrations of all the species decreased compared to the sample collected at the end of the SRP 2018 campaign, which may be caused by precipitation during storage over four years. The campaign used a total inventory of 400 gallons. The important operational changes in the campaign are listed in Table 5-6.

Table 5-6: Important process changes in the SRP 2022 campaign

Operating Time (hrs)	Important Process Changes
264	Start
523	1 ppm of NO_2 in inlet gas
737	Increase residence time in warm rich bypass
761	N_2 sparging at 6 scfm
811	N_2 sparging at 10 scfm
832	Stop N_2 sparging
956	Treat 1.55 gpm of solvent with 3.5 kg carbon

The accumulation rate of the degradation and corrosion products, together with the PZ oxidation rate is summarized in Table 5-7. A more detailed discussion is provided in the rest of the chapter.

Table 5-7: Accumulation rate of chemicals in the solvent

	Baseline	**NO_2**	**Warm rich (N_2)**	**Warm rich (No N_2)**	**Warm rich (Carbon)**
PZ (mmol/kg-hr)	-1.2	-2.5	4.1	-1.2	1.6
PZ-one (mmol/kg-hr)	0.04 ± 0.04	0.10 ± 0.02	0.09 ± 0.03	-0.15 ± 0.05	0.03 ± 0.15
320 nm Absorbance (A/hr)	0.003 ± 0.002	0.008 ± 0.000	0.005 ± 0.001	0.004 ± .003	-0.004 ± 0.003
Fe (mmol/kg-hr)	-5E-6 ± 1E-05	3E-05 ± 1E-05	Step Increase	-4E-05 ± 1E-05	-3E-05 ± 2E-05
Total formate (mmol/kg-hr)	0.0015 ± 0.0005	0.0065 ± 0.0006	0.0047 ± 0.0002	0.0042 ± 0.0016	-0.0005 ± 0.0029
FPZ (mmol/kg-hr)	0.0007 ± 0.0009	0.0045 ± 0.0007	-0.001 ± 0.021	-0.0062 ± 0.0011	-0.0035 ± 0.0012
Formate (mmol/kg-hr)	0.0006 ± 0.0004	0.0023 ± 0.0005	-0.0005 ± 0.0006	0.0014 ± 0.0005	0.0003 ± 0.0017
Total acetate (mmol/kg-hr)	0.003 ± 0.000	0.012 ± 0.001	0.002 ± 0.001	0.010 ± 0.003	-0.005 ± 0.005
Total nitrate	Negligible	0.0003 ±	Negligible	Negligible	Negligible

(mmol/kg-hr)	0.000

Four species were used as tracers in the SRP campaign to account for water balance and errors in the analytical measurements. The concentrations in lean samples are plotted in Figure 5-36 Li is used to correct for metals, sulfate for anions, total sulfate for total anions, and PZ for cations. Here PZ can be treated as a tracer because the degradation rate is low, and the amount of PZ oxidized is small compared to the total inventory. The slight decrease in the sulfate and total sulfate concentration may suggest that there is a little precipitation of sulfate occurring during the operation. The Li concentration was also used to estimate the solvent inventory. A total of 255.6 g of $LiOH \cdot H_2O$ was added into the system, and the solvent inventory fluctuates around 400 gallons in the campaign.

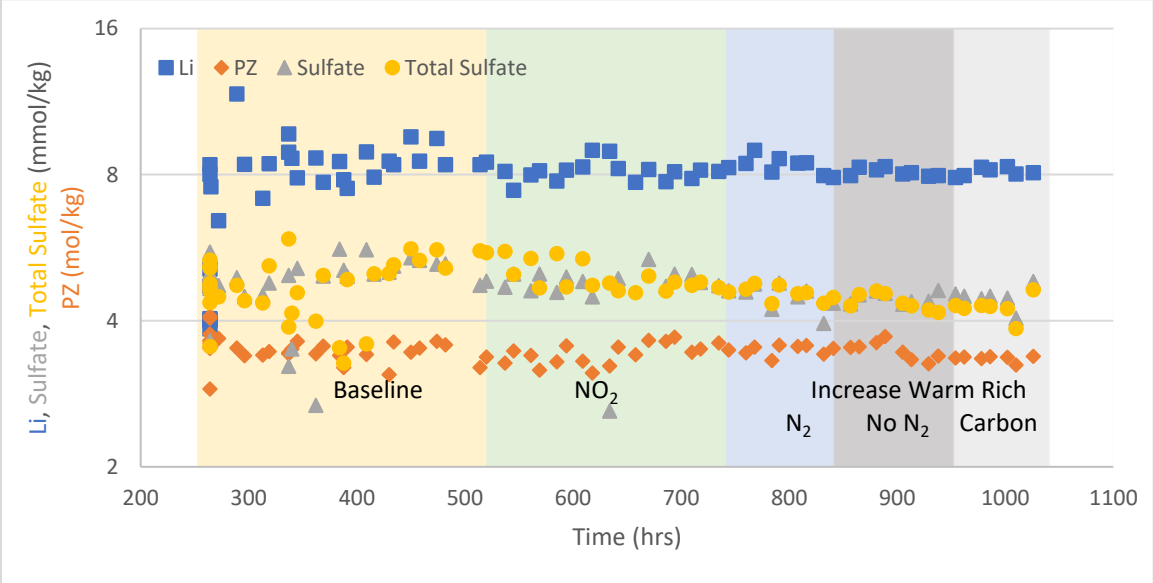

Figure 5-36: Tracer concentrations in SRP lean samples

The tracers in rich samples are plotted in Figure 5-37. The same four species: Li, sulfate, total sulfate, and PZ are used. The sulfate, total sulfate, and PZ had similar trend as observed in lean samples and were relatively stable throughout the campaign. An increase was observed in Li concentration. Since all three other species in the rich samples

suggested constant water balance, the Li tracer was not representative of the water balance. Therefore, the metal concentrations in rich samples are not normalized to avoid introduction of more errors.

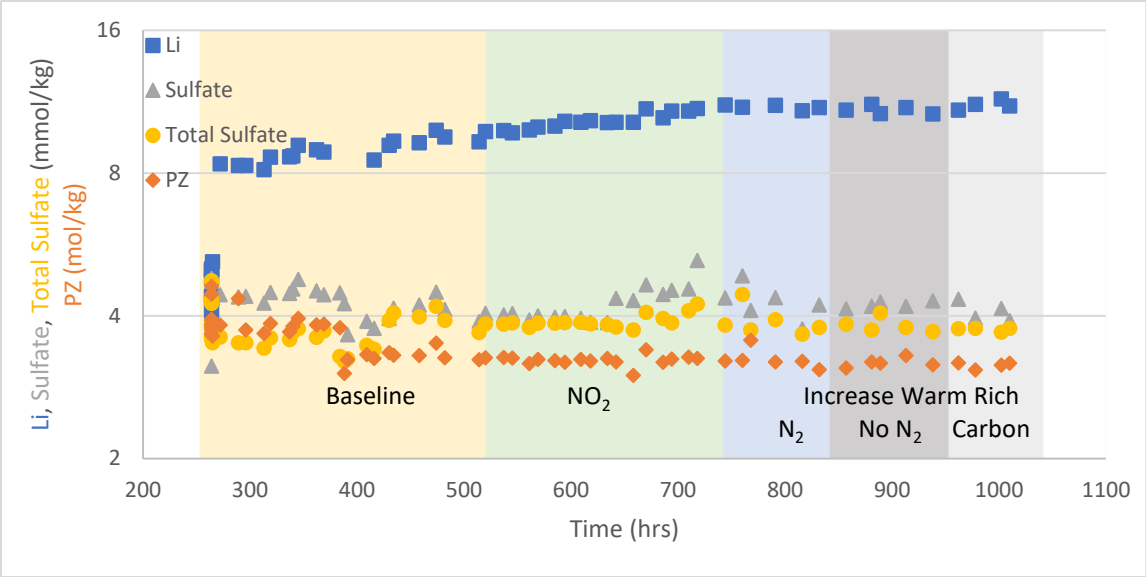

Figure 5-37: Tracer concentrations in SRP rich samples

The samples from the SRP campaign only had one absorbance peak at 320 nm, and the dilution-corrected absorbance is plotted in Figure 5-38. Since the absorbance is related to the Fe concentration, which is solubility limited, the non-normalized data were reported. During the baseline condition, the absorbance increases at 0.003 A/hr, and this rate increases to 0.006 in the NO_2 region. This means that NO_2 can accelerate the production of the UV-absorbing component. No difference was observed in regions with or without N_2 sparging, but this does not mean N_2 sparging has no effect at all. One possible reason for the constant rate is that in the N_2 sparging region, the MNPZ was not depleted and caused oxidation, cancelling out the mitigation of the N_2 sparging. The MNPZ was depleted when the N_2 sparging was turned off, so there appeared to be no changes at any of the three operating conditions. When the carbon bed was turned on, the absorbance decreased at

0.004 A/hr. The carbon testing only lasted three days and equilibrium was not reached, but it was proved that carbon treating is capable of removing the UV-absorbing component at a fast rate. The peak at 538 nm was not observed in any SRP samples, possibly because the intensity was below detection limit. In the NCCC campaigns, as shown in Figure 5-18, the intensity of the 538-nm peak is only 0.5% the intensity of the 320-nm peak. Given the small 320 nm peak intensity in the SRP samples, the intensity at 538 nm is too low to be detected if the ratio in NCCC kept constant.

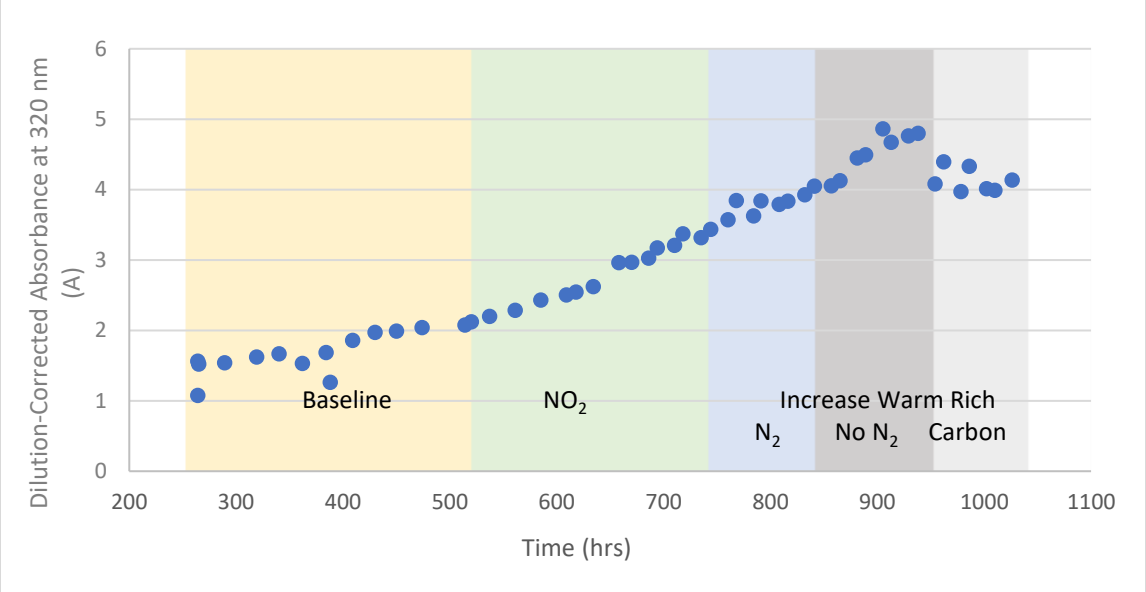

Figure 5-38: Dilution-corrected absorbance at 320 nm in SRP 2022 campaign

The lean and rich Fe concentrations are plotted in Figure 5-39. Since the Fe is solubility limited, the concentration is not normalized by the tracer. For most of the data points, the Fe in the lean samples matched the rich samples, indicating that no dissolution or precipitation of Fe occurred in the absorber. The concentrations in the SRP samples are low compared to the results from NCCC and bench-scale experiments. The Fe was relatively stable during the baseline condition and started to increase steadily when NO_2 was fed, which was a result of the higher oxidation rate. At 784 hrs, there was a step

increase in the Fe concentration, which then started decreasing at a steady rate. This can be a result of mixing of the solvent left in the newly installed warm rich bypass section. The solvent in the section was not heated and was at a lower temperature. Since the Fe solubility was higher at low temperature, the Fe concentration in the solvent residue in warm rich bypass section was higher than the Fe in the system, which is limited by the solubility at high temperature. As a result of the mixing, there was a step increase in Fe concentration, which surpassed the solubility limit at high temperature and resulted in the decrease of Fe afterwards.

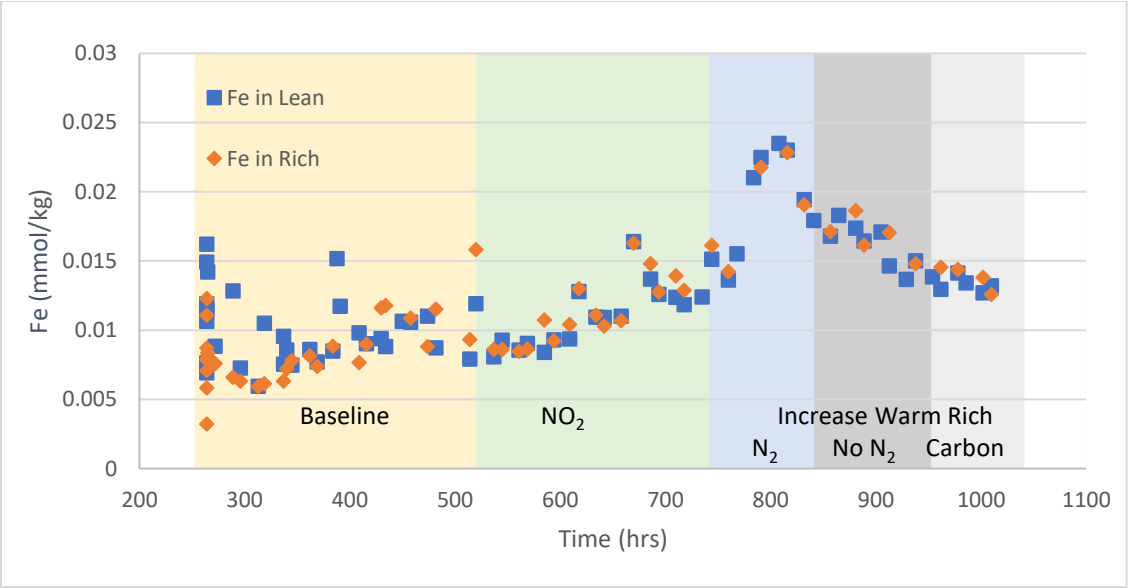

Figure 5-39: Non-normalized Fe in SRP 2022 campaign

The total mols of PZ was calculated from the IC method results and solvent inventory was estimated from the Li tracer concentration. As shown in Figure 5-40, the PZ loss rate was 1.2 mmol/kg-hr during the baseline region, and 2.5 mmol/kg-hr during the NO_2 region. However, since the starting PZ concentration is very high relative to the PZ lost over the campaign, it is difficult to get an accurate oxidation rate from the PZ data. The data suggest qualitatively that 1 ppm NO_2 can cause an increase in the PZ oxidation rate.

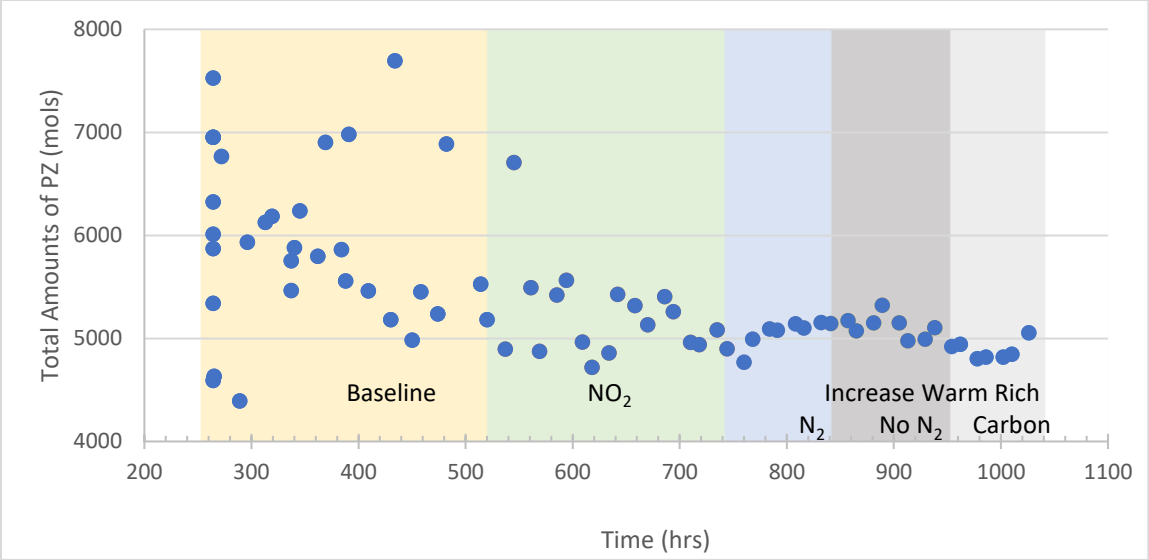

Figure 5-40: PZ inventory in SRP 2022 campaign

Normalized PZ-one, the degradation product which accumulated at the highest concentration during this campaign, is shown in Figure 5-41. PZ-one fluctuated at the beginning of the campaign because of multiple shutdowns due to cold weather and equipment failure. If these outliers are disregarded, the PZ-one accumulated at 0.04 mmol/kg-hr. This rate increased to 0.1 mmol/kg-hr after NO_2 was blended into the flue gas at 1 ppm, indicating that NO_2 is important in PZ-one production. The decrease in PZ-one concentration at 640 hrs was due to a plug in the warm rich bypass, where an uneven mixing occurred when the precipitation was redissolved. Similar behavior was also observed in EDA and formate concentrations. After the NO_2 was turned off, the PZ-one continued to increase at 0.09 mmol/kg-hr, suggesting that the effects of NO_2 continued until the MNPZ was depleted. After depleting the MNPZ, the PZ-one became stable and stopped increasing. Carbon treating did not remove PZ-one from the solvent.

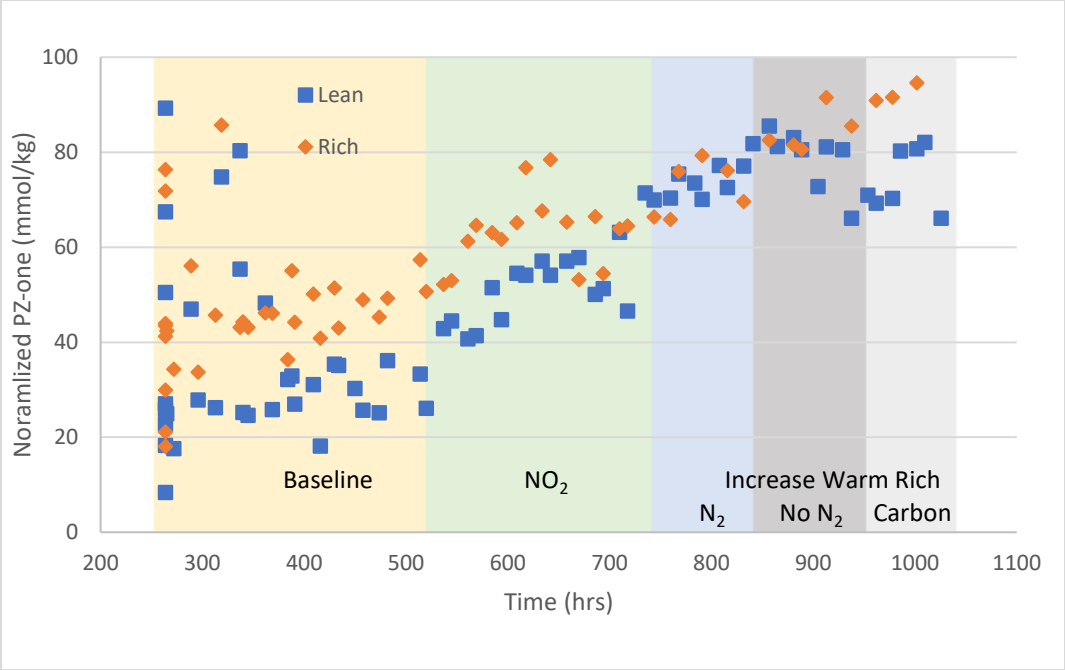

Figure 5-41: Normalized PZ-one (the major degradation product) in SRP 2022 campaign

Normalized EDA which is the degradation product with the second largest concentration, is plotted in Figure 5-42. The EDA in rich samples and lean samples followed the same trend. The EDA in rich is consistently higher than the EDA in lean samples, which may be due to the thermal degradation of EDA into 2-imidazolidone at high temperature (Freeman, 2011). In the first 744 hrs, the EDA increased at 0.03 mmol/kg-hr, and this rate did not change as NO_2 was fed, indicating that NO_2 had no effect on EDA production. After EDA reached 25 mmol/kg, it stopped increasing and started to decrease. This has been observed in multiple plants (Nielsen, 2018), and is believed to be unrelated related to the operational changes in the system.

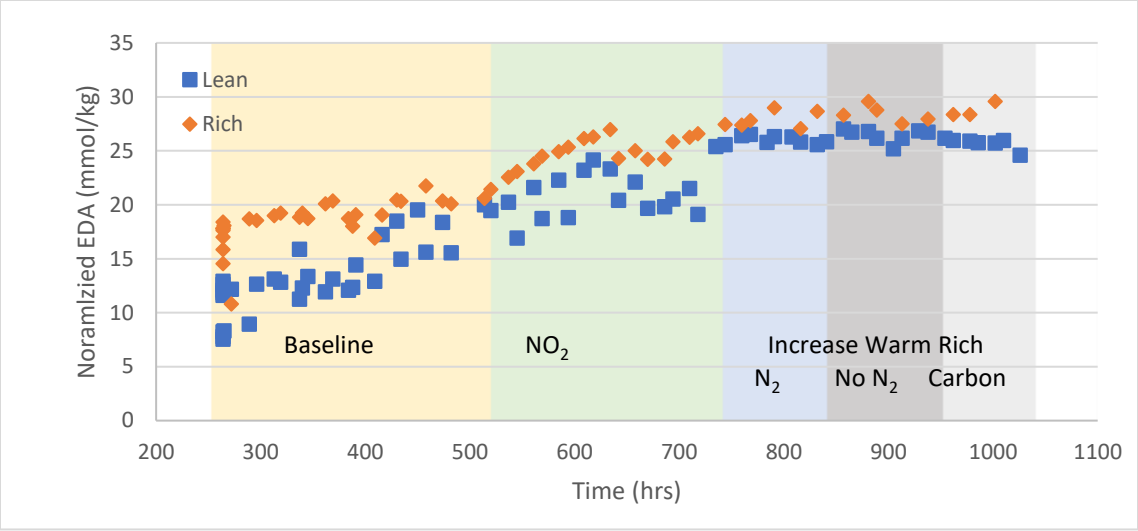

Figure 5-42: EDA normalized by PZ in SRP 2022 campaign

As shown in Figure 5-43, the normalized AEP, a thermal degradation product, accumulated steadily at 0.014 mmol/kg-hr before the carbon bed was turned on, indicating that AEP production was not affected by NO_2, warm rich residence time change, or N_2 sparging. After the carbon treating was applied, the AEP concentration decreasedNo significant difference was observed between the AEP in rich and lean.

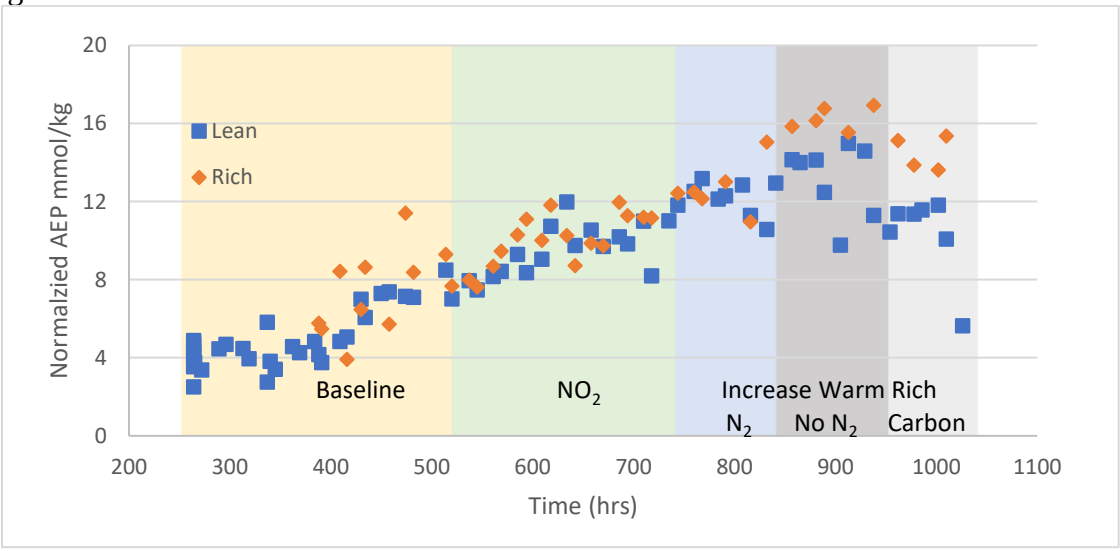

Figure 5-43: AEP normalized by PZ in SRP 2022 campaign

The ammonium in the solvent was normalized and plotted in Figure 5-44. The

ammonium is consistently higher in rich samples than in lean samples, indicating that it is removed in the stripper with the CO_2. It is still unclear why the ammonium data became less scattered in the latter half of the campaign.

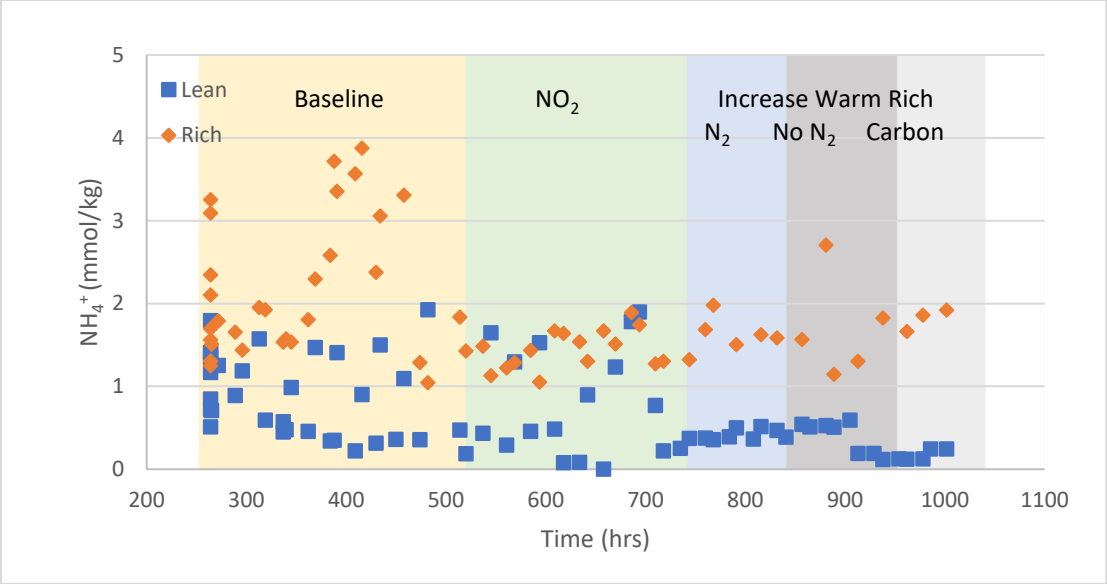

Figure 5-44: NH_4^+ normalized by PZ in SRP 2022 campaign

The HEP and MPZ normalized by PZ are plotted in Figure 5-45. The HEP stayed constant until 900 hrs, meaning that it was not a degradation product in the SRP campaign. A step decrease was observed afterwards, the reason for which is still unclear. The MPZ increased steadily and is not related to the operating conditions.

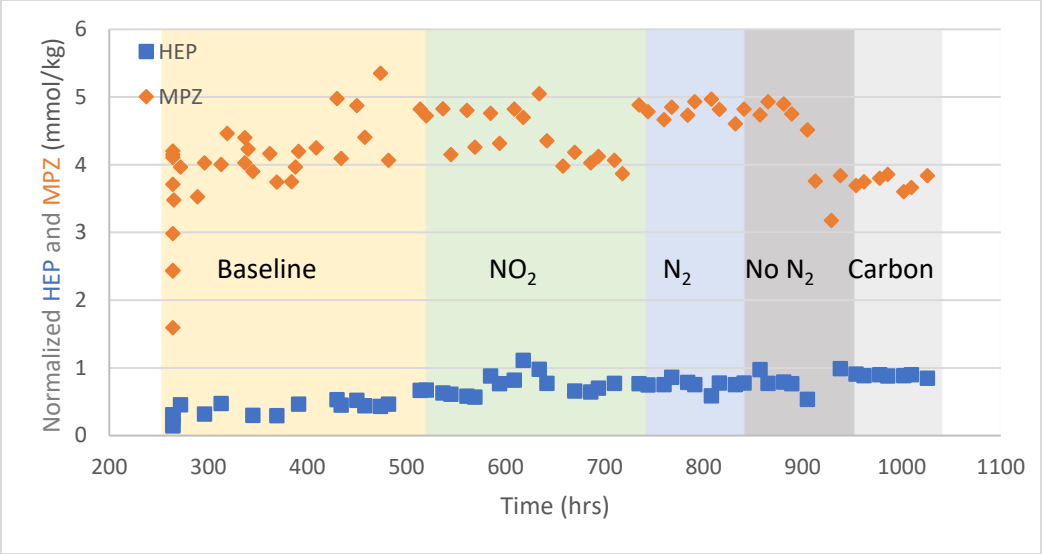

Figure 5-45: HEP and MPZ normalized by PZ in SRP 2022 campaign

The normalized formate, total formate, and FPZ are shown in Figure 5-46. The formate is normalized with sulfate, total formate is normalized with total sulfate, and FPZ is normalized with PZ. All three species had a low accumulation rate during the baseline condition, and a higher rate during the NO_2 condition, suggesting the NO_2 accelerates formate production. The NO_2 also shifted the equilibrium towards FPZ. The total formate continued to increase when the NO_2 was turned off, but the concentration of formate and FPZ did not increase, meaning that amides other than FPZ were produced in that period. When the carbon bed was turned on, the FPZ and total formate decreased, but the rate of total formate is much lower than the FPZ, which indicates that the carbon may remove a small portion of FPZ, but there are other degradation products that also formed amides with formate.

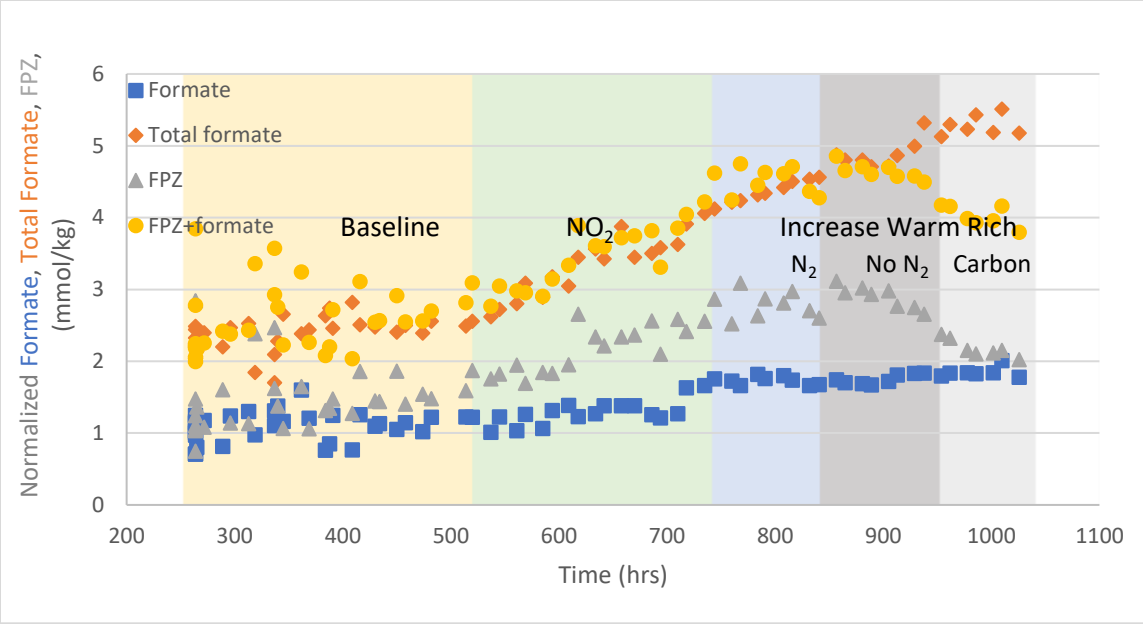

Figure 5-46: Normalized formate, total formate, and FPZ in SRP 2022 campaign.

Although formate was normally the heat stable salt with the highest concentration, acetate had the fastest accumulation rate in the SRP campaign. The acetate normalized by sulfate and the total acetate normalized by total sulfate are plotted in Figure 5-47. Although there is some scatter in the region between 400 hrs and 700 hrs in the acetate, the acetate and total acetate are close to each other, indicating that most of the acetate is in the salt form instead of the amide form. The accumulation rate of total acetate was 0.003 mmol/kg-hr in baseline, 0.012 mmol/kg-hr in baseline with NO_2, 0.001 mmol/kg-hr in baseline with high warm rich residence time and N_2 sparging, 0.010 mmol/kg-hr in baseline with high warm rich residence time and no N_2 sparging, and -0.003 mmol/kg-hr in baseline with carbon bed. This suggests that NO_2 accelerated acetate production, but the effect diminished quickly and MNPZ had little or no effect on acetate production. N_2 sparging reduced the acetate production by 10 times, and carbon treating removed the acetate from the solvent.

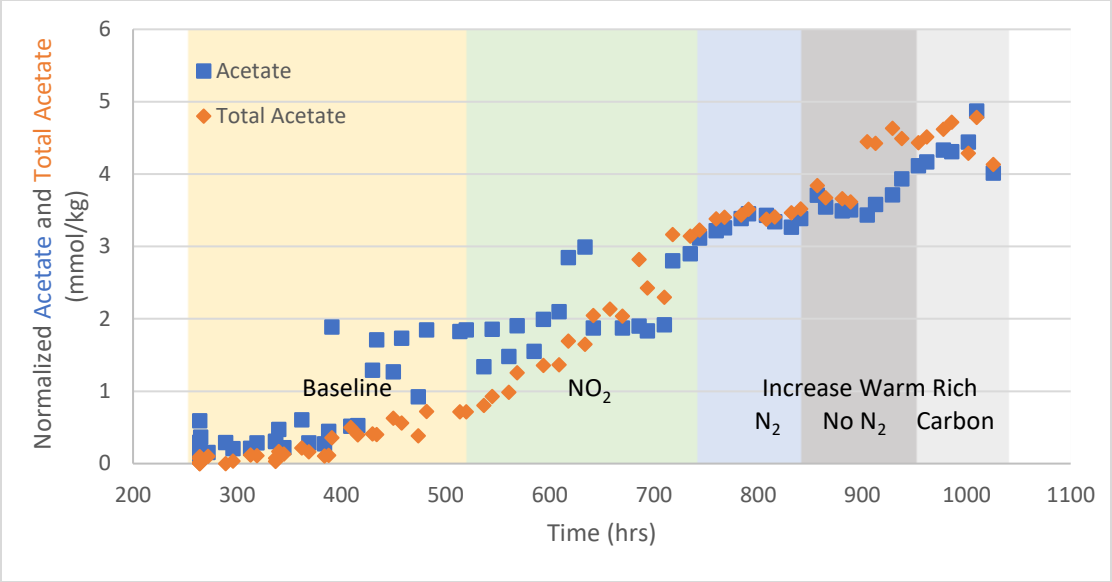

Figure 5-47: Normalized acetate and total acetate in SRP 2022 campaign

As shown in Figure 5-48, the total oxalate concentration is low and increases at a low rate. No significant difference was observed before the carbon treating. The oxalate matched the total oxalate before 670 hours, but decreased afterwards, indicating that the equilibrium between the salt form and the amide form shifted, and more oxalate was in amide form as the solvent became more degraded. Both the oxalate and total oxalate decreased after carbon treating, showing the ability of the carbon to remove oxalate from the solvent.

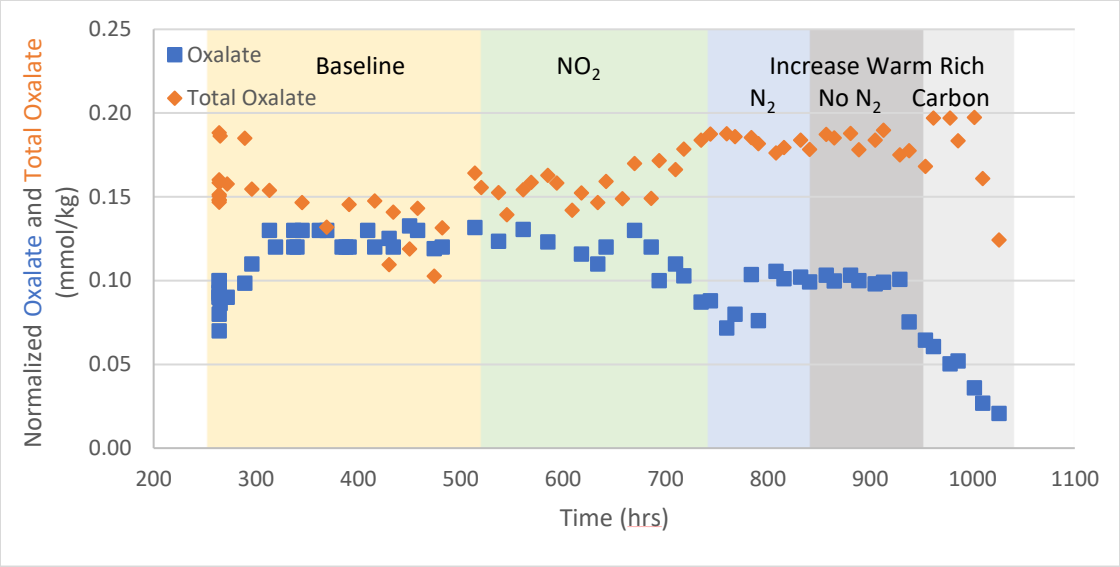

Figure 5-48: Normalized oxalate and total oxalate in SRP 2022 campaign

The normalized nitrate and total nitrate are shown in Figure 5-49. Similar to the acetate, the nitrate and total nitrate concentrations are very close to each other. The nitrate concentration only increased during the NO_2 condition at a rate of 0.0003 mmol/kg-hr, which means that nitrate is not a degradation product from PZ oxidation, but a product completely of NO_2. Thus, the concentration of the nitrate can be used as an indicator of NO_2 level in the flue gas. Another valuable point is that the solvent absorbed 2.5 mmol/kg of NO_2 in total, but the nitrate concentration only increased by 0.08 mmol/kg, so 1 mol of NO_2 only produces 0.032 mol of nitrate. No nitrite peak was observed in the SRP samples, so the nitrite concentration was less than 0.02 mmol/kg, the detection limit on the IC.

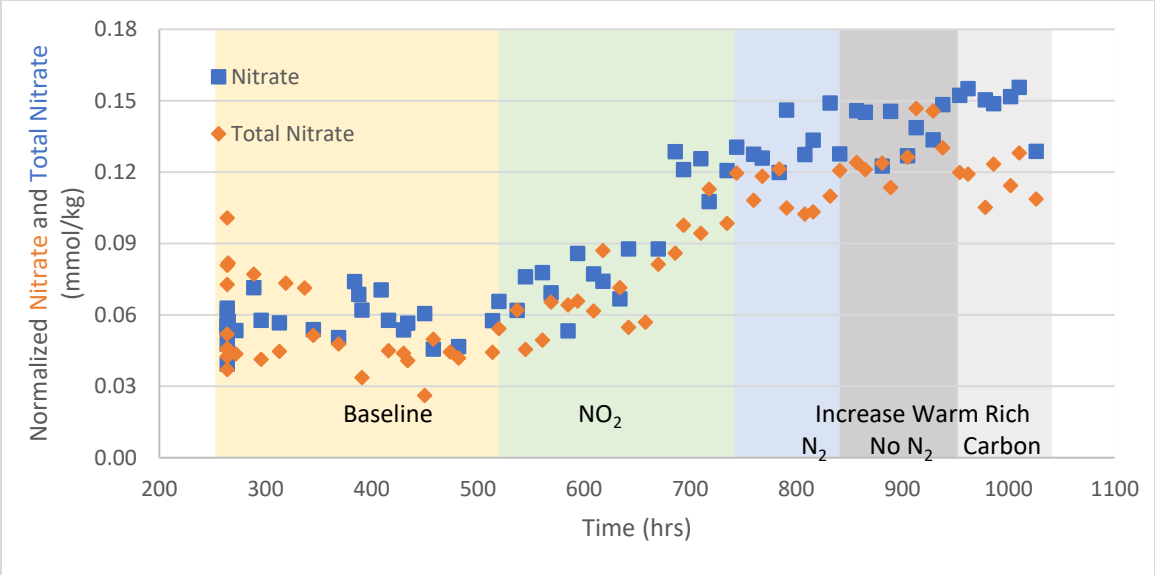

Figure 5-49: Normalized nitrate and total nitrate in SRP 2022 campaign

The anions and total anions in the rich samples were quantified and compared with the results in lean samples, as shown from Figure 5-50 to Figure 5-57. No significant differences were observed in any species, indicating that the cycling between high and low temperatures and pressures had little effects on the anion species. The nitrate in the lean solvent is 0.05 mmol/kg higher than the nitrate in the rich solvent, so there might be an unknown anion species exists only in the lean solution, and elutes at the same time as nitrate on anion IC.

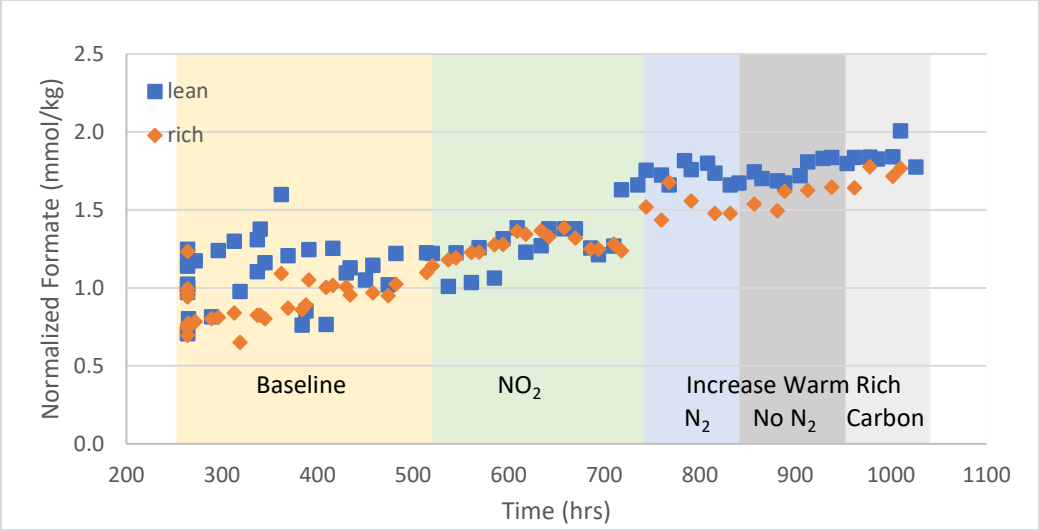

Figure 5-50: Normalized formate in SRP 2022 lean and rich samples

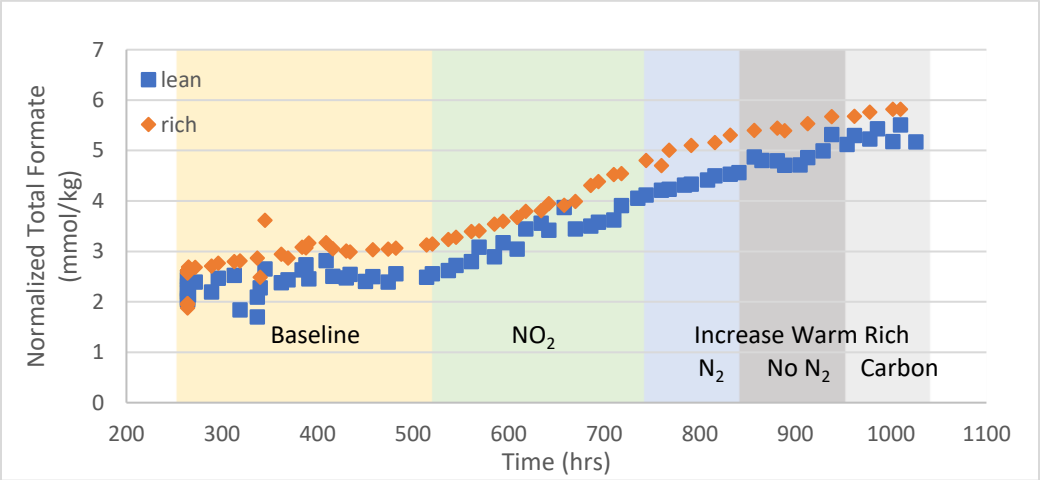

Figure 5-51: Normalized total formate in SRP 2022 lean and rich samples

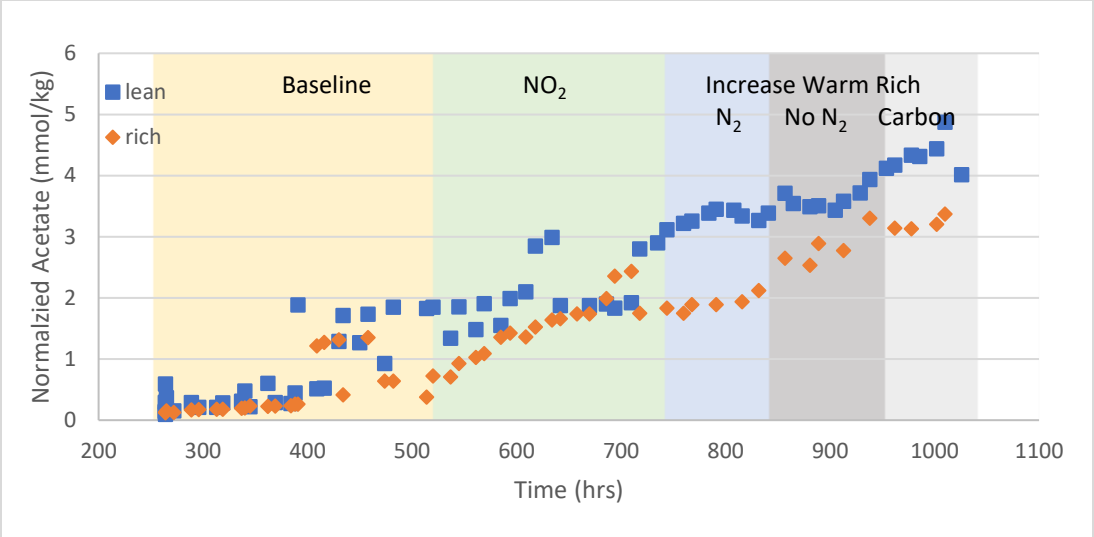

Figure 5-52: Normalized acetate in SRP 2022 lean and rich samples

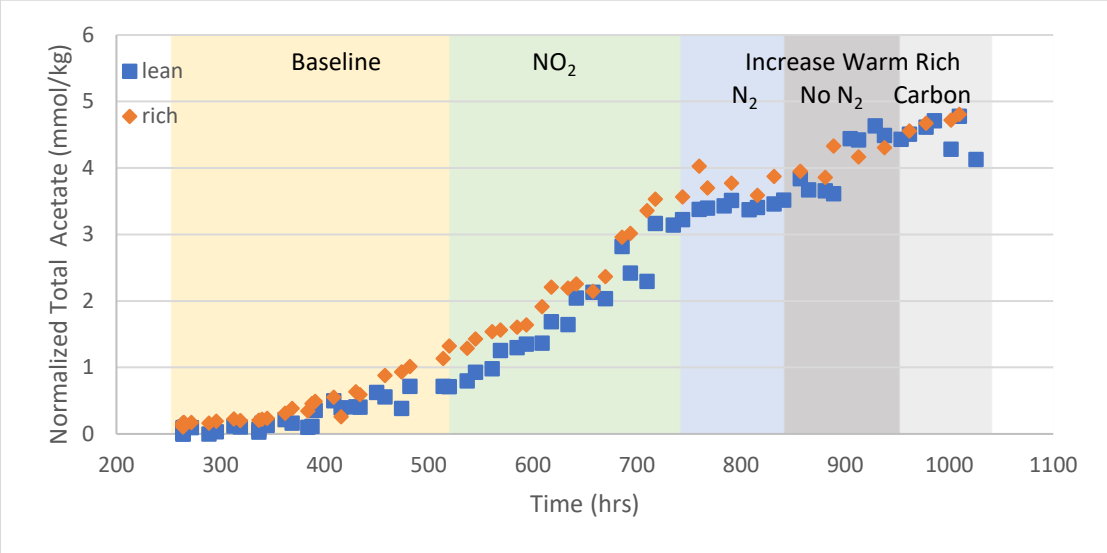

Figure 5-53: Normalized total acetate in SRP 2022 lean and rich samples

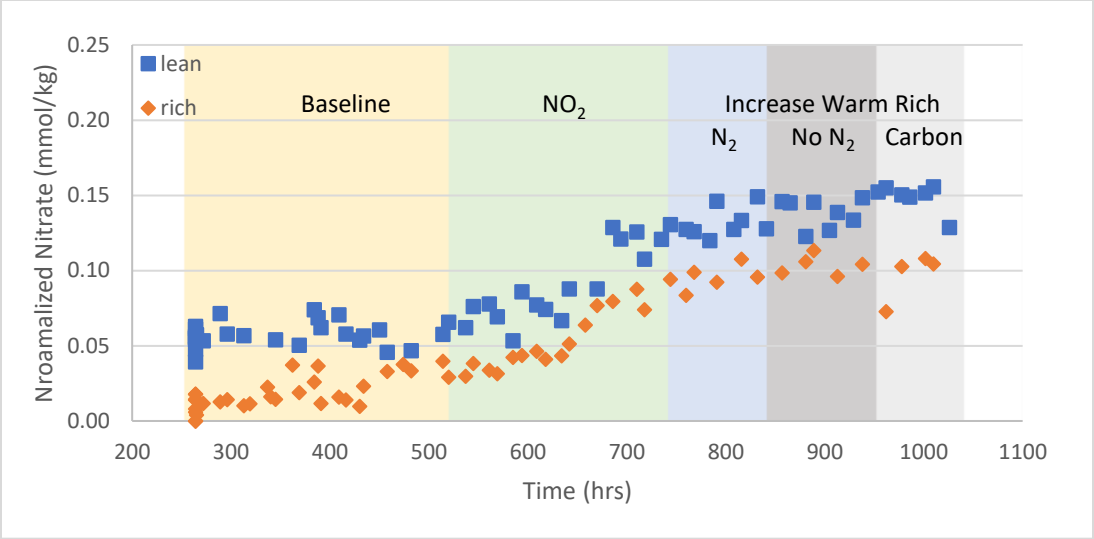

Figure 5-54: Normalized nitrate in SRP 2022 lean and rich samples

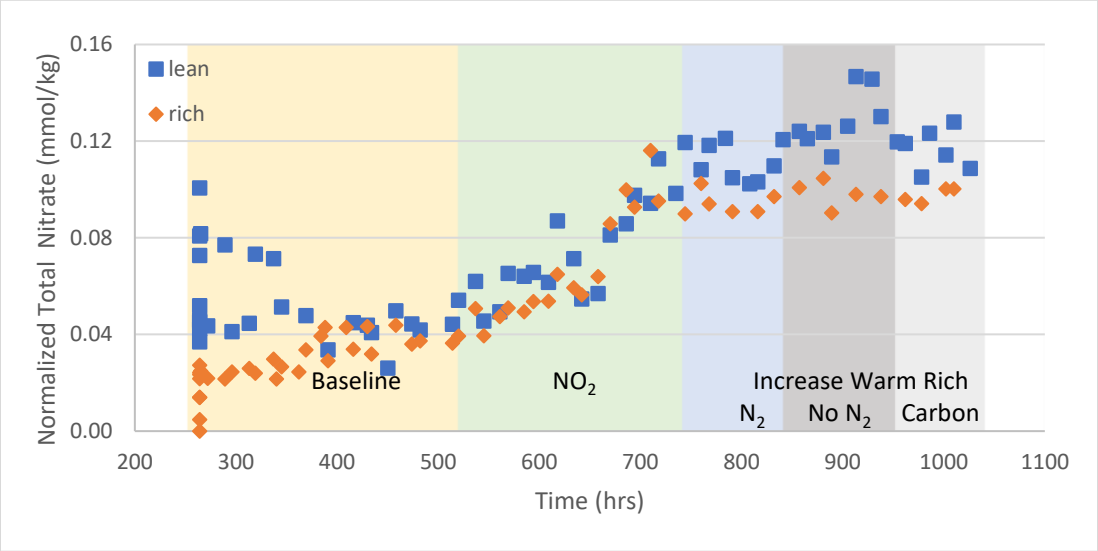

Figure 5-55: Normalized total nitrate in SRP 2022 lean and rich samples

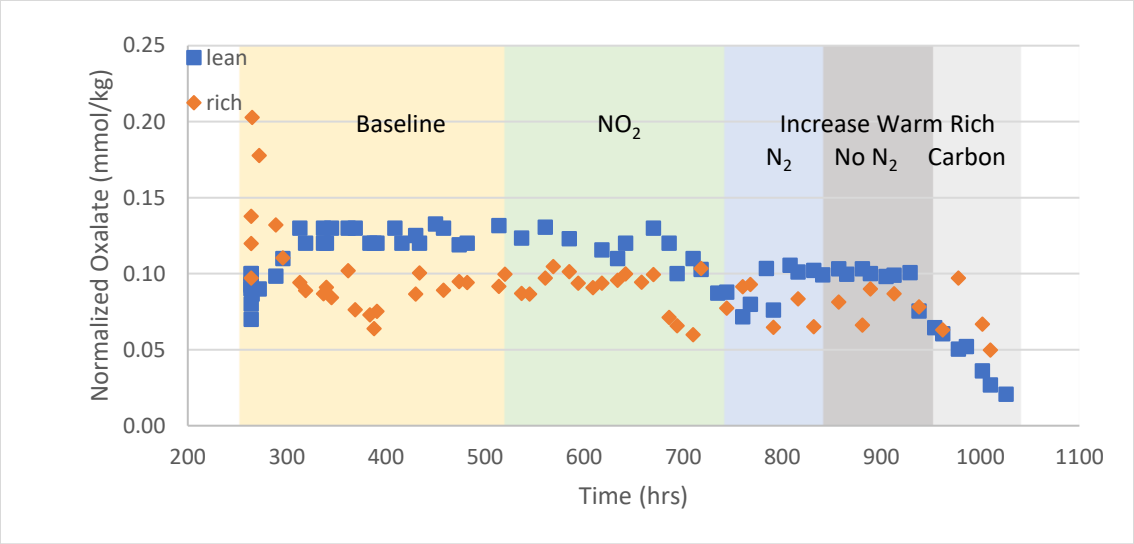

Figure 5-56: Normalized oxalate in SRP 2022 lean and rich samples

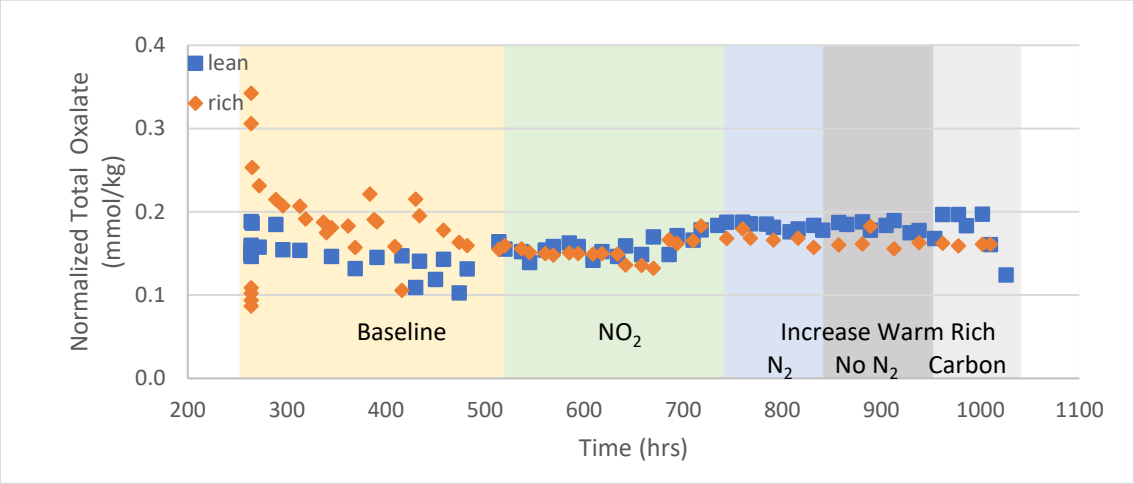

Figure 5-57: Normalized total oxalate in SRP 2022 lean and rich samples

The normalized stainless steel metal ion concentrations are plotted in Figure 5-58. the concentrations of all the metal ions are low. The Cr has a faster accumulation rate with NO_2, but no significant difference was observed in data for the other metal ions. The carbon did not remove any of the metals, which was different from the bench-scale results that carbon can remove Cr and Mn. This is possibly because the concentration of Cr and Mn are low in the solvent, and the driving force is too small to provide a detectable rate of

removal.

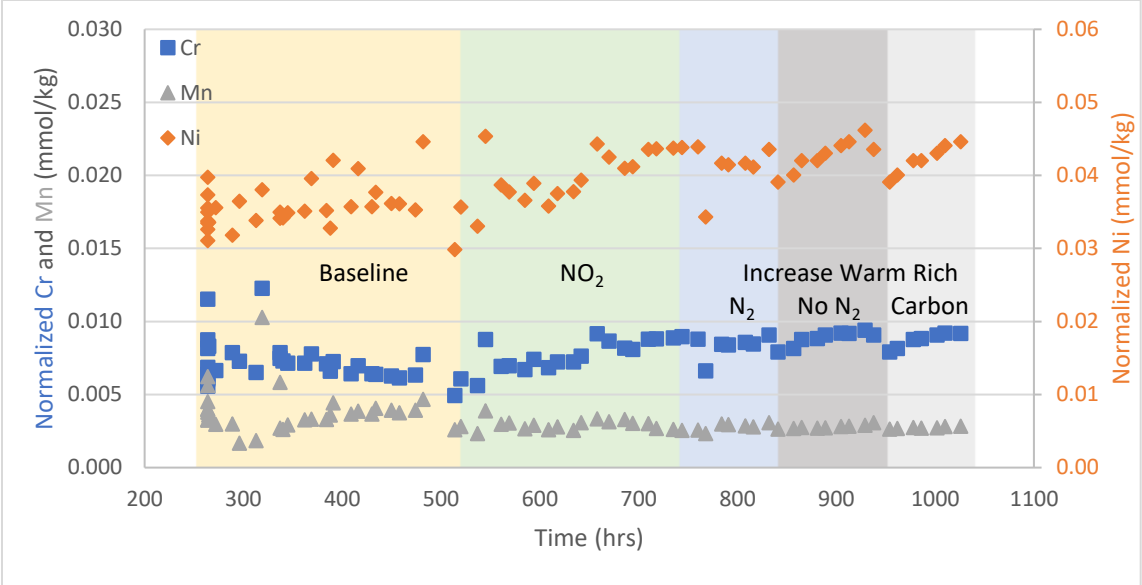

Figure 5-58: Normalized Ni, Cr, and Mn in SRP 2022 lean samples

Since the Li in rich samples increased continuously and was not caused by dilution factor, the Ni, Cr, and Mn were not normalized, and the raw data was shown in Figure 5-59. Similar trends were observed in the rich samples as in the lean samples.

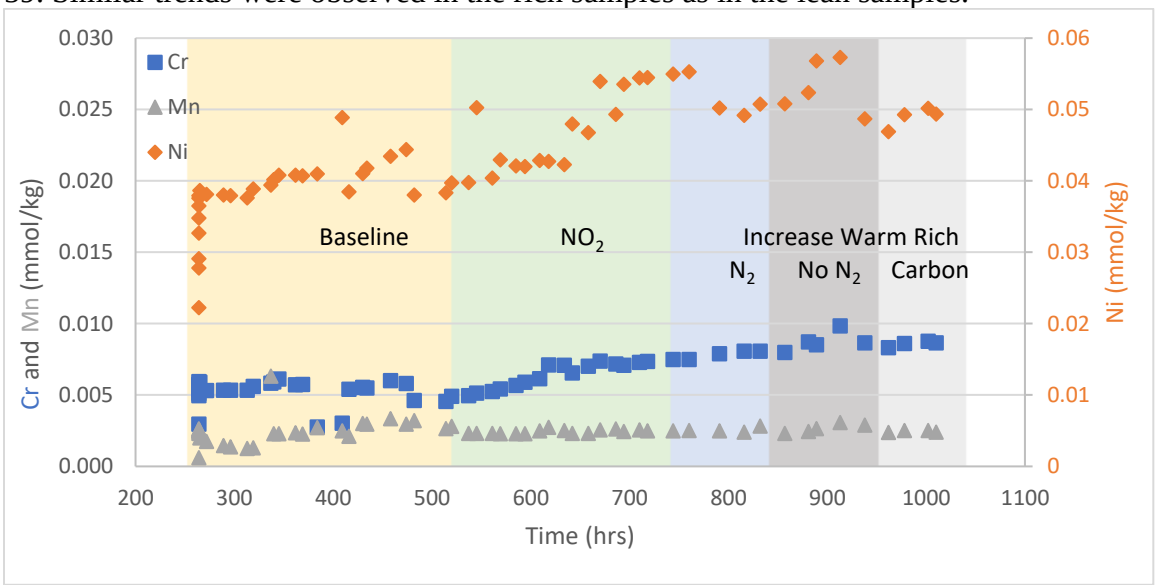

Figure 5-59: Unnormalized Ni, Cr, and Mn in SRP 2022 rich samples

Excess 0.2 N H_2SO_4 was added to 3.3478 g of SRP used carbon to quantify the Fe removed more accurately. Eight batches of H_2SO_4 were added, and each batch was drained completely before the new batch was added. The time and amount of H_2SO_4 added is shown in Table 5-8. The Fe concentration became negligible after 264.78 g of 0.2 N H_2SO_4 was used to rinse the carbon, and almost all the Fe was removed from the carbon. From the Fe concentration and the mass of 0.2 N H_2SO_4, it is calculated that there was 54.5 mmol Fe/kg of carbon on the SRP used carbon. Since there was 36.3 mmol Fe/kg of carbon on the clean carbon, a total of 63.6 mmol Fe was adsorbed by the carbon in the SRP campaign, which corresponds to 0.04 mmol Fe/kg solvent with a total inventory of 1500 kg, compared to 0.012 mmol Fe/kg solvent measured at the end of the campaign. Therefore, as the carbon bed removes dissolved Fe, the Fe is replaced (and some of it removed), presumably by dissolving soluble iron solids from some point in the system.

Table 5-8: 0.2 N H_2SO_4 addition in SRP used carbon

Time (hours)	Mass of 0.2 N H_2SO_4 (g)	[Fe] in H_2SO_4 Eluent (mmol/kg)
0.17	66.56	0.09
0.34	67.53	1.16
0.67	62.02	1.09
1	68.65	0.28
1.33	64.94	0.08
1.67	66.49	0.06
2	66.60	0.03
2.5	67.39	0.02

5.4 Comparisons between Different Pilot Plant Campaigns

The N balance of the PZ oxidation in all the pilot plant campaigns is shown in Tables 6-9, which includes the newly produced degradation products, the amount of volatile amine loss, and the total loss of PZ. The units for all the species are in mmol/kg. The small fraction of N accounted for in all campaigns indicates that PZ may be lost through other outlets that were not monitored, for example, the stripper gas outlet. Compounds with high molecular weight were present in the solvent, as shown in Figure 5-25 and 6-26, indicating that PZ could have polymerized, and these losses were not included in the degradation products that have been analyzed. The use of carbon has removed some degradation products, which underestimates the degradation products produced, therefore, the %N is smaller in the NCCC 2019 and SRP 2022 campaigns.

Table 5-9: N balance of the pilot plant campaigns (mmol/kg)

	NCCC 2018	NCCC 2019	SRP 2022
NH_3	104	182.1	27.9
Volatile PZ by FTIR	109	29.3	30.3
PZ-one	9.67	24.61	66.1
PZ-ol	49.25	1.25	28.43
EDA	21.13	-14.27	17.04
AEP			10.09
MPZ	4.83	11.67	0.99
HEP			4.49
MNPZ	0.4	0.5	
FPZ	2.42	26.09	2.02
liquid phase PZ loss	646	900	680
N(%)	38.5	18.9	25.5

The comparison of Fe concentration at SRP, NCCC, PP2, and CSIRO Tarong is shown in Figure 5-60. The Fe in PP2 and CSIRO Tarong is significantly higher than in SRP and NCCC. Since the Fe concentration was found to be directly related to degradation extent, it is possible that the use of the AFS reduced the oxidation rate by having only a portion of solvent heated to high temperature and flashing out the O_2 before the solvent reached high temperature. As a result, the oxidation was low in SRP and NCCC, causing a lower Fe concentration. As tested in SRP 2022, the existence of NO_2 in flue gas can increase the Fe accumulation rate, therefore, the 1-5 ppm NO_2 in PP2 and CSIRO Tarong can also cause a higher Fe rate. The SRP campaigns had the lowest Fe, which is because

of the synthetic flue gas used. Since the Fe shuttle mechanism requires a dissolved Fe concentration that is larger than the 0.05 to 0.2 mmol/kg dissolved oxygen concentration, the low Fe in SRP and NCCC indicated that the amount of oxidation due to the Fe shuttle mechanism is small.

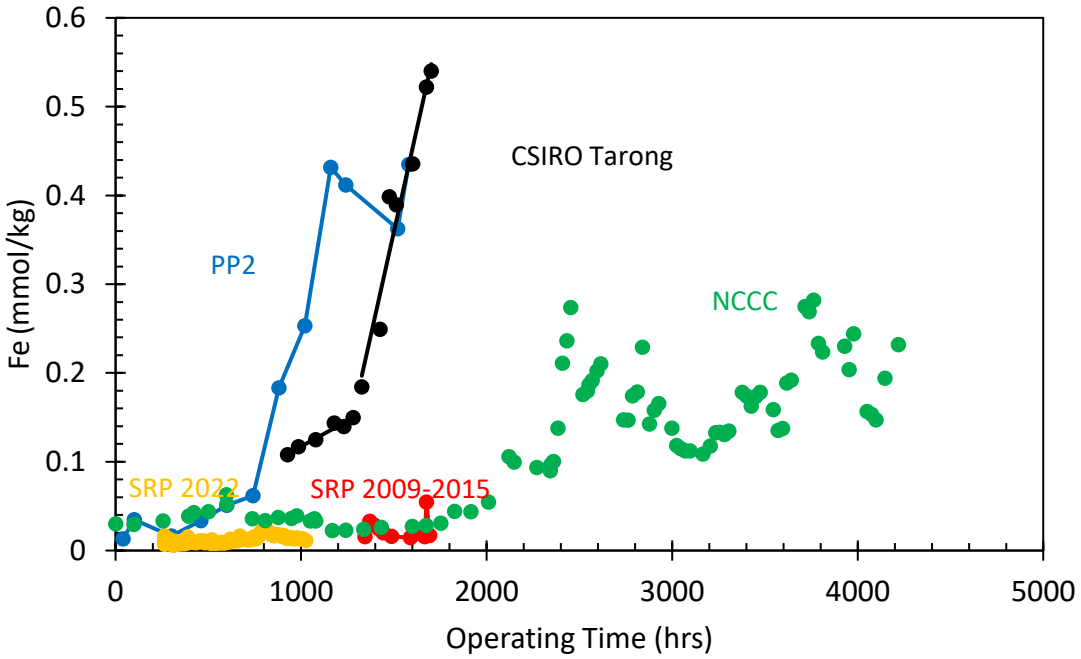

Figure 5-60: Comparisons of Fe in different pilot plant campaigns (CSIRO Tarong, PP2, SRP, and NCCC)

The comparison of total formate in different campaigns is shown in Figure 5-61. PP2 and CSIRO Tarong had a higher total formate concentration than SRP and NCCC and is most likely due to the high NO_2 concentration in the flue gas. It was also shown in the SRP 2022 campaign that NO_2 can cause a higher total formate production rate.

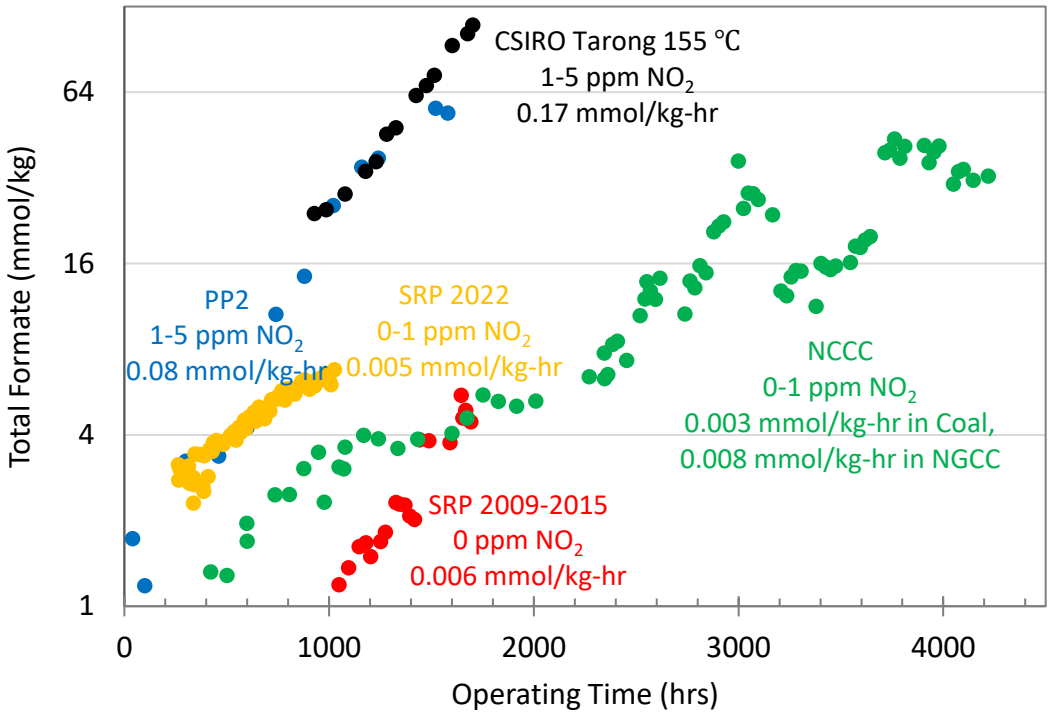

Figure 5-61: Comparisons of total formate in different pilot plant campaigns (CSIRO Tarong, PP2, SRP, and NCCC)

The EDA comparison is shown in Figure 5-62. In most of the campaigns, EDA decreased after reaching 30 to 40 mmol/kg-hr, indicating that EDA is in equilibrium with 2-imidazolidone, and any newly produced EDA would be degraded. Greater EDA was observed in NCCC samples when the stripper temperature was reduced to 140 ℃ , which shows that the EDA equilibrium is related to temperature, and a lower temperature favors the equilibrium towards EDA. No decrease was observed in SRP 2009-2015 samples because the EDA concentration was still low in these solvents. Another difference between SRP 2009-2015 and all other campaigns was that 1 wt% Inh A was added into the solvent.

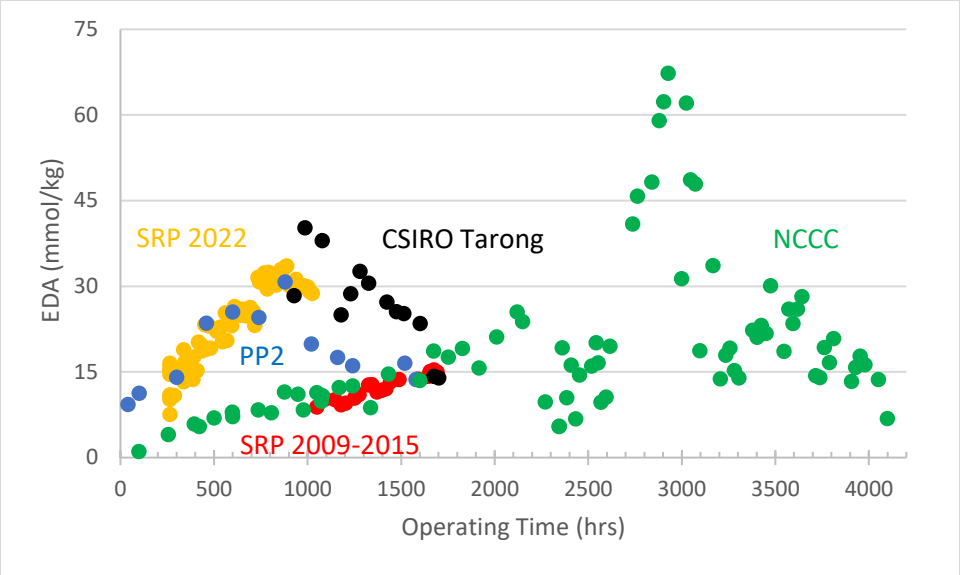

Figure 5-62: Comparisons of EDA in different pilot plant campaigns (CSIRO Tarong, PP2, SRP, and NCCC)

The total nitrogen of all the degradation products are compared and plotted in Figure 5-63. The species accounted for includes gas-phase NH_3 and liquid phase NH_4^+, PZ-ol, PZ-one, FPZ, EDA, MPZ, AEP, and MNPZ. No FTIR measurements were performed in PP2, CSIRO Tarong, and SRP 2009-2015 Campaign, therefore, the gas-phase NH_3 was estimated from total formate. The accumulation of total nitrogen was much faster with NO_2 present, indicating that NO_2 can increase PZ oxidation significantly.

Inhibitor A (1 wt% potassium iodide) was added to the solvent used at SRP from 2009-2015. However it appears that the low oxidation rate in that period resulted from the absence of NO_2. Experiments with inhibitor A in the HTOR also suggest that it does not reduce piperazine oxidation with temperature cycling (reference the experiments).

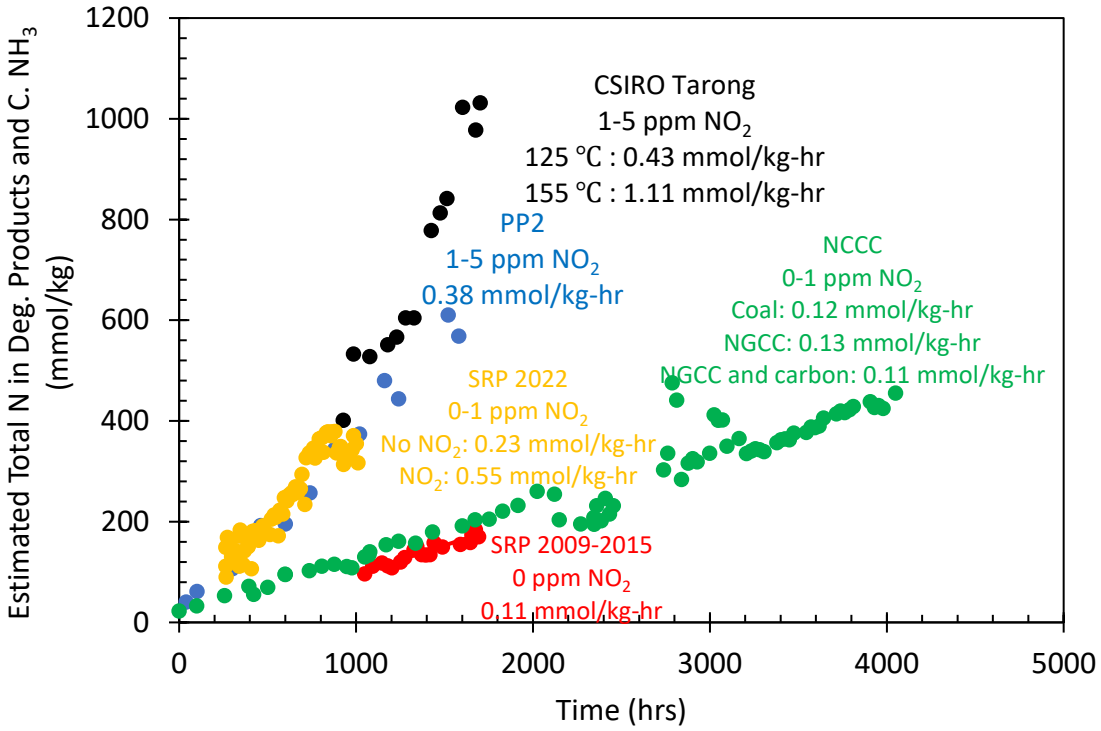

Figure 5-63: Comparisons of total nitrogen in degradation products in different pilot plant campaigns (CSIRO Tarong, PP2, SRP, and NCCC)

5.5 CONCLUSIONS

5.5.1 NCCC Campaigns

1. In the NCCC campaigns, PZ oxidizes at a slow rate.
    a. Low NH_3 emission (280 mmol/kg over 4000 hrs)
    b. Low PZ oxidation rate (0.07 mmol/kg-hr from NH_3 results, and 4.1 mmol/kg-hr from PZ results)
    c. Possible reasons: use of advanced flash stripper, absence of NO_2 in inlet gas
    d. Total formate is high due to carry over from carbon bed
2. The oxidation rate of PZ can be reduced by lowering the stripper sump level, applying nitrogen sparging, and removing NO_2 in inlet gas. A combination of these

three methods reduced the PZ oxidation rate by 13%.

3. Dissolved iron concentration is correlated with the solvent oxidation rate rather than the extent of solvent degradation.
4. More PZ was lost due to aerosol and volatile loss than due to oxidation in NCCC campaigns.
5. The dissolved Fe increased from 0.06 mmol/kg to 0.29 mmol/kg in NCCC 2019, and the rate of increase is much faster than in NCCC 2018. This could be due to the high temperature in the stripper sump.
6. EDA reached a high concentration when the stripper temperature was low, indicating that the equilibrium between EDA production and degradation is highly correlated to stripper temperature. When the stripper temperature was 150 ℃ , EDA started decreasing after reaching 30 mmol/kg.
7. Carbon treating removes complexes of PZ and degradation products that catalyze oxidation
    a. The NH_3 production rate decreased from 0.1 mmol/kg-hr to 0.056 mmol/kg-hr after 400 hrs of operation
8. Carbon treating removes Fe and Cr from the solvent.
    a. The carbon removed 6.6 mmol Fe/kg solvent from the solvent, but the Fe concentration in solvent stayed constant at 0.1 mmol/kg.
    b. Whenever the carbon removes the dissolved Fe, more Fe as soluble solid will dissolve into the solvent. Therefore, the whole inventory of soluble Fe must be removed to result in a decrease in Fe concentration.

5.5.2 SRP Campaigns

1. The PZ loss rate is low in SRP campaigns. The highest loss rate (1.67 mmol/kg-hr)

was observed with NO_2 injection.

2. PZ-one is the dominant cation product. The accumulation rate increases with NO_2, and the effect of NO_2 lasts until the MNPZ is depleted.
3. EDA and AEP are not affected by NO_2. EDA levelled out at 25 mmol/kg, and AEP was removed by the carbon bed.
4. Acetate is the dominant anion product. The accumulation rate was relatively constant throughout the campaign, and very little acetate exists in its amide form.
5. Total formate production is accelerated by NO_2, and the carbon bed can remove FPZ.
6. Total nitrate only increased w/ NO_2. 2.5 mmol/kg of NO_2 absorbed results in a 0.08 mmol/kg increase in total nitrate. Nitrite was less than 0.02 mmol/kg.
7. 0.04 mmol Fe/kg solvent was removed by the activated carbon while the Fe in the solvent stayed constant at 0.01 mmol/kg. More Fe dissolved into the solvent when the Fe in solvent was removed by the carbon, similar to the results observed in NCCC campaign.

5.5.3 Comparisons between All Pilot-plant Campaigns Using 5 m PZ as Solvent

1. Dissolved Fe in the SRP and NCCC campaigns was significantly lower than in PP2 and CSIRO Tarong, possible due to the use of PZAS^{TM} and low NO_2 in the flue gas.
2. The total formate in SRP and NCCC campaigns is significantly lower than in PP2 and CSIRO Tarong, possible due to the low NO_2 in flue gas.
3. In all campaigns, EDA started to decrease after reaching 30 to 40 mmol/kg when the stripper temperature is 150 ℃ . When the stripper temperature is 140 ℃ , the EDA concentration can reach 70 mmol/kg. Therefore, EDA equilibrium is highly related to temperature, and a lower temperature favors the equilibrium towards

EDA.

4. The total nitrogen products from all degradation products accumulated from 0.11 mmol/kg-hr to 1.11 mmol/kg-hr in different campaigns. The existence of NO_2 increased the accumulation rate significantly, showing the catalytic effect of NO_2 on PZ oxidation.

Chapter 6. Mitigation Methods and Costs

6.1 Overview of Mitigation Methods and Cost Analysis

From bench-scale and pilot testing, the mitigation methods of N_2 sparging and carbon treating are found effective in mitigating PZ oxidation. This chapter shows the designs and the cost analysis of N_2 sparging columns for NCCC and a 460 MW FEED (Front End Engineering Design) (Rochelle et al, 2021) and the cost analysis to apply carbon treating at NCCC and the 460 MW FEED.

6.2 N_2 Sparging

Bench-scale studies suggest that the application of 1 L/min of N_2 with a liquid depth of 15 cm can reduce the PZ oxidation rate by 50% (Nielsen, 2018). However, the test of N_2 sparging at NCCC achieved a reduction of <13% when applied at 1 scfm N_2 in the absorber sump. This suggests that the N_2 flow was insufficient to remove the dissolved oxygen in the solvent at NCCC, and a higher N_2 flow rate or liquid depth is required. A model is needed to estimate the removal of dissolved oxygen by N_2 sparging to optimize the size of the sparging column and the flow rate of N_2.

6.2.1 N_2 Sparging Model

The model assumes that the mass transfer in the liquid phase is the limiting factor. There is no back-mixing in the column, and the k_La is calculated based on equation 6.1 (Hikita et al, 1981). Other different equations for k_La were also investigated, (Akita et al, 1974; Kang et al,1999, Kawase et al, 1987, Schumpe et al, 1986; Shah et al, 1982; öztürk et al, 1987), and the relationship by Hikita matched the sparging of N_2 into PZ solvent best. The packed height is calculated by multiplying the number of transfer units (NTU) and height of transfer units (HTU).

$$\frac{(k_L a)u_G}{g} = 14.9\left(\frac{U_G \mu_L}{\sigma}\right)^{1.76}\left(\frac{{\mu_L}^4 g}{\rho_L \sigma^3}\right)^{-0.248}\left(\frac{\rho_G}{\rho_L}\right)^{0.243}\left(\frac{\mu_L}{\rho_L D_{G/L}}\right)^{-0.604} \quad (6\text{-}1)$$

The bubble rise speed of N_2 gas in 5 m PZ solvent was measured with a 1000-mL graduate cylinder. 800 mL of clean 5 m PZ was added into the graduate cylinder, and nitrogen was fed into the bottom of the column. The distance from the bottom to the top and the time for one bubble to rise from the bottom to top were measured to calculate the bubble rise speed. The bubble rise speed is related to temperature and sparger pore size, and not related to the nitrogen flow rate. As shown in Table 6-1, the average bubble rise speed is 0.23 m/s at 50 ℃ and 0.27 m/s at 25 ℃ , so the liquid rate is kept constant at 0.23 m/s in the column design to achieve maximum mass transfer.

Table 6-1: N_2 bubble rise speed in 5 m PZ

T = 50 ℃			T = 40 ℃		
Travel Distance (cm)	**Time (s)**	**Bubble Rise Speed (m/s)**	**Travel Distance (cm)**	**Time (s)**	**Bubble Rise Speed (m/s)**
29.845	1.26	0.237	28.575	1.16	0.246
29.845	1.31	0.228	28.575	1.05	0.272
29.845	1.27	0.235	28.575	1.00	0.286
29.845	1.29	0.231	28.575	1.13	0.253
29.845	1.31	0.228	28.575	1.14	0.251
29.845	1.29	0.231	28.575	1.06	0.270
29.845	1.30	0.230	28.575	1.10	0.260
29.845	1.29	0.231	28.575	1.06	0.270
29.845	1.32	0.226	28.575	1.09	0.262
29.845	1.26	0.237	28.575	1.05	0.272
29.845	1.31	0.228	28.575	1.01	0.283

6.2.2 Design Case for NCCC

A sensitivity analysis was performed for the NCCC design. N_2 sparging treats all the solvent before the cross exchanger, and the liquid rate is set to be 1.89 kg/s, equivalent to 15000 lb/hr as used in the NCCC 2019 campaign. The sparging column is designed to remove 90% of the dissolved oxygen. The relationship between the column height and the gas rate is shown as in Figure 6-1.

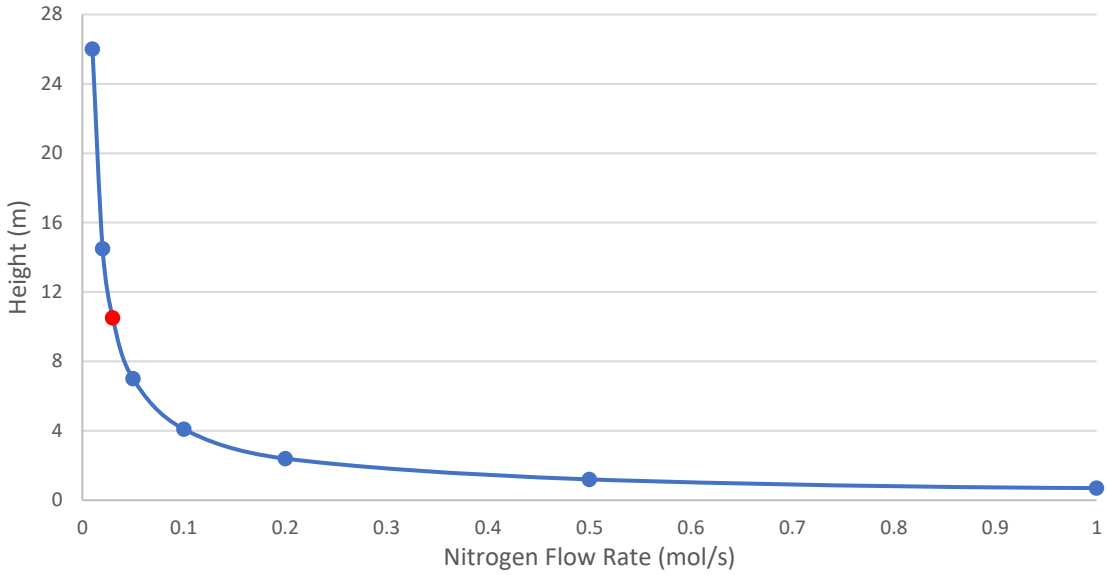

Figure 6-1: Sensitivity analysis between column height and gas rate for N_2 sparging at NCCC

Since the price of N_2 is high, the column is designed to be 10.5 m tall and 0.1 m in diameter, and 0.03 mol/s (0.025 scfm) of N_2 is required to treat the solvent. The CO_2 capture rate in this case is 1.26 mol/s. The design of the column and the absorber are plotted in Figure 6-2.

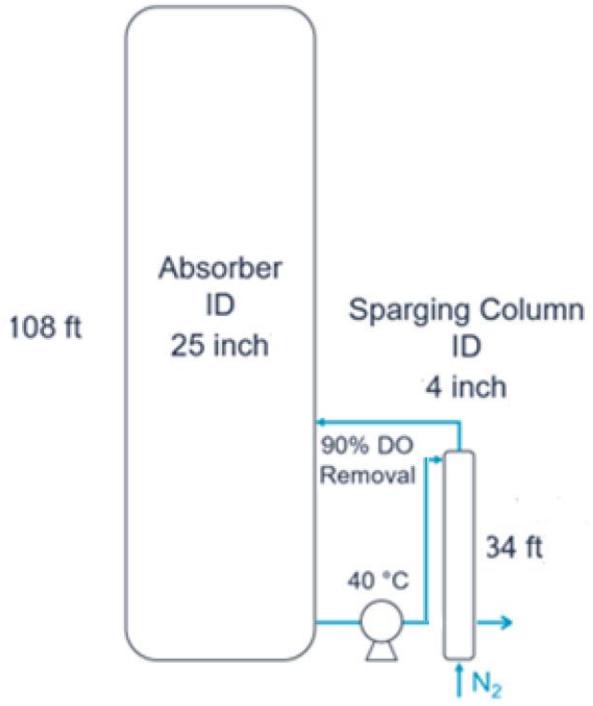

Figure 6-2: Design of a N_2 sparging column for NCCC

6.2.3 Design for a 460 MW FEED Study

The NGCC plant of interest is 460 MW, and the solvent inventory is estimated to be 4,200 tonne by scaling up from the NCCC operation, which is 5,400 kg solvent per 0.6 MW. 68% piperazine (PZ) costs $1.70/lb, or $5512/tonne of PZ. All estimation is done assuming that the plant load factor is 70% (6132 hrs/yr). A reclaimer is used to keep the concentration of the degradation products constant at a low level. Capital costs are estimated as 4 times the cost of purchased equipment. Annualized capital costs are 0.25 times the total capital cost.

The nitrogen sparging column is 2.8 m in diameter and 10.5 m tall with a N_2 sparging rate of 23 mol/s. The current design and the modification with a nitrogen sparging column are shown in Figure 6-3.

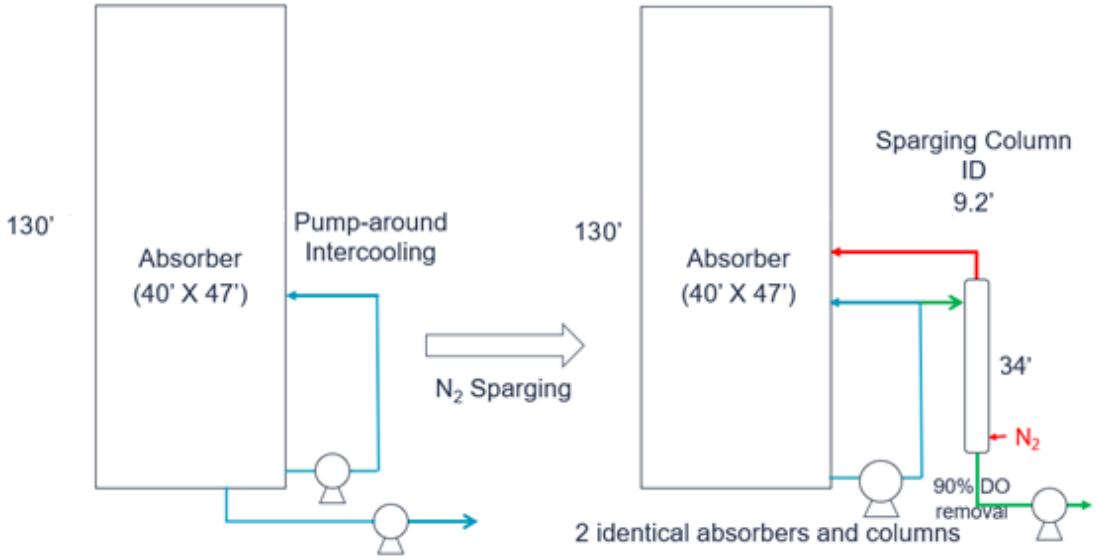

Figure 6-3: Original design of absorber column and modified absorber with a nitrogen sparging column

The cost includes the operating cost of nitrogen, the annualized capital cost of the column, and the enlargement of 2 pumps previously designed for pump-around intercooling. An on-site nitrogen plant operated by the gas company is used, and the cost is $960k per year estimated by Praxair on Oct. 8, 2021. The purchase cost of the column is $103k. The cost of the pumps was estimated by AECOM to be $560k each, and the cost to enlarge each pump is estimated to be $136k. The annualized capital cost of the column and pumps is $657k, and the total annual cost is $1.558M.

The savings are realized from the lower cost of PZ makeup and reduced waste disposal necessary. The PZ oxidation rate is estimated based on data from a 2019 NCCC campaign, and the mitigation effects of N_2 sparging is based on HTOR experiments (Nielsen, 2018). It is estimated from bench-scale data that 220 tonnes PZ/yr are oxidized without N_2 sparging, and 110 tonnes PZ/yr with N_2 sparging, suggesting that N_2 sparging can reduce PZ oxidation by 50%. This results in an annual saving of $606k. The waste

disposal is assumed to cost the same as the PZ saved, and the total saving is $1,212k/yr. In conclusion, applying N_2 sparging will incur a net cost of $404k/yr. However, N_2 sparging benefits the environment by producing fewer degradation products and waste that must be treated. Environmentally, this is a worthwhile mitigation method. N_2 sparging should also satisfy the expected requirement for less than 10 ppm oxygen in the CO_2 product.

Table 6-2: Summary of costs and savings to apply N_2 sparging

	Equipment Purchase Cost ($)	Annualized Cost ($/yr)
Column	103,000	104,000
Pump (two)	546,000	553,000
N_2 plant		960,000
PZ saving		-606,000
Waste saving		-606,000
Total Annualized Cost		404,000

6.3 CARBON TREATING

In bench-scale experiments, a linear relationship was discovered between the equilibrium absorbance of the solvent and the carbon loading. This relationship is used to estimate the amount of degradation products that the carbon can adsorb, and therefore the lifetime of the carbon is calculated. The average accumulation rate of the dilution-corrected absorbance at 320 nm at the NCCC 2018 and 2019 campaigns are 0.0168 A/hr, and this rate is used in the design case for NCCC and the 460 MW FEED.

6.3.1 Design for NCCC

The carbon bed at NCCC can hold 28 canisters of carbon, each canister containing 34 lb of 8 * 39 mesh, lignite based, granular activated carbon. To understand the carbon better, a test plan is created to deplete the carbon with six weeks of testing. The campaign will start with 6000 kg of 5 m degraded PZ solvent with an initial dilution-corrected absorbance of 16.74. It is calculated that 76.3 kg of carbon, which is equivalent to 5 canisters, is required for the carbon to reach equilibrium after 5 weeks of operation. Therefore, only 5 canisters of carbon will be used in the upcoming NCCC 2022 campaign to confirm the lifetime estimation of carbon.

6.3.2 Design Case for a 460 MW FEED Study

The capital cost of the carbon treating process consists of the cost of the carbon bed and the cartridges. The equipment purchase cost of the carbon bed is estimated by AECOM to be $115 k. The bed holds 24 refillable carbon cartridges, each costing $900. The annualized capital cost for the carbon bed is $138k. According to the bench-scale experiments, the equilibrium solvent absorbance is linearly related to the carbon loading in ranges of low absorbance. From this relationship, the operating cost is estimated with a target of 10 A at 320 nm, which corresponds to a carbon loading of 3563 A*g of solvent/g of carbon. The accumulation rate of the compounds during a 2019 NCCC campaign was 0.0146 A/hr. 75 tonne of carbon is required annually, and the cost is $105k per year quoted by Riley Equipment Company. The total annualized cost is $243k. Similar to the calculation done for N_2 sparging, the savings are realized on the cost of PZ and waste disposal. The PZ oxidation rate without the carbon bed is 220 tonne per year, and the PZ oxidation rate with carbon bed is estimated to be 110 tonne per year based on the assumption that the carbon bed reduces oxidation by 50%, so the total annual saving is

$1.21M. In conclusion, using a carbon bed will yield an annual saving of $1.07M. Considering the added effect of producing fewer degradation products and waste solvent, the carbon bed is an excellent method to mitigate PZ oxidation.

Table 6-3: Summary of costs and savings to apply carbon treating

	Equipment Purchase Cost ($)	Annualized Cost ($/yr)
Carbon bed	115,000	116,000
Cartridge (24)	21,600	21,800
Carbon		105,000
PZ saving		-606,000
Waste saving		-606,000
Total Annualized Cost		-1,074,000

6.4 COMBINED TREATING FOR A 460 MW FEED STUDY

Applying N_2 sparging and a carbon bed will mitigate oxidation further. The total annualized cost is $1.801M. The oxidation rate is estimated to be 55 tonne per year compared to 220 tonne per year without N_2 sparging or carbon bed, so the annual saving is $1.819M. As a result, applying both N_2 sparging and carbon treating yields an annual saving of $18k with the benefits environmentally by producing much fewer degradation products and waste.

Table 6-4: Summary of costs and savings to apply N_2 sparging and carbon treating

	Equipment Purchase Cost ($)	Annualized Cost ($/yr)
Column (2)	103,000	104,000
Pump Enlargement (4)	546,000	553,000
N_2 plant		960,000
Carbon bed	115,000	116,000
Cartridge (24)	21,600	21,800
Carbon		105,000
PZ saving		-909,000
Waste saving		-909,000
Total Annualized Cost		-18,000

6.5 CONCLUSIONS

1. Applying N_2 sparging on the absorber sump requires a large expensive N_2 supply and using a sparger column after the absorber sump is more efficient and cost effective.
2. To achieve 90% dissolved oxygen removal at NCCC, a column 10.5 m tall and 0.1 m in diameter is designed. The N_2 flow rate is 0.03 mol/s (0.025 scfm), which is small compared to the 1.26 mol/s CO_2 capture rate.
3. For a 460 MW FEED study, the N_2 sparging column is 10.5 m tall and 2.8 m in diameter, and 23 mol/s (19 scfm) N_2 is required to achieve 90% dissolved oxygen removal. The design utilizes the pump-around intercooling pump.

4. The major cost to do N_2 sparging is the N_2 source. Applying N_2 sparging in a 460 MW FEED study incurs a cost of $404k/yr. However, environmentally this is worth doing since fewer NH_3 and other degradation products are produced.
5. 5 canisters of carbon will be depleted after 5 weeks of operation at NCCC.
6. Applying carbon treating in a 460 MW FEED study yields an annual saving of $1.07 M.
7. A combined mitigation of carbon treating and N2 sparging in a 460 MW FEED study yields a saving of $18k/yr. The oxidation is estimated to be mitigated by 75% with the combined treatments.

Chapter 7. Conclusions and Recommendations

This chapter provides an overview of Bench-scale experiments in the Carbon Adsorption Column (CAC) and the High Temperature Oxidation Reactor (HTOR) and pilot-scale results from the National Carbon Capture Center (NCCC) and the Separations Research Program (SRP). It also includes designs for future testing and commercial units and recommendations to further study and mitigate the piperazine (PZ) oxidation.

The four most important results include:

1. Carbon treating will be useful for removing Fe, Cr, ligands, and foaming agents from the solvent, and it reduces NH_3 production and amine oxidation.
2. When Fe is removed by carbon treating or other methods, the soluble Fe in the system dissolves and replaces the dissolved Fe. Therefore, all available Fe and ligands need to be removed for the mitigation to be effective. The sources of soluble Fe include fly ash and the corrosion of stainless steel, and the ligands are degradation products.
3. All PZ degraded solvents have two absorbance peaks at 320 nm and 538 nm. The 320 nm peak is caused by dissolved metals, especially Fe, complexed by degradation products. The 320 nm peak is related to the amine degradation level and can be used as a simple and efficient estimate method to quantify amine degradation rate.
4. NO_2 can oxidize PZ significantly, possibly through radical reactions. 0.01 mmol/kg-hr absorption of NO_2 increased the PZ oxidation rate from 1.2 mmol/kg-hr to 2.5 mmol/kg-hr. This conclusion was developed with the combined efforts of several Texas Carbon Engineers and the SRP staff.

7.1 SUMMARY OF RESULTS

7.1.1 Bench-Scale Results

The degraded PZ samples collected in both bench-scale and pilot-scale shared two universal UV-Vis absorbance peaks, 320 nm and 528 nm. The 528 nm is responsible for the color of the solvent, but the absorbance in much lower than the 320 nm. Both peaks increase as the solvent becomes more degraded and can be removed by carbon treating. The 320 nm peak is highly related to the dissolved metals (especially Fe) creating a ligand with the degradation products and can be used as an immediate measurement of the solvent degradation level.

The effect of carbon treating on degraded solvent was quantified in the CAC, where no water loss or further solvent degradation occurs. The activated carbon does not adsorb PZ, which makes it possible to treat degraded PZ. Carbon treating can remove up to 70% of dissolved Fe, Cr, and Mn, and the selectivity for Fe and Cr is higher than Mn. Ni is not removed by carbon treating. The carbon has a small removal effect on heat stable salts including formate, sulfate, nitrate, and oxalate, and degradation products including n-formyl-piperazine (FPZ), ethylenediamine (EDA), and 1-methyl-piperazine (MPZ), but these effects are much smaller compared to the removal effects of metals. When treating degraded solvent, the alkalinity of the solvent decreased by up to 6%, indicating that the carbon adsorbs degradation products with alkalinity. The carbon removes all the degradation products that can complex with Fe^{3+}, even if they are not complexed.

The equilibrium loading of the carbon is linearly related to the equilibrium absorbance of the solvent, and this relationship is not related to the initial Fe concentration or degradation level. After the carbon has reached equilibrium, it can still treat solvents

with high absorbance. The rate of treatment becomes slower, and the second equilibrium absorbance is higher due to the decrease in active sorption sites.

The Fe and Mn adsorbed by the carbon can be removed from the carbon by treating with H_2SO_4, therefore the amount of removal can be quantified. The 320 nm peak in the solvent shifts to 303 nm in the H_2SO_4, indicating that the ligand speciates differently depending on the pH of the solvent.

The PZ loss in the HTOR varied between 0.5 mmol/kg-hr and 1.5 mmol/kg-hr. The oxidation rate is higher with degraded solvent. The previous observation of 1 mol of NH_3 production per mol of PZ oxidation (Nielsen, 2018) only holds true in less degraded solvent. When the solvent is more degraded, different oxidation pathways exist and 1 mol of PZ only produces 0.23 mol of NH_3. For every mol of PZ oxidized, 0.05 mols of total formate were produced. Although a linear relationship was observed between NH_3 production and total formate production, the slopes are not consistent in different HTOR experiments.

Increasing the temperature of the trim cooler from 62 to 75 ℃ increased the NH_3 production rate. Therefore, in commercial units, the locations above 75 ℃ are of interest when studying PZ oxidation.

Adding ethylenediamine (EDA) into PZ solvent does not affect the oxidation rate of PZ. More NH_3 is observed in the experiment due to EDA degradation, but the NH_3 from PZ holds constant. EDA always accumulates at the beginning of degradation. After EDA concentration reaches 40 to 50 mmol/kg in the HTOR, the rate of EDA degradation is faster than the rate of EDA production. Such behavior is not affected by the operational changes.

Adding antifoam diminishes the effect of N_2 sparging. It is possible that the foaming produced extra surface area that strengthens the effects of N_2 sparging. Formaldehyde increases NH_3 production, and a larger increase is observed in more

degraded samples. Dissolved Fe increased along with the increase in NH_3 production. Formaldehyde can accelerate PZ oxidation.

Carbon treating was effective in removing degradation and corrosion products and mitigating oxidation in the HTOR. When carbon treating was applied, the increase in NH_3 rate slowed down, the dilution-corrected absorbance at 320 nm decreased, and the accumulation rate of Fe and total formate decreased. Carbon treating can remove Cr and Mn from the solvent and stop the solvent from foaming. 15.5 g of carbon on 1.6 L of NCCC degraded solvent reduced PZ oxidation rate by 0.4 mmol/kg-hr. The Fe removed by the carbon bed was larger than the result calculated from the solvent inventory and concentration difference of Fe in solvent. This is because other "soluble" Fe can dissolve into the solvent when the Fe in solvent is adsorbed by the carbon.

Combining carbon treating and nitrogen sparging is more effective in oxidation mitigation than applying the methods separately. Observations included decrease in NH_3 production rate, UV-Vis absorbance at 320 nm, and accumulation rate of Fe and total formate. The effects of carbon treating continue when the carbon is bypassed, which is possibly due to the removal of catalytic degradation products. Therefore, it is better to apply carbon treating in the early stages of oxidation.

7.1.2 Pilot-Scale Results

PZ in the NCCC campaign oxidized at a slow rate. After 4100 hrs of operation, the solvent produced 280 mmol/kg NH_3, which corresponds to 0.07 mmol/kg-hr PZ oxidation rate if assuming 1 mol of PZ finally oxidizes into 1mol NH_3 (Nielsen, 2018). The possible reasons include the use of the advanced flash stripper and the absence of NO_2 in the inlet gas. The overall PZ loss rate was 4.1 mmol/kg-hr calculated from PZ concentration data and make-up inventories. The most significant cause of PZ loss was aerosol and volatile

PZ. Some other loss may also occur from leaks and when solvent was drained and replaced into the system. Recent HTOR experiments suggest that 1 mol of PZ might only degrade into 0.23 mol NH_3, so the total PZ oxidation rate may be underestimated.

Dissolved iron concentration is correlated with the solvent oxidation rate rather than the extent of solvent degradation. The dissolved Fe increased from 0.06 mmol/kg to 0.29 mmol/kg in NCCC 2019, and the rate of increase was much faster than in NCCC 2018. This could be due to the high temperature in the stripper sump. EDA reached a high concentration when the stripper temperature was low, indicating that the equilibrium between EDA production and degradation is highly correlated to stripper temperature. When the stripper temperature was 150 ℃ , EDA started decreasing after reaching 30 mmol/kg.

The oxidation rate of PZ can be reduced by lowering the stripper sump level, applying nitrogen sparging, and removing NO_2 in inlet gas. A combination of these three methods reduced the PZ oxidation rate by 13%. Carbon treating removes complexes of PZ and degradation products that catalyze oxidation. The NH_3 production rate decreased from 0.1 mmol/kg-hr to 0.056 mmol/kg-hr after 400 hrs of carbon treating. Carbon treating also removes Fe and Cr from the solvent. The carbon removed 6.6 mmol Fe/kg solvent from the solvent, but the Fe concentration in solvent stayed constant at 0.1 mmol/kg, which matched the results observed in the HTOR.

The PZ loss rate was lower at SRP than at NCCC. The highest loss rate (1.67 mmol/kg-hr) was observed with NO_2 injection. PZ-one was the dominant cation product. The accumulation rate of PZ-one increased with NO_2, and the effect of NO_2 lasted until the mononitrosopiperazine (MNPZ) was depleted. EDA and aminoethylpiperazine (AEP) were not affected by NO_2. EDA levelled out at 25 mmol/kg, and AEP was removed by the carbon bed. Acetate was the dominant anion product. The accumulation rate was relatively

constant throughout the campaign, and very little acetate existed in its amide form. Total formate production was accelerated by NO_2, and the carbon bed can remove FPZ. Total nitrate only increased with NO_2. 2.5 mmol/kg of NO_2 absorbed resulted in a 0.08 mmol/kg increase in total nitrate. Nitrite was less than 0.02 mmol/kg.

No significant NH_3 or liquid-phase product concentration changes were observed when N_2 sparging was applied, possibly because the solvent was allowed to reach steady state after the NO_2 was turned off, and the effects of NO_2 lasted during the period of N_2 sparging tests. When the carbon bed was tested, the UV-Vis absorbance of the solvent decreased, but no other significant changes were observed, because the time of carbon treating was too short, and the reduction was not great enough to be measured. 0.04 mmol Fe/kg solvent was removed by the activated carbon while the Fe in the solvent stayed constant at 0.01 mmol/kg. Additional Fe dissolved into the solvent when the Fe in solvent was removed by the carbon, similar to the results observed in the HTOR and NCCC campaign. Whenever the carbon removes the dissolved Fe, more Fe as soluble solid will dissolve into the solvent. Therefore, the whole inventory of soluble Fe must be removed to result in a decrease in Fe concentration.

Previous campaigns (PP2 and CSIRO Tarong) that used PZ as the solvent were compared with the newly performed campaigns. Dissolved Fe and total formate in the SRP and NCCC campaigns was significantly lower than in PP2 and CSIRO Tarong, possible due to the use of the Advanced Stripper and low NO_2 in the flue gas. The total nitrogen products from all degradation products accumulated from 0.11 mmol/kg-hr to 1.11 mmol/kg-hr in different campaigns. The existence of NO_2 affected the accumulation rate significantly, showing the catalytic effect of NO_2 on PZ oxidation. In all campaigns, EDA started to decrease after reaching 30 to 40 mmol/kg when the stripper temperature is 150 °C . When the stripper temperature is 140 °C , the maximum EDA concentration was 70

mmol/kg. Therefore, EDA equilibrium is highly related to temperature, and a lower temperature favors the equilibrium towards EDA.

7.1.3 Mitigation Designs

Applying N_2 sparging in the absorber sump requires a large amount of N_2 and using a sparger column after the absorber sump is more efficient and cost effective. To achieve 90% dissolved oxygen removal at NCCC, a column 10.5 m tall and 0.1 m in diameter would be required. The N_2 flow rate is 0.03 mol/s (0.025 scfm), which is small compared to the 1.26 mol/s CO_2 capture rate. For a 460 MW plant, the N_2 sparging column would be 10.5 m tall and 2.8 m in diameter, and 23 mol/s (19 scfm) N_2 is required to achieve 90% dissolved oxygen removal. The design utilizes the pump-around intercooling pump. The major cost to do N_2 sparging is the N_2 source. Applying N_2 sparging in a 460 MW plant incurs a net cost of $404k/yr. However, environmentally this is worth doing since less NH_3 and other degradation products would be produced.

Compared to N_2 sparging, carbon treating is much less expensive due to the low cost of activated carbon. 5 canisters of carbon will be depleted after 5 weeks of operation at NCCC. Applying carbon treating in a 460 MW plant yields an annual saving of $1.07 M. A combined mitigation of carbon treating and N_2 sparging in a 460 MW FEED study yields a saving of $18k/yr. The oxidation is assumed to be mitigated by 75% with the combined treatments.

7.2 RECOMMENDATIONS

The pilot plant results suggest that NO_2 has a much more significant effect on PZ oxidation than understood previously. It is important to understand the mechanisms of NO_2 reactions better in bench-scale apparatus and find a stoichiometric correlation between the

amount of NO_2 absorbed and the total amount of PZ oxidized. The pretreatment of NO_2 in the flue gas is critical in mitigating oxidation. The bag house at NCCC showed significant removal of NO_2. NO_2 pretreatment was also tested at a post-combustion capture pilot plant at Niederaussem, Germany on CESAR-1, blend of 2-amino-2-methyl-1-propanol (AEP) and PZ, but the oxidation rate increased after the pretreatment (Moser, 2022). The NO in the flue gas may also react to form NO_2. Therefore, further study of reactions with NO_2 and NO is important to mitigate oxidation.

More work needs to be done to understand the two other oxidation mechanisms better. The reaction with dissolved oxygen was tested and verified by applying N_2 sparging in bench-scale experiments but testing in pilot plant did not match the bench-scale results. Dissolved oxygen concentration will be measured to confirm the effectiveness of the sparger, and longer tests will be performed at NCCC to understand how much of the oxidation is caused by the dissolved oxygen mechanism in pilot or commercial scale.

The Fe^{2+}/Fe^{3+} shuttle mechanism also requires more study. The Fe is currently quantified with ICP, and the oxidation states cannot be differentiated. The X-ray photoelectron spectroscopy can be one promising method to identify the atomic ratio between Fe^{2+} and Fe^{3+}. Identifying the ligands that increases Fe solubility in the solvent is also one potential direction.

Foaming was observed in both HTOR and SRP as the solvent becomes more degraded. Carbon treating can stop foaming in HTOR after a short treatment. Since foaming can affect CO2 absorption and desorption and cause solvent carryover into undesired locations, the mitigation of foaming by carbon treating should be quantified.

This work focuses on the study of a single source of 8*30 mesh, lignite-based granular activated carbon, and the source of carbon has not been optimized to achieve the best removal. Future studies can study the adsorption rate and selectivity of variable carbon

on the degradation and corrosion products. Ion exchange resins can also be a potential method to reduce oxidation rate. Moser reported removal of Fe and heat stable salts by ion exchange resins with CESAR-1 (Moser, 2022). Therefore, it is promising to remove similar products in PZ.

Appendix

APPENDIX A. SCRIPTS FOR ANALYTICAL METHODS

Table A-1. Scripts for Cation IC

{Initial Time}	Instrument Setup	
	DC.Compartment_TC.AcquireExclusiveAccess	
	DC.Column_TC.AcquireExclusiveAccess	
	Sampler.AcquireExclusiveAccess	
	Wait	Sampler.Ready,
Run=Hold, Timeout=Infinite		
	DC.Suppressor1.PowerMode	Legacy
	Sampler.DiverterValve	Position_2
	Wait	Sampler.Ready,
Run=Hold, Timeout=Infinite		
	CationPump.Flow	1 [ml/min]
	CationPump.Pressure.UpperLimit	5000 [psi]
	CationPump.%A.Equate	%A
	CationPump.Pressure.LowerLimit	200 [psi]
	Sampler.CycleTime	0 [min]
	Sampler.LoopOverfill	5
	Sampler.InjectMode	PushSeqFull
	Sampler.BufferWashFactor	2
	Sampler.WashDispSpeed	20.0 [µl/s]
	Sampler.InjectWash	Both
	Sampler.WashSpeed	20.0 [µl/s]
	Sampler.WashVolume	500.0 [µl]
	Sampler.SampleHeight	2.000 [mm]
	Sampler.WasteSpeed	20.0 [µl/s]
	Sampler.DispenseDelay	2.0 [s]
	Sampler.DispSpeed	5.0 [µl/s]
	Sampler.DrawSpeed	10.0 [µl/s]
	Sampler.DrawDelay	2.0 [s]
	Sampler.DilutionMixDispenseSpeed	60.0 [µl/s]
	Sampler.DilutionMixIterations	3
	Sampler.DilutionMixSpeed	30.0 [µl/s]
	DC.Column_TC.Mode	On
	DC.Column_TC.TemperatureSet	30.00 [°C]

	DC.Compartment_TC.Mode	On
	DC.Compartment_TC.TemperatureSet	15.00 [°C]
	DC.Suppressor1.Type	CDRS_4mm
	DC.Suppressor1.H2SO4	0.0 [mM]
	DC.Suppressor1.MSA	11.0 [mM]
	DC.Suppressor1.RecommendedCurrent	33 [mA]
	DC.Suppressor1.OtherEluent	0.0 [mN]
	DC.Suppressor1.CurrentSet	33 [mA]
	CDet1.Rise_Time	1.00 [s]
	CDet1.Data_Collection_Rate	5.0 [Hz]
	CDet1.CellHeater.Mode	On
	CDet1.CellHeater.TemperatureSet	35.00 [°C]
	CDet1.Temperature_Compensation	1.7 [%/°C]
	CationPump.Curve	5
	EluentGenerator.EGC_1.CR_TC	On
	Sampler.PunctureOffset	3 [mm]
-3	Equilibration	Duration = 3.000 [min]
	EluentGenerator.EGC_1.Concentration	5.50 [mM]
0	Inject	
	Wait	Sampler.CycleTimeState,
Run=Hold,		
Timeout=Infinite		
	Sampler.Inject	
0	Start Run	
	CationPump.CationPump_Pressure.AcqOn	
	CDet1.CD_1.AcqOn	
	CDet1.CD_1_Total.AcqOn	
	CDet1.Autozero	
0	Run	Duration = 50.000 [min]
0.1		
	Sampler.ReleaseExclusiveAccess	
	DC.Column_TC.ReleaseExclusiveAccess	
	DC.Compartment_TC.ReleaseExclusiveAccess	
8.5		
	EluentGenerator.EGC_1.Concentration	5.50 [mM]
17		
	EluentGenerator.EGC_1.Concentration	11.00 [mM]
37		
	EluentGenerator.EGC_1.Concentration	11.00 [mM]
40		

	EluentGenerator.EGC_1.Concentration	5.50 [mM]
50		
	EluentGenerator.EGC_1.Concentration	5.50 [mM]
50	Stop Run	
	CationPump.CationPump_Pressure.AcqOff	
	CDet1.CD_1.AcqOff	
	CDet1.CD_1_Total.AcqOff	
50	Post Run	Duration = 0.000 [min]
End		

Table A-2. Scripts for Cation Standby

{Initial Time}	Instrument Setup		
	Sampler.AcquireExclusiveAccess		
	Wait	Sampler.Ready,	
Run=Hold, Timeout=Infinite			
	DC.Suppressor1.PowerMode	Legacy	
	Sampler.DiverterValve	Position_2	
	Wait	Sampler.Ready,	
Run=Hold, Timeout=Infinite			
	CationPump.Flow	0.2 [ml/min]	
	CationPump.Pressure.UpperLimit	5000 [psi]	
	CationPump.%A.Equate	%A	
	CationPump.Pressure.LowerLimit	200 [psi]	
	EluentGenerator.EGC_1.Concentration	5.50 [mM]	
	EluentGenerator.EGC_1.CR_TC	On	
	Sampler.CycleTime	0 [min]	
	Sampler.LoopOverfill	5	
	Sampler.InjectMode	PushSeqFull	
	Sampler.BufferWashFactor	2	
	Sampler.WashDispSpeed	20.0 [µl/s]	
	Sampler.InjectWash	AfterInj	
	Sampler.WashSpeed	20.0 [µl/s]	
	Sampler.WashVolume	500.0 [µl]	
	Sampler.SampleHeight	2.000 [mm]	
	Sampler.WasteSpeed	20.0 [µl/s]	
	Sampler.DispenseDelay	2.0 [s]	
	Sampler.DispSpeed	5.0 [µl/s]	
	Sampler.DrawSpeed	10.0 [µl/s]	
	Sampler.DrawDelay	2.0 [s]	
	Sampler.DilutionMixDispenseSpeed	60.0 [µl/s]	
	Sampler.DilutionMixIterations		3
	Sampler.DilutionMixSpeed	30.0 [µl/s]	
	DC.Suppressor1.Type	CDRS_4mm	
	DC.Suppressor1.H2SO4	0.0 [mM]	
	DC.Suppressor1.MSA	5.0 [mM]	
	DC.Suppressor1.RecommendedCurrent	3 [mA]	
	DC.Suppressor1.OtherEluent	0.0 [mN]	
	DC.Suppressor1.CurrentSet	3 [mA]	

		CDet1.Rise_Time	0.50 [s]
		CDet1.Data_Collection_Rate	5.0 [Hz]
		CDet1.CellHeater.Mode	Off
		CationPump.Curve	5
		Sampler.PunctureOffset	3 [mm]
	0	Inject	
		Wait	Sampler.CycleTimeState,
Run=Hold,			
Timeout=Infinite			
		Sampler.Inject	
	0	Start Run	
		CationPump.CationPump_Pressure.AcqOn	
		CDet1.CD_1.AcqOn	
		CDet1.CD_1_Total.AcqOn	
		CDet1.Autozero	
	0	Run	Duration = 100000.000 [min]
	0.1		
		Sampler.ReleaseExclusiveAccess	
		DC.Column_TC.ReleaseExclusiveAccess	
		DC.Compartment_TC.ReleaseExclusiveAccess	
	100000	Stop Run	
		CationPump.CationPump_Pressure.AcqOff	
		CDet1.CD_1.AcqOff	
		CDet1.CD_1_Total.AcqOff	
	100000	Post Run	Duration = 0.000 [min]
End			

Table A-3. Scripts for Anion

{Initial Time}	Instrument Setup	
	DC.Compartment_TC.AcquireExclusiveAccess	
	DC.Column_TC.AcquireExclusiveAccess	
	Sampler.AcquireExclusiveAccess	
	Wait	Sampler.Ready,
Run=Hold, Timeout=Infinite		
	DC.Suppressor1.PowerMode	Legacy
	Sampler.DiverterValve	Position_1
	Wait	Sampler.Ready,
Run=Hold, Timeout=Infinite		
	Pump_1.Flow	1.6 [ml/min]
	Pump_1.Pressure.UpperLimit	5000 [psi]
	Pump_1.%A.Equate	%A
	Pump_1.Pressure.LowerLimit	200 [psi]
	Sampler.CycleTime	0 [min]
	Sampler.LoopOverfill	5
	Sampler.InjectMode	PushSeqFull
	Sampler.BufferWashFactor	2
	Sampler.WashDispSpeed	20.0 [µl/s]
	Sampler.InjectWash	Both
	Sampler.WashSpeed	20.0 [µl/s]
	Sampler.WashVolume	500.0 [µl]
	Sampler.SampleHeight	2.000 [mm]
	Sampler.WasteSpeed	20.0 [µl/s]
	Sampler.DispenseDelay	2.0 [s]
	Sampler.DispSpeed	5.0 [µl/s]
	Sampler.DrawSpeed	10.0 [µl/s]
	Sampler.DrawDelay	2.0 [s]
	Sampler.DilutionMixDispenseSpeed	60.0 [µl/s]
	Sampler.DilutionMixIterations	3
	Sampler.DilutionMixSpeed	30.0 [µl/s]
	DC.Column_TC.Mode	On
	DC.Column_TC.TemperatureSet	30.00 [°C]
	DC.Compartment_TC.Mode	On
	DC.Compartment_TC.TemperatureSet	15.00 [°C]
	DC.Suppressor1.Type	ADRS_4mm
	DC.Suppressor1.Carbonate	0.0 [mM]

	DC.Suppressor1.Bicarbonate	0.0 [mM]
	DC.Suppressor1.Hydroxide	40.0 [mM]
	DC.Suppressor1.Tetraborate	0.0 [mM]
	DC.Suppressor1.OtherEluent	0.0 [mN]
	DC.Suppressor1.RecommendedCurrent	159 [mA]
	DC.Suppressor1.CurrentSet	159 [mA]
	CDet1.Rise_Time	0.50 [s]
	CDet1.Data_Collection_Rate	5.0 [Hz]
	CDet1.CellHeater.Mode	On
	CDet1.CellHeater.TemperatureSet	35.00 [°C]
	CDet1.Temperature_Compensation	1.7 [%/°C]
	Pump_1.Curve	5
	EluentGenerator.EGC_1.CR_TC	On
	Sampler.PunctureOffset	3 [mm]
-3	Equilibration	Duration = 3.000 [min]
	EluentGenerator.EGC_1.Concentration	2.00 [mM]
0	Inject	
	Wait	Sampler.CycleTimeState, Run=Hold, Timeout=Infinite
	Sampler.Inject	
0	Start Run	
	Pump_1.Pump_1_Pressure.AcqOn	
	CDet1.CD_1.AcqOn	
	CDet1.CD_1_Total.AcqOn	
	CDet1.Autozero	
0	Run	Duration = 50.000 [min]
0.1		
	Sampler.ReleaseExclusiveAccess	
	DC.Column_TC.ReleaseExclusiveAccess	
	DC.Compartment_TC.ReleaseExclusiveAccess	
17		
	EluentGenerator.EGC_1.Concentration	2.00 [mM]
27		
	EluentGenerator.EGC_1.Concentration	40.00 [mM]
40		
	EluentGenerator.EGC_1.Concentration	40.00 [mM]
45		
	EluentGenerator.EGC_1.Concentration	2.00 [mM]
50		

		EluentGenerator.EGC_1.Concentration	2.00 [mM]
	50	Stop Run	
		Pump_1.Pump_1_Pressure.AcqOff	
		CDet1.CD_1.AcqOff	
		CDet1.CD_1_Total.AcqOff	
	50	Post Run	Duration = 0.000 [min]
end			

Table A-4. Scripts for Anion Standby

{Initial Time}	Instrument Setup	
	Sampler.AcquireExclusiveAccess	
	Wait	Sampler.Ready,
Run=Hold, Timeout=Infinite		
	DC.Suppressor1.PowerMode	Legacy
	Sampler.DiverterValve	Position_1
	Wait	Sampler.Ready,
Run=Hold, Timeout=Infinite		
	Pump_1.Flow	0.3 [ml/min]
	Pump_1.Pressure.UpperLimit	5000 [psi]
	Pump_1.%A.Equate	%A
	Pump_1.Pressure.LowerLimit	200 [psi]
	EluentGenerator.EGC_1.Concentration	2.00 [mM]
	EluentGenerator.EGC_1.CR_TC	On
	Sampler.CycleTime	0 [min]
	Sampler.LoopOverfill	5
	Sampler.InjectMode	PushSeqFull
	Sampler.BufferWashFactor	2
	Sampler.WashDispSpeed	20.0 [µl/s]
	Sampler.InjectWash	AfterInj
	Sampler.WashSpeed	20.0 [µl/s]
	Sampler.WashVolume	500.0 [µl]
	Sampler.SampleHeight	2.000 [mm]
	Sampler.WasteSpeed	20.0 [µl/s]
	Sampler.DispenseDelay	2.0 [s]
	Sampler.DispSpeed	5.0 [µl/s]
	Sampler.DrawSpeed	10.0 [µl/s]
	Sampler.DrawDelay	2.0 [s]
	Sampler.DilutionMixDispenseSpeed	60.0 [µl/s]
	Sampler.DilutionMixIterations	3
	Sampler.DilutionMixSpeed	30.0 [µl/s]
	DC.Suppressor1.Type	ADRS_4mm
	DC.Suppressor1.Carbonate	0.0 [mM]
	DC.Suppressor1.Bicarbonate	0.0 [mM]
	DC.Suppressor1.Hydroxide	2.0 [mM]
	DC.Suppressor1.Tetraborate	0.0 [mM]
	DC.Suppressor1.OtherEluent	0.0 [mN]

	DC.Suppressor1.RecommendedCurrent	2 [mA]
	DC.Suppressor1.CurrentSet	2 [mA]
	CDet1.Rise_Time	0.50 [s]
	CDet1.Data_Collection_Rate	5.0 [Hz]
	Pump_1.Curve	5
	Sampler.PunctureOffset	3 [mm]
	CDet1.CellHeater.Mode	Off
0	Inject	
	Wait	Sampler.CycleTimeState,
Run=Hold,		
Timeout=Infinite		
	Sampler.Inject	
0	Start Run	
	Pump_1.Pump_1_Pressure.AcqOn	
	CDet1.CD_1.AcqOn	
	CDet1.CD_1_Total.AcqOn	
	CDet1.Autozero	
0	Run	Duration = 100000.000 [min]
0.1		
	Sampler.ReleaseExclusiveAccess	
	DC.Column_TC.ReleaseExclusiveAccess	
	DC.Compartment_TC.ReleaseExclusiveAccess	
100000	Stop Run	
	Pump_1.Pump_1_Pressure.AcqOff	
	CDet1.CD_1.AcqOff	
	CDet1.CD_1_Total.AcqOff	
100000	Post Run	Duration = 0.000 [min]
End		

Table A-5. Scripts for Nitrosamines

Column_A.ActiveColumn =	No
TempCtrl =	On
Temperature.Nominal =	30.0 [°C]
Column_B.ActiveColumn =	No
Pressure.LowerLimit =	25 [bar]
Pressure.UpperLimit =	450 [bar]
MaximumFlowRampDown =	Infinite
MaximumFlowRampUp =	Infinite
%A.Equate =	%A
%B.Equate =	%B
%C.Equate =	%C
%D.Equate =	%D
Pump_Pressure.Average =	On
DrawSpeed =	5.000 [µl/s]
DrawDelay =	3000 [ms]
DispSpeed =	20.000 [µl/s]
DispenseDelay =	0 [ms]
WasteSpeed =	32.000 [µl/s]
SampleHeight =	2.000 [mm]
InjectWash =	NoWash
LoopWashFactor =	2
PunctureOffset =	0.0 [mm]
PumpDevice =	Pump
InjectMode =	Normal
SyncWithPump =	On
Data_Collection_Rate =	10.0 [Hz]
;Data_Collection_Rate =	2.5 [Hz]
;TimeConstant =	0.60 [s]
;ELS_1.Step =	0.10 [s]
;ELS_1.Average =	Off
UV_VIS_1.Wavelength =	240 [nm]
;EvaporatorTemperature.Nominal =	50 [°C]
;NebuliserTemperature =	90 [°C]
;LightSourceIntensity =	85 [%]
;CarrierFlow.Nominal =	1.60 [slm]
;SmoothWidth =	20
;PMTGain =	1
UV.LeakSensorMode =	Disabled

-4	Flow =	1.000 [ml/min]
	%B =	5.0 [%]
	%C =	0.0 [%]
	%D =	0.0 [%]
0	UV.Autozero	
	;ELSD.Autozero	
		UV.Ready ;and ELSD.Readynd
	Wait	PumpModule.Ready
	Inject	
	Pump_Pressure.AcqOn	
	UV_VIS_1.AcqOn	
5	Flow =	1.000 [ml/min]
	%B =	5.0 [%]
10	Flow =	1.000 [ml/min]
	%B =	20.0 [%]
	Flow =	1.000 [ml/min]
	%B =	50.0 [%]
20	;ELS_1.AcqOff	
	Pump_Pressure.AcqOff	
	UV_VIS_1.AcqOff	
	Flow =	1.000 [ml/min]
	%B =	50.0 [%]
	%C =	0.0 [%]
	%D =	0.0 [%]
	End	

Table A-6. Scripts for Aldehydes

Column_A.ActiveColumn =	No
	On
TempCtrl =	
	30.0 [°C]
Temperature.Nominal =	
	No
Column_B.ActiveColumn =	
	25 [bar]
Pressure.LowerLimit =	
	450 [bar]
Pressure.UpperLimit =	
	Infinite
MaximumFlowRampDown =	
	Infinite
MaximumFlowRampUp =	
	%A
%A.Equate =	
	%B
%B.Equate =	
	%C
%C.Equate =	
	%D
%D.Equate =	
	5.000 [µl/s]
DrawSpeed =	
	3000 [ms]
DrawDelay =	
	20.000 [µl/s]
DispSpeed =	
	0 [ms]
DispenseDelay =	
	32.000 [µl/s]
WasteSpeed =	
	2.000 [mm]
SampleHeight =	
	NoWash
InjectWash =	
	2
LoopWashFactor =	
	0.0 [mm]
PunctureOffset =	

		Pump
	PumpDevice =	
		Normal
	InjectMode =	
		On
	SyncWithPump =	
		2.5 [Hz]
	;Data_Collection_Rate =	
		0.60 [s]
	;TimeConstant =	
		0.10 [s]
	;ELS_1.Step =	
		Off
	;ELS_1.Average =	
		365 [nm]
	UV_VIS_1.Wavelength =	
	;EvaporatorTemperature.Nominal =	50 [°C]
		90 [°C]
	;NebuliserTemperature =	
		85 [%]
	;LightSourceIntensity =	
		1.60 [slm]
	;CarrierFlow.Nominal =	
		20
	;SmoothWidth =	
		1
	;PMTGain =	
		Disabled
	UV.LeakSensorMode =	
		1.000 [ml/min]
-4	Flow =	
		0.0 [%]
	%B =	
		65.0 [%]
	%C =	
		0.0 [%]
	%D =	
0		
	UV.Autozero ;ELSD.Autozero	

		AZ_Done
	Wait	UV.Ready ;and ELSD.Ready
	Wait Inject ;ELS_1.AcqOn UV_VIS_1.AcqOn Pump_Pressure.AcqOn	
6	Flow =	1.000 [ml/min]
	%B =	0.0 [%]
	%C =	65.0 [%]
	%D =	0.0 [%]
10	Flow =	1.000 [ml/min]
	%B =	0.0 [%]
	%C =	85.0 [%]
	%D =	0.0 [%]
15	Flow =	1.000 [ml/min]
	%B =	0.0 [%]
	%C =	82.5 [%]
	%D =	0.0 [%]
15.001	Flow =	1.000 [ml/min]
	%B =	0.0 [%]

	65.0 [%]
%C =	
	0.0 [%]
%D =	
;ELS_1.AcqOff	
UV_VIS_1.AcqOff	
Pump_Pressure.AcqOff	

APPENDIX B. DATA OF CAC EXPERIMENTS

Table B-1. Detailed Data of CAC 1 w/ #3537 and no carbon

Time (hr)	Solvent (g)	Abs (A)	Fe (mmol/kg)	Ni (mmol/kg)	Cr (mmol/kg)	Mn (mmol/kg)
0.0	72.6	26.19	0.07	0.04	0.15	0.11
2.0	69.8	26.05	0.07	0.04	0.15	0.11
4.9	65.5	26.33	0.07	0.04	0.15	0.10
23.6	60.8	26.24	0.07	0.04	0.15	0.09
47.0	56.9	26.16	0.07	0.04	0.14	0.10
73.6	52.2	25.99	0.07	0.04	0.14	0.10
170.8	49.3	26.32	0.07	0.04	0.15	0.10

Time (hr)	Acetate (mmol/kg)	Formate (mmol/kg)	Chloride (mmol/kg)	Sulfate (mmol/kg)	Oxalate (mmol/kg)	Nitrate (mmol/kg)
0.0	5.2	13.7	0.6	32.8	1.5	1.1
2.0	5.1	13.5	0.5	32.2	1.5	1.1
4.9	5.2	13.6	0.6	32.0	1.5	1.1
23.6	5.2	13.8	0.6	32.7	1.4	1.1
47.0	5.5	14.3	0.6	33.3	1.5	1.1
73.6	5.4	14.1	0.5	32.4	1.4	1.1
170.8	5.5	14.2	0.6	32.5	1.4	1.1

Time (hr)	FPZ (mmol/kg)	EDA (mmol/kg)	MPZ (mmol/kg)
0.0	8.7	27.9	2.5
2.0	7.5	28.1	2.3
4.9	7.6	26.9	2.4
23.6	8.8	27.0	2.5
47.0	8.1	26.4	2.5
73.6	7.9	26.8	2.5
170.8	7.8	27.6	2.5

Table B-2. Detailed Data of CAC 2 w/ PZ and #3706

Time (hr)	Solvent (g)	C/S (g/g)	Alkalinity (mol/kg)
0.0	89.3	0.037	6.49
0.3	88.4	0.038	6.43
1.0	87.5	0.038	6.44
1.6	87.1	0.039	6.51
2.8	86.5	0.039	6.50
14.6	85.5	0.039	6.53
16.6	84.7	0.039	6.51
20.6	83.9	0.040	6.46
22.5	83.0	0.040	6.51
24.5	81.7	0.041	6.48
26.9	81.3	0.041	6.54
28.6	80.5	0.042	6.49
38.6	79.6	0.042	6.50
44.5	78.6	0.042	6.51
50.6	78.3	0.043	6.46
70.4	77.7	0.043	6.47
Drain and fill with 82.4 g of #3706			
Time (hr)	Solvent (g)	C/S (g/g)	Alkalinity (mol/kg)
0.0	81.8	0.041	6.724542
22.5	80.8	0.042	6.430196
89.1	80.0	0.042	6.311784
161.8	78.6	0.043	6.224231
192.4	77.6	0.043	6.246459

Table B-3. Detailed Data of CAC 3 w/ #3537

Time (hr)	Abs (A)	Solvent (g)	C/S (g/g)	Fe (mmol/kg)	Ni (mmol/kg)	Cr (mmol/kg)
0.0	10.19	104.07	0.029	0.06	0.09	0.08
0.3	8.46	103.43	0.029	0.04	0.09	0.05
0.6	7.29	102.99	0.029	0.04	0.08	0.05
1.0	6.20	102.17	0.029	0.03	0.08	0.04
1.5	5.38	101.44	0.029	0.03	0.08	0.04
2.0	4.95	100.79	0.029	0.02	0.08	0.04
19.3	1.37	100.07	0.030			
20.3	1.35	99.61	0.030			
22.3	1.31	99.02	0.030			
24.4	1.24	98.21	0.030			
26.0	1.22	97.40	0.030			
43.8	0.94	96.98	0.031	0.01	0.08	0.03
45.8	0.95	95.51	0.031			
68.0	0.91	93.38	0.032	0.01	0.08	0.03
73.9	0.81	90.82	0.033			
89.6	0.76	89.21	0.033			
97.5	0.83	87.21	0.034			
162.4	0.73	83.75	0.035			
186.7	0.72	80.77	0.037			
213.2	0.72	76.28	0.039	0.01	0.08	0.02

Time (hr)	Mn (mmol/kg)	Formate (mmol/kg)	Sulfate (mmol/kg)	Oxalate (mmol/kg)	Nitrate (mmol/kg)	Alkalinity (mol/kg)
0.0	0.06	14.47	15.42	2.60	0.89	6.5
0.3	0.05	13.58	13.09	2.40	0.80	6.4
0.6	0.04	12.87	13.35	2.06	0.61	6.4
1.0	0.04	12.78	13.49	2.00	0.63	6.3
1.5	0.04	12.69	13.68	1.93	0.59	6.3
2.0	0.04	11.75	13.69	1.91	0.57	6.2
19.3						6.2
20.3						6.2
22.3						6.2
24.4						6.2
26.0						6.3
43.8	0.02	11.58	12.99	1.95	0.60	6.2
45.8						6.2
68.0	0.01	11.42	12.68	1.95	0.59	6.2
73.9						6.2

89.6						6.2
97.5						6.2
162.4						6.2
186.7						6.2
213.2	0.01	10.58	12.70	1.93	0.59	6.2

Time (hr)	FPZ (mmol/kg)	EDA (mmol/kg)	MPZ (mol/kg)
0.0	3.93	36.72	1.31
0.3	3.83	35.92	1.32
0.6	3.78	34.59	1.13
1.0	3.71	33.84	1.08
1.5	3.73	33.23	1.06
2.0	3.69	32.69	1.04
19.3	3.61	31.85	1.07
20.3	3.59	31.79	1.01
22.3	3.53	31.23	0.89
24.4	3.39	30.02	0.92
26.0	3.25	29.37	0.86
43.8	3.04	29.34	0.83
45.8	3.09	28.95	0.67
68.0	2.86	28.42	0.72
73.9	2.73	28.37	0.74
89.6	2.75	28.19	0.73
97.5	2.68	27.82	0.76
162.4	2.69	28.03	0.72
186.7	2.67	27.96	0.73
213.2	2.64	27.83	0.75

Table B-4. Detailed Data of CAC 4 w/ #3537

Time (hr)	Abs (A)	Solvent (g)	C/S (g/g)	Fe (mmol/kg)	Ni (mmol/kg)	Cr (mmol/kg)	Mn (mmol/kg)
0.0	10.19	96.7	0.045	0.06	0.07	0.07	0.07
21.3	1.55	96.7	0.045	0.05	0.07	0.06	0.06
52.0	0.95	93.6	0.046	0.02	0.07	0.02	0.02
91.3	0.77	88.9	0.048	0.00	0.07	0.02	0.02
97.9	0.72	84.1	0.051	0.00	0.07	0.01	0.02
331.7	0.72	78.8	0.055	0.00	0.07	0.01	0.01

Table B-5. Detailed Data of CAC 5 w/ #3537

Time (hr)	Abs (A)	Solvent (g)	C/S (g/g)	Fe (mmol/kg)	Ni (mmol/kg)	Cr (mmol/kg)	Mn (mmol/kg)
0.0	10.19	86.0	0.012	0.06	0.07	0.07	0.07
1.4	9.50	86.0	0.012	0.02	0.08	0.06	0.05
50.6	3.86	84.6	0.012	0.01	0.08	0.02	0.04
120.0	2.68	77.7	0.013	0.01	0.08	0.02	0.04
145.9	2.55	71.1	0.015	0.01	0.09	0.02	0.04
194.1	2.36	66.9	0.016	0.01	0.08	0.02	0.03
247.4	2.31	61.2	0.017				
312.1	2.24	56.7	0.018				
319.2	2.24	51.7	0.020	0.01	0.08	0.02	0.03

Table B-6. Detailed Data of CAC 6 w/ #3537

Time (hr)	Abs (A)	Solvent (g)	C/S (g/g)
0.0	9.94	94.5	0.037
0.4	7.89	93.7	0.037
0.7	6.61	93.3	0.037
1.1	6.69	92.6	0.038
2.1	3.33	92.0	0.038
2.8	3.48	91.1	0.038
4.8	2.62	90.3	0.039
6.1	2.46	89.5	0.039
71.6	1.26	88.6	0.039
95.6	0.74	86.2	0.041
120.5	0.66	81.4	0.043
231.1	0.66	75.5	0.046

Table B-7. Detailed Data of CAC 7 w/ #3537

Time (hr)	Abs (A)	Solvent (g)	C/S (g/g)	Fe (mmol/kg)	Ni (mmol/kg)	Cr (mmol/kg)
0.0	10.15	87.9	0.042	0.02	0.09	0.07
42.4	0.78	85.1	0.043	0.01	0.09	0.02
122.3	0.60	78.9	0.047	0.00	0.09	0.01
286.3	0.58	73.5	0.050	0.00	0.09	0.01

Time (hr)	Mn (mmol/kg)	Formate (mmol/kg)	Sulfate (mmol/kg)	Oxalate (mmol/kg)	Nitrate (mmol/kg)	Alkalinity (mol/kg)
0.0	0.07	13.4	15.0	2.3	0.8	6.4
42.4	0.03	10.8	12.7	2.0	0.7	6.2
122.3	0.03	11.2	12.6	1.9	0.7	6.2
286.3	0.02	10.2	12.6	1.8	0.6	6.3

Table B-8. Detailed Data of CAC 8 w/ #3537

Time (hr)	Abs (A)	Solvent (g)	C/S (g/g)
0.0	10.39	87.5	0.024
1.2	7.95	86.7	0.024
2.3	6.74	86.0	0.024
3.7	5.73	85.4	0.024
5.7	5.03	84.7	0.024
71.6	1.47	83.8	0.025
78.1	1.52	83.0	0.025
101.1	1.48	78.4	0.026

Table B-9. Detailed Data of CAC 9 w/ #3537

Time (hr)	Abs (A)	Solvent (g)	C/S (g/g)	Fe (mmol/kg)	Ni (mmol/kg)	Cr (mmol/kg)	Mn (mmol/kg)
0.0	9.96	88.6	0.019	0.03	0.08	0.07	0.07
71.9	1.51	87.4	0.019	0.01	0.09	0.03	0.03
95.7	1.42	86.5	0.020	0.01	0.09	0.02	0.03
166.7	1.27	82.2	0.021	0.01	0.09	0.02	0.03

Table B-10. Detailed Data of CAC 10 w/ #3537

Time (hr)	Abs (A)	Solvent (g)	C/S (g/g)
0.0	9.96	89.2	0.015
0.3	9.80	89.2	0.015
71.4	1.87	88.3	0.015
91.8	1.79	87.8	0.015
96.0	1.78	83.8	0.016

Table B-11. Detailed Data of CAC 11 w/ #3537

Time (hr)	Abs (A)	Solvent (g)	C/S (g/g)	Formate (mmol/kg)	Sulfate (mmol/kg)	Oxalate (mmol/kg)
0.0	11.01	86.6	0.053	0.06	0.07	0.07
25.5	1.17	85.1	0.054	0.05	0.07	0.06
49.2	0.65	82.5	0.056	0.02	0.07	0.02
68.4	0.66	76.9	0.060	0.00	0.07	0.02
93.6	0.60	70.5	0.065	0.00	0.07	0.01
171.4	0.63	64.5	0.071	0.00	0.07	0.01

Time (hr)	Nitrate (mmol/kg)	Alkalinity (mol/kg)	FPZ (mmol/kg)	EDA (mmol/kg)	MPZ (mmol/kg)
0.0	0.07	6.5	3.73	34.72	1.25
25.5	0.06	6.3			
49.2	0.02	6.1	3.22	34.30	0.84
68.4	0.02	6.1	3.43	33.99	0.90
93.6	0.02	6.1	3.08	30.00	0.65
171.4	0.01	6.1	2.74	27.03	0.82

Table B-12. Detailed Data of CAC 12 w/ #3706

Time (hr)	Abs (A)	Solvent (g)	C/S (g/g)	Fe (mmol/kg)	Ni (mmol/kg)	Cr (mmol/kg)	Mn (mmol/kg)
0.0	35.58	78.6	0.024	0.06	0.12	0.03	0.06
0.1	34.20	77.8	0.025	0.06	0.11	0.03	0.05
0.2	33.07	76.4	0.025	0.06	0.11	0.03	0.05
0.4	32.00	75.1	0.025	0.05	0.11	0.03	0.05
0.6	31.32	73.5	0.026	0.08	0.12	0.04	0.06
0.9	30.11	72.8	0.026	0.05	0.11	0.03	0.05
1.3	29.44	71.6	0.027	0.05	0.12	0.03	0.05
1.8	28.07	70.5	0.027	0.06	0.11	0.03	0.05
2.3	24.87	68.9	0.028	0.05	0.11	0.03	0.05
3.1	25.84	67.7	0.028	0.05	0.12	0.03	0.05
5.3	21.95	66.9	0.029	0.05	0.11	0.03	0.05
7.4	20.88	65.4	0.029	0.05	0.11	0.03	0.05
23.8	8.81	64.3	0.030	0.04	0.12	0.03	0.05
31.4	7.51	62.0	0.031	0.04	0.11	0.03	0.04
71.9	2.80	59.1	0.032				
95.7	2.78	54.7	0.035				
175.2	2.78	50.0	0.038				
366.6	2.79	45.8	0.042				

Table B-13. Detailed Data of CAC 13 w/ #3706

Time (hr)	Abs (A)	Solvent (g)	C/S (g/g)	Fe (mmol/kg)	Ni (mmol/kg)	Cr (mmol/kg)
0.0	35.60	87.9	0.059	0.08	0.12	0.08
80.7	1.33	85.1	0.061	0.01	0.11	0.02
104.2	1.25	78.9	0.065	0.01	0.11	0.02
171.4	1.16	73.5	0.069	0.01	0.12	0.03
246.6	1.13	69.4	0.074	0.01	0.11	0.02
272.6	1.14	63.6	0.081	0.01	0.12	0.02

Time (hr)	Mn (mmol/kg)	Sulfate (mmol/kg)	Oxalate (mmol/kg)	Nitrate (mmol/kg)	Alkalinity (mol/kg)	FPZ (mmol/kg)
0.0	0.18	23.3	4.0	1.9	6.7	8.29
80.7	0.12				6.2	6.83
104.2	0.12	18.9	2.6	1.4	6.3	7.40
171.4	0.13				6.3	6.76
246.6	0.12	19.5	2.6	1.3	6.3	6.78
272.6	0.13	19.5	2.3	1.3	6.3	6.67

Time (hr)	EDA (mmol/kg)	MPZ (mmol/kg)
0.0	55.43	2.18
80.7	53.63	1.82
104.2	53.15	1.75
171.4	53.71	1.65
246.6	49.04	1.58
272.6		1.57

Table B-14. Detailed Data of CAC 14 w/ #3706

Time (hr)	Abs (A)	Solvent (g)	C/S (g/g)	Formate (mmol/kg)	Sulfate (mmol/kg)	Oxalate (mmol/kg)
0.0	32.33	86.0	0.025	22.7	23.7	3.7
24.1	7.57	85.3	0.025			
45.9	5.77	80.4	0.027	18.4	22.0	2.2
68.2	4.51	76.8	0.028			
88.7	4.12	69.5	0.031	16.1	19.0	2.0
168.9	3.99	64.3	0.033			
189.2	3.62	61.3	0.035	16.2	18.7	2.1

Time (hr)	Nitrate (mmol/kg)	Alkalinity (mol/kg)	FPZ (mmol/kg)	EDA (mmol/kg)	MPZ (mmol/kg)	
0.0	1.8	6.7	7.91	57.43	1.98	
24.1		6.3	6.17	47.76	1.82	
45.9	1.4	6.4	6.98	52.81	1.52	
68.2		6.3	5.15	45.01	1.33	
88.7	1.2	6.3				
168.9		6.3				
189.2	1.1	6.3	5.08	45.80	1.27	

Table B-15. Detailed Data of CAC 15 w/ #3706

Time (hr)	Abs (A)	Solvent (g)	C/S (g/g)	Fe (mmol/kg)	Ni (mmol/kg)	Cr (mmol/kg)
0.0	29.09	82.8	0.042	0.06	0.14	0.09
21.9	3.43	80.7	0.043	0.02	0.15	0.03
93.9	1.69	81.5	0.043	0.01	0.14	0.03
144.7	1.58	80.9	0.043	0.01	0.14	0.02
215.9	1.55	78.5	0.045	0.01	0.14	0.02
453.8	1.55	80.7	0.043	0.01	0.14	0.02

Time (hr)	Mn (mmol/kg)	Formate (mmol/kg)	Sulfate (mmol/kg)	Oxalate (mmol/kg)	Nitrate (mmol/kg)	Alkalinity (mol/kg)
0.0	0.19	21.6	24.7	3.9	1.8	6.7
21.9	0.14					
93.9	0.15	16.9	21.2	2.0	1.3	6.8
144.7	0.13					
215.9	0.15	17.4	20.9	2.1	1.3	6.5
453.8	0.12	17.4	19.1	2.3	1.2	6.1

Table B-16. Detailed Data of CAC 16 w/ #3706

Time (hr)	Abs (A)	Solvent (g)	C/S (g/g)	Fe (mmol/kg)	Ni (mmol/kg)	Cr (mmol/kg)
0.0	26.18	87.0	0.060	0.06	0.14	0.08
47.4	1.50	85.1	0.061	0.01	0.15	0.03
72.9	1.00	83.7	0.062	0.01	0.14	0.03
145.0	0.74	82.2	0.064	0.01	0.14	0.02
338.3	0.71	80.9	0.065	0.01	0.14	0.02

Time (hr)	Mn (mmol/kg)	Formate (mmol/kg)	Sulfate (mmol/kg)	Oxalate (mmol/kg)	Nitrate (mmol/kg)	Alkalinity (mol/kg)
0.0	0.18	21.6	23.3	3.9	1.8	6.6
47.4	0.13					
72.9	0.14	15.6	19.8	1.9	1.3	6.3
145.0	0.15					
338.3	0.13	15.7	18.2	2.4	1.2	6.1

Table B-17. Detailed Data of CAC 17 w/ #3706

Time (hr)	Abs (A)	Solvent (g)	C/S (g/g)
0.0	24.99	82.4	0.074
0.9	13.65	78.3	0.097
21.7	2.67	72.9	0.103
24.7	2.54	68.1	0.110
43.3	2.54	63.1	0.117

Table B-18. Detailed Data of CAC 18 w/ #3706 + External Fe^{3+}

Time (hr)	Abs (A)	Solvent (g)	C/S (g/g)	Fe (mmol/kg)
0.0	56.25	78.0	0.040	9.88
0.2	53.06	74.8	0.042	7.86
0.4	51.55	71.7	0.043	7.70
0.5	50.47	68.6	0.045	5.89
0.9	48.34	65.8	0.047	5.92
1.3	45.40	63.7	0.049	5.02
1.6	44.51	61.1	0.051	5.47
1.9	42.93	58.7	0.053	4.23
2.4	42.05	55.9	0.056	4.76
2.9	40.41	54.2	0.057	4.70
4.5	37.45	52.7	0.059	4.17
6.1	35.30	50.8	0.061	4.36
7.2	33.99	49.0	0.064	3.52
23.6	26.20	47.1	0.066	1.85
25.9	25.24	45.8	0.068	3.04
29.6	24.32	44.4	0.070	1.86
48.6	21.12	42.0	0.074	2.73
54.3	19.29	40.3	0.077	2.19
75.8	15.88	38.0	0.082	1.47
167.5	7.14	37.0	0.084	1.32
215.5	5.25	35.5	0.088	0.93
239.9	3.93	34.3	0.091	0.67
383.7	2.60	28.9	0.108	0.12
409.7	2.25	27.5	0.113	0.13
505.6	2.25	26.1	0.119	0.09

Table B-19. Detailed Data of CAC 19 w/ #3706 + External Fe^{3+}

Time (hr)	Abs (A)	Solvent (g)	C/S (g/g)	Fe (mmol/kg)	Ni (mmol/kg)	Cr (mmol/kg)	Mn (mmol/kg)
0.0	30.48	78.7	0.042	0.16	0.11	0.03	0.06
0.2	27.61	76.3	0.043	0.16	0.11	0.03	0.06
0.5	24.41	73.8	0.044	0.16	0.10	0.03	0.06
0.9	22.34	71.7	0.045	0.16	0.10	0.03	0.06
1.2	20.70	69.0	0.046	0.16	0.11	0.03	0.06
1.5	19.90	67.0	0.047	0.16	0.11	0.03	0.06
2.0	17.70	64.2	0.048	0.15	0.11	0.03	0.05
2.5	16.05	61.5	0.051	0.15	0.11	0.03	0.05
3.1	14.94	59.3	0.053	0.15	0.11	0.03	0.05
3.5	14.39	59.3	0.053	0.15	0.11	0.03	0.05
4.7	11.99	53.5	0.061	0.14	0.11	0.03	0.05
20.6	5.36	51.5	0.067	0.11	0.11	0.03	0.04
23.1	5.30	48.9	0.073	0.10	0.11	0.03	0.04
27.5	4.57	46.3	0.076	0.10	0.11	0.02	0.04
45.9	3.87	44.1	0.081	0.09	0.11	0.02	0.03
52.4	3.43	41.6	0.086	0.09	0.12	0.02	0.03
73.0	3.00	39.1	0.106	0.08	0.12	0.02	0.03
189.1	2.79	36.5	0.042	0.05	0.11	0.02	0.02
218.4	2.39	34.9	0.043	0.04	0.11	0.01	0.02
236.9	2.04	33.6	0.044	0.04	0.11	0.01	0.02
266.3	2.02	31.7	0.045	0.04	0.11	0.01	0.02
335.5	2.04	29.2	0.046	0.04	0.11	0.01	0.02

Table B-20. Detailed Data of CAC 20 w/ #3706

Time (hr)	Abs (A)	Solvent (g)	C/S (g/g)
0.0	32.79	81.8	0.0035
2.0	30.66	80.1	0.0035
20.4	27.37	78.3	0.0036
26.4	26.87	77.1	0.0037
140.2	23.27	74.2	0.0038
145.8	22.73	72.0	0.0039
165.2	22.44	69.2	0.0041
169.9	22.40	65.6	0.0043
Take out and refill with 58.59 g #3706			
170.3	32.80	46.1	0.0061
187.5	30.78	43.6	0.0065
194.5	30.06	41.5	0.0068
212.5	29.5	38.7	0.0073
218.8	28.58	36.8	0.0077
240.6	28.35	34.6	0.0082
335.4	26.97	32.2	0.0088

Table B-21. Detailed Data of CAC 21 w/ NCCC Used Carbon

Time (hr)	Solvent (g)	Fe (mmol/kg)
0.0	78.5	0.031
1.1	74.2	0.007
2.9	69.8	0.008
Drain and Fill 74.6 g 0.2 N H_2SO_4		
3.0	74.6	1.244
4.2	72.4	1.234
93.8	67.9	1.225
99.3	57.7	1.165
Drain and Fill 77.8 g 0.2 N H_2SO_4		
99.4	77.8	0.702
117.9	73.9	1.182
124.6	69.4	1.214
146.6	63.4	1.343
286.7	58.7	1.482
Drain and Fill 70.0 g 25 mmol/kg EDTA		
286.7	68.0	0.197
313.3	63.3	0.259
315.2	59.3	0.268
337.2	55.1	0.270
360.8	50.8	0.271
433.4	68.0	0.291

Table B-22. Detailed Data of CAC 22 w/ NCCC Clean Carbon

Time (hr)	H_2SO_4 (g)	Fe (mmol/kg)
22.5	83.1	0.163
22.7	58.7	0.072
23.0	61.5	0.011
23.2	61.6	0.004
23.5	63.5	0.004
23.9	60.8	0.004
24.2	58.0	0.004

Table B-23. Detailed Data of CAC 23 Treating AEP w/ Clean Carbon

Time (hr)	Sample (g)	C/S	AEP (mmol/kg)
0.0	4.99	0.020	17.33
0.1	0.61	0.020	14.10
0.2	1.36	0.020	13.65
0.4	0.96	0.020	12.74
0.9	0.95	0.021	12.19
1.4	1.49	0.021	10.93
1.9	1.30	0.021	10.54
2.9	2.29	0.022	10.46
3.9	1.46	0.022	9.83
4.9	1.11	0.023	9.77
21.8	1.65	0.023	9.58
27.9	1.23	0.024	9.49
94.5	1.47	0.024	9.39
119.0	2.05	0.025	9.38
146.2	2.48	0.026	9.42
172.0		0.026	9.44

APPENDIX C. DATA OF HTOR EXPERIMENTS

Table C-1. Detailed Data of HTOR 22

Time (hr)	PZ (mol/kg)	320 Abs (A)	EDA (mmol/kg)	FPZ (mmol/kg)	PZ-one (mmol/kg)	PZ-ol (mmol/kg)
5.3	3.76	149.61	20.53	15.78	16.85	3.68
14.6	3.79	152.94	19.69	18.15	16.15	4.10
61.5	3.63	157.96	16.49	26.29	16.92	4.09
153.6	4.38	191.63	13.69	33.72	16.90	4.04
206.0	4.03	214.31	16.42	33.73	17.12	3.29
274.6	2.98	243.16	12.86	29.61	15.88	3.66
324.6	4.40	250.22	13.23	50.45	16.56	3.08
373.0	4.37	264.28	12.49	56.22	16.83	3.97
397.0	3.58	266.86	9.92	29.87	14.85	2.83
495.9	4.14	278.43	10.51	50.51	16.54	3.06
541.7	3.80	281.44	9.08	43.44	14.51	2.37
587.8	3.79	290.07	11.44	39.18	14.87	2.13
657.9	3.48	326.11	14.51	57.08	14.14	2.28

Time (hr)	T. Sulfate (mmol/kg)	T. Oxalate (mmol/kg)	T. Formate (mmol/kg)	T. Acetate (mmol/kg)	T. Nitrate (mmol/kg)	Fe (mmol/kg)
5.3	3.09	5.70	46.23	3.32	2.69	0.42
14.6	3.65	7.58	50.66	5.79	3.28	0.28
61.5	3.98	9.10	56.38	7.06	3.19	0.32
153.6	4.10	9.96	71.92	7.20	3.46	0.36
206.0	5.08	11.43	75.82	7.74	3.23	0.47
274.6	4.28	12.54	86.31	10.13	3.67	0.52
324.6	4.38	12.75	96.60	8.10	3.48	0.66
373.0	4.52	13.74	104.78	8.25	3.74	0.81
397.0	4.20	11.94	99.20	9.98	3.42	0.70
495.9	4.29	14.03	111.37	11.20	3.60	0.69
541.7	3.59	12.15	110.47	11.58	3.33	0.65
587.8	4.02	15.13	129.90	13.31	3.49	0.57
657.9	3.64	16.49	129.84	12.00	3.23	

Time (hr)	Cr (mmol/kg)	Mn (mmol/kg)	Ni (mmol/kg)
5.3	1.61	0.13	1.55
14.6	1.53	0.12	1.51
61.5	1.60	0.13	1.58
153.6	1.67	0.13	1.69
206.0	1.65	0.14	1.64
274.6	1.66	0.14	1.68
324.6	1.77	0.14	1.80

373.0	1.87	0.15	1.90
397.0	1.69	0.14	1.74
495.9	1.81	0.15	1.87
541.7	1.72	0.15	1.81
587.8	1.66	0.15	1.75
657.9			

Table C-2. Detailed Data of HTOR 23

Time (hr)	PZ (mol/kg)	320 Abs (A)	EDA (mmol/kg)	MPZ (mmol/kg)	T. Formate (mmol/kg)	Fe (mmol/kg)
23.4	3.69	5.77	120.65	0.00	2.83	0.03
23.8	3.61	7.38	117.96	0.00	2.42	0.31
28.1	3.66	8.42	119.13	0.00	2.72	0.12
52.5	3.66	14.22	114.21	0.76	3.66	0.04
76.8	3.66	19.83	108.40	0.96	4.59	0.03
101.0	3.62	22.49	106.25	1.45	4.46	0.04
149.5	3.56	30.75	102.39	1.81	6.07	0.05
195.7	3.61	36.74	96.88	2.28	6.46	0.04
243.9	3.57	45.97	89.53	2.78	7.99	0.06
294.4	3.57	56.64	67.54	0.00	9.81	0.08
340.1	3.53	70.22	66.15	0.00	11.96	0.10
411.9	3.42	80.67	51.09	0.00	13.46	0.12
432.6	3.46	92.12	48.17	1.95	16.03	0.11
508.9	3.42	114.89	46.53	7.08	19.55	0.13
579.8	3.41	131.87	38.56	8.75	25.81	0.15
602.7	3.34	149.98	35.67	9.04	28.78	0.17
629.1	3.40	151.96	34.47	10.05	29.63	0.16

Time (hr)	Cr (mmol/kg)	Mn (mmol/kg)	Ni (mmol/kg)	Li (mmol/kg)	K (mmol/kg)
23.4	0.03	0.01	0.04	9.21	3.13
23.8	0.03	0.01	0.04	9.08	3.09
28.1	0.02	0.01	0.04	9.13	3.06
52.5	0.02	0.01	0.06	9.16	3.13
76.8	0.03	0.01	0.08	9.58	3.31
101.0	0.04	0.01	0.09	9.12	3.05
149.5	0.05	0.01	0.12	9.35	3.16
195.7	0.06	0.01	0.15	9.32	3.09
243.9	0.08	0.01	0.17	9.21	2.99
294.4	0.09	0.01	0.20	9.53	3.13
340.1	0.12	0.02	0.25	10.43	3.44
411.9	0.11	0.02	0.23	8.38	3.06
432.6	0.12	0.02	0.25	8.86	3.24
508.9	0.13	0.02	0.28	8.80	3.26
579.8	0.15	0.02	0.30	8.58	3.09
602.7	0.16	0.02	0.32	8.99	3.27
629.1	0.16	0.03	0.34	9.27	3.37

Table C-3. Detailed Data of HTOR 25

Time (hr)	PZ (mol/kg)	320 Abs (A)	EDA (mmol/kg)	PZ-one (mmol/kg)	FPZ (mmol/kg)	HEP (mmol/kg)
4.6	3.73	0.17	7.82		0.76	2.24
23.9	3.80	3.3	10.27	8.85	1.45	4.84
28.5	3.80	3.73	10.59	8.81	1.44	5.10
76.2	2.95	4.27	13.73		1.07	6.28
123.3	3.52	5.94	24.70		2.23	8.90
147.4	3.76	7.79	27.36		2.36	10.21
171.9	3.65	19.8	30.70	26.59	4.35	9.12
215.0	3.58	25.43	34.59	29.27	4.79	8.47
268.2	3.95	41.12	45.38	63.54	7.80	9.37
334.8	3.51	41.56	46.56	40.26	7.42	7.93
340.6	3.41	62.8	48.15	38.33	16.08	7.55
387.0	3.33	88.02	50.26	51.37	13.52	7.44
454.3	3.04	85.12	47.48	47.70	13.67	6.25
501.8	3.59	101.63	53.76	107.74	18.88	11.39
550.5	3.29	105.15	47.25	58.50	15.56	6.43
554.7	3.33	111.54	49.92	49.08	33.70	6.31
558.4	3.07	107.75	48.84	46.26	17.42	5.80
579.8	3.26	127.32	47.96	56.83	19.81	5.53
622.4	3.11	127.87		40.40	18.77	5.25
696.2	2.96	172.61	41.17	32.21	22.30	6.91
790.3	2.89	190.76	40.57	29.35	29.65	4.56
866.7	2.81	202.84	38.36	30.08	39.13	4.19

Time (hr)	MPZ (mmol/kg)	Li (mmol/kg)	K (mmol/kg)	Fe (mmol/kg)	Cr (mmol/kg)	Ni (mmol/kg)
4.6	0.48	20.85	4.74	0.01	0.01	0.01
23.9	3.18	21.44	4.94	0.01	0.01	0.02
28.5	3.17	21.73	5.05	0.06	0.01	0.02
76.2	4.68	16.64	3.73	0.02	0.02	0.03
123.3	5.42	19.04	4.41	0.02	0.02	0.06
147.4	8.12	21.55	4.89	0.02	0.03	0.07
171.9	10.47	21.11	4.83	0.03	0.04	0.08
215.0	11.37	20.85	4.76	0.03	0.05	0.10
268.2	13.97	22.03	5.10	0.04	0.07	0.12
334.8	13.45	20.90	4.74	0.05	0.08	0.14
340.6	17.24	21.47	4.87	0.15	0.10	0.14
387.0	20.74	21.96	5.04	0.08	0.11	0.16
454.3	19.49	20.59	2.50	0.09	0.13	0.18
501.8	24.36	23.17	2.77	0.10	0.17	0.23

550.5	20.88	22.22	2.61	0.08	0.16	0.24
554.7	23.87	21.86	2.67	0.14	0.15	0.22
558.4	23.77	21.48	2.53	0.18	0.17	0.22
579.8	24.62	22.65	2.73	0.10	0.15	0.24
622.4	24.98	21.66	2.57	0.09	0.17	0.24
696.2	25.68	20.96	2.87	0.10	0.19	0.27
790.3	27.48	20.83	2.54	0.12	0.21	0.32
866.7	27.82	20.55	2.49	0.11	0.24	0.31

Time (hr)	Mn (mmol/kg)	Formate (mmol/kg)	T. Formate (mmol/kg)	T. Acetate (mmol/kg)	T. Glycolate (mmol/kg)	T. Oxalate (mmol/kg)
4.6	0.00	0.57	1.33	0.32	0.22	0.02
23.9	0.00	0.13	1.54	1.32	0.04	0.07
28.5	0.00	0.13	1.51	1.42	0.04	0.06
76.2	0.00	1.23	2.87	2.00	0.06	0.10
123.3	0.00	1.47	4.05	2.24	0.11	0.14
147.4	0.01	1.63	3.86	2.14	0.12	0.16
171.9	0.01	3.25	7.51	4.78	0.18	0.69
215.0	0.01	3.18	7.97	5.91	0.20	0.45
268.2	0.01	2.72	9.95	7.23	0.25	0.68
334.8	0.01	4.85	12.24	8.19	0.25	0.84
340.6	0.01	5.88	21.33	8.70	0.27	1.67
387.0	0.02	5.75	18.29	11.88	0.32	1.68
454.3	0.02	4.00	20.98	13.95	0.34	2.13
501.8	0.02	7.05	20.59	13.63	0.32	0.47
550.5	0.02	8.64	25.53	16.61	0.35	2.83
554.7	0.02	11.64	33.82	17.70	0.41	3.60
558.4	0.02	11.47	32.90	18.18	0.42	3.59
579.8	0.02	13.16	30.34	20.19	0.38	3.58
622.4	0.02	16.06	28.71	20.53	0.44	3.63
696.2	0.02	18.95	46.01	33.60	0.80	6.50
790.3	0.04	20.52	50.22	30.61	0.83	10.82
866.7	0.03	23.24	63.29	31.62	0.75	8.60

Table C-3. Detailed Data of HTOR 27

Time (hr)	PZ (mol/kg)	320 Abs (A)	EDA (mmol/kg)	MPZ (mmol/kg)	FPZ (mmol/kg)	PZ-ol (mmol/kg)
18.6	2.66	97.75	8.87	0.66	4.73	7.73
25.8	2.49	73.92	8.31	0.85	2.83	8.70
67.0	2.68	87.64	12.86	1.57	4.59	7.03
90.5	2.28	59.92	12.33	1.58	2.10	7.86
162.7	2.17	57.00	17.32	2.96	2.75	9.61
211.6	2.02	52.89	17.27	3.69	2.69	8.24
234.5	2.10	52.22	21.42	4.20	3.55	8.06
263.6	1.84	51.27	23.19	4.26	3.52	7.13
330.7	2.32	50.01	28.72	4.67	8.71	12.16
357.3	2.01	48.80	24.72	4.83	6.20	13.86
403.8	2.22	40.12	21.28	5.25	8.98	14.90
427.2	1.36	44.00	18.86	5.55	2.31	11.04
498.7	1.00	47.98	17.03	6.29	0.81	13.38
522.6	0.94	51.30	15.54	6.97	0.83	13.66
570.6	0.89	62.44	16.43	7.09	1.21	15.75
594.7	0.87	68.47	15.33	7.46	1.61	14.08
675.7	0.80	85.03	12.42	8.56	1.93	12.87
699.7	0.76	76.60	10.87	9.43	1.98	7.22
766.7	0.68	80.92	9.03	10.02	3.28	6.35

Time (hr)	Li (mmol/kg)	K (mmol/kg)	Fe (mmol/kg)	Cr (mmol/kg)	Ni (mmol/kg)	Mn (mmol/kg)
18.6	2.93	2.55	0.08	0.58	0.53	0.05
25.8	2.70	2.24	0.04	0.47	0.46	0.04
67.0	3.03	2.49	0.06	0.47	0.52	0.04
90.5	2.68	2.05	0.04	0.37	0.45	0.03
162.7	2.70	2.03	0.04	0.33	0.46	0.03
211.6	2.60	1.92	0.04	0.28	0.44	0.03
234.5	2.61	1.90	0.04	0.27	0.44	0.03
263.6	2.49	1.78	0.04	0.24	0.42	0.03
330.7	2.51	1.75	0.05	0.23	0.42	0.03
357.3	2.40	1.61	0.04	0.21	0.40	0.03
403.8	1.94	1.25	0.06	0.16	0.33	0.02
427.2	2.00	1.25	0.02	0.14	0.33	0.02
498.7	1.85	1.13	0.03	0.10	0.31	0.02
522.6	1.88	1.11	0.03	0.10	0.31	0.02
570.6	1.93	1.12	0.04	0.10	0.32	0.02
594.7	2.03	1.14	0.05	0.11	0.32	0.02
675.7	2.22	1.18	0.05	0.11	0.34	0.02

699.7	2.03	1.06	0.03	0.10	0.31	0.02
766.7	2.07	1.05	0.04	0.12	0.31	0.02

Time (hr)	Formate (mmol/kg)	Acetate (mmol/kg)	Oxalate (mmol/kg)	T. Formate (mmol/kg)	T. Acetate (mmol/kg)	T. Oxalate (mmol/kg)
18.6	28.65	8.35	3.54	47.02	11.25	5.43
25.8				41.95	9.94	4.97
67.0	32.42	10.38	4.09	30.06	7.34	3.33
90.5	29.93	9.64	3.67	28.35	7.10	3.25
162.7	33.63	11.77	4.39	48.45	13.04	6.38
211.6	36.54	12.31	4.65	31.36	8.13	3.83
234.5	36.20	12.84	4.79	49.81	13.72	6.65
263.6	36.23	13.14	4.90	47.78	12.78	6.36
330.7	36.91	14.08	5.28	52.00	14.21	7.17
357.3	37.75	14.24	5.27	49.83	13.38	6.92
403.8	30.71	11.59	4.19	40.76	10.51	5.38
427.2	35.76	12.47	4.39	41.76	11.12	5.45
498.7	40.27	13.44	4.56	46.49	11.46	5.43
522.6	42.02	14.17	4.60	50.44	12.75	5.81
570.6	46.33	16.42	5.21	58.39	14.74	10.88
594.7	46.66	16.67	5.30	63.58	17.13	11.11
675.7	60.60	21.22	6.99	75.39	19.11	8.71
699.7	55.67	20.01	6.71	72.14	18.33	8.61
766.7	60.51	21.99	7.75	78.11	19.21	9.76

Table C-4. Detailed Data of HTOR 28

Time (hr)	PZ (mol/kg)	320 Abs (A)	EDA (mmol/kg)	MPZ (mmol/kg)	FPZ (mmol/kg)	PZ-one (mmol/kg)
140.0	3.08	109.16	58.69	6.61	17.30	110.25
166.2	3.09	122.84	61.47	8.11	23.66	142.13
185.5	3.25	150.12	66.80	8.92	29.98	167.67
190.8	3.33	157.89	63.85	9.84	22.70	158.43
213.8	3.54	179.37	64.31	9.58	39.86	186.46
214.7	3.57	172.54	63.06	10.50	34.03	197.48
220.8	3.58	170.53	65.81	11.61	42.79	197.76
237.9	3.32	176.48	57.25	11.17	39.13	187.61
262.6	3.41	192.37	58.38	11.61	44.96	215.57
266.7	3.22	194.03	52.17	11.67	43.37	194.60
285.6	3.14	197.71	50.22	13.02	48.90	217.21
291.8	3.19	198.84	48.38	12.93	46.12	220.71
317.1	3.03	199.48	42.76	12.52	46.23	180.32
339.5	3.31	201.37	38.01	12.31	46.53	203.74
363.7	2.98	200.44	33.15	14.55	51.26	196.02
383.6	2.83	200.08	29.95	15.89	53.88	199.44
405.6	3.21	195.96	32.55	19.25	71.46	200.67
434.3	2.84	194.77	23.23	17.13	62.72	191.54
458.8	2.79	199.17	22.57	28.44	55.04	174.22
482.8	2.93	220.28	20.83	28.16	65.77	168.16
506.8	2.92	234.39	21.44	27.12	64.82	151.72
532.0	2.90	243.15	20.56	28.73	71.11	145.48
554.8	2.83	263.34	17.77	28.30	72.66	151.07

Time (hr)	AEP (mmol/kg)	Li (mmol/kg)	Fe (mmol/kg)	Cr (mmol/kg)	Ni (mmol/kg)	Mn (mmol/kg)
140.0	1.94	1.65	0.40	0.38	0.39	0.26
166.2	5.70	1.73	0.45	0.42	0.40	0.28
185.5	4.19	1.93	0.51	0.47	0.44	0.31
190.8	4.39	1.94	0.53	0.48	0.45	0.31
213.8	5.03	2.07	0.61	0.50	0.47	0.33
214.7	5.60	2.06	0.61	0.49	0.47	0.32
220.8	8.05	2.04	0.58	0.45	0.47	0.33
237.9	5.28	2.00	0.57	0.43	0.46	0.31
262.6	5.09	1.92	0.55	0.43	0.45	0.30
266.7	4.91	1.92	0.55	0.43	0.46	0.30
285.6	3.96	1.91	0.53	0.42	0.45	0.29
291.8	3.80	2.11	0.57	0.46	0.51	0.32
317.1	4.71	1.85	0.55	0.36	0.45	0.28

339.5	4.08	2.04	0.57	0.40	0.50	0.30
363.7	3.56	2.13	0.56	0.42	0.52	0.31
383.6	2.84	1.89	0.57	0.37	0.47	0.28
405.6	3.28	2.17	0.56	0.42	0.54	0.32
434.3	1.91	2.00	0.54	0.41	0.50	0.29
458.8	3.05	1.93	0.53	0.39	0.47	0.28
482.8	2.66	2.13	0.58	0.43	0.52	0.30
506.8	3.60	2.15	0.63	0.48	0.53	0.31
532.0	3.61	2.16	0.72	0.50	0.54	0.31
554.8	2.79	2.15	0.74	0.50	0.54	0.31
140.0	3.09	2.24	0.81	0.54	0.57	0.33

Time (hr)	Formate (mmol/kg)	Acetate (mmol/kg)	Propionate (mmol/kg)	Sulfate (mmol/kg)	Oxalate (mmol/kg)	Nitrate (mmol/kg)
140.0	23.03	9.80	1.40	8.25	5.34	1.01
166.2	24.07	10.72	1.58	9.29	6.63	1.11
185.5	26.93	12.06	1.87	11.21	8.38	1.24
190.8	27.02	12.14	1.78	11.14	7.97	1.27
213.8	27.91	13.34	2.18	10.70	9.56	1.31
214.7	26.88	12.97	1.99	10.54	9.09	1.29
237.9	29.23	12.74	2.12	10.00	9.60	1.17
262.6	32.81	12.86	2.30	10.14	10.88	1.16
266.7	33.45	13.00	2.26	11.04	11.00	1.08
285.6	35.79	13.24	2.24	9.26	12.40	1.11
291.8	36.56	13.56	2.33	9.25	12.61	1.13
317.1	34.39	13.45	2.21	9.07	11.87	0.99
339.5	39.18	14.10	2.42	8.96	13.61	0.96
363.7	40.63	14.35	2.13	8.67	15.33	0.97
383.6	41.83	15.97	2.43	8.94	17.63	1.01
405.6	45.77	18.95	2.94	10.12	21.16	1.08
434.3	47.61	18.70	3.85	9.19	20.40	0.99
458.8	61.79	18.92	4.48	9.95	21.21	1.46
482.8	68.44	22.64	4.45	11.15	24.59	1.79
506.8	66.07	22.40	4.59	10.59	23.48	1.53
532.0	62.38	22.55	4.63	10.67	22.53	1.44
554.8	67.86	23.14	4.64	10.67	23.94	1.46

Time (hr)	T. Formate (mmol/kg)	T. Acetate (mmol/kg)	T. Propionate (mmol/kg)	T. Sulfate (mmol/kg)	T. Oxalate (mmol/kg)	T. Nitrate (mmol/kg)
140.0	21.43	7.30	1.50	8.65	5.98	1.20
166.2	23.99	8.39	2.81	9.48	7.10	1.36
185.5	29.68	8.92	3.39	10.35	8.65	1.52
190.8	30.42	8.69	3.19	10.43	8.48	1.50

213.8	38.06	9.45	3.86	11.67	8.96	1.74
214.7	41.21	9.25	3.63	11.39	9.03	1.66
237.9	44.68	9.53	4.00	10.73	9.69	1.54
262.6	47.15	9.14	4.09	10.63	11.08	1.61
266.7	51.00	11.04	2.21	10.00	13.25	1.60
285.6	51.84	12.68	2.31	9.00	14.99	1.11
291.8	57.54	13.59	2.54	9.74	14.09	1.17
317.1	52.34	13.30	2.45	9.16	13.46	1.01
339.5	59.08	13.99	2.36	8.58	14.82	1.12
363.7	62.55	15.47	2.51	8.72	15.63	0.95
383.6	60.80	16.16	2.59	8.44	15.59	0.93
405.6	68.59	21.68	3.46	11.39	19.48	1.22
434.3	68.60	22.96	2.86	9.15	17.56	1.44
458.8	66.37	26.42	3.73	9.77	17.44	1.53
482.8	73.82	30.56	4.31	10.91	20.48	1.57
506.8	76.30	31.74	4.34	10.44	21.39	1.50
532.0	76.84	31.36	4.17	10.32	20.20	1.54
554.8	80.78	33.92	4.50	10.32	21.87	1.52

Table C-5. Detailed Data of HTOR 29

Time (hr)	PZ (mol/kg)	320 Abs (A)	EDA (mmol/kg)	MPZ (mmol/kg)	FPZ (mmol/kg)	PZ-one (mmol/kg)
0.8	2.97	21.33	42.98	6.51	11.21	121.83
19.8	4.41	20.83	69.78	8.07	16.79	154.72
24.4	3.40	21.13	50.11	8.92	17.94	130.46
48.8	3.30	24.62	51.93	9.36	18.20	131.15
70.3	3.60	29.64	55.13	10.82	19.40	127.79
75.9	3.49	30.75	53.86	10.31	19.78	130.00
100.2	3.18	35.05	53.84	10.92	20.04	128.00
124.3	3.25	42.49	60.04	12.47	22.45	120.00
142.4	3.38	43.88	61.36	12.57	23.76	124.00
167.6	3.32	61.05	65.06	14.72	26.38	140.00
238.5	3.27	73.49	63.98	14.91	29.45	148.00
288.7		100.95			27.45	154.00
288.7	3.02	102.49	53.15	17.47	29.82	123.27
294.1	3.04	107.11	49.79	15.06	30.53	136.56
318.1	3.38	132.75	50.33	19.07	42.54	180.27
336.7	3.00	138.92	45.89	17.48	38.85	173.49
366.3	2.80	146.68	35.33	17.21	36.83	157.23
386.3	2.64	163.13	36.88	20.27	42.49	178.60
393.9	2.41	167.73	34.67	19.99	45.38	165.34
416.5	2.25	173.41	29.64	19.09	48.64	168.61
487.2	2.25	183.85	24.32	21.52	51.32	160.21
510.9	2.13	188.28	22.61	23.92	53.44	178.29
588.9	2.10	207.86	17.61	26.53	58.98	149.87
612.9	1.90	208.29	17.02	27.40	57.06	159.95
634.9	2.13	219.37	16.48	32.37	62.45	162.89
663.9	2.13	224.26	15.55	31.85	64.02	143.03

Time (hr)	AEP (mmol/kg)	Li (mmol/kg)	Fe (mmol/kg)	Cr (mmol/kg)	Ni (mmol/kg)	Mn (mmol/kg)
0.8	12.22	1.70	0.14	0.35	0.32	0.22
19.8	12.44	2.61	0.13	0.29	0.47	0.32
24.4	14.56	1.99	0.09	0.27	0.40	0.22
48.8	13.69	1.96	0.08	0.18	0.41	0.21
70.3	13.82	2.18	0.05	0.17	0.41	0.23
75.9	14.15	2.12	0.06	0.19	0.40	0.26
100.2	13.46	1.95	0.07	0.16	0.41	0.22
124.3	13.88	2.01	0.07	0.15	0.39	0.22
142.4	13.25	2.07	0.07	0.13	0.39	0.23
167.6	13.33	2.11	0.09	0.13	0.43	0.24

238.5	13.08	2.14	0.22	0.15	0.42	0.27
288.7		2.09	0.33	0.22	0.44	0.28
288.7	8.24	2.05	0.36	0.25	0.49	0.28
294.1	8.81	2.09	0.39	0.29	0.43	0.29
318.1	7.39	2.25	0.45	0.29	0.43	0.31
336.7	7.44	2.20	0.49	0.28	0.47	0.31
366.3	6.18	1.96	0.60	0.35	0.49	0.31
386.3	4.13	2.00	0.68	0.34	0.49	0.30
393.9	4.62	2.11	0.71	0.45	0.47	0.32
416.5	4.55	1.94	0.79	0.43	0.49	0.32
487.2	3.03	1.90	0.83	0.44	0.49	0.32
510.9	1.46	1.93	0.89	0.49	0.49	0.33
588.9	0.95	1.84	1.11	0.51	0.49	0.31
612.9	0.74	1.80	1.10	0.51	0.49	0.32
634.9	0.69	2.01	1.19	0.59	0.53	0.34
663.9	0.97	1.83	1.21	0.58	0.57	0.33

Time (hr)	Formate (mmol/kg)	Acetate (mmol/kg)	Propionate (mmol/kg)	Sulfate (mmol/kg)	Oxalate (mmol/kg)	Nitrate (mmol/kg)
0.8	15.51	8.34	1.17	7.95	1.83	0.96
19.8	13.22	9.30	1.35	8.50	2.29	1.02
24.4	13.49	9.67	1.44	8.62	2.38	1.04
48.8	14.78	10.10	1.54	8.76	2.61	1.00
70.3	15.06	10.73	1.71	8.56	2.84	0.99
75.9	14.87	10.43	1.68	8.58	2.69	0.99
100.2	16.29	10.56	1.64	8.30	3.05	0.97
124.3	17.71	11.65	1.82	8.52	3.66	0.99
142.4	18.33	11.94	1.87	8.33	3.85	0.98
167.6	19.67	13.10	2.10	8.74	4.29	1.03
238.5	19.65	13.17	1.85	8.54	4.17	0.96
288.7	20.67	13.97	2.30	8.35	4.65	1.00
288.7	21.91	13.25	2.26	7.14	4.45	1.04
294.1	21.96	13.41	2.16	7.36	4.68	1.07
318.1	22.26	16.22	2.37	8.30	6.15	1.19
336.7	22.25	16.17	2.55	8.00	6.23	1.19
366.3	22.09	16.23	2.96	7.12	6.79	1.09
386.3	22.22	18.56	2.03	7.20	7.68	1.12
393.9	22.31	19.45	2.04	7.65	8.21	1.19
416.5	25.08	18.68	2.28	6.85	8.08	1.08
487.2	22.38	24.04	2.57	6.96	11.18	1.14
510.9	22.41	27.00	2.28	6.83	11.57	1.16
588.9	22.49	31.06	2.6	6.52	14.64	1.10

612.9	22.53	31.33	2.42	6.41	15.24	1.10
634.9	25.82	36.49	2.54	7.12	18.11	1.26
663.9	25.70	35.67	2.81	6.63	17.25	1.19

Time (hr)	T. Formate (mmol/kg)	T. Acetate (mmol/kg)	T. Propionate (mmol/kg)	T. Sulfate (mmol/kg)	T. Oxalate (mmol/kg)	T. Nitrate (mmol/kg)
0.8	29.80	10.00	1.42	7.64	3.43	0.98
19.8	33.47	11.55	1.53	8.26	10.87	1.08
24.4	33.97	11.86	1.59	8.22	4.19	1.07
48.8	36.11	12.28	1.61	8.27	4.76	1.07
70.3	37.08	13.88	1.70	8.16	5.09	0.98
75.9	38.40	13.73	1.69	8.02	5.00	0.98
100.2	40.37	14.02	1.80	7.88	5.80	0.97
124.3	43.00	15.31	1.78	7.88	6.32	0.99
142.4	44.64	15.72	1.88	7.83	7.30	1.05
167.6	48.10	17.21	1.90	8.17	7.75	1.02
238.5	54.68	18.18	2.07	8.13	7.05	1.00
288.7	56.86	19.48	2.31	7.79	7.88	0.92
288.7	56.01	19.62	2.40	7.90	7.66	1.04
294.1	61.55	21.90	2.65	8.80	8.55	0.99
318.1	63.23	22.55	2.55	8.51	10.30	1.07
336.7	67.88	25.76	3.02	8.94	11.26	1.23
366.3	67.99	24.03	2.29	7.48	12.43	1.10
386.3	69.13	25.58	2.44	7.77	13.09	1.11
393.9	70.98	25.09	2.25	7.02	13.00	1.03
416.5	73.53				13.90	
487.2	82.35	24.78	2.59	7.10	15.08	1.12
510.9	85.39	29.00	2.80	7.06	17.39	1.13
588.9	86.95	29.83	2.80	6.98	18.26	1.12
612.9	89.36	30.10	2.87	4.58	18.28	0.78
634.9	91.72	34.68	2.71	3.89	21.24	0.69

APPENDIX D. DATA OF PILOT PLANTS

Table D-1. Detailed Data of NCCC 2018 Campaign

Time (hr)	PZ (mol/kg)	320 Abs (A)	EDA (mmol/kg)	MPZ (mmol/kg)	FPZ (mmol/kg)	PZ-one (mmol/kg)
0.0	3.20	1.36		0	0.28	
99.2	3.39	1.58	1.09	0	0.30	2.49
256.0	3.23	2.39	4.04	0	0.34	1.69
394.0	3.04	2.94	7.90	0	0.61	2.98
421.2	3.08	3.05		0	0.58	4.28
500.8	2.98	3.16		0	0.56	2.37
598.2	3.13	4.83	9.54	0	0.83	5.47
600.0	3.18	5.53	7.18	0	0.76	4.45
736.4	3.21	6.88	8.46	0	0.88	5.44
806.2	3.24	8.02	8.24	0	0.83	3.72
876.3	3.00	8.05	11.30	0	1.16	6.01
948.1	3.72	10.84	9.88	0	1.22	1.88
977.0	2.64	10.84	5.88	0	0.71	1.09
1048.6	3.40	10.36	10.46	0	0.82	5.45
1072.5	3.21	10.92	9.13	0	1.00	4.92
1078.2	3.29	11.79	10.17	0	1.24	2.32
1169.2	3.36	12.97	11.91	0.13	1.43	5.29
1241.1	3.08	12.72	11.31	0.25	1.30	6.13
1336.6	3.15	13.52	7.77	0.93	1.31	6.14
1432.8	3.00	16.15	13.39	1.08	1.14	4.42
1599.9	2.85	16.98	12.20	0.98	1.42	6.64
1673.0	2.87	17.7	16.76	2.37	1.57	8.55
1752.3	2.86	17.82	15.88	2.07	1.31	7.72
1827.5	2.78	20.04	17.33	2.75	1.49	6.73
1915.8	2.73	19.68	14.18	3.37	1.70	7.46
2010.0	3.10	22.95	19.82	3.89	2.42	10.05

Time (hr)	MNPZ (mmol/kg)	Li (mmol/kg)	K (mmol/kg)	Fe (mmol/kg)	Cr (mmol/kg)	Ni (mmol/kg)
0.0				0.03	0.00	0.02
99.2	1.05			0.03	0.01	0.02
256.0	1.55	8.20	1.08	0.03	0.01	0.03
394.0	2.01	7.63	1.00	0.04	0.01	0.03
421.2	2.04	8.70	0.96	0.04	0.01	0.04
500.8	2.08	7.91	0.94	0.04	0.01	0.04
598.2	2.72	8.64	0.90	0.05	0.01	0.05
600.0	2.76	7.22	1.06	0.05	0.01	0.06

736.4	2.72	7.31	1.03	0.03	0.02	0.07
806.2	2.17	7.56	1.06	0.03	0.02	0.08
876.3	2.17	7.10	1.13	0.04	0.02	0.08
948.1	3.36	6.44	1.06	0.04	0.02	0.08
977.0		5.08	0.98	0.04	0.01	0.07
1048.6	3.40	6.64	0.98	0.03	0.02	0.07
1072.5		6.68	0.99	0.03	0.02	0.08
1078.2		6.77	0.99	0.03	0.02	0.08
1169.2	2.71	7.00	1.03	0.02	0.02	0.08
1241.1		6.52	0.84	0.02	0.02	0.07
1336.6	2.89	6.42	0.82	0.02	0.02	0.07
1432.8		6.62	0.85	0.02	0.02	0.08
1599.9	2.20	6.54	0.84	0.02	0.02	0.08
1673.0		6.49	0.83	0.02	0.02	0.08
1752.3		6.51	0.87	0.02	0.02	0.08
1827.5		6.55	0.84	0.03	0.02	0.09
1915.8	3.41	6.52	0.85	0.03	0.02	0.09
2010.0	4.24	6.78	0.91	0.05	0.02	0.10

Time (hr)	Mn (mmol/kg)	Formate (mmol/kg)	Acetate (mmol/kg)	Sulfate (mmol/kg)	Oxalate (mmol/kg)	Nitrate (mmol/kg)
0.0	0.01	0.27	21.10	1.61		0.03
99.2	0.01	0.13	24.06	8.61		
256.0	0.02	0.27	23.91	10.12		0.20
394.0	0.02	0.38	21.87	11.51		0.29
421.2	0.03	0.46	18.43	10.69	0.11	0.37
500.8	0.02	0.50	19.99	10.91		0.35
598.2	0.03	0.55	22.32	12.84	0.01	0.45
600.0	0.03	0.47	23.33	12.19	0.01	0.31
736.4	0.03	1.30	21.17	19.37		0.39
806.2	0.03	0.94	22.00	13.19	0.01	0.47
876.3	0.03	0.96	20.89	11.37	0.04	0.44
948.1	0.05	0.76	26.59	12.17	0.08	0.47
977.0	0.04	0.97	19.45	10.90	0.04	0.32
1048.6	0.04	1.55	21.14	10.65	0.07	0.56
1072.5	0.04	1.62	23.09	10.59	0.07	0.45
1078.2	0.05	1.36	22.27	10.70	0.05	0.53
1169.2	0.05	1.60	23.57	11.37	0.07	0.51
1241.1	0.04	1.22	22.70	10.71	0.08	0.76
1336.6	0.04	1.28	23.20	11.08	0.10	0.65
1432.8	0.04	1.49	0.10	12.66	0.09	0.85
1599.9	0.04	1.59	0.17	12.50	0.11	0.72

1673.0	0.05	1.64	0.16	13.38	0.12	1.03
1752.3	0.05	1.77		12.16	0.00	
1827.5	0.05	2.11		11.52	0.17	
1915.8	0.05	1.85		9.98	0.27	
2010.0	0.06	0.27				

Time (hr)	T. Formate (mmol/kg)	T. Acetate (mmol/kg)	T. Sulfate (mmol/kg)	T. Oxalate (mmol/kg)	T. Nitrate (mmol/kg)
0.0	0.52	0.00	1.46	0.00	0.00
99.2	0.39	0.00	2.15	0.00	0.00
256.0	0.87	0.51	10.94	0.00	0.00
394.0	0.91	0.59	9.95	0.00	0.00
421.2	1.32	0.47	11.59	0.00	0.15
500.8	1.28	0.39	9.76	0.00	0.00
598.2	1.95	0.73	12.95	0.00	0.18
600.0	1.69	0.81	11.10	0.01	0.18
736.4	2.46	0.91	12.99	0.03	0.19
806.2	2.47	0.95	11.76	0.08	0.45
876.3	3.04	1.44	11.44	0.07	0.37
948.1	3.48	1.18	13.02	0.18	0.41
977.0	2.32	0.88	7.77	0.13	0.49
1048.6	3.08	0.50	9.82	0.11	0.55
1072.5	3.04	0.23	8.00	0.16	0.80
1078.2	3.62	1.00	8.93	0.13	0.50
1169.2	3.99	1.32	9.66	0.15	0.48
1241.1	3.88	1.55	12.23	0.20	0.83
1336.6	3.59	1.58	10.96	0.18	0.59
1432.8	3.87	0.75	11.87	0.15	0.85
1599.9	4.05	0.97	14.01	0.14	0.70
1673.0	4.59	1.30	30.54	0.13	1.00
1752.3	5.53	1.85	13.31	0.14	
1827.5	5.24	1.93	11.97	0.18	
1915.8	5.04	2.14	13.11	0.18	

Table D-2. Detailed Data of NCCC 2019 Campaign

Time (hr)	PZ (mol/kg)	320 Abs (A)	EDA (mmol/kg)	PZ-one (mmol/kg)	MNPZ (mmol/kg)	Li (mmol/kg)
2120.6	3.11	26.91	25.48	7.29	2.08	3.80
2148.2	2.41		14.59			2.33
2270.6	2.91		9.87		2.58	3.84
2343.5	2.72	26.99	5.61	5.40	6.27	3.90
2345.5	2.93	28.59	5.09	2.15	2.98	3.54
2360.7	2.99	29.95	19.53	7.06	3.23	3.86
2384.8	2.92	35.07	9.87	6.55	2.76	3.58
2408.8	3.57	34.64	14.65	5.86	3.08	3.44
2432.8	3.68	35.88	6.70		3.72	3.76
2453.5	3.25	32.11	11.35	5.14	2.80	2.98
2518.9	2.87	33.72	11.41	2.94	3.40	2.70
2542.8	2.90	35.59	14.09	2.82	4.00	2.66
2551.8	3.02	38.34	11.69	2.46	5.12	2.68
2568.5	3.05	36.67	7.41	2.70	4.11	2.91
2594.7	2.86		7.45	2.04		2.67
2615.8	2.97	37.89	14.60	2.66	4.68	2.84
2737.5	2.98		31.57	7.20	4.63	2.93
2762.5	3.09	43.25	37.62	7.39	4.76	3.12
2786.5	3.05	45.31	108.69	3.35	4.25	3.01
2811.7	3.07	47.83	94.29	6.50	5.13	3.01
2840.5	3.10	49.69	35.70		6.00	2.81
2878.4	3.15		32.46	9.51	4.49	2.09
2903.2	3.31	40.53	34.78	9.12	4.15	2.12
2927.3	3.38	41.65	37.78	9.52	5.67	2.13
2998.4	3.59	41.79	20.43	9.38	5.47	2.48
3024.0	2.98	43.53	49.98	3.99	5.44	3.05
3046.8	2.95	45.06	39.23	7.48	5.98	3.06
3071.6	3.07		39.65	5.92	6.34	3.14
3096.2	2.94	45.32	15.57	4.56	6.51	3.15
3166.1	2.85	46.19	26.96	3.35	5.77	3.04
3206.2	2.70	47.58	10.56	3.43	5.28	2.91
3234.7	2.73	49.3	12.75	1.57	4.87	2.70
3257.0	2.67	48.68	13.48	1.68	5.11	2.67
3281.0	2.62	49.8	11.08	2.29	5.48	2.76
3305.8	2.48	52.25	10.06	1.97	5.46	2.73
3378.6	2.63	53.99	12.49	2.79	5.53	2.13
3402.1	2.78	53.23	11.79	3.02	5.58	2.12

3425.4	2.76	54.65	13.03	2.77	5.74	2.14
3449.8	2.86	54.02	12.29	2.14	5.74	2.15
3474.1	2.83	54.92	16.47	3.11	6.19	2.08
3545.6	2.79	56.01	12.88	2.42	6.72	2.63
3571.3	2.87	58.26	15.84	3.35	6.53	2.31
3594.6	3.00		14.18	2.81	18.61	2.29
3617.8	2.94	27.32	14.28	3.01	10.49	2.09
3642.2	2.89	27.69	14.33		10.25	1.93
3715.1	2.96	29.87	9.65	5.10	11.34	2.55
3738.4	2.79	24.69	9.64	4.88	12.06	2.61
3761.7		24.89	12.06	3.00	10.48	2.38
3788.6	2.80	22.53	10.85	3.72	11.36	2.47
3811.4	2.94	21.91	13.52	3.34	10.81	2.46
3907.0	2.69	21.8	16.46	3.98	11.78	
3930.1	2.82	22.76	7.94	4.32	11.83	1.91
3953.8	2.73	19.77	7.49	4.92	11.02	1.60
3978.6	2.86	18.88	8.54	5.91	11.77	2.00
4050.1	2.79	18.65	9.39	16.24	12.28	2.61
4073.9	2.83	18.09	15.40	16.48	13.03	2.40
4098.2	2.90	17.78	4.48	17.86	12.54	2.48
4146.2	2.77	17.39	9.57	13.93	12.21	1.98
4219.6	2.76	20.94	4.69	7.69	12.07	2.20

Time (hr)	K (mmol/kg)	Fe (mmol/kg)	Cr (mmol/kg)	Ni (mmol/kg)	Mn (mmol/kg)	T. Formate (mmol/kg)
2120.6	0.77	0.11	0.03	0.09	0.08	
2148.2	0.48	0.06	0.02	0.06	0.07	
2270.6	0.56	0.09	0.04	0.09	0.09	6.40
2343.5	0.54	0.09	0.07	0.11	0.08	7.76
2345.5	0.51	0.09	0.07	0.11	0.08	6.30
2360.7	0.56	0.10	0.09	0.13	0.09	6.52
2384.8	0.55	0.13	0.15	0.16	0.08	8.31
2408.8	0.53	0.19	0.17	0.18	0.12	8.53
2432.8	0.58	0.23	0.19	0.20	0.12	
2453.5	0.45	0.21	0.18	0.18	0.11	7.31
2518.9	0.57	0.12	0.20	0.22	0.15	10.49
2542.8	0.49	0.13	0.20	0.22	0.14	12.02
2551.8	0.49	0.13	0.21	0.24	0.14	13.80
2568.5	0.54	0.15	0.23	0.26	0.16	12.80
2594.7	0.52	0.14	0.23	0.26	0.15	11.99
2615.8	0.53	0.16	0.24	0.27	0.16	14.21

2737.5	0.46	0.11	0.17	0.19	0.13	10.63
2762.5	0.48	0.12	0.19	0.21	0.14	13.88
2786.5	0.48	0.14	0.20	0.23	0.14	13.16
2811.7	0.47	0.14	0.20	0.22	0.13	15.72
2840.5	0.44	0.17	0.21	0.23	0.13	14.86
2878.4	0.35	0.08	0.14	0.16	0.08	20.70
2903.2	0.35	0.09	0.14	0.17	0.08	21.65
2927.3	0.35	0.09	0.14	0.17	0.08	22.44
2998.4	0.31	0.09	0.14	0.16	0.08	36.64
3024.0	0.38	0.10	0.16	0.18	0.09	25.00
3046.8	0.37	0.09	0.16	0.19	0.09	28.27
3071.6	0.37	0.09	0.16	0.19	0.09	28.18
3096.2	0.38	0.09	0.16	0.19	0.09	26.87
3166.1	0.36	0.09	0.15	0.18	0.09	23.75
3206.2	0.35	0.09	0.15	0.17	0.09	12.82
3234.7	0.34	0.09	0.15	0.17	0.09	12.34
3257.0	0.33	0.09	0.14	0.17	0.09	14.36
3281.0	0.34	0.09	0.15	0.17	0.09	15.13
3305.8	0.34	0.10	0.15	0.17	0.09	15.03
3378.6	0.35	0.10	0.15	0.17	0.10	11.32
3402.1	0.36	0.10	0.15	0.17	0.09	15.99
3425.4	0.37	0.09	0.14	0.16	0.09	15.57
3449.8	0.37	0.10	0.15	0.17	0.09	15.25
3474.1	0.39	0.10	0.14	0.16	0.09	15.70
3545.6	1.86	0.11	0.13	0.20	0.17	16.14
3571.3	1.53	0.08	0.12	0.18	0.14	18.40
3594.6	1.39	0.08	0.12	0.17	0.14	18.24
3617.8	0.98	0.10	0.14	0.16	0.12	19.35
3642.2	0.87	0.10	0.13	0.15	0.12	19.88
3715.1	1.92	0.18	0.10	0.17	0.17	39.25
3738.4	1.94	0.19	0.10	0.18	0.18	39.99
3761.7	1.85	0.18	0.09	0.16	0.17	43.80
3788.6	1.96	0.15	0.09	0.17	0.18	37.53
3811.4	2.06	0.15	0.09	0.17	0.19	41.27
3907.0						41.65
3930.1	2.10	0.12	0.07	0.16	0.21	36.20
3953.8	1.88	0.09	0.06	0.14	0.17	39.43
3978.6	2.31	0.13	0.07	0.17	0.21	41.38
4050.1	2.35	0.11	0.07	0.20	0.21	30.42
4073.9	2.23	0.10	0.07	0.18	0.20	33.65

4098.2	2.27	0.10	0.06	0.19	0.20	34.27
4146.2	1.92	0.10	0.05	0.16	0.17	31.38
4219.6	2.16	0.13	0.06	0.18	0.20	32.45

Time (hr)	T. Acetate (mmol/kg)	T. Sulfite (mmol/kg)	T. Sulfate (mmol/kg)	T. Oxalate (mmol/kg)	T. Nitrate (mmol/kg)	
2120.6	2.35	0.64	3.17	1.38	0.89	
2270.6	2.24	0.74	2.59	1.45	0.72	
2343.5	3.65	0.77	2.53	2.34	0.74	
2345.5	2.57	0.81	2.57	1.63	0.75	
2360.7	2.51	0.81	2.62	1.50	0.75	
2384.8	3.19	0.77	2.91	1.87	0.86	
2453.5	2.51	0.69	2.21	1.53	0.67	
2518.9	3.09	0.81	2.12	1.72	0.69	
2542.8	3.07	0.81	2.06	1.70	0.67	
2551.8	3.83	0.77	2.20	2.31	0.72	
2568.5	3.38	0.78	2.16	1.84	0.71	
2615.8	3.68	0.83	2.12	1.96	0.69	
2737.5	3.77	0.84	1.95	2.03	0.69	
2762.5	4.15	0.82	2.17	2.12	0.74	
2786.5	4.26	0.82	2.19	2.11	0.75	
2811.7	4.40	0.82	2.18	2.17	0.79	
2840.5	4.49	0.82	2.14	2.31	0.75	
2878.4	3.81	0.83	1.87	1.76	0.67	
2903.2	3.98	0.73	1.85	1.78	0.68	
2927.3	3.97	0.88	1.84	1.79	0.65	
2998.4	4.93	1.09	2.14	2.17	0.75	
3024.0	4.30	0.88	1.85	1.91	0.72	
3046.8	4.40	0.85	1.86	1.95	0.69	
3071.6	4.53	0.88	1.85	2.04	0.72	
3096.2	5.34	0.89	2.39	2.49	0.78	
3166.1	4.60	0.80	1.72	1.90	0.67	
3234.7	7.07	2.94	1.97	4.02	1.06	
3257.0	7.05	3.03	1.74	3.51	0.92	
3281.0	6.62	3.31	1.77	3.64	1.39	
3378.6	8.03	3.45	1.72	3.38	0.88	
3402.1	8.09	3.45	1.76	3.30	0.90	
3425.4	8.88	3.51	1.97	3.58	0.97	
3449.8	7.69	3.66	1.73	3.19	0.90	
3474.1	7.13	3.92	1.69	3.05	0.89	
3545.6	8.95	3.80	1.71	3.40	0.88	
3571.3	8.45	3.76	1.74	3.21	0.91	

3617.8	10.13	3.67	2.02	3.95	1.01
3642.2	8.41	3.80	1.73	3.74	0.93
3715.1	8.86	3.78	1.74	3.63	0.93
3738.4	8.59	3.78	1.77	3.55	1.00
3761.7	9.71	3.80	1.67	3.63	0.94
3788.6	8.73	3.78	1.68	3.80	0.99
3811.4	9.35	2.38	1.68	3.70	0.97
3907.0	9.49	2.54	1.81	4.16	1.08
3930.1	10.41	2.50	1.60	3.63	0.95
3953.8	9.50	2.47	1.66	3.57	1.03
3978.6	10.05	2.49	1.73	3.74	1.06
4050.1	9.65	2.50	1.70	3.72	1.10
4073.9	10.56	2.45	1.66	3.94	1.07

Table D-3. Detailed Data of SRP 2018 Campaign

Time (hr)	PZ (mol/kg)	EDA (mmol/kg)	Li (mmol/kg)	Fe (mmol/kg)	Cr (mmol/kg)	Ni (mmol/kg)
8.5	3.58	3.98	1.1	0.07	0.02	0.04
103.5	3.43	5.66	1.0	0.04	0.02	0.03
126.5	3.40	7.28	1.1	0.04	0.02	0.03
150.5	3.20	10.08	1.0	0.04	0.02	0.03
164.5	3.48	11.25	32.1	0.04	0.01	0.03
199.0	3.18	12.71	28.0	0.05	0.01	0.03
221.3	3.26	15.43	30.0	0.04	0.01	0.03
264.0	3.19	17.12	30.7	0.03	0.01	0.03

Time (hr)	Mn (mmol/kg)	Fe (mmol/kg)	Cr (mmol/kg)	Ni (mmol/kg)	Mn (mmol/kg))	Formate (mmol/kg)
8.5	0.02	0.11	0.03	0.09	0.08	2.62
103.5	0.01	0.06	0.02	0.06	0.07	
126.5	0.01	0.09	0.04	0.09	0.09	
150.5	0.01	0.09	0.07	0.11	0.08	
164.5	0.01	0.09	0.07	0.11	0.08	
199.0	0.01	0.10	0.09	0.13	0.09	
221.3	0.01	0.13	0.15	0.16	0.08	
264.0	0.01	0.19	0.17	0.18	0.12	2.06

Time (hr)	Acetate (mmol/kg)	Chloride (mmol/kg)	Sulfate (mmol/kg)	Oxalate (mmol/kg)	T. Formate (mmol/kg)	T. Acetate (mmol/kg)
8.5	0.52	0.14	1.73	0.12	5.12	0.60
264.0	1.21	0.13	6.32	0.17	3.85	1.00

Time (hr)	T. Chloride (mmol/kg)	T. Sulfate (mmol/kg)	T. Oxalate (mmol/kg)
8.5	0.11	1.62	0.29
264.0	0.11	8.04	0.34

Table D-4. Detailed Data of SRP 2022 Campaign Lean Samples

Time (hr)	PZ (mol/kg)	320 Abs (A)	EDA (mmol/kg)	PZ-one (mmol/kg)	NH_4^+ (mmol/kg)	FPZ (mmol/kg)
264	2.89	1.08	7.55	89.30	0.85	2.84
264	3.63		14.56	10.54	2.25	1.29
264	4.05		16.55	31.78	1.96	1.73
264	4.09		10.98	95.36	1.02	2.93
264	3.76	1.56	10.68	65.51	0.67	1.92
264	3.51		15.28	22.11	1.42	0.91
264	3.59		16.03	32.03	1.67	1.31
264	3.65		15.23	34.07	1.78	1.39
265	3.54	1.52	10.19	30.52	0.87	1.67
272	3.68		15.46	22.38	1.59	1.37
289	3.52	1.54	10.86	57.08	1.08	1.95
296	3.39		14.80	32.61	1.39	1.33
313	3.40		15.39	30.83	1.85	1.33
319	3.46	1.62	15.30	89.30	0.71	2.84
337	3.44		18.86	95.36	0.68	2.93
337	3.42		13.31	65.51	0.53	1.92
340	3.50	1.67	14.87	30.52	0.58	1.67
345	3.63		16.76	30.87	1.24	1.34
362	3.42	1.53	14.10	57.08	0.54	1.95
369	3.55		16.07	31.68	1.80	1.30
384	3.40	1.68	14.16	37.72	0.40	1.54
388	3.20	1.26	13.67	36.40	0.39	1.49
391	3.53		17.59	32.95	1.72	1.80
409	3.41	1.86	15.22	36.64	0.26	1.50
416	3.40		20.26	21.30	1.06	2.18
430	3.10	1.97	19.80	37.84	0.34	1.55
434	3.62		18.67	43.89	1.87	1.80
450	3.45	1.99	23.25	36.10	0.43	2.22
458	3.51		18.94	31.18	1.33	1.70
474	3.63	2.04	23.03	31.51	0.45	1.93
482	3.57		19.17	44.52	2.37	1.82
514	3.21	2.07	22.16	36.89	0.52	1.76
520	3.37	2.12	22.66	30.38	0.22	2.18
537	3.27	2.20	22.88	48.47	0.49	1.98
545	3.47		20.28	53.30	1.97	2.18
561	3.39	2.29	25.34	47.76	0.34	2.28
569	3.16		20.49	45.27	1.42	1.85

585	3.30	2.43	25.37	58.58	0.52	2.10
594	3.55		23.08	54.89	1.87	2.25
609	3.30	2.50	26.44	62.15	0.55	2.23
618	3.12	2.55	26.05	58.34	0.08	2.87
634	3.23	2.62	26.03	63.72	0.09	2.61
642	3.53		24.92	66.07	1.10	2.70
658	3.40	2.96	26.01	67.17	0.00	2.75
670	3.65	2.97	24.80	72.85	1.55	2.98
686	3.63	3.03	24.86	62.85	2.23	3.22
694	3.70	3.17	26.27	65.60	2.43	2.69
710	3.44	3.21	25.59	75.16	0.92	3.08
718	3.50	3.37	23.12	56.33	0.27	2.92
735	3.6	3.32	31.57	88.82	0.32	3.18
744	3.48	3.44	30.78	84.22	0.45	3.45
760	3.44	3.57	31.38	83.59	0.45	2.99
768	3.53	3.84	32.34	91.99	0.44	3.77
784	3.31	3.63	29.51	84.21	0.45	3.02
791	3.57	3.84	32.43	86.36	0.61	3.53
808	3.54	3.79	32.16	94.47	0.45	3.44
816	3.56	3.83	31.72	89.25	0.63	3.65
832	3.42	3.92	30.18	90.95	0.55	3.19
841	3.51	4.05	31.31	99.11	0.47	3.16
857	3.53	4.06	32.94	104.25	0.66	3.79
865	3.54	4.12	32.65	99.15	0.63	3.61
881	3.61	4.45	33.39	103.51	0.65	3.77
889	3.71	4.50	33.56	103.32	0.65	3.76
905	3.45	4.86	30.02	86.74	0.70	3.55
913	3.33	4.67	30.12	93.36	0.22	3.18
929	3.27	4.76	30.28	90.87	0.22	3.10
938	3.38	4.80	31.23	77.29	0.14	3.10
954	3.36	4.08	30.33	82.24	0.15	2.75
962	3.37	4.39	30.23	80.70	0.14	2.70
978	3.35	3.97	29.95	81.23	0.14	2.48
986	3.38	4.33	30.04	93.55	0.28	2.45
1002	3.36	4.01	29.88	93.80	0.28	2.46
1010	3.24	3.99	29.08	92.03		2.41
1026	3.38	4.14	28.73	77.22		2.36

Time (hr)	AEP (mmol/kg)	HEP (mmol/kg)	MPZ (mmol/kg)	Li (mmol/kg)	K (mmol/kg))	Fe (mmol/kg)
264	4.71	1.60		5.12	0.35	0.012
264	4.45	3.05	0.18	4.00	0.37	0.007

264	5.01	3.41	0.36	3.85	0.38	0.008
264	6.92	4.22		8.39	0.54	0.016
264	3.26	4.82		8.02	0.58	0.015
264	5.05	4.98	0.19	4.04	0.41	0.012
264	5.35	5.15	0.37	4.02	0.36	0.011
264	5.08	5.30	0.39	4.71	0.41	0.011
265	4.62	4.25		7.56	0.54	0.014
272	4.30	5.04	0.57	6.44	0.38	0.009
289	5.42	4.28		11.75	0.56	0.013
296	5.49	4.72	0.37	8.40	0.40	0.007
313	5.26	4.70	0.56	7.16	0.39	0.006
319	4.71	5.33		8.42	0.39	0.011
337	6.92	5.22		8.90	0.42	0.008
337	3.26	4.76		9.71	0.44	0.010
340	4.62	5.12		8.65	0.42	0.009
345	4.30	4.90	0.37	7.88	0.41	0.007
362	5.42	4.92		8.66	0.42	0.009
369	5.23	4.59	0.36	7.72	0.36	0.008
384	5.68	4.40		8.52	0.41	0.008
388	4.61	4.39		7.81	0.41	0.015
391	4.60	5.12	0.56	7.49	0.36	0.012
409	5.71	5.01		8.92	0.44	0.010
416	5.96	4.28	0.18	7.90	0.38	0.009
430	7.49	5.32	0.57	8.53	0.42	0.009
434	7.59	5.12	0.56	8.39	0.33	0.009
450	8.70	5.81	0.62	9.57	0.49	0.011
458	8.96	5.35	0.53	8.53	0.46	0.011
474	8.98	6.72	0.54	9.50	0.49	0.011
482	8.76	5.01	0.57	8.39	0.37	0.009
514	9.41	5.34	0.74	8.39	0.41	0.008
520	8.18	5.50	0.78	8.49	0.46	0.012
537	8.99	5.46	0.71	8.13	0.47	0.008
545	8.97	4.97	0.73	7.43	0.37	0.009
561	9.58	5.63	0.68	7.99	0.44	0.009
569	9.21	4.66	0.62	8.15	0.46	0.009
585	10.59	5.42	1.00	7.77	0.43	0.008
594	10.26	5.30	0.94	8.17	0.45	0.009
609	10.34	5.50	0.93	8.31	0.47	0.009
618	11.58	5.07	1.20	8.99	0.47	0.013
634	13.39	5.64	1.09	8.95	0.47	0.011

642	11.91	5.31	0.94	8.24	0.46	0.011
658	12.40	4.68		7.73	0.45	0.011
670	12.23	5.27	0.83	8.20	0.50	0.016
686	12.80	5.05	0.81	7.74	0.47	0.014
694	12.59	5.27	0.90	8.11	0.50	0.013
710	13.09	4.84	0.92	7.87	0.46	0.012
718	9.91	4.68	0.00	8.18	0.47	0.012
735	13.72	6.07	0.95	8.13	0.47	0.012
744	14.23	5.76	0.90	8.28	0.47	0.015
760	14.89	5.55	0.89	8.44	0.48	0.014
768	16.08	5.92	1.05	8.98	0.48	0.016
784	13.89	5.42	0.90	8.10	0.46	0.021
791	15.16	6.08	0.92	8.64	0.50	0.022
808	15.74	6.08	0.72	8.46	0.49	0.023
816	13.90	5.92	0.96	8.47	0.49	0.023
832	12.49	5.43	0.89	7.97	0.47	0.019
841	15.70	5.84	0.94	7.90	0.48	0.018
857	17.25	5.77	1.19	7.97	0.48	0.017
865	17.10	6.02	0.94	8.29	0.49	0.018
881	17.61	6.10	0.98	8.19	0.49	0.017
889	16.00	6.09	0.98	8.32	0.49	0.016
905	11.65	5.38	0.64	8.03	0.47	0.017
913	17.25	4.32		8.08	0.47	0.015
929	16.47	3.58		7.95	0.46	0.014
938	13.21	4.49	1.15	7.97	0.47	0.015
954	12.11	4.28	1.05	7.90	0.48	0.014
962	13.27	4.36	1.03	7.97	0.48	0.013
978	13.14	4.39	1.04	8.29	0.49	0.014
986	13.50	4.50	1.03	8.19	0.49	0.013
1002	13.74	4.19	1.03	8.32	0.49	0.013
1010	11.31	4.11	1.01	8.03	0.47	0.013
1026	6.60	4.49	0.99	8.08	0.47	0.011

Time (hr)	Cr (mmol/kg)	Ni (mmol/kg)	Mn (mmol/kg)	Formate (mmol/kg)	Acetate (mmol/kg)	Propionate (mmol/kg)
264	0.007	0.024	0.004	1.00	0.59	0.11
264	0.004	0.022	0.003	1.38	0.18	
264	0.004	0.022	0.003	1.48	0.14	0.04
264	0.008	0.034	0.005	1.06	0.44	0.10
264	0.008	0.033	0.005	1.03	0.42	0.06
264	0.004	0.023	0.002	1.60	0.19	
264	0.004	0.024	0.002	1.54	0.17	

264	0.005	0.025	0.002	1.57	0.20	0.04
265	0.008	0.032	0.003	1.05	0.48	0.07
272	0.005	0.024	0.002	1.52	0.20	0.05
289	0.008	0.032	0.003	1.10	0.39	0.11
296	0.005	0.026	0.001	1.53	0.26	0.05
313	0.005	0.023	0.001	1.61	0.26	0.07
319	0.009	0.027	0.007	1.28	0.37	0.11
337	0.006	0.025	0.002	1.51	0.42	0.10
337	0.006	0.027	0.005	1.16	0.27	0.06
340	0.005	0.025	0.002	1.32	0.46	0.07
345	0.005	0.025	0.002	1.64	0.31	0.10
362	0.005	0.026	0.002	1.18	0.44	0.11
369	0.005	0.025	0.002	1.64	0.39	0.09
384	0.005	0.025	0.002	1.18	0.42	0.11
388	0.005	0.024	0.003	1.19	0.62	0.05
391	0.005	0.027	0.003	1.69	2.56	0.12
409	0.005	0.028	0.003	1.18	0.79	0.05
416	0.005	0.028	0.003	1.72	0.72	0.14
430	0.005	0.027	0.003	1.52	1.78	0.12
434	0.004	0.022	0.002	1.61	2.43	0.14
450	0.005	0.031	0.003	1.56	1.88	0.14
458	0.005	0.029	0.003	1.68	2.54	0.17
474	0.005	0.031	0.003	1.47	1.33	0.15
482	0.005	0.029	0.003	1.76	2.66	0.19
514	0.004	0.022	0.002	1.59	2.37	0.17
520	0.005	0.029	0.002	1.62	2.45	0.21
537	0.005	0.028	0.002	1.30	1.73	0.16
545	0.006	0.029	0.003	1.68	2.54	0.23
561	0.005	0.030	0.002	1.31	1.88	0.23
569	0.006	0.031	0.002	1.72	2.61	0.22
585	0.005	0.028	0.002	1.34	1.95	0.27
594	0.006	0.031	0.002	1.78	2.69	0.26
609	0.006	0.030	0.002	1.83	2.77	0.27
618	0.006	0.031	0.002	1.51	3.50	0.25
634	0.006	0.031	0.002		2.14	0.18
642	0.006	0.032	0.002	1.85	2.52	0.30
658	0.007	0.035	0.003			0.44
670	0.008	0.038	0.003	2.03	2.76	0.33
686	0.007	0.034	0.003	1.63	2.46	0.31
694	0.007	0.036	0.003	1.66	2.52	0.37

710	0.007	0.035	0.002	1.73	2.62	0.37
718	0.007	0.036	0.002	2.15	3.69	0.44
735	0.007	0.036	0.002	2.15	3.76	0.42
744	0.007	0.036	0.002	2.22	3.95	0.39
760	0.007	0.037	0.002	2.17	4.05	0.40
768	0.007	0.037	0.002	2.17	4.26	0.34
784	0.007	0.034	0.002	2.10	3.93	0.43
791	0.007	0.036	0.003	2.31	4.53	0.47
808	0.007	0.036	0.002	2.22	4.22	0.39
816	0.007	0.036	0.002	2.20	4.22	0.50
832	0.008	0.036	0.003	1.80	3.55	0.41
841	0.007	0.033	0.002	2.00	4.04	0.48
857	0.007	0.034	0.002	2.07	4.41	0.56
865	0.008	0.037	0.002	2.11	4.41	0.58
881	0.008	0.037	0.002	2.13	4.42	0.54
889	0.008	0.038	0.002	2.09	4.39	0.55
905	0.008	0.037	0.002	2.04	4.08	0.51
913	0.008	0.037	0.002	2.18	4.31	0.57
929	0.008	0.038	0.002	2.20	4.47	0.62
938	0.008	0.036	0.003	2.33	5.00	0.64
954	0.007	0.033	0.002	2.24	5.14	0.66
962	0.007	0.034	0.002	2.27	5.14	0.69
978	0.008	0.037	0.002	2.24	5.28	0.69
986	0.008	0.037	0.002	2.25	5.32	0.72
1002	0.008	0.038	0.002	2.25	5.43	0.70
1010	0.008	0.037	0.002	2.23	5.42	0.82
1026	0.008	0.037	0.002	2.35	5.31	0.81

Time (hr)	Chloride (mmol/kg)	Sulfate (mmol/kg)	Oxalate (mmol/kg)	Nitrate (mmol/kg)	Glycolate* (mmol/kg)	T. Formate (mmol/kg)
264	0.07	3.64	0.09	0.06		2.03
264	0.23	4.91		0.05	5.50	2.92
264	0.23	5.54		0.07	6.09	3.27
264	0.10	5.49	0.14	0.08		3.12
264	0.09	5.30	0.13	0.09		3.00
264	0.24	4.67		0.07	4.37	3.01
264	0.25	4.83		0.07	4.91	3.25
264	0.28	5.02		0.09	4.74	3.14
265	0.09	4.75	0.11	0.07		2.78
272	0.26	4.73		0.07	4.60	3.03
289	0.10	4.91	0.13	0.10		2.94
296	0.25	4.49		0.07	4.24	3.07

313	0.24	4.51		0.07	4.11	3.11
319	0.08	4.79		0.29		2.70
337	0.13	4.96		0.25		2.83
337	0.11	3.22		0.18		2.30
340	0.12	3.50		0.17		2.67
345	0.25	5.13		0.08	4.42	3.43
362	0.12	2.68		0.14		2.69
369	0.25	4.95		0.07	4.20	3.42
384	0.11	5.62		0.11		2.62
388	0.12	5.08		0.10		2.53
391	0.29	4.94		0.08	4.22	3.38
409	0.12	5.61		0.11		2.85
416	0.26	5.00		0.08	4.05	3.54
430	0.12	5.04	0.17	0.07	6.69	3.50
434	0.29	5.19		0.08	4.60	3.75
450	0.12	5.40	0.20	0.09	7.08	3.83
458	0.29	5.33		0.07	4.56	3.76
474	0.13	5.23	0.17	0.21	5.37	3.79
482	0.31	5.24		0.07	4.28	3.71
514	0.13	4.73	0.17	0.07	6.18	3.92
520		4.83		0.09	3.94	3.99
537	0.14	4.69	0.16	0.08	4.77	4.12
545	0.32	4.99		0.10	4.00	3.83
561	0.15	4.62	0.17	0.10	4.60	4.25
569	0.30	4.99		0.09	4.12	4.08
585	0.14	4.58	0.15	0.07	4.56	4.50
594	0.33	4.92		0.12	3.85	4.21
609	0.35	4.82		0.10	3.68	4.62
618	0.16	4.48	0.14	0.09	5.84	4.61
634	0.18	2.61		0.05	3.30	4.81
642	0.35	4.89		0.12	3.68	4.46
658	0.31			0.19		5.00
670	0.38	5.35		0.13	4.03	4.82
686	0.44	4.71		0.17	2.64	4.56
694	0.43	5.00		0.17	3.23	4.86
710	0.39	4.98		0.17	3.43	4.85
718	0.20	4.80	0.14	0.14	4.43	5.31
735	0.22	4.72	0.11	0.16	4.60	5.37
744	0.32	4.61	0.11	0.17	4.43	5.33
760	0.20	4.59	0.09	0.16	4.39	5.53

768	0.23	4.76	0.10	0.16	4.50	5.72
784	0.21	4.22	0.12	0.14	3.71	5.30
791	3.64	4.78	0.10	0.19	4.26	5.81
808	1.96	4.48	0.13	0.16	3.98	5.68
816	2.51	4.60	0.13	0.17	4.00	5.81
832	2.98	3.95	0.11	0.16	2.76	5.57
841	2.62	4.35	0.12	0.15	3.70	5.76
857	2.70	4.33	0.12	0.17	3.74	5.92
865	2.64	4.53	0.12	0.18	3.83	6.15
881	2.67	4.61	0.13	0.15	3.83	6.24
889	2.67	4.56	0.13	0.18	3.92	6.06
905	2.70	4.33	0.12	0.15	3.53	5.79
913	0.25	4.38	0.12	0.17	3.61	5.91
929	0.27	4.39	0.12	0.16	3.69	5.94
938	0.37	4.62	0.10	0.19	4.22	6.25
954	0.30	4.54	0.08	0.19	4.00	6.23
962	0.30	4.49	0.07	0.19	3.97	6.35
978	0.28	4.44	0.06	0.18	4.11	6.36
986	0.33	4.50	0.06	0.18	4.10	6.58
1002	0.33	4.45	0.04	0.19	4.07	6.20
1010	0.32	4.05	0.03	0.17	3.67	6.00
1026	0.36	4.82	0.03	0.17	3.68	6.78

Time (hr)	T. Acetate (mmol/kg)	T. Propionate (mmol/kg)	T. Chloride (mmol/kg)	T. Sulfate (mmol/kg)	T. Oxalate (mmol/kg)	T. Nitrate (mmol/kg)
264		0.07	0.10	3.54	0.15	0.10
264	0.09	0.23	0.11	4.71	0.20	0.05
264	0.10	0.23	0.11	5.14	0.22	0.07
264		0.10	0.11	5.34	0.22	0.11
264		0.09	0.11	5.19	0.28	0.12
264	0.02	0.24	0.09	4.36	0.20	0.05
264	0.03	0.25	0.12	4.62	0.21	0.07
264	0.13	0.28	0.12	4.78	0.20	0.06
265		0.09	0.11	4.60	0.24	0.11
272	0.13	0.26	0.12	4.48	0.20	0.06
289		0.10	0.12	4.74	0.25	0.10
296	0.04	0.25	0.12	4.40	0.19	0.05
313	0.15	0.24	0.12	4.35	0.19	0.05
319	0.16	0.08	0.15	5.20	0.81	0.11
337	0.05	0.13	0.05	5.90	1.03	0.12
337	0.08	0.11	0.04	3.89	1.01	0.13
340	0.19	0.12	0.05	4.15	0.97	0.15

345	0.17	0.25		4.57	0.19	0.07
362	0.25	0.12	0.08	3.99		0.15
369	0.23	0.25	0.11	4.96	0.18	0.07
384	0.10	0.11	0.06	3.52	0.55	0.12
388	0.11	0.12	0.14	3.27	0.38	0.13
391	0.49	0.29	0.15	4.86	0.20	0.05
409	0.51	0.12	0.12	3.59	0.25	0.10
416	0.56	0.26	0.16	5.00	0.21	0.06
430	0.58	0.12	0.18	5.01	0.15	0.06
434	0.59	0.29	0.18	5.22	0.21	0.06
450	0.99	0.12	0.21	5.63	0.19	0.04
458	0.84	0.29	0.15	5.33	0.22	0.08
474	0.61	0.13	0.19	5.61	0.16	0.07
482	1.04	0.31	0.15	5.14	0.19	0.06
514	1.13	0.13	0.24	5.57	0.26	0.07
520	1.12		0.26	5.53	0.24	0.08
537	1.26	0.14	0.28	5.56	0.24	0.10
545	1.31	0.32	0.23	4.98	0.20	0.06
561	1.50	0.15	0.27	5.38	0.23	0.08
569	1.66	0.30	0.20	4.68	0.21	0.09
585		0.14	0.29	5.50	0.25	0.10
594	1.80	0.33	0.21	4.70	0.21	0.09
609	2.07	0.35	0.31	5.37	0.22	0.09
618	2.26	0.16	0.23	4.73	0.20	0.12
634	2.23	0.18	0.27	4.79	0.20	0.10
642	2.67	0.35	0.22	4.61	0.21	0.07
658	2.76	0.31	0.28	4.57	0.19	0.07
670	2.85	0.38	0.22	4.95	0.24	0.11
686	3.67	0.44	0.20	4.61	0.19	0.11
694	3.29	0.43	0.27	4.81	0.23	0.13
710	3.07	0.39	0.22	4.74	0.22	0.13
718	4.30	0.20	0.27	4.81	0.24	0.15
735	4.16	0.22	0.32	4.68	0.24	0.13
744	4.18	0.32	0.43	4.58	0.24	0.15
760	4.44	0.20	0.41	4.65	0.25	0.14
768	4.59	0.23	0.32	4.78	0.25	0.16
784	4.21	0.21	0.32	4.34	0.23	0.15
791	4.71	3.64	0.35	4.74	0.24	0.14
808	4.34	1.96	0.33	4.55	0.23	0.13
816	4.40	2.51	0.36	4.57	0.23	0.13

832	4.26	2.98	0.37	4.35	0.23	0.14
841	4.44	2.62	0.38	4.47	0.23	0.15
857	4.66	2.70	0.38	4.30	0.23	0.15
865	4.70	2.64	0.40	4.53	0.24	0.15
881	4.76	2.67	0.40	4.60	0.24	0.16
889	4.65	2.67	0.37	4.55	0.23	0.15
905	5.46	2.70	0.38	4.35	0.23	0.16
913	5.37	0.25	0.39	4.30	0.23	0.18
929	5.51	0.27	0.25	4.21	0.21	0.17
938	5.28	0.37	0.41	4.16	0.21	0.15
954	5.39	0.30	0.44	4.30	0.20	0.15
962	5.41	0.30	0.43	4.24	0.24	0.14
978	5.62	0.28	0.46	4.31	0.24	0.13
986	5.71	0.33	0.45	4.29	0.22	0.15
1002	5.13	0.33	0.05	4.24	0.24	0.14
1010	5.20	0.32	0.41	3.85	0.18	0.14
1026	5.41	0.36	0.51	4.64	0.16	0.14

*The glycolate peaks disappeared after treating the samples with NaOH. Therefore, the glycolate peak may represent an amide eluting at the same time as glycolate. The concentration is reported with the glycolate calibration curve.

Table D-5. Detailed Data of SRP 2022 Campaign Rich Samples

Time (hr)	EDA (mmol/kg)	PZ-one (mmol/kg)	NH_4^+ (mmol/kg)	FPZ (mmol/kg)	AEP (mmol/kg)	HEP (mmol/kg)
264	9.11	81.69	3.70	7.10	0.00	1.92
264	17.19	21.39	3.65	7.00	0.00	2.06
264	15.85	21.11	2.10	3.46	0.00	3.22
264	15.94	71.52	1.22	3.08	0.00	2.77
264	17.88	30.09	1.57	3.70	0.00	5.48
264	17.03	42.00	1.64	3.01	0.00	4.73
264	17.62	39.55	2.25	3.24	0.00	5.25
264	17.44	43.01	1.22	3.52	0.00	5.19
265	16.53	39.31	1.40	3.62	0.00	4.90
272	17.69	33.55	1.75	3.66	0.00	4.86
289	12.03	62.36	1.84	5.30	0.00	4.51
296	17.87	32.25	1.38	3.52	0.00	5.01
313	17.40	42.92	1.83	3.51	0.00	4.83
319	18.69	84.45	1.90	3.64	0.00	5.00
337	18.20	40.86	1.45	3.34	0.00	4.93
340	18.32	43.05	1.53	3.52	0.00	5.19
345	19.41	43.56	1.55	3.57	0.00	5.25
362	18.32	45.19	1.77	3.70	0.00	5.27
369	19.74	45.32	2.26	4.17	0.00	4.92
384	19.66	35.07	2.49	3.83	0.00	5.08
388	14.49	42.57	2.88	1.74	3.93	4.79
391	14.89	36.57	2.77	2.00	3.99	5.49
409	16.19	42.55	3.03	2.18	6.29	5.47
416	14.08	34.02	3.23	1.86	2.87	5.29
430	16.31	44.02	2.03	2.25	4.88	5.49
434	17.28	36.33	2.58	2.23	6.43	5.55
458	17.17	41.32	2.79	2.11	4.25	5.32
474	19.51	40.59	1.15	2.49	9.00	6.04
482	17.00	41.13	0.87	2.09	6.16	5.43
514	16.61	47.41	1.52	2.43	6.76	5.34
520	17.18	42.31	1.19	2.57	5.63	5.55
537	17.92	43.64	1.24	2.23	5.88	5.44
545	18.80	44.18	0.94	2.26	5.60	5.51
561	18.73	49.71	0.99	2.44	6.20	5.28
569	19.71	53.50	1.07	2.63	6.89	5.33
585	20.18	51.94	1.18	2.55	7.46	5.35
594	20.36	50.40	0.86	2.47	7.97	5.34

609	20.97	53.98	1.38	2.65	7.30	5.38
618	21.46	63.04	1.34	2.58	8.54	5.41
634	21.86	56.27	1.28	2.76	7.51	5.43
642	22.07	64.20	1.07	2.63	6.28	5.16
658	18.64	50.04	1.28	1.64	6.66	4.35
670	21.70	46.12	1.31	1.89	7.43	5.01
686	19.78	54.28	1.54	1.78	8.60	4.71
694	20.12	45.16	1.44	1.85	8.23	4.72
710	21.63	53.48	1.06	2.19	8.25	4.82
718	21.83	53.61	1.09	2.23	8.17	4.91
744	21.84	54.54	1.09	2.23	8.98	4.74
760	22.61	54.27	1.39	2.22	9.05	4.71
768	24.90	69.08	1.80	2.36	9.73	5.37
791	22.74	64.88	1.23	2.21	9.36	4.87
816	23.77	62.48	1.33	2.13	7.92	4.86
832	21.31	54.86	1.25	2.25	10.43	4.59
857	22.77	65.61	1.24	2.24	11.09	4.57
881	23.13	66.64	2.21	2.27	11.61	4.82
889	24.06	65.55	0.93	2.68	12.00	4.74
913	24.30	77.26	1.10	2.71	11.54	5.15
938	22.19	69.03	1.47	2.35	12.03	4.81
962	22.76	73.99	1.35	2.60	10.84	4.93
978	22.31	72.01	1.46	2.53	9.60	5.13
1002	22.87	76.26	1.55	2.68	9.65	5.08
1010	24.06	65.55	0.93	2.68	11.00	4.74

Time (hr)	MPZ (mmol/kg)	Li (mmol/kg)	K (mmol/kg))	Fe (mmol/kg)	Cr (mmol/kg)	Ni (mmol/kg)
264	0.19	4.10	0.23	0.006	0.005	0.028
264	0.00	4.37	0.25	0.007	0.005	0.029
264	0.18	5.03	0.29	0.008	0.006	0.033
264		4.40	0.26	0.008	0.005	0.035
264	0.52	4.99	0.35	0.009	0.006	0.038
264	0.18	4.80	0.33	0.012	0.006	0.037
264	0.51	4.98	0.34	0.011	0.006	0.038
264	0.55	1.01	0.10	0.003	0.003	0.022
265	0.50	5.20	0.37	0.008	0.006	0.039
272	0.38	8.37	0.40	0.008	0.005	0.038
289	0.37	8.31	0.39	0.007	0.005	0.038
296	0.55	8.30	0.39	0.006	0.005	0.038
313	0.37	8.13	0.38	0.006	0.005	0.038
319	0.38	8.64	0.40	0.006	0.006	0.039

337	0.35	8.65	0.40	0.006	0.006	0.039
340	0.37	8.70	0.40	0.007	0.006	0.040
345	0.37	9.16	0.42	0.008	0.006	0.041
362	0.58	8.96	0.41	0.008	0.006	0.041
369	0.39	8.86	0.40	0.007	0.006	0.041
384	0.60	0.05	0.36	0.009	0.003	0.041
388	0.55					
391	0.63					
409	0.73		0.41	0.008	0.003	0.049
416	0.58	8.52	0.39	0.009	0.005	0.038
430	0.75	9.16	0.41	0.012	0.006	0.041
434	0.62	9.34	0.42	0.012	0.005	0.042
458	0.88	9.27	0.42	0.011	0.006	0.043
474	0.70	9.85	0.45	0.009	0.006	0.044
482	0.53	9.54	0.42	0.012	0.005	0.038
514	0.81	9.31	0.41	0.009	0.005	0.038
520	0.72	9.79	0.43	0.016	0.005	0.040
537	0.75	9.83	0.43	0.009	0.005	0.040
545	0.95	9.73	0.43	0.009	0.005	0.050
561	0.85	9.86	0.43	0.008	0.005	0.040
569	0.73	10.00	0.44	0.009	0.005	0.043
585	0.89	10.06	0.45	0.011	0.006	0.042
594	1.03	10.28	0.44	0.009	0.006	0.042
609	1.11	10.24	0.45	0.010	0.006	0.043
618	1.08	10.33	0.45	0.013	0.007	0.043
634	0.96	10.22	0.45	0.011	0.007	0.042
642	1.10	10.25	0.45	0.010	0.007	0.048
658	1.03	10.24	0.45	0.011	0.007	0.047
670	0.99	10.92	0.48	0.016	0.007	0.054
686	0.93	10.46	0.46	0.015	0.007	0.049
694	0.97	10.81	0.47	0.013	0.007	0.054
710	1.10	10.82	0.48	0.014	0.007	0.054
718	0.93	10.95	0.48	0.013	0.007	0.054
744	0.93	11.14	0.49	0.016	0.007	0.055
760	0.93	11.02	0.49	0.014	0.007	0.055
768	1.18					
791	0.93	11.12	0.49	0.022	0.008	0.050
816	1.07	10.83	0.49	0.023	0.008	0.049
832	0.94	10.99	0.49	0.019	0.008	0.051
857	1.12	10.86	0.47	0.017	0.008	0.051

881	1.14	11.17	0.50	0.019	0.009	0.052
889	1.12	10.68	0.48	0.016	0.009	0.057
913	1.13	11.00	0.51	0.017	0.010	0.057
938	1.18	10.67	0.48	0.015	0.009	0.049
962	1.27	10.86	0.48	0.015	0.008	0.047
978	1.23	11.17	0.50	0.014	0.009	0.049
1002	1.31	11.46	0.52	0.014	0.009	0.050
1010	1.12	11.08	0.50	0.013	0.009	0.049

Time (hr)	Mn (mmol/kg)	Formate (mmol/kg)	Acetate (mmol/kg)	Propionate (mmol/kg)	Chloride (mmol/kg)	Sulfate (mmol/kg)
264	0.002	0.97	0.13	0.13	0.08	3.79
264	0.003	0.98	0.12	0.12	0.08	3.74
264	0.003	0.95	0.16	0.16	0.09	3.81
264	0.002	1.02	0.10	0.10	0.06	3.13
264	0.003	0.88	0.21	0.21	0.10	4.80
264	0.003	0.87	0.20	0.20	0.09	4.43
264	0.002	0.88	0.21	0.21	0.10	4.41
264	0.001	0.90	0.21	0.21	0.10	4.44
265	0.002	0.89	0.22	0.22	0.09	4.37
272	0.002	0.92	0.24	0.24	0.09	4.43
289	0.001	0.93	0.27	0.27	0.09	4.38
296	0.001	0.94	0.26	0.26	0.09	4.40
313	0.001	0.94	0.26	0.26	0.11	4.25
319	0.001	0.77	0.28	0.28	0.12	4.48
337	0.006	0.97	0.31	0.31	0.10	4.46
340	0.002	0.99	0.32	0.32	0.10	4.56
345	0.002	1.01	1.53	1.53	0.11	4.77
362	0.002	1.30	1.52	1.52	0.26	4.52
369	0.002	1.02	1.54	1.54	0.52	4.43
384	0.003	1.02	0.49	0.49	0.18	4.47
388		1.00	1.51	1.51	0.14	4.25
391		1.01	0.62	0.62	0.15	3.65
409	0.002	1.03	0.66	0.66	0.14	3.89
416	0.002	1.01	0.37	0.37	0.11	3.76
430	0.003	1.05	0.75	0.75	0.12	3.95
434	0.003	1.05	0.77	0.77	0.12	4.15
458	0.003	1.08	1.03	1.03	0.13	4.22
474	0.003	1.13	1.22	1.22	0.13	4.49
482	0.003	1.12	1.18	1.18	0.12	4.13
514	0.003	1.13	1.39	1.39	0.15	3.89
520	0.003	1.22	1.52	1.52	0.14	4.05

537	0.002	1.25	1.45	1.45	0.21	4.02
545	0.002	1.27	1.62	1.62	0.16	4.04
561	0.002	1.27	1.69	1.69	0.16	3.92
569	0.002	1.30	1.75	1.75	0.16	4.00
585	0.002	1.34	1.82	1.82	0.16	3.98
594	0.002	1.35	1.83	1.83	0.17	3.99
609	0.003	1.42	2.07	2.07	0.17	3.95
618	0.003	1.38	2.41	2.41	0.18	3.88
634	0.003	1.40	2.48	2.48	0.19	3.87
642	0.002	1.53	2.01	2.01	0.20	4.36
658	0.002	1.58	2.08	2.08	0.29	4.31
670	0.003	1.62	2.15	2.15	0.28	4.65
686	0.003	1.46	2.22	2.22	0.23	4.44
694	0.002	1.49	2.26	2.26	0.29	4.53
710	0.003	1.54	2.33	2.33	0.30	4.56
718	0.002	1.71	2.93	2.93	0.13	5.23
744	0.002	1.75	3.05	3.05	0.12	4.36
760	0.003	1.84	3.25	3.25	0.14	4.85
768		1.82	3.13	3.13	0.11	4.11
791	0.003	1.80	3.20	3.20	0.12	4.37
816	0.002	1.46	3.27	3.27	0.14	3.75
832	0.003	1.64	3.49	3.49	0.14	4.21
857	0.002	1.68	3.42	3.42	0.19	4.14
881	0.002	1.65	3.55	3.55	0.14	4.19
889	0.003	1.83	3.80	3.80	0.18	4.27
913	0.003	1.80	3.81	3.81	0.17	4.19
938	0.003	1.87	3.92	3.92	0.16	4.30
962	0.002	1.88	3.98	3.98	0.18	4.34
978	0.003	1.86	4.06	4.06	0.18	3.96
1002	0.003	1.88	4.49	4.49	0.17	4.14
1010	0.002	1.82	4.42	4.42	0.18	3.90

Time (hr)	Nitrate (mmol/kg)	Glycolate* (mmol/kg)	T. Formate (mmol/kg)	T. Acetate (mmol/kg)	T. Propionate (mmol/kg)	T. Chloride (mmol/kg)
264		3.18	1.96	0.10	0.16	0.12
264		3.55	2.09	0.13	0.18	0.14
264	0.015	5.19	2.44	0.15	0.16	0.17
264	0.005	4.63	2.21	0.12	0.19	0.13
264	0.023	5.29	2.59	0.15	0.07	0.16
264	0.021	4.68	2.45	0.16	0.06	0.15
264	0.009	4.74	2.49	0.16	0.07	0.16
264	0.016	4.66	2.50	0.17	0.06	0.17

265	0.005	4.46	2.47	0.17	0.07	0.17
272	0.013	4.38	2.53	0.17	0.07	0.17
289	0.015	4.35	2.49	0.16	0.07	0.17
296	0.016	4.32	2.54	0.19	0.10	0.16
313	0.011	4.02	2.50	0.22	0.10	0.18
319	0.013	4.27	2.65	0.20	0.10	0.18
337	0.026	4.35	2.67	0.21	0.11	0.17
340	0.019	4.39	2.41	0.22	0.11	0.18
345	0.018	4.65	3.55	0.23	0.11	0.18
362	0.044	4.07	2.77	0.31	0.13	0.18
369	0.022	3.90	2.79	0.38	0.12	16.85
384	0.030	4.05	2.65	0.35	0.10	0.25
388	0.041	3.48	2.58	0.46	0.12	0.29
391	0.011	3.94	2.69	0.49	0.12	
409	0.016	4.33	2.88	0.55	0.12	0.28
416	0.014	4.52	2.71	0.26	0.09	
430	0.010	4.09	3.08	0.63	0.15	0.31
434	0.025	4.43	3.17	0.59	0.11	0.25
458	0.037	4.23	3.16	0.88	0.15	0.28
474	0.045	4.75	3.33	0.93	0.18	0.29
482	0.036	4.04	3.14	1.02	0.20	0.27
514	0.041	3.59	3.02	1.14	0.20	0.29
520	0.031	4.15	3.17	1.33	0.19	0.30
537	0.032	4.14	3.25	1.29	0.17	0.32
545	0.041	4.17	3.31	1.43	0.20	0.31
561	0.035	3.94	3.36	1.54	0.23	0.29
569	0.033	3.99	3.44	1.57	0.23	0.30
585	0.044	3.94	3.57	1.61	0.27	0.32
594	0.046	3.88	3.64	1.64	0.23	0.33
609	0.048	4.07	3.72	1.92	0.23	0.34
618	0.042	3.57	3.82	2.21	0.27	0.33
634	0.044	3.50	3.82	2.20	0.29	0.35
642	0.059	3.49	3.91	2.26	0.30	0.34
658	0.073	3.42	3.82	2.15	0.31	0.89
670	0.094	3.77	4.24	2.37	0.33	2.35
686	0.093	3.44	4.45	2.96	0.40	0.30
694	0.321	3.55	4.43	3.02	0.40	0.30
710	0.106	3.59	4.85	3.36	0.45	0.33
718	0.102	5.39	5.03	3.53	0.47	0.33
744	0.108	4.28	4.80	3.57	0.47	0.31

760	0.107	4.72	5.46	4.03	0.52	0.34
768	0.107	3.92	4.89	3.70	0.51	0.33
791	0.106	4.17	5.23	3.78	0.54	0.36
816	0.107	3.37	4.94	3.59	0.53	0.35
832	0.107	4.21	5.25	3.87	0.59	0.37
857	0.108	4.11	5.42	3.95	0.62	0.37
881	0.117	4.07	5.32	3.86	0.60	0.35
889	0.128	3.95	5.72	4.33	0.61	0.38
913	0.106	4.01	5.47	4.17	0.65	0.38
938	0.118	4.09	5.50	4.31	0.67	0.36
962	0.083	4.06	5.59	4.56	0.68	0.41
978	0.107	3.81	5.67	4.68	0.71	0.40
1002	0.118	3.66	5.62	4.72	0.74	0.42
1010	0.108	3.39	5.72	4.81	0.75	0.43

Time (hr)	T. Sulfate (mmol/kg)	T. Oxalate (mmol/kg)	T. Nitrate (mmol/kg)
264	3.83	0.09	
264	4.25	0.10	0.016
264	4.74	0.13	0.017
264	4.34	0.12	0.005
264	3.85	0.57	0.024
264	3.58	0.39	0.020
264	3.64	0.33	0.023
264	3.64	0.29	0.026
265	3.51	0.23	0.023
272	3.61	0.22	0.021
289	3.51	0.20	0.020
296	3.51	0.19	0.023
313	3.42	0.18	0.023
319	3.59	0.18	0.023
337	3.56	0.17	0.028
340	3.70	0.17	0.021
345	3.76	0.18	0.026
362	3.60	0.17	0.023
369	3.72	0.15	0.033
384	3.29	0.19	0.034
388	3.21	0.16	0.036
391	3.25	0.16	0.025
409	3.47	0.14	0.039
416	3.40	0.09	0.030
430	3.92	0.22	0.044

434	4.05	0.21	0.034
458	3.98	0.19	0.046
474	4.19	0.18	0.039
482	3.92	0.16	0.038
514	3.69	0.15	0.035
520	3.85	0.16	0.040
537	3.84	0.16	0.051
545	3.86	0.15	0.040
561	3.78	0.15	0.047
569	3.86	0.15	0.051
585	3.86	0.15	0.050
594	3.87	0.15	0.054
609	3.88	0.15	0.054
618	3.85	0.15	0.065
634	3.84	0.15	0.060
642	3.79	0.13	0.056
658	3.73	0.13	0.062
670	4.07	0.14	0.091
686	3.95	0.17	0.103
694	3.86	0.16	0.094
710	4.10	0.18	0.124
718	4.23	0.20	0.105
744	3.82	0.17	0.090
760	4.44	0.21	0.119
768	3.73	0.16	0.092
791	3.92	0.17	0.093
816	3.66	0.16	0.087
832	3.78	0.16	0.096
857	3.84	0.16	0.101
881	3.73	0.16	0.102
889	4.06	0.19	0.096
913	3.78	0.15	0.097
938	3.71	0.16	0.094
962	3.76	0.16	0.094
978	3.77	0.16	0.093
1002	3.69	0.16	0.097
1010	3.76	0.16	0.099

*The glycolate peaks disappeared after treating the samples with NaOH. Therefore, the glycolate peak may represent an amide eluting at the same time as glycolate. The concentration is reported with the glycolate calibration curve.

References

Akinpelumi K, Saha C, Rochelle GT. Piperazine aerosol mitigation for post-combustion carbon capture. *International Journal of Greenhouse Gas Control*. 2019; 91: 102845.

Akita K, Yoshida F. "Bubble size, interfacial area, and liquid-phase mass transfer coefficient in bubble columns." *Industrial & Engineering Chemistry Process Design and Development*. **1974**; 13(1): 84–91.

Beaudry MR. *Aerosol Measurement and Mitigation in CO2 Capture by Amine Scrubbing*. The University of Texas at Austin. Ph.D. Dissertation. **2017**.

Benquet C, Knarvik AB, Gjernes E, Hvidsten OA, Romslo Kleppe E, Akhter S. "First process results and operational experience with CESAR1 solvent at TCM with high capture rates (align-CCUS project)" Presented at *GHGT-15*, Abu Dhabi. Mar 15–18, **2021**.

Closmann FB. *Oxidation and thermal degradation of methyldiethanolamine/piperazine in CO_2 Capture*, Ph.D. dissertation, University of Texas at Austin. **2011**.

Chakravarti S, Gupta A. "Carbon Dioxide Recovery Plant", Patent Appl. No. 09/774,031.**1999**.

Cousins A, Nielsen P, Huang S, Cottrell A, Chen E, Rochelle GT, Feron PH. "Pilot-scale evaluation of concentrated piperazine for CO_2 capture at an Australian coal-fired power station: Duration experiments." *Greenhouse Gases: Science and Technology* **2015**;5(4):363-73.

da Silva EF, Lepaumier H, Grimstveldt A, Vevelstad SJ, Einbu A, Vernstad K, Svendsen HF, Zahlsen K. "Understanding 2-Ethanolamine Degradation in Post-Combustion

CO2 Capture." *Industrial & Engineering Chemistry Research*. **2012**; 51:13329–13338.

Davis JD. *Thermal Degradation of Aqueous Amines Used for Carbon Dioxide Capture*. The University of Texas at Austin. Ph. D. Dissertation. **2009**.

Dugas RE. *Carbon Dioxide Absorption, Desorption, and Diggusion in Aqueous Piperazine and Monoethanoalamine.* The University of Texas at Austin. Ph.D. Dissertation. **2009**.

EIA. "May 2022 Monthly Energy Review." U.S. Energy Information Administration. **2022**. < https://www.eia.gov/totalenergy/data/monthly/pdf/mer.pdf>

Fine NA. *Nitrosamine Management in Aqueous Amines for Post-Combustion Carbon Capture*, Ph.D. dissertation, University of Texas at Austin. **2015**.

Flø NE, Faramarzi L, Cazenove TD, Hvidsten OA, Morken AK, Hamborg ES, Vernstad K, Watson G, Pedersen S, Cents T, Fostås BF, Shah MI, Lombardo G, Gjernes E. "Results from MEA Degradation and Reclaiming Processes at the CO_2 Technology Centre Mongstad. "*Energy Procedia*, **2017**;114:1307–1324.

Freeman SA, Dugas R, Wagener DH, Nguyen T, Rochelle GT. "Carbon dioxide capture with concentrated, aqueous piperazine." *International Journal of Greenhouse Gas Control*. **2010**; 4(2):119-24.

Freeman SA. *Thermal Degradation and Oxidation of Aqueous Piperazine for Carbon Dioxide Capture*. The University of Texas at Austin. Ph.D. Dissertation. **2011**.

Gao T, Rochelle GT. CO2 Absorption from Gas Turbine Flue Gas by Aqueous Piperazine with Intercooling. *Industrial & Engineering Chemistry Research*, **2020**; 59(15): 7174-7181.

Goff GS. *Oxidative Degradation of Aqueous Monoethanolamine in CO_2 Capture Process: Iron and Copper Catalysis, Inhibition, and O_2 Mass Transfer*. The University of Texas at Austin. Ph.D. Dissertation. **2005**.

Hikita H, Asai S, Tanigawa K, Segawa K, Kitao M. "The volumetric liquid-phase mass transfer coefficient in bubble columns." *The Chemical Engineering Journal*. **1981**; 22(1): 61-69.

Hilliard MD. *A Predictive Thermodynamic Model for an Aqueous Blend of Potassium Carbonate, Piperazine, and Monoethanolamine for Carbon Dioxide Capture from Flue Gas*. The University of Texas at Austin. Ph.D. Dissertation. **2008**.

H R P, "Kapillarchemie, Eine Darstellung der Chemie der Kolloide und verwandter Gebiete". *Nature.* **1911**; 85: 534–535.

Kang Y, Cho YJ, Woo KJ, Kim SD. "Diagnosis of bubble distribution and mass transfer in pressurized bubble columns with viscous liquid medium." *Chemical Engineering Science*, **1999**; *54*(21): 4887–4893.

Kawase Y, Halard B, Moo-Young M. "Theoretical prediction of volumetric mass transfer coefficients in bubble columns for newtonian and non-newtonian fluids." *Chemical Engineering Science*. **1987**; *42*(7): 1609–1617.

Polderman LD, Dillon CP, Steele AB. "Why Monoethanolamine Solution Breaks Down in Gas-Treating Services." *Oil and Gas Journal*. **1955**; 54(2):180-183.

Kohl, AL, Nielsen RB. **1997**. Gas Purification, fifth ed. Gulf Pub, Houston.

Langmuir I. "The Adsorption of Gases on Plane Surface of Glass, Mica and Platinum". *Journal of American Chemical Soc*iety. **1918**; 40 (9): 1361–1402.

Lin Y, Rochelle GT. "Optimization of Advanced Flash Stripper for CO_2 Capture using Piperazine." *Energy Procedia*. **2014**; 63:1504-13.

Morken AK, Pedersen S, Nesse SO, Flø NE, Johnsen K, Feste JK, Cazenove TD, Faramarzi L, Vernstad K. "CO_2 Capture with Monoethanolamine: Solvent Management and Environmental Impacts During Long Term Operation at the Technology Centre Monstad (TCM)". *International Journal of Greenhouse Gas Control.* **2019**; 82:175-183.

Moser P, Wiechers G, Schmidt S, Rochelle GT, Knuutila HK, Vevelstad SJ, Moretz-Sohn Monteiro JG, Gravesteijn,P, Figueiredo RV, Goetheer E. "Demonstrating Solvent Management Technologies for an aqueous AMP/PZ solvent" Presented at *GHGT-15*, Abu Dhabi. Mar 15–18, **2021**.

Namjoshi OA. *Thermal Degradation of PZ-Promoted Tertiary Amines for CO2 Capture.* The University of Austin. Ph. D. Dissertation. **2015**.

Nielsen PT, Li L, Rochelle GT. "Piperazine Degradation in Pilot Plants." *Energy Procedia*. **2016**; 37: 1912-23.

Nielsen PT, Rochelle GT. "Effects of Catalysts, Inhibitors, and Contaminants on Piperazine Oxidation". *Energy Procedia*. **2017**; 114: 1919-29.

Nielsen PT. *Oxidation of Piperazine in Post-Combustion Carbon Capture.* The University of Texas at Austin. Ph.D. Dissertation. **2018**.

Ocampo-Perez R., Leyva-Ramos R, Alonso-Davila P, Rivera-Utrilla J, Sanchez-Polo M.. "Modeling Adsorption Rate of Pyridine onto Granular Activated Carbon." *Chemical Engineering Journal*. **2010**; 165(1):133–141.

Ogata Y, Kawasaki A. "The Kinetics of the Reaction of Formaldehyde with Nmmonia". *Bulletin of the Chemical Society of Japan*.1964; 37(4), 514–519.

öztürk SS, Schumpe A, Deckwer WD. "Organic Liquids in a Bubble Column: Holdups and Mass Transfer Coefficients". *AIChE Journal*. **1987**; *33*(9): 1473–1480.

Rao AB, Rubin ES. “A Technical, Economic, and Environmental Assessment of Amine-Based CO2 Capture Technology for Power Plant Greenhouse Gas Control.” *Environmental Science and Technology*. **2002**; 36(20):4467-4475.

Reynolds AJ, Verheyen TV, Adeloju SB, Chaffee AL, Meuleman E. “Evaluation of Methods for Monitoring MEA Degradation during Pilot Scale Post-Combustion Capture of CO_2.” *International Journal of Greenhouse Gas Control*. **2015**; 39: 407-419.

Rochelle GT, Chen E, Freeman SA, Wagener DV, Xu Q, Voice AK. “Aqueous piperazine as the new standard for CO_2 capture technology.” *Chemical Engineering Journal*. **2011**; 171(3):725-733.

Rochelle GT, Wu Y, Chen E, Akinpelumi K, Fischer KB, Gao T, Liu CT, Selinger JL. “Pilot Plant Demonstration of Piperazine with the Advanced Flash Stripper.” *International Journal of Greenhouse Gas Control*. **2021**; 84: *72–81*.

Rochelle GT, Akinpelumi K, Gao T, Liu CT, Suresh Babu A, Wu Y. “Pilot Plant Results with the Piperazine Advanced Stripper at NGCC Conditions.” Presented at *GHGT-15*, Abu Dhabi. Mar 15–18, **2021**.

Rooney PC, DuPart MS, Bacon TR. “Oxygen’s Role in Alkanolamine Degradation.” *Hydrocarbon Processes, International Edition*. **1998**; 77(7):109-113.

Schumpe A, Grund G. (1986). The gas disengagement technique for studying gas holdup structure in bubble columns. *The Canadian Journal of Chemical Engineering*. **1986**; 64(6): 891–896.

Sexton AJ. *Amine Oxidation in CO_2 Capture Process*. The University of Texas at Austin. Ph.D. Dissertation. **2008**.

Shah YT, Kelkar BG, Godbole SP, Deckwer WD. “Design parameters estimations for bubble column reactors.” *AIChE Journal*. **1982**; 28(3): 353–379.

Strazisar BR, Anderson RR, White CM. “Degradation Pathways for Monoethanolamine in a CO_2 Capture Facility.” *Energy Fuels*. **2003**; 17(4):1034–1039.

Suresh Babu, A, Rochelle, GT. “Energy Use of Piperazine with the Advanced Stripper Based on Pilot Plant Testing.” Presented at *GHGT-15*, Abu Dhabi. Mar 15–18, **2021**.

Voice AK. *Amine Oxidation in Carbon Dioxide Capture by Aqueous Scrubbing*. The University of Texas at Austin. Ph.D. Dissertation. **2013**.

Walker JF. **1964**. Formaldehyde, third ed. Reinhold Publ. Corp, New York.

Wu Y, Rochelle GT. “Effects of Carbon Treating on Piperazine Oxidation in Pilot Plant Testing of PZAS^{TM}”. *International Journal of Greenhouse Gas Control*. **2021**; 112:103502

Vita

Yuying Wu was born in Shanghai, China and finished her high school in Shanghai Foreign Language School. She earned a Bachelor of Science in Chemical and Biomolecular Engineering from the University of Illinois at Urbana-Champaign in May 2017, where she conducted research in the research group of Dr. Huimin Zhao. She started her graduate study in the University of Texas at Austin in August 2017 and joined the research group of Dr. Gary T. Rochelle. She has accepted full-time employment with Honeywell UOP in Des Plaines, IL.

Permanent email: amyyuying130@gmail.com

This dissertation was typed by Yuying Wu.